More than a ligand: PD-L1 promotes oncolytic virus infection via a metabolic shift that inhibits the type I interferon pathway

Jonathan James Hodgins

Thesis submitted to the University of Ottawa
in partial Fulfillment of the requirements for the
Ph.D. in Microbiology and Immunology

Department of Biochemistry, Microbiology, and Immunology
Faculty of Medicine
University of Ottawa

Abstract

Targeting the PD-1/PD-L1 axis has transformed the field of immune-oncology. While conventional wisdom initially postulated that PD-L1 serves as the inert ligand for PD-1, an emerging body of literature suggests that PD-L1 has cell intrinsic functions in immune and cancer cells. In line with these studies, here we show that engagement of PD-L1 via cellular ligands or agonistic antibodies potently inhibits the type I interferon pathway in cancer cells. Hampered type I interferon responses in PD-L1-expressing cells resulted in enhanced infection with oncolytic viruses in cancer cells in vitro and in vivo. Consistently, PD-L1 expression marked tumour explants from cancer patients that were best infected by oncolytic viruses, indicating PD-L1 could be a biomarker for tumours that will best respond to oncolytic viruses. Mechanistically, PD-L1 suppressed type I interferon by promoting Warburg metabolism, characterized by enhanced glucose uptake and glycolysis rate. Lactate generated from glycolysis was the key metabolite responsible for inhibiting type I interferon responses and enhancing oncolytic virus infection in PD-L1 expressing cells. In addition to adding mechanistic insight into PD-L1 intrinsic function, this work suggests that PD-L1 has a broader impact on immunity and cancer biology besides acting as a ligand for PD-1.

Table of Contents

List of Figures

List of Tables

Abbreviations

2-DG – 2-deoxy-D-glucose
ANOVA – analysis of variance
APC – antigen presenting cell
β-TRCP - β-transducin repeat containing E3 ubiquitin protein ligase
CARD – caspase recruitment domain
CBP – CREB binding protein
CD – cluster of differentiation
cGAS – cyclic GMP-AMP synthase
CLR – C-type lectin receptor
CMTM – CKLF-like MARVEL transmembrane domain-containing
CSS – charcoal stripped serum
CTLA-4 – cytotoxic T-lymphocyte associated protein 4
CXCL10 – C-X-C motif chemokine ligand 10
CXCL9 – C-X-C motif chemokine ligand 9
DAMP – damage-associated molecular pattern
DC – dendritic cell
DFX - desferrioxamine
DHT – dihydrotestosterone
DMEM – Dulbecco's modified Eagle medium
DMOG – dimethyloxallyl glycine
DMSO – dimethyl sulfoxide
DNA-PK – DNA-dependent protein kinase
E2 – estrogen
ECAR – extracellular acidification rate
EGFR – epidermal growth factor receptor
eIF2α – eukaryotic translation initiation factor 2α
FACS – fluorescent-associated cell sorting
FBS – fetal bovine serum
FDA – Food and Drug Administration
FDG – fluorodeoxyglucose
FIH – factor inhibiting HIF-1
FOXO1 – forkhead box protein O1
GFP – green fluorescent protein
GPCR – G-protein coupled receptor
GSK3β – glycogen synthase kinase 3β
HEPES – 4-(2-hydroxyethyl)-1-piperazineethanesulfonic acid
HIF – hypoxia-inducible factor
HRE – hypoxia response element

ICOS – inducible T cell costimulator
IFN - interferon
IFNAR – interferon α/β receptor
IgC – immunoglobulin constant
IgV – immunoglobulin variable
IHC - immunohistochemistry
IKK – IκB kinase
IL-12 – interleukin-12
irAEs – immune-related adverse events
IRF – interferon regulatory factor
ISG – interferon stimulated gene
ISGF3 – interferon stimulated gene factor 3
ISRE – interferon stimulated response element
JAK – Janus kinase
LDL-R – low density lipoprotein receptor
MAPK – mitogen-activated protein kinase
MAVS – mitochondrial antiviral-signaling protein
MHC – major histocompatibility complex
miR – microRNA
MOI – multiplicity of infection
mtDNA – mitochondrial DNA
mTOR – mechanistic target of rapamycin
NAC – N-acetyl cysteine
nDNA – nuclear DNA
NFAT – nuclear factor of activated T cells
NK – natural killer
NLR – NOD-like receptor
NPC – nasopharyngeal cancer
NRF2 – nuclear factor erythroid 2–related factor 2
OAS – oligoadenylate synthase
OCR – oxygen consumption rate
OV – oncolytic virus
OXPHOS – oxidative phosphorylation
PAMP – pathogen-associated molecular pattern
PARP – poly(ADP) ribose polymerase
PBS – phosphate buffered saline
PD-1 – programmed cell death protein 1
PDAC – pancreatic ductal adenocarcinoma
PD-L1 – programmed cell death ligand 1
PET – positron emission tomography

PHD-2 – prolyl hydroxylase domain-containing protein 2
PI3K – phosphoinositide 3-kinase
PIAS1 – protein inhibitor of activated STAT1
PKC – protein kinase C
PKR – protein kinase RNA-activated
PROGENy – Pathway RespOnsive GENes for activity inference
PRR – pattern recognition receptor
PTP1B – protein tyrosine phosphatase 1B
PYK2 – protein tyrosine kinase 2
RIG-I – retinoic acid-inducible gene I
RLR – RIG-I-like receptor
ROS – reactive oxygen species
RPMI – Roswell Park Memorial Institute
SCC – squamous cell carcinoma
scRNA-seq – single-cell RNA-sequencing
SD – standard deviation
sgRNA – single guide RNA
SHP-2 – Src homology region 2 domain-containing phosphatase-2
SIN3A - SIN3 transcription regulator family member A
SOCS – suppressor of cytokine signaling
SP1 – specificity protein 1
STAT – signal transducer and activation of transcription
STING – stimulator of interferon genes
TAM – Tyro3, Axl, Mertk
TBK1 – TANK binding kinase 1
TF – transcription factor
TGF – transforming growth factor
TLR – Toll-like receptor
TOMM20 – translocase of the outer mitochondrial membrane 20
TRAMP – transgenic adenocarcinoma of the mouse prostate
TYK2 – tyrosine kinase 2
USP18 – ubiquitin specific peptidase 18
USP22– ubiquitin specific peptidase 22
VEGF – vascular endothelial growth factor
VSV – vesicular stomatitis virus
YFP – yellow fluorescent protein

Significant Contributions

Dr. Mathieu Crupi generated the microscopy images of vaccinia virus-infected TRAMP-C2 cells in Figure 3.5.

Christiano Tanese de Souza injected TRAMP-C2 cells into NCG mice, subsequently infected those tumours with oncolytic virus, and performed IVIS imaging on the infected tumours.

Dr. David Cook and Edward Yakubovich performed all bioinformatic analyses in this thesis.

Claire Fong-McMaster performed mitochondrial DNA and nuclear DNA extractions from TRAMP-C2 cells.

Dr. Shama Naz at the uOttawa Metabolomics Core Facility performed the LC-MS on extracted aqueous metabolites, and analysis of the resulting data.

Ariel Buchler and Dr. Benjamin Rotstein performed the [^{18}F]-FDG PET scanning procedure, and analysis of the resulting data.

Paraffin-embedding, tissue sectioning, and hematoxylin/eosin staining of patient tumour biopsies was performed by the uOttawa Louise Pelletier Histology Core Facility.

Dr. Saleh Fadel quantified PD-L1 expression and necrosis on patient tumour biopsies.

Acknowledgements

It has been said that behind every success there is effort; behind every effort, is passion. But behind all passion, there is someone with the courage to try. I have done my best to live by this inspirational Pinterest quote in the last few years.

However, none of this would have been possible without the circle of remarkable people I've had the privilege of meeting during this degree. Any success I might (humbly) claim can largely be credited to these amazing individuals.

I would first like to thank my supervisor Dr. Michele Ardolino for providing an outstanding training environment, for your mentorship, and for your friendship. Despite my best efforts, it will be hard for me to re-pay the huge debt I owe you; in the meantime, you will have to accept this simple acknowledgement!

I would also like to thank my TAC members Dr. Barbara Vanderhyden, Dr. Subash Sad, and Dr. Tommy Alain, who were an invaluable part of my training. Additionally, I have been lucky to collaborate with notable experts in different fields: Dr. Mary-Ellen Harper, Dr. Ben Rotstein, Dr. Doug Gray, Dr. Marie-Claude Bourgeois-Daigneault, and Dr. David Cook. Thank you all for your patient help!

As labs go, the Ardolino lab is not a bad one to end up in. Without a doubt, it's full of the most interesting, unique, funny, and kind people I've ever met. There are many I would like to thank: Maria Park, Serena Cortés-Kaplan, Cynthia Chan, Amit Scheer, Ash Hagerman, Lysanne Desharnais, Shaad Hasim, Arwa Alrehaili, Marie Marotel, Sara Asif, Colin O'Dwyer, Reem Kurdieh, and Olivia Makinson. I couldn't imagine doing this without you all.

Moreover, the 3rd floor Cancer Center is not a bad spot to spend your weekdays…and weekends. I've been truly fortunate to spend my days with such great people! Special shout-out to John Abou-Hamad, who has been there right from the start in 2017, when we knew nothing, to now (where we still know nothing, but it doesn't bother us as much). Thanks for keeping things entertaining during long days in the lab, "interesting" TA jobs, conferences, intramurals, and 20-minute lunch breaks.

Finally, thank you to my big family for their endless love and support. Special thanks to my mom Zarouhie and brother Justin, for inspiring me and keeping me grounded. This degree is as much yours, as it is mine.

Chapter 1

General Introduction

1.1 The PD-1/PD-L1 axis.

PD-1 and its ligands PD-L1/PD-L2 belong to a family of immune proteins termed co-inhibitory receptors. These receptors deliver signals to immune cells to modulate their function and activity and as such are dynamically regulated during an immune response (*1*). Co-inhibitory receptors are best studied in conventional T cells, where they are well-known to counteract the activity of co-stimulatory receptors that promote T cell activation (*2*–*4*). Multiple lines of evidence, including genetic mouse models and clinical therapies targeting these proteins, highlight their role in maintaining peripheral tolerance, preventing autoimmunity, and resolving inflammatory and immune responses (*5*, *6*).

PD-1 is a member of the CD28 family, sharing ~15% amino acid sequence similarity with other family members CD28, CTLA-4, and ICOS (*5*). It is a 288-residue transmembrane protein expressed on a variety of immune cells, including T cells, B cells (*7*, *8*), innate lymphoid cells including NK cells (*9*–*11*), and macrophages (*12*–*14*).

The ligands of PD-1, PD-L1 and PD-L2, are distinct in terms of expression. PD-L1 is widely expressed, often constitutively, on immune cells like antigen-presenting cells (APCs) and on non-immune cells such as vascular endothelial cells and pancreatic islet cells, among others (*15*). Importantly, PD-L1 expression is inducible on almost every cell type by a wide variety of stimuli, particularly pro-inflammatory cytokines such as type I and II interferons, TNF-α, and IL-6 (*16*). Therefore, PD-L1 is a readily available ligand for PD-1 engagement in vivo. On the other hand, PD-L2 expression is restricted to a handful

of cell types, with expression on dendritic cells, macrophages, and particular B cell subsets (*16*). Like PD-L1, it can be up-regulated by pro-inflammatory cytokines.

The PD-1 pathway suppresses the activity of effector T cells to maintain self-tolerance and promote resolution of inflammation. This role of PD-1 in maintaining peripheral tolerance was first noted in aged PD-1-deficient mice on the C57BL/6 background, which developed lupus-like glomerulonephritis and arthritis (*17*). Similarly, aged PD-1-deficient mice on the BALB/C background develop dilated cardiomyopathy (*18*). In other genetic backgrounds, PD-1-deficiency leads to the development of organ-specific autoimmunity, the characteristics of which depend on the type(s) of autoimmunity to which each particular mouse strain is predisposed (*19*, *20*).

Given the role of PD-1 in blocking effector T cell activity, therapies were later developed inhibiting the PD-1/PD-L1 pathway to boost the immune response against cancer (*5*). Antibodies binding to either PD-1 (pembrolizumab, nivolumab, cemiplimab, dostarlimab) or PD-L1 (atezolizumab, avelumab, durvalumab) and preventing interactions between PD-1 and PD-L1 are now clinically approved. These therapies have had success in different cancer indications, while also representing a paradigm shift in oncology and cancer immunology that re-invigorated the field of cancer immunotherapy.

Additionally, PD-1/PD-L1 blockade therapy confirmed the critical role of this pathway in maintaining immune tolerance in humans. Individuals undergoing PD-1/PD-L1 blockade

therapy develop characteristic side effects, termed immune-related adverse events (irAEs), involving autoimmune responses and autoinflammation (*21*). Recently, the consequences of PD-1 deficiency in an individual has been described, and includes dramatic immune dysfunction and autoimmunity (*22*).

1.2. PD-L1 structure, interactions, and localization

PD-L1 is a 290-residue type I transmembrane protein belonging to the B7 family, along with CD80, CD86, PD-L2 and others. It is made up of 5 major regions: the N-terminal signal peptide, the extracellular IgV and IgC domains, the transmembrane domain, and the C-terminal intracellular tail (*15*, *23*, *24*). However, smaller PD-L1 variants exist in humans due to deletion of specific regions or sequences (*16*).

PD-L1 is known to bind and interact with the co-inhibitory receptor PD-1 and CD80 (which also serves as a ligand for the co-stimulatory receptor CD28). The interaction between PD-1 and PD-L1 is very well-described, and the functional consequences are well-characterized, whereas less is known about CD80-PD-L1 interactions. PD-L1 binds PD-1 and CD80 via partially overlapping interfaces in their extracellular domains (*25*, *26*). The dissociation constant (K_D) for the PD-L1:CD80 interaction is in the range of 1-2 μM, whereas the K_D for the PD-L1:PD-1 interaction is lower (~0.5 μM) (*25*, *27*), suggesting that the affinity of PD-L1 for PD-1 is stronger than for CD80. Furthermore, recent evidence suggests that the interaction between PD-L1 and CD80 can only occur in cis on the same cell surface, and requires flexibility in a 11-residue stalk on the structure of PD-L1 (*26*, *28*,

29). Conversely, the interaction between PD-L1 and PD-1 occurs in trans between two cell membranes (*30*). Therefore, PD-1 and CD80 can competitively block each other from binding to PD-L1; further, PD-1:PD-L1 and CD80:PD-L1 interactions impact other binding interactions with related proteins, including CTLA-4 and CD28, in a complex system (*29*). The immunological consequences of these competing binding interactions are just starting to be described.

The complexity of PD-L1 biology is not limited to its extracellular domain. PD-L1 contains a 30-residue cytoplasmic tail, which lacks any conventional domains or motifs associated with protein-protein interactions or enzymatic activity. The 30-residue cytoplasmic tail of PD-L1 also lacks any evident secondary or tertiary structure and is predicted to be intrinsically disordered. In line with literature on intrinsically-disordered domains, the intracellular tail of PD-L1 has been described to bind multiple proteins, including STAT3 (*31*, *32*), as well as nucleic acids like DNA promoter regions, to alter gene expression patterns (*33*), and mRNA molecules, promoting their stability (*34*). The short cytoplasmic tail of PD-L1 contains sites for acetylation (impacting subcellular localization) (*33*), palmitoylation (*35*) and phosphorylation (*36–38*) (impacting ubiquitination and stability).

Canonically, PD-L1 is considered to be an integral cell surface protein. However, several lines of evidence have shown that PD-L1 can also localize to the nucleus (*39–41*), although its specific location in the nucleus, and any potential alterations in its three-dimensional structure in that compartment, are as-of-yet unknown. The nuclear

localization of PD-L1 is dependent on its acetylation status at Lys263 (in the cytoplasmic tail), which is controlled by the opposing actions of the histone acetyltransferase p300 and HDAC2 (*33*). PD-L1 relies on clathrin-dependent endocytosis and vimentin/importin-1α to transport it from the plasma membrane into the nucleus (*33*). In the nucleus, PD-L1 has been shown to bind to the transcription factor SP1 (*42*), the cohesion complex subunits SA1 (*43*) and PDS5B (*44*), and DNA-dependent protein kinase (DNA-PK) (*45*). It has also been characterized to impact gene expression, in particular those genes related to immune responses (*33*).

In other intracellular compartments, PD-L1 has been described to bind glycogen synthase kinase 3β (GSK3β) and β-transducin repeats-containing protein (β-TRCP) (*46*), ubiquitin specific peptidase 22 (USP22) (*47*), protein tyrosine phosphatase 1B (PTP1B) (*48*), CKLF-like MARVEL transmembrane domain-containing protein 6 (CMTM6) and CMTM4 (*49*, *50*), all of which impact protein stability. For many of these intracellular protein-protein interactions, the binding residues on PD-L1 are unknown. Interestingly, PD-L1 has been suggested to bind to AKT in the intracellular environment via its IgC extracellular domain (*51*), hinting that not all intracellular binding partners of PD-L1 dock onto its 30-residue cytoplasmic domain.

1.3. PD-L1 intrinsic function in cancer

Recent literature has revealed a new angle on PD-L1, beyond its unidimensional role as the ligand for the PD-1 receptor. PD-L1 is now linked to the regulation of many important pathways and processes in cancer cells.

In several different contexts, PD-L1 expression on cancer cells promotes proliferation and survival, and the mechanism by which it does so has been variously attributed to regulation of mTOR and autophagy (*52*, *53*), PI3K/Akt (*54*), c-Myc (*55*), or by undetermined mechanisms (*56–59*). PD-L1 has also been suggested to promote tumour initiation *in vitro* (*60*), invasion of cancer cells and fibroblasts (*51*, *61*), and the epithelial-to-mesenchymal transition process (*48*, *62*). Additionally, one report suggests that PD-L1 can recruit phospholipase C-γ1 to its cytoplasmic tail, and in this manner promote EGFR function to drive tumour formation and metastasis (*63*), consistent with another paper that used an unbiased proteomic approach to show PD-L1 promotes EGFR signaling (*64*).

PD-L1 prevents cell death in response to a variety of chemotherapeutics, including cisplatin, paclitaxel, and the PARP inhibitors olaparib and talazoparib. Consistently, this function of PD-L1 has been linked to its ability to protect cancer cells from DNA damage, as PD-L1 promotes expression of proteins involved in homologous recombination (*34*, *65*, *66*) and promotes the activity of DNA-PKc (*45*), a kinase involved in regulating the DNA damage response. PD-L1 also protects cancer cells from the damaging effects of ionizing radiation (*34*, *67*).

PD-L1 also regulates cellular metabolism in cancer. Via the regulation of mTOR, PD-L1 promotes glucose uptake and glycolysis in B16-F10, MC38, and the d42m1 murine tumour models (*68*). Further, in renal cell carcinoma cells, PD-L1 is a key player in the pro-glycolytic metabolic shift following treatment with IFN-γ (*69*). In the clinical space, PD-L1 expression in tumours is associated with [^{18}F]-fluorodeoxyglucose (FDG) uptake of those tumours during FDG-PET scans (summarized in (*70*)), suggestive of increased glucose metabolism. Lastly, a recent report revealed a positive correlation between PD-L1 and glycolysis-related gene signatures, as well as a negative correlation between PD-L1 and OXPHOS-related gene signatures, in hundreds of patient tumours (*71*). PD-L1 has also been suggested to regulate choline metabolism (*72*), hinting that the metabolic roles of PD-L1 extend beyond glycolysis and glucose metabolism.

1.4. Oncolytic viruses (OVs)

Oncolytic viruses (OVs) are a group of viruses with natural or engineered tropism for cancer cells over healthy cells. The use of OVs as a therapeutic modality in cancer, termed oncolytic virotherapy, represents a more selective therapy than traditional treatments like radiation and chemotherapy. There are now multiple OV “platforms”, including (but not limited to) adenoviruses, herpesviruses, poxviruses, reoviruses, and rhabdoviruses, each with unique properties and coding capacities.

The origins of the OV field can be traced back 100 years, with case reports observing remission of leukemia in association with influenza and other types of infection (*73–76*). Later, it was shown that vaccinia virus can slow the growth of mouse and rat tumours

(*77*), leading to clinical trials using viruses to treat cancer in the 1950s (*78*). These early clinical trials consisted of transferring serum or tissues from infected individuals to cancer patients, which showed unacceptable toxicity and highly variable efficacy (*79*, *80*). Today, there are 2 clinically approved OVs: in 2005, an adenovirus OV (Oncorine) was approved in China for the treatment of head and neck cancer (*81*), and in 2015, a herpes simplex OV (talimogene laherparepvec or T-Vec) was approved by the FDA for the treatment of melanoma (*82*). There are many OVs in preclinical and clinical testing, using different viruses and combination treatments. Since the 1950s, there has been tremendous progress in the selection, engineering, and understanding of OVs, driven by advances in basic research which will be summarized here.

The efficacy of OVs stems from two major mechanisms: direct infection/lysis of tumour cells and other cells in the tumour microenvironment, and induction/stimulation of an anti-tumour immune response. Tumour cell lysis occurs after replication of the OV in tumour cells, which can be driven by natural mechanisms encoded by the virus or engineered genetic modifications that force the virus to preferentially replicate in tumour cells (*83*). A classic example of such engineering is the removal of the viral thymidine kinase gene, which attenuates viral replication in healthy tissues with a relatively low abundance of nucleotides to support viral replication (*84–90*). In contrast, tumours with relatively high abundance of nucleotides (allowing for uncontrolled growth) can support viral replication, producing a degree of selectivity. Other examples of engineered specificity include replacing viral promoters with tissue-specific promoters (*91–97*) or modification of viral surface proteins to alter entry receptor utilization (*98–104*).

Regardless of the mechanism of specificity, viral replication allows for amplification and spread of the therapeutic virus in tumours.

OVs have also been shown to replicate within non-cancer cells in the tumour microenvironment. OVs can invade vascular endothelial cells that make up the vasculature, and OV vessel infection can reduce tumour vasculature (*105*, *106*). Additionally, OVs can infect cancer-associated fibroblasts (CAFs), which make up the stromal component and predominate in some tumour types like pancreatic cancer (*107*). OV infection of stromal cells in the tumour microenvironment offers a unique opportunity to destroy the structure of the tumour, in addition to the tumour debulking caused by OV-mediated cancer cell lysis and the immune-stimulating properties of OVs. Lastly, recent evidence suggests that OVs also replicate in immune cells (*108*). In patients with B cell lymphoma treated with the FDA-approved OV T-VEC, viral transcripts were detected in many cells in the tumour microenvironment, including nearly every immune cell subset. Entry and replication of T-VEC in these diverse cell types was independent of malignancy status, HSV-1 entry receptor expression, and status of pathways previously characterized to target OVs to cancer cells (type I interferon anti-viral signaling, PKR, and RAS mutations). A similar observation was made in vitro with the OV Newcastle disease virus, which infected monocytes, macrophages, and dendritic cells (DCs) (*109*). Interestingly, this infection was non-productive in the sense that there was no boost in Newcastle disease virus titers post-infection, despite evidence of viral replication and gene expression.

The second major mechanism of OV efficacy is the induction and/or stimulation of an anti-tumour immune response. Generally, tumours are inherently immunosuppressive for several reasons, including low expression of MHC, active anti-inflammatory programs, co-inhibitory ligand expression, and poor immune cell infiltration (*110*–*112*). Infection of tumour cells by OVs leads to a localized inflammatory response, characterized by cytokine secretion and infiltration of innate immune cells, including DCs and neutrophils (*113*–*115*). Additionally, OV infection leads to generation of virus-derived pathogen-associated molecular patterns (PAMPs), which act as an adjuvant to boost the immune response (*116*). OV-stimulated lysis of tumour cells leads to release of both viral and cancer cell antigens, allowing for boosting and induction of adaptive immune responses following antigen uptake by APCs infiltrating the tumour and activated by the now inflammatory cytokine-rich and PAMP-dense tumour microenvironment (*117*–*120*). Lastly, OV infection up-regulates MHC I expression on infected and bystander cells due to autocrine and paracrine effects of the cytokines produced as a result of infection (*121*). MHC I expression subsequently allows for recognition and tumour cell lysis by $CD8^+$ T cells, which require MHC I on target cells. Oncolytic virotherapy is unique in that with one biological therapy, there is multi-pronged stimulation of the immune system and the chance to turn a “cold” tumour into a “hot” tumour. Indeed, this innate and adaptive immune response to tumours induced by OV infection are now considered essential for efficacy and long-term protection against tumour recurrence, owing to the memory response induced by the immune system (*122*, *123*).

1.5. The type I interferon pathway

Interferons are cytokines able to inhibit viral infection, alter cancer cell proliferation, and modulate immune responses. There are three main families of interferons: type I interferons (IFN-α and IFN-β, among others), type II interferons (IFN-γ), and type III interferons (IFN-λ1, IFN-λ2, and IFN-λ3) (*124*). The three families are distinguished by the cell types that produce them, the cellular receptors they bind to (and the pattern of receptor expression), and their signaling pathways and resulting gene expression programs.

The type I interferon family is made up of 13 partially homologous IFN-α subtypes (14 in mice), IFN-β, IFN-ε, IFN-τ, IFN-κ, IFN-ω, IFN-δ, and IFN-ζ (*124*). All type I interferon cytokines bind to a common heterodimeric cell-surface receptor composed of IFN-α receptor I and 2 (IFNAR1 and IFNAR2). IFNAR1 and IFNAR2 constitutively interact with the intracellular tyrosine kinases TYK2 and JAK1, respectively. When type I interferon cytokines bind to IFNAR2, they induce a conformational change that causes dimerization of the two receptor subunits, which allows for autophosphorylation and activation of JAK1. The transcription factors STAT1 and STAT2, inactive in the cytoplasm, can then dock onto the phosphorylated IFNAR and become phosphorylated by JAK1, which allows them to dimerize and form a complex along with IRF-9, termed the interferon-stimulated gene factor 3 (ISGF3).

The ISGF3 complex translocates to the nucleus, where it can bind to interferon-stimulated response elements (ISREs) in the promoters of genes and induce expression of hundreds of interferon-stimulated genes (ISGs), which exert both anti-viral and immune-stimulating functions (*125*, *126*). The oligoadenylate synthase (OAS) enzymes are ISGs that allow for detection of viral RNAs, which can then be degraded by the latent endoribonuclease RNAseL, itself an ISG (*127*). Protein kinase R (PKR) is an ISG that binds to dsRNA and halts cellular translation of mRNAs, including viral RNAs, by phosphorylating and inactivating the key eukaryotic translational initiation factor eIF2α (*128*). PKR is a critical component of the interferon-induced resistance to many viruses. Mx proteins are dynamin-like GTPases effective against a broad range of RNA viruses, including VSV (*129*). The chemokines CXCL9 and CXCL10 are ISGs that regulate immune cell migration, and lead to the recruitment of macrophages, T cells, and NK cells (*130*).

Type I interferon cytokines are generated during a viral infection in response to activation of pattern recognition receptors (PRRs), which are grouped into 5 families: Toll-like receptors (TLRs), NOD-like receptor (NLRs), RIG-I-like receptors (RLRs), C-type lectin receptor (CLRs), and cGAS/STING (*131–133*). PRRs are distributed in different subcellular compartments and are activated by PAMPs and damage-associated molecular patterns (DAMPs) generated by infection or damage, respectively. PRRs all recognize distinct molecules that are either not found in the host, or are in the incorrect subcellular compartment, either of which is indicative of infection and/or damage. These receptors are an early system to alert the host that a foreign agent is present, and work to stimulate the immune system.

The molecular methods used by each PRR to trigger immune responses are distinct; given its importance in the rest of this thesis, the response to the RNA virus vesicular stomatitis virus (VSV) will be discussed. VSV primarily triggers the PRR retinoic acid-inducible-gene-I (RIG-I), which recognizes short double-stranded RNA generated in the cytosol during infection (*134–137*). Upon dsRNA binding, a conformational change in RIG-I exposes its caspase activation and recruitment domain (CARD), which allows for interaction with the CARD of mitochondrial antiviral signaling protein (MAVS). This leads to the recruitment, autophosphorylation, and activation of the serine/threonine kinase TANK-binding-kinase-1 (TBK1). Activated TBK1 and another kinase, inhibitor of NF-κB kinase ε (IKKε), phosphorylate the transcription factor interferon regulatory factor-3 (IRF-3), which homodimerizes and translocates to the nucleus to transcribe type I interferon cytokines and a subset of ISGs (*131*). IRF-3 is aided in this by two co-factors, CBP and p300, in the nucleus (*138*). Type I interferon cytokine expression is also promoted by the transcription factor IRF-7, which is itself an ISG that allows for a second wave of interferon-stimulated interferon expression in a feed-forward loop (*124*). Other PRRs, like TLR-4 (*139*) and TLR-13 (*140*), have also been implicated in the control of VSV infection.

The molecular players involved in the type I interferon pathway are broadly expressed, and therefore most cell types can generate a type I interferon response and/or produce type I interferon cytokines. Indeed, many cells exhibit a constitutive type I interferon

response in the absence of infection (tonic signaling), maintained by small amounts of IFN-β production in an autocrine loop (*141–145*). In immune cells, this constitutive low-level IFN-β production drives high basal expression of ISGs (such as STAT1 and IRF-9), allowing those cells to respond rapidly with anti-microbial gene expression patterns upon infection (*146–148*). In cancer cells, tonic type I interferon production is thought to be a consequence of the DNA damage common in rapidly proliferating cells (*149–153*). Additionally, tonic signals from other immunoreceptors can amplify type I interferon signaling; for example, tonic signaling from ITAM-containing receptors activates protein tyrosine kinase 2 (PYK2), which amplifies type I interferon-induced JAK1 phosphorylation and activation (*154*). At the same time, tonic type I interferon signaling is restrained by inhibitory mechanisms that limit expression and activation of IFNAR, JAK, and STAT molecules (*155–157*).

There are numerous proteins and pathways that inhibit the type I interferon pathway. Surface IFNAR expression is often down-regulated, for example by a pathway involving p38 MAPK phosphorylation of IFNAR, allowing for casein kinase II-mediated phosphorylation of a degron sequence in IFNAR and subsequent internalization, ubiquitination, and proteasomal degradation of the receptor (*158–160*). Viruses have other distinct mechanisms to induce IFNAR degradation to evade the anti-viral effects of type I interferons (*161*). The phosphatase SHP-2 can also dephosphorylate signaling intermediates downstream of the type I interferon receptor (*162*); in these contexts, SHP-2 activation is mediated by PKCβ and PKCδ activated downstream of other receptors, such as TLRs (*163*, *164*). Importantly, some negative regulators are

themselves ISGs and are therefore induced as part of the type I interferon response, including SOCS1, SOCS3, and USP18. SOCS proteins compete with STAT molecules for binding to IFNAR, thus suppressing their phosphorylation and activation by JAK1 (*165*). Expression of SOCS proteins involves the TAM (Tyro3, Axl, Mer) family of receptor tyrosine kinases. USP18, on the other hand, displaces JAK1 from IFNAR2 (*166*, *167*). Therefore, some of these regulators of the type I interferon pathway are involved in a negative feedback loop.

Regulation of the type I interferon pathway can also occur farther downstream, at the gene/ISG expression level. For example, type I interferon-activated STAT3 can diminish ISG expression and the anti-viral response (*168*, *169*), and this inhibition can be relieved by STAT3 binding to the co-repressor complex SIN3A (*170*). Additionally, PIAS1 can suppress STAT1 function and ISG expression by blocking the binding of STAT1 to DNA and enabling histone marks that repress transcription (*171*). Lastly, several studies have revealed that miRNAs can regulate the type I interferon pathway by targeting transcripts encoding STAT1, STAT2, and IFN-β, such as miR-146a and miR-155 (*155*, *157*).

Beyond individual regulators, the type I interferon pathway can cross-talk with many other pathways that either promote or inhibit type I interferon responses. For example, the cellular response to hypoxia has been well-characterized to impact type I interferon responses and viral infection (*172–175*). Generally, hypoxia has been found to inhibit the type I interferon response, and promote virus (including VSV) infection. Signaling

downstream of the VEGF receptor can repress the type I interferon pathway and promote OV infection (*106*, *176*). The transcription factor p53 has been shown to suppress innate immune signaling and the subsequent generation of type I interferon responses (*177*); alternatively, in other contexts p53 has been shown to promote type I interferon signaling and therefore block viral infection (*178–180*). In a similar fashion, TGF-β signaling has variously been shown to promote or inhibit type I interferon signaling and responses in different contexts (*181–184*). Lastly, EGFR signaling has consistently been shown to inhibit type I interferon responses and anti-viral signaling, in several different contexts (*185–187*).

Besides their anti-viral functions, type I interferons are critical for the generation of an effective immune response, both in infection and in cancer. Type I interferons have effects on both innate and adaptive immune cell responses, and therefore their ability to impact the host response to infection is not limited to the cell-intrinsic anti-viral response. Type I interferons promote the maturation of immature DCs and enhance their ability to stimulate T cells and trigger IL-12 production (*124*). In NK cells, type I interferons are important for the activation and expression of IFN-γ and cytotoxic molecules; during influenza and vaccinia virus infection, these cytokines are required for cytolytic functions of NK cells (*124*). Type I interferons enhance the ability of $CD4^+$ T cells to help B cells and have been shown to promote differentiation into the T_H1 lineage (*124*). In $CD8^+$ T cells, type I interferons promote survival and clonal expansion during immune responses and promote their cytotoxic functions (*124*). Lastly, type I interferons promote B cell activation and antibody class switching (*124*).

The important role of type I interferons during anti-microbial immunity extends to the anti-tumour immune response. In murine models of graft-versus-leukemia, the anti-tumour efficacy of allotransplanted T cells requires them to express IFNAR1 (*188*). In murine models of melanoma, the synthetic TLR7/8 agonist imiquimod promotes IFNAR1-dependent recruitment of plasmacytoid DCs in the tumour bed, which abundantly secrete type I interferons that further triggers production of cytotoxic molecules and tumour cell killing (*189*). Absence of IFNAR1 abolishes the therapeutic efficacy of imiquimod in these models. Mice deficient for the PRR and type I interferon trigger STING have reduced efficacy of combined checkpoint blockade therapy (anti-CTLA-4 and anti-PD-L1) in murine models of melanoma, suggesting a potential role for these cytokines in checkpoint blockade therapy (*190*).

Given the importance of type I interferons in anti-microbial immunity and in the generation of adaptive immune responses, it is no surprise that type I interferons play an important role in oncolytic virotherapy. The OV Newcastle disease virus, in combination with anti-CTLA-4, eliminates murine B16-F10 melanoma tumours via an immune response that requires cytotoxic T cells, NK cells, and IFNAR (*191*). Additionally, the OV Semliki Forest virus elicits tumour-specific cytotoxic T cells only in IFNAR-expressing mice (*192*). These data suggest that rather than posing an obstacle to oncolytic virotherapy, type I interferons are key molecules in the resulting anti-tumour immune response that plays a prominent role in the efficacy of OVs.

Beyond their impact on anti-tumour immune responses, several lines of evidence suggest that type I interferons inhibit the process of transformation and oncogenesis. At high doses, they are well-known to have anti-proliferative and pro-apoptotic effects on cancer cells, and have also been shown to inhibit metastatic dissemination of tumour cells (*193*). In many instances, the role of type I interferons in preventing oncogenesis and metastasis lies in the immune cells, as shown in mouse models with hematopoietic-specific expression of IFNAR (*194*, *195*). In other cases, type I interferons directly impact the cancer cell itself. Deletion of IFNAR or IFN-β from mouse embryonic fibroblasts predisposes these cells to transformation in vitro (*196*). In vivo, specific IFNAR deletion in intestinal epithelial cells increases intestinal tumour burden in mice treated with dextran sodium sulfate (*197*). In agreement with the direct impact of these cytokines on cancer cells, many tumours exhibit reduced type I interferon signaling via a variety of mechanisms, including downregulation of IFNAR (*198*), loss-of-function mutations in JAK1 (*199–201*), and/or reduced expression of other type I interferon signaling components, such as STAT1 (*202*). Therefore, type I interferon responses are unfavourable to tumours via cell-intrinsic and cell-extrinsic mechanisms. This likely imposes a selective pressure on cancer cells to dampen type I interferon responsiveness. However, this defective type I interferon response in cancer cells leads to a proverbial Achilles heel: cancer cells have defective anti-viral responses, and thus are more readily infected with OVs than healthy cells (*83*). It should be noted that this is by no means a universal phenomenon; a subset of tumours/cancer cells retain the capacity to generate effective anti-viral responses, rendering them relatively resistant to OV therapy (*203–205*).

1.6. Vesicular stomatitis virus (VSV and VSVΔ51)

VSV is a negative sense ssRNA rhabdovirus that primarily infects rodents, cattle, swine, and horses, where it results in a mild and non-fatal illness. Human infection is rare and usually asymptomatic (*206*).

The ~11 kb VSV genome, like other rhabdoviruses, is made up of 5 genes: nucleoprotein (N), phosphoprotein (P), matrix (M), glycoprotein (G), and the viral RNA-dependent RNA polymerase (L), listed in order from 3' to 5'. In the virion, viral RNA forms a helical complex with the nucleocapsid, composed of the nucleoprotein N and the phosphoprotein P (*206*). The virion also packages the RNA-dependent RNA polymerase (L). This nucleocapsid is enveloped in a lipid bilayer acquired from host cell membranes during budding (*206*). The matrix protein (M) and glycoprotein (G) are membrane-associated proteins. M associates with both the nucleocapsid and the lipid bilayer, which maintain the virion structure (*206*). G is an integral membrane protein that controls viral tropism and entry, mediated by cell attachment via the LDL receptor (LDL-R) and related family members, followed by membrane fusion (*206*).

Briefly, the VSV lifecycle begins when the VSV G protein binds to the target cell membrane via LDL-R (*207*), following which the virion enters the cells by clathrin-dependent endocytosis (*208*, *209*). Upon acidification of the endosome and fusion of the viral and endosomal membranes, the ribonucleocapsid is released into the cytoplasm. The RNA-dependent RNA polymerase (L) then proceeds to synthesize genomic RNAs

and mRNAs in the cytoplasm (*206*). Host cell ribosomes translate viral mRNAs to synthesize viral proteins, which assemble into a virion structure that buds off the host cell plasma membrane (*206*).

VSV is highly sensitive to the anti-viral effects of type I interferons (*210–213*), and has developed a key mechanism to shut off the virus-induced type I interferon response. Through an incompletely understood mechanism that may involve inhibition of host mRNA export from the nucleus, the VSV M protein blocks production of type I interferon cytokines (*214–223*), among other host genes, preventing type I interferon-mediated anti-viral response. A variant generated with deletion of the methionine 51 residue prevents VSV M from blocking type I interferon production and is permissive to the development of an effective anti-viral response. This VSV variant, termed VSVΔ51, replicates more effectively in transformed over healthy cells due to the blunted type I interferon response that characterizes many cancer cells (*224*, *225*), whereas in healthy cells an intact type I interferon response is likely to oppose to VSVΔ51 replication and infection.

Due to the relatively low rate of pre-existing immunity to VSV in humans and its cytoplasmic life cycle, VSVΔ51 is a viable candidate as a therapeutic OV platform. Further, the genome of VSV, although small, does allow for genetic manipulation to encode transgenes that boost efficacy. VSV engineered to encode IFN-β was tested in a phase I clinical trial and deemed safe in patients with solid tumours (NCT02923466), and

is now being tested as a monotherapy in a clinical trial for patients with liquid and solid tumours (NCT03017820, NCT01628640), as well as in combination with anti-PD-1 (pembrolizumab) in lung and neuroendocrine cancer (NCT03647163).

1.7. OV Therapy and Anti-PD-L1

OV infection of tumours results in a remodeling of the tumour microenvironment, and greater understanding of those changes will facilitate the rational combination of therapies to enhance anti-tumour efficacy. A frequent change in the tumour microenvironment is the up-regulation of PD-L1 that occurs upon OV infection, often triggered by type I interferons (*226*).

Given the importance of the anti-tumour immune response in the efficacy of OV therapy, and the immunosuppressive function of the PD-1/PD-L1 axis, several studies have shown synergistic effects of combining OV therapy with anti-PD-L1 or other methods that would prevent signaling downstream of PD-1. In mouse models of colon and ovarian cancer, vaccinia virus injection induced PD-L1 expression in cancer cells and tumour-infiltrating immune cells, including macrophages and DCs. Combination of vaccinia virus with anti-PD-L1 therapy led to reduced tumour burden and improved survival in these models, which was associated with a reduction in checkpoint receptor expression on immune cells and increased expression of immune activation markers like IFN-γ, granzyme B, perforin, and ICOS. Anti-PD-L1 therapy also reduced PD-L1 surface expression on tumour and immune cells (*227*).

In murine B16-F10 melanoma tumours, infection with Newcastle disease virus led to up-regulation of PD-L1 in immune and non-immune cells. Blockade of IFNAR1 abolished OV-induced PD-L1 up-regulation in the tumour microenvironment. Combination treatment of Newcastle disease virus with anti-PD-L1 or anti-PD-1 reduced tumour burden and improved survival in this model, which was similarly associated with a re-invigoration of the immune response in these tumours (*228*). In a similar vein, another group has shown that the combination of VSVΔ51 infection with anti-IFNAR1 (to prevent virus-induced PD-L1 up-regulation in the tumour) or anti-PD-L1 showed synergistic effects on tumour burden in the B16-F10 and MC38 murine models of cancer (*229*).

Alternatively, in murine B16-F10 melanoma tumours, infection with oncolytic myxoma virus engineered to express and secrete a soluble PD-1 molecule resulted in improved tumour control compared to a control virus. This was associated with changes in the tumour immune infiltrate, presumably due to the soluble PD-1 molecule preventing PD-L1 from engaging PD-1 on T cells that would suppress their activity (*230*).

Lastly, in a mouse model of acute myeloid leukemia using intravenously delivered C1498 cancer cells (engineered to encode GFP), the combination of VSV with anti-PD-L1 significantly decreased tumour burden and improved survival compared to either treatment alone. Improved outcomes in this murine model was associated with increases in VSV- and tumour-specific T cells (*231*).

1.8. Rationale and Aim

Over the past 5 years, different research groups have observed that PD-L1 regulates the type I interferon response in cancer and immune cells (*33*, *232–234*), which has been shown using transcriptome-based studies or direct biochemical methods. Interestingly, the connection between PD-L1 and type I interferon responses has been studied only in the context of interferon-induced cell death (*232*) and interferon responses triggered by DNA damage (*234*). PD-L1 inhibition of type I interferon responses has not been studied in the context of viral infection.

While PD-L1 has been shown to modulate type I interferon responses in different contexts, there is a gap in the literature regarding its role in controlling viral infections. The interplay between PD-L1, type I interferons, and OVs is especially interesting considering the enthusiasm for combining oncolytic virotherapy with PD-L1 blockade in preclinical studies and clinical trials, as mentioned previously. Given that PD-L1 alters the type I interferon pathway, which is critical to the cellular anti-viral response, we investigated the ability of PD-L1 to modulate OV infection in cancer. Further, we sought to identify the mechanism by which PD-L1 alters type I interferon responses and OV infection in cancer cells.

Chapter 2

Materials and Methods

2.1. Cell Culture

2.1.1. Cell lines

All cell lines were cultured at 37°C in a humidified atmosphere containing 5% CO_2. TRAMP-C2 were maintained in DMEM supplemented with 5% FBS, 5% NuSerum, 0.005 mg/mL bovine insulin, 10 nM dehydroisoandrosterone, 100 U/mL penicillin, 100 µg/mL streptomycin, 10 µg/mL gentamicin sulfate, and 20 mM HEPES. B16-BL6, MB49, YUMM1.1., MC38, 786-0, Hs746, HEK293T, L929-ISRE, and Vero cells were maintained in DMEM supplemented with 10% FBS, 100 U/mL penicillin, 100 µg/mL streptomycin, 10 µg/mL gentamicin sulfate, and 20 mM HEPES. C1498 cells were maintained in RPMI supplemented with 5% FBS, 100 U/mL penicillin, 100 µg/mL streptomycin, 10 µg/mL gentamicin sulfate, and 20 mM HEPES. Cells were regularly tested for mycoplasma using PCR protocol adapted from (*235*). MB49 cells were a gift from Dr. Bob Korneluk (CHEO), YUMM1.1. cells were a gift from Dr. Luc Sabourin (OHRI), 786-0 and Vero cells were a gift from Dr. John Bell (OHRI), Hs746 were purchased from ATCC, L929-ISRE generated by Dr. Bruce Beutler (UT Southwestern) were a gift from Dr. Subash Sad (uOttawa), and HEK293T were a gift from Dr. Ian Lorimer (OHRI).

2.1.2. Generation of PD-L1-deficient TRAMP-C2, B16-BL6, MB49, MC38, C1498, and YUMM1.1.

Single-guide RNA (sgRNA) targeting exon 3 of the *Cd274* gene (sequence: GTATGGCAGCAACGTCACGA) was cloned into the Cas9-expressing lentiCRISPR v2 vector according to lentiCRISPR cloning protocol from the Zhang lab (*236*); lentiCRISPR v2 was a gift from Feng Zhang (Addgene plasmid 52961). Murine cancer cell lines were

transiently transfected with this plasmid using Lipofectamine 3000 as per manufacturer's instructions, and subsequently treated with murine IFN-γ (Peprotech) which induced up-regulation of PD-L1 in all cells, except those with deletion of PD-L1. PD-L1^{-} cells were isolated by FACS.

2.1.3. Retroviral production and transduction

To produce retroviral particles, HEK293T cells were seeded in 10 cm plates to 70-80% confluency. HEK293T cells were transfected using Lipofectamine 3000 as per the manufacturer's protocol with 10 µg of retroviral construct, 8 µg of pCL-Eco (a gift from Inder Verma; Addgene plasmid 12371), and 2 µg of pCMV-VSV-G (a gift from Bob Weinberg; Addgene plasmid 8454) to generate retrovirus. The next day, media was removed and replaced with 5 mL of TRAMP-C2 media. 48-72 hours later, the culture supernatant (containing retrovirus) was removed from cells and filtered using a 0.45 µm filter.

2.1.4. Stable expression of PD-L1 or empty vector in TRAMP-C2 *Cd274*$^{-/-}$

To stably express PD-L1 or control vector in TRAMP-C2-*Cd274*$^{-/-}$, the cDNA encoding full-length murine PD-L1 was cloned into the retroviral vector pQCXIN-IRES-Thy1.1, and the resulting pQCXIN-PD-L1-IRES-Thy1.1 plasmid was used to make retrovirus. TRAMP-C2-*Cd274*$^{-/-}$ were infected with this retrovirus (or retrovirus encoding pQCXIN-IRES-Thy1.1 as empty vector control) supplemented with 8 µg/mL polybrene. Cells staining positively for PD-L1 and Thy1.1 (or Thy1.1 only for empty vector control) were isolated by FACS.

2.1.5. Generation of 786-0 *CD274*$^{-/-}$ and Hs746 *CD274*$^{-/-}$

To generate 786-0 and Hs746 *CD274*$^{-/-}$, cells were electroporated with a ribonucleoprotein complex of ATTO550-labeled gRNA (IDT; sequences: UGG CUG CAC UAA UUG UCU AUG UUU UAG AGC UAU GCU; AUU UAC UGU CAC GGU UCC CAG UUU UAG AGC UAU GCU; AGC UAC UAU GCU GAA CCU UCG UUU UAG AGC UAU GCU; UUG AAG GAC CAG CUC UCC CUG UUU UAG AGC UAU GCU) and recombinant Cas9 (IDT) using protocols modified from the Alt-R CRISPR-Cas9 system (IDT), and subsequently treated with human IFN-γ (Peprotech) to up-regulate PD-L1 in all cells except those with deletion of PD-L1. PD-L1^{-} cells were isolated by FACS.

2.1.6. In vitro treatments

Cells were treated with the following reagents, at concentrations and times indicated in figure legends: recombinant murine IFN-β (PBL Assay Sciences), poly(I:C) (Invivogen), actinomycin D (Sigma), recombinant mouse PD-1-Fc chimeric protein (R&D Systems) or human IgG1 control (R&D Systems), afatinib (Selleck Chemicals), SB431542 (Selleck Chemicals), estradiol/E2 (Sigma), dihydrotestosterone/DHT (Sigma), ML385 (Selleck Chemicals), N-acetyl-L-cysteine (Sigma), 10058-F4 (Selleck Chemicals), DMOG (Selleck Chemicals), deferoxamine mesylate (DFX, Selleck Chemicals), sodium oxamate (Selleck Chemicals), (R)-GNE-140 (Selleck Chemicals), sodium lactate (Sigma), oligomycin A (Selleck Chemicals), or Torin1 (Selleck Chemicals).

2.1.7. In vitro antibody treatment

Anti-IFNAR1 (clone MAR1-5A3) was purchased from Leinco. PD-L1 monoclonal antibody clones 6E11, 17H9, and 27C11 were gifts from Dr. Ira Mellman (Genentech). Tecentriq® (atezolizumab) was obtained from The Ottawa Hospital Pharmacy department. TRAMP-

C2, 786-0, or Hs746 cells were pre-treated with these antibodies or appropriate isotype controls (Leinco) for 24 hours prior to further manipulation/analysis at concentrations indicated in figure legends.

2.1.8. Hypoxia

TRAMP-C2 cells were seeded in normoxic conditions and transferred to a humidified hypoxic glove box (Coy Labs) maintained at 37°C and 1% O_2. All subsequent manipulations were performed in the hypoxia chamber, with solutions equilibrated to the low oxygen environment prior to use.

2.2. Oncolytic viruses

2.2.1. Oncolytic virus production

VSVΔ51-YFP, VSV WT, VSVΔ51-firefly luciferase, and vaccinia virus were gifts from Dr. John Bell (OHRI). Original VSV virus stocks were propagated on Vero cells (at MOI 0.01) and cell supernatant isolated 20-24 hours later for concentration of virus by high-speed centrifugation at 10,000 rpm for 2 hours at 4°C. All subsequent VSV virus stocks were generated from the original stock to avoid genetic drift.

2.2.2. Oncolytic virus infection

TRAMP-C2, 786-0, and Hs746 were infected with VSVΔ51-YFP, VSV WT, or GFP-expressing vaccinia virus (Copenhagen strain) by first removing and washing out culture media with PBS, followed by the addition of a low volume of virus diluted in cold DMEM at MOIs ranging from 0.001 to 100. After incubation at 37°C + 5% CO_2 for 1 hour,

supplemented growth media were added to each well, and cells incubated at 37°C + 5% CO_2 prior to analysis.

2.2.3. Plaque assay

VSVΔ51 and vaccinia virus titers were quantified by plaque assay. Confluent monolayers of Vero cells were plated 24 hours prior to plaque assay. Virus samples were serially diluted in cold DMEM, and 100 µL of dilutions added onto Vero cells for 1 hour at 37°C + 5% CO_2. After 1 hour, a 0.5% agarose in DMEM + 10% FBS overlay was applied to each well and incubated at 37°C + 5% CO_2 for 24 hours to allow infection and plaque formation. After 24 hours, plaques were counted for each dilution.

2.2.4. Coomassie staining for cell viability

Culture media was removed and washed out with PBS, and cells were fixed with 3:1 methanol:acetic acid solution for 1-3 hours. Cells were then rinsed in tap water and stained with Coomassie Blue solution for 30 minutes. Cells were rinsed with tap water to remove excess dye, dried overnight, and imaged using an iPhone 5S.

2.2.5. Ex vivo virion quantification of infected mouse tumours

Tumours were resected, weighed, and flash frozen in dry ice. Later, tumours were mechanically lysed using a TissueLyser II (Qiagen), in PBS supplemented with cOmplete protease inhibitor cocktail (Roche), using glass beads. Cell debris was removed via centrifugation, and supernatant serially diluted for plaque assay as described above. Titers are reported in PFU/mg of tumour to correct for tumour mass.

2.2.6. Ex vivo infection of patient tumours

Fresh patient tumour biopsies were cut into 2 x 2 x 2 cm cores using a biopsy punch and scalpel. Each tumour core placed into individual wells of 24-well plate with DMEM supplemented with 10% FBS, 100 U/mL penicillin, 100 µg/mL streptomycin, 10 µg/mL gentamicin sulfate, and 20 mM HEPES. Cores were infected in quadruplicate with MOI 100, 30, 3, 1, or 0.1 of VSVΔ51-YFP (assuming ~$1*10^6$ cells per core) or uninfected control. Concurrently, 3-4 tumour cores were analyzed by alamarBlue Assay (ThermoFisher) as per manufacturer's protocol to assess biopsy viability. Tumours were infected for 48 hours prior to imaging YFP reporter from the virus using EVOS Imaging System (ThermoFisher). Virus infection was quantified by quantifying percentage of tumour area that is YFP^+, using ImageJ (in a blinded fashion). The only exclusion criterion for a tumour biopsy sample was lack of viability based on alamarBlue results; otherwise, all collected biopsies were included in the analysis.

2.3. Protein analysis

2.3.1. Flow cytometry and FACS

Cells were briefly trypsinized, washed and resuspended in PBS for staining. The cell suspension was stained with Zombie NIR Fixable Viability Dye or Zombie Aqua Fixable Viability Dye (BioLegend) for 10 minutes on ice to label dead cells, followed by incubation with rat anti-mouse CD16/CD32 (clone 2.4G2, BD Biosciences) for 10 minutes on ice. Cells were then washed and incubated with fluorescently-labeled antibodies for 20 minutes on ice. Cells were washed and resuspended in PBS and analyzed using an LSRFortessa (BD Biosciences) or Celesta (BD Biosciences), or isolated using MoFlo XDP (Beckman Coulter) or MA900 (SONY). Data were analyzed using FlowJo (Tree Star Inc.).

For experiments with murine cells, the following antibodies were used: BV421-anti-PD-L1 (BD, clone MIH5 or clone 10F.9G2), PE-Cy5-anti-CD80 (BioLegend, clone 16-10A1), PE-Cy7-anti-PD-1 (BioLegend, clone 29F.1A12), PE-anti-LDLR (R&D Systems, clone 263123). For experiments with human cells, the following antibodies were used: BV421-anti-PD-L1 (BD, clone MIH1), PE-Cy5-anti-CD80 (BioLegend, clone 2D10), PE-Cy7-anti-PD-1 (BD, clone EH12.1).

2.3.2. ELISA

IFN-β was analyzed in culture supernatant following VSVΔ51-YFP/VSV WT infection or transfection with poly(I:C) (Invivogen), using Mouse IFN-β Quantikine ELISA Kit (R&D Systems), as per manufacturer's instructions.

2.3.3. Western blotting

Following infection or treatment with recombinant murine IFN-β (PBL Assay Sciences), cells were lysed in RIPA (0.05% SDS, 1% Triton X-100, 1% NP-40, 50 mM Tris-HCl pH 7.5, 150 mM NaCl, 2 mM EDTA pH 8.0, 12 mM sodium deoxycholate) supplemented with cOmplete protease inhibitor cocktail (Roche) and PhosSTOP phosphatase inhibitor cocktail (Roche). Protein concentration was quantified by BCA Assay using MicroBCA Protein Assay Kit (ThermoFisher), and samples were denatured in Laemmli buffer (Bio-Rad) supplemented with 5% β-mercaptoethanol. Proteins were separated on 8-12% polyacrylamide (acrylamide/bis-acrylamide 37.5:1, Bio-Rad) gels at 60 mA, and then transferred to a PVDF membrane for 90 minutes at 100V. Membranes were probed with the following primary antibodies diluted in 5% w/v BSA in 1X TBS + 0.1% Tween20: anti-pIRF3 S396, anti-IRF3, anti-pTBK1 S172, anti-TBK1, anti-pSTAT1 Y701, anti-STAT1,

anti-pSTAT3 Y705, anti-STAT3, anti-PD-L1, anti-HIF-1α, anti-HIF-1β, anti-FIH, anti-PHD2, anti-p-p70 S6K T389, anti-S6K, anti-p4E-BP1 T37/46, anti-4E-BP1, anti-pAkt S473, anti-Akt, and anti-β-actin. All antibodies were purchased from Cell Signaling Technologies, with the exception of anti-PD-L1 which was purchased from Abcam. Membranes were further probed with appropriate species-specific HRP-conjugated secondary antibodies (purchased from Cell Signaling Technologies), developed using ECL reagent (Bio-Rad) and X-ray film.

2.3.4. Type I interferon reporter assay

Cell culture supernatant (100-200 µL) was isolated from cultured cells and placed on adherent L929-ISRE cells (mouse fibroblast cell line expressing luciferase under the control of a type I interferon-sensitive ISRE promoter) in a 96-well plate for 4-6 hours. Luciferase expression was assessed using Luciferase Assay System (Promega) and luminescence measured on a plate reader (BioTek).

2.3.5. Immunohistochemistry

Fresh patient tumour biopsies were fixed in 10% neutral-buffered formalin for 24 hours prior to paraffin-embedding and sectioning. Sections were rehydrated using xylene and ethanol and subjected to heat-induced antigen retrieval using 10 mM citrate buffer (pH 6.0) in a pressure cooker for 10 minutes. Sections were blocked in 10% normal goat serum (BioLynx) and incubated with anti-PD-L1 (clone 28-8, Abcam) overnight at 4˚C. Endogenous peroxidase activity was quenched using 3% hydrogen peroxide and sections were incubated with HRP-conjugated goat anti-rabbit (Cell Signaling Technologies) for 1 hour at room temperature. Detection was performed using DAB Substrate (Vector

Laboratories), followed by hematoxylin counterstaining. Sections were dehydrated and stabilized with mounting medium (ThermoFisher). PD-L1 expression was scored by a blinded trained pathologist (Dr. Saleh Fadel). The percentage of tumour cells that stained with the PD-L1 antibody was estimated on each slide. The average intensity of staining was scored as 0 (no staining), 1+ (weak intensity), 2+ (moderate intensity), and 3+ (strong intensity). The cellular compartment with positive staining was noted; this included nuclear, cytoplasmic, or membranous. Inflammatory cells were examined for positive staining as well, and the percentage of necrotic cells was quantified.

2.3.6. Signosis Plate Array

Nuclear extracts were isolated from mock-infected TRAMP-C2 and TRAMP-C2-*Cd274*$^{-/-}$ cells and those same cells infected with VSVΔ51-YFP at MOI 0.1 for 12 hours, with the nuclear extraction performed as per manufacturer's protocol (Signosis, SK-0001). Nuclear protein extracts (10 µg measured by Bradford assay) were used for Transcription Factor Activation Profiling Plate Array I (Signosis, FA-1001) as per manufacturer's protocol.

2.3.7. HIF reporter assay

TRAMP-C2 cells were transiently transfected with 10 µg of HRE-luciferase (a gift from Navdeep Chandel, Addgene plasmid 26731) or pGL2 (Addgene) using Lipofectamine 3000 as per manufacturer's instructions. Cells were cultured for 24 hours in normoxic conditions, and subsequently transferred to the hypoxia chamber for 24 hours. Cells were lysed with Passive Lysis Buffer (Promega), and luminescence measured using the Luciferase Assay System (Promega) on a plate reader (BioTek).

2.3.8. Immunocytochemistry

Cells were plated and cultured on coverslips prior to staining. Cells were fixed with 4% paraformaldehyde for 10 minutes at room temperature. The fixative was washed out 5X with PBS, and cells were permeabilized with 0.3% Triton X-100 diluted in PBS for 10 minutes at room temperature. Detergent was washed out 3-5X with PBS, and coverslips were blocked with 5% v/v of donkey or goat serum in PBS for 1 hour at room temperature. The blocking agent was washed out with PBS, and coverslips were incubated with diluted rabbit anti-TOM20 (PTGLabs) primary antibody (in PBS with blocking agent) for 1-2 hours at room temperature. Antibody was washed 5X with PBS, and coverslips were incubated with AF488-conjugated goat anti-rabbit antibody (ThermoFisher, diluted in PBS with blocking agent) for 1 hour at room temperature, protected from light. Antibody was washed 5X with PBS, and coverslips were mounted using Prolong Gold Antifade Reagent with DAPI (ThermoFisher) and sealed with nail polish. Slides were imaged using ZEISS AxioScan (ZEISS).

2.4. RNA expression analysis

2.4.1. RNA isolation, cDNA synthesis, and qPCR

RNA was isolated using GenElute RNA Miniprep Kit (Sigma) as per manufacturer's protocol. cDNA was synthesized using iScript Reverse Transcription Supermix (Bio-Rad), containing a mix of oligo(dT) primers and random primers, as per manufacturer's protocol. qPCR was run using iTaq Universal SYBR Green Supermix (Bio-Rad), using primers listed in Table 2.1. qPCR data was normalized to murine *Gapdh* gene or human *18S* gene using the $2^{-\Delta\Delta Ct}$ method.

2.4.2. RNA-seq sample preparation

RNA (3 biological replicates per condition) was collected as described above from mock-infected TRAMP-C2 cells and TRAMP-C2-*Cd274*$^{-/-}$ or those same cells infected with VSVΔ51-YFP at MOI 0.1 for 8 hours.

2.4.3. RNA-seq library preparation and sequencing

Total RNA was quantified using a NanoDrop Spectrophotometer ND-1000 (NanoDrop Technologies, Inc.) and its integrity was assessed on a 2100 Bioanalyzer (Agilent Technologies). Libraries were generated from 250 ng of total RNA as follows: mRNA enrichment was performed using the NEBNext Poly(A) Magnetic Isolation Module (New England BioLabs). cDNA synthesis was performed using the NEBNext RNA First Strand Synthesis and NEBNext Ultra Directional RNA Second Strand Synthesis Modules (New England BioLabs). The remaining steps of library preparation were done using the NEBNext Ultra II DNA Library Prep Kit for Illumina (New England BioLabs). Adapters and PCR primers were purchased from New England BioLabs. Libraries were quantified using the Quant-iT™ PicoGreen® dsDNA Assay Kit (Life Technologies) and the Kapa Illumina GA with Revised Primers-SYBR Fast Universal kit (Kapa Biosystems). Average size fragment was determined using a LabChip GX (PerkinElmer) instrument. Libraries were then sequenced on a NovaSeq6000 S4 200 cycle (2 x 100bp) flow cell to an approximate depth of 30M reads per sample.

2.4.4. RNA-seq processing and differential expression

Transcript quantification for each sample was performed using Kallisto (v0.45.0) (*237*) with the GRCm38 transcriptome reference and the -b 50 bootstrap option. The R package

Sleuth (v0.30.0) (*238*) was then used to construct general linear models for the log-transformed expression of each gene across experimental conditions. Wald's test was used to test for differential expression between groups and the resultant *p*-values were adjusted to *q*-values using the Benjamini-Hochberg false discovery rate method.

2.4.5. Signalling inference and gene set scoring

Relative activities of 14 signalling pathways were inferred using the R package PROGENy (v.1.9.6) (*239*), which provides a prebuilt regression model for signalling activity based on consistently responsive genes. Single-sample gene set scoring was performed using the R package singscore (v1.17.) (*240*), which computes independent scores for each sample from rank-based statics for each gene in the set.

2.5. Metabolic analyses

2.5.1. MitoTracker/MitoSOX

TRAMP-C2 cells were briefly trypsinized and re-suspended in PBS. Cells were counted and 500,000 cells were stained with 500 nM MitoTracker Deep Red FM (ThermoFisher) and 10 µM MitoSOX Red Mitochondrial Superoxide Indicator (ThermoFisher) for 10 minutes at 37˚C. Dye was washed out with PBS and cells were analyzed by flow cytometry within 1 hour.

2.5.2. Mitochondrial DNA and nuclear DNA quantification

Mitochondrial DNA and nuclear DNA were isolated using organic solvent extraction-based protocol adapted from Guo *et al* (*241*). qPCR performed as described above using primers amplifying MT-ND1 (for mitochondrial DNA) and 18S rRNA (for nuclear DNA).

2.5.3. Seahorse extracellular flux analysis

TRAMP-C2 cells (20,000/well) were seeded into 96-well Seahorse plate one day prior to the Seahorse assay. On the day of the assay, cells were equilibrated for one hour in DMEM supplemented with 4 mM glutamine, 1 mM sodium pyruvate, 25 mM glucose, at pH 7.4. Oxygen consumption rate (OCR) and extracellular acidification rate (ECAR) were measured by monitoring dissolved oxygen and pH using the XF96 extracellular flux analyzer (Seahorse Bioscience) above the cell monolayer under basal conditions and following treatment with oligomycin (1 μM), FCCP (0.5 μM), and rotenone + antimycin A (1 μM each). Protein content of each well was measured by BCA Assay using MicroBCA Protein Assay Kit (ThermoFisher), to normalize OCR/ECAR data and correct for potential differences in cell numbers.

2.5.4. Glucose uptake

In vitro glucose uptake was measured following 10 minutes of uptake by 10,000 TRAMP-C2 cells using the Glucose Uptake-Glo Assay kit (Promega), as per manufacturer's instructions.

2.5.5. Metabolomic analysis

Levels of metabolites from TRAMP-C2 cell lysates and cell culture supernatant (corrected using culture media in the absence of cells) following 48 hours of culture were quantified by liquid chromatography mass spectrometry (LC-MS). Sample temperature was maintained on ice or dry ice where possible, and all solvents were MS grade and pre-equilibrated to -20°C.

Cell pellets and media/supernatant were collected to a pre-chilled 2 mL tube containing 6 washed ceramic beads (1.4 mm) and 230 µl of methanol:water (1:1). Samples were vortexed 10s and cell lysis was done by beating for 60 s at 2000 rpm (bead beating was done twice) after adding 220 µL of acetonitrile. Samples were then incubated with a 2:1 dichloromethane:water solution on ice for 10 minutes. The polar and non-polar phases were separated by centrifugation at 4000g for 10 minutes at 1°C. The upper polar phase was dried using a refrigerated CentriVap Vacuum Concentrator at -4°C (LabConco Corporation, Kansas City, MO). Samples were resuspended in water and run on an Agilent 6470A tandem quadruple mass spectrometer equipped with a 1290 Infinity II ultra-high-performance LC (Agilent Technologies) using the Metabolomics Dynamic MRM Database and Method (Agilent), which uses an ion-pairing reverse phase chromatography. This method was further optimized for phosphate-containing metabolites with the addition of 5 µM InfinityLab deactivator (Agilent) to mobile phases A and B, which requires decreasing the backflush acetonitrile to 90%. Multiple reaction monitoring (MRM) transitions were optimized using authentic standards and quality control samples. Metabolites were quantified by integrating the area under the curve of each compound using external standard calibration curves with Mass Hunter Quant (Agilent). No corrections for ion suppression or enhancement were performed, as such, uncorrected metabolite concentrations are presented.

2.5.6. Enzymatic measurement of L-lactate

L-lactate was quantified in culture supernatant using colorimetric assay (Abcam), as per manufacturer's protocol.

2.6. Bioinformatic analysis

2.6.1. Bioinformatic analyses of human cell line RNA-seq

Analysis of expression levels of *CD274* transcript and HALLMARK_GLYCOLYSIS gene module (*242*, *243*) in cell lines was performed using information from the RNA-Seq dataset E-MTAB-2706, which contains genome-wide transcriptome profiles of 675 cancer cell lines. Briefly, we downloaded the Reads Per Kilobase of transcript, per Million (RPKM) file containing all sequencing reads for each cell line, along with a file containing the gene names in various formats and a metadata file describing the samples. We then converted gene IDs in the expression matrix to gene symbols and removed duplicates and missing values. We next added sample names to the columns of the expression matrix, before leveraging the R-based package singscore (*240*) that allows for rank-based statistics to score a sample's gene expression profile according to the activities of genes provided by curated gene modules. We set a cut-off on each axis at the mean of each value plus two standard deviations.

2.6.2. Malignant cell PD-L1 expression and gene set activity

We analyzed a pre-existing collection of scRNA-seq data from 266 epithelial tumours (*244*). Automated annotation of cell types had been performed in conjunction with a copy number alteration inference to identify the malignant population of each data set. Only tumours with >200 malignant cells were retained in the cohort. Average PD-L1 expression (log-transformed counts per 10k transcripts) was calculated from this fraction. Gene set scores for the MSigDB Hallmark Hypoxia and Glycolysis gene sets were calculated for individual cells using the R package Ucell, which implements a rank-based signature scoring method based on the Mann-Whitney U statistic.

2.7. In vivo experiments

2.7.1. Mice and tumour injection

NCG mice (NOD-*Prkdc*^{em26Cd52}*Il2rg*^{em26Cd22}/NjuCrl, lacking functional T, B, and NK cells) were purchased from Charles River Laboratory and maintained at the University of Ottawa. For all experiments, male mice were used to match the male origin of injected prostate cancer cell lines (TRAMP-C2). To generate subcutaneous tumours, 1-2*10^6 cancer cells were resuspended in Matrigel (BD Biosciences) and injected in the left flank. Mice were monitored once weekly until palpable tumours were observed, following which tumour growth was assessed every 3 days.

2.7.2. In vivo VSVΔ51 infection and bioluminescence imaging

For in vivo treatments of NCG mice with VSVΔ51-firefly luciferase, subcutaneous TRAMP-C2 tumours were injected with 10^8 PFU of virus by intra-tumoural injection of 100 µL of a 10^9 PFU/mL solution in sterile PBS. Mice were injected when tumours reached 750 mm^3.

Twenty-four hours post-infection with VSVΔ51-firefly luciferase, tumour-bearing mice were subjected to IVIS imaging. Mice were injected intraperitoneally with D-luciferin (Perkin Elmer) at a dose of 150 mg/kg for 15 minutes prior to isoflurane anesthesia. Mice were imaged using an IVIS Spectrum (Perkin Elmer). Investigators were not blinded during imaging, but all mice were subjected to identical imaging conditions.

2.7.3. [^{18}F]-FDG PET

Tumour-bearing mice (tumour volume 750 mm^3, n = 5-6 per group) fasted 5-8 hours before the imaging session were anesthetized with 2% isoflurane and intravenously injected with [^{18}F]-FDG (5.98 ± 1.92 MBq) as a bolus over 30 sec via the lateral tail vein. Mice remained under isoflurane anesthesia in an induction chamber and body temperature was maintained with a heat lamp. Blood glucose measurements (mM) were taken via tail vein blood sampling before and after the PET scan using a MediSure Blood Glucose Monitoring System. Forty minutes after radiotracer delivery, mice were positioned in the PET scanner and a 10 min transmission scan was performed. A whole-body static scan was immediately acquired between 50-60 min using a Siemens DPET scanner. Emission data were corrected for attenuation and scatter, then reconstructed using the 3D-OSEM/MAP algorithm. Volumetric regions of interest (ROIs) were drawn conforming to tumour margins and quantified using a threshold of 25% of SUVmax (SUV_{25}) (*245*). Uptake values obtained in $Bq \cdot cc^{-1}$ were converted to SUV using the injected dose (Bq) and animal body weight (kg).

2.7.4. Study approvals

Mouse studies were reviewed and approved by Animal Care and Veterinary Services at the University of Ottawa in accordance with the guidelines of the Canadian Council on Animal Care. For human studies, informed and written consent in accordance with the Declaration of Helsinki was obtained from all patients, and approval was obtained from The Ottawa Hospital (REB 20180221-02H).

2.8. Reproducibility and Statistical Analyses

All in vitro experiments were repeated at least 3 times, unless otherwise stated. Mouse studies were performed twice, unless otherwise stated.

Statistical analyses were performed using GraphPad Prism (GraphPad). Experiments with two independent conditions were analysed by two-tailed unpaired Student's t test, one-way ANOVA to compare three or more conditions, and two-way ANOVA (with Sidak's correction for multiple comparisons) to compare groups influenced by two variables. Differences between experimental groups were considered significant when $p < 0.05$. In all figures, ns represents not significant ($p > 0.05$); * represents $p \leq 0.05$; ** represents $p \leq 0.01$; *** represents $p \leq 0.001$; **** represents $p \leq 0.0001$.

Table 2.1. Primers used in qPCR analyses.

Target	Primer Sequence	
VSV N	Forward	GAT AGT ACC GGA GGA TTG ACG ACT A
	Reverse	TCA AAC CAT CCG AGC CAT TC
Ifnb1	Forward	CGC TGC GTT CCT GCT GTG
	Reverse	GAT CTT GAA GTC CGC CCT GTA G
Mx1	Forward	GAC CAT AGG GGT CTT GAC CAA
	Reverse	AGA CTT GCT CTT TCT GAA AAG CC
Oas1b	Forward	TTC TAC GCC AAT CTC ATC AGT G
	Reverse	GGT CCC CCA GCT TCT CCT TAC
Eif2ak	Forward	ATG CAC GGA GTA GCC ATT ACG
	Reverse	TGA CAA TCC ACC TTG TTT TCG T
Isg15	Forward	TGA CGC AGA CTG TAG ACA CG
	Reverse	TGG GGC TTT AGG CCA TAC TC
Gapdh	Forward	CAT CAC CAT CTT CCA GGA GCG
	Reverse	GAG GGG CCA TCC ACA GTC TTC
MT-ND1	Forward	AACATACCCATGGCCAACCT
	Reverse	AGCGAAGGGTTGTAGTAGCCC
IFNB1	Forward	TCCAAATTGCTCTCCTGTTG
	Reverse	GCAGTATTCAAGCCTCCCAT
MX1	Forward	CTGCGAGGAGATCGGTTCTG
	Reverse	CTGCACCTCCTTGGAATGGT
18S	Forward	GTAACCCGTTGAACCCCATT
	Reverse	CCATCCAATCGGTAGTAGCG

Chapter 3

PD-L1 promotes oncolytic virus infection via inhibition of the type I interferon pathway.

3.1 Introduction and Rationale

Type I interferon cytokines are critical to the induction of effective anti-viral responses, as evidenced by the frequency of viral infections in individuals with loss-of-function mutations in molecules of the type I interferon pathway (*246–248*). Importantly, most OVs are sensitive to the anti-viral effects of type I interferons, and these cytokines are thought to control, in part, the specificity of OVs for cancer cells over healthy cells.

PD-L1 has been shown to modulate type I interferon responses in different contexts but, surprisingly, not in viral infections. The interplay between PD-L1, type I interferons, and OVs becomes particularly important considering the enthusiasm for combining oncolytic virotherapy with PD-L1 blockade in preclinical studies and clinical trials. The potential for synergy, or antagonism, between targeting PD-L1 and oncolytic viral infection should be investigated prior to clinical translation to favour rational combination of the two strategies.

Given that PD-L1 alters type I interferon responses, which are well-known to induce cellular anti-viral responses, we investigated the ability of PD-L1 to modulate OV infection in cancer cells. Additionally, we examined the ability of PD-L1 to alter type I interferon responses in cancer cells.

3.2 PD-L1 (*Cd274*) promotes oncolytic virus infection

The murine prostate cancer cell line TRAMP-C2 was used as a model for initial experiments. These cells express PD-L1 (Figure 3.1) and are widely used in preclinical studies of oncolytic viruses (*121*, *249*, *250*). To investigate PD-L1 function, CRISPR/Cas9-mediated recombination was used to delete PD-L1 expression from TRAMP-C2 cells (Figure 3.1). From here on, these PD-L1-deficient cells are referred to as TRAMP-C2 *Cd274*$^{-/-}$.

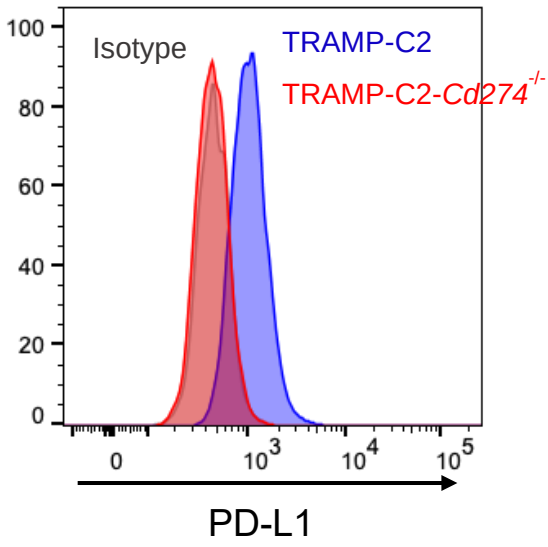
Isotype
TRAMP-C2
TRAMP-C2-Cd274-/-
100
80
60
40
20
0
0
10^3
10^4
10^5
PD-L1

Figure 3.1. TRAMP-C2 cells express PD-L1, which is absent following CRISPR-Cas9-mediated recombination. TRAMP-C2 cells (blue) were transfected with Cas9 and gRNA targeting PD-L1 to generate TRAMP-C2 *Cd274*$^{-/-}$ (red). A representative plot of flow cytometry analysis for PD-L1 is shown.

To assess whether PD-L1 expression impacts OV infection, parental and *Cd274*$^{-/-}$ TRAMP-C2 cells were infected with the oncolytic virus VSVΔ51, which is highly sensitive to the anti-viral effects of type I interferons. PD-L1 deletion resulted in a dramatic reduction of infection, which was tracked using the viral YFP reporter (Figure 3.2A) and by plaque assay (Figure 3.2B). Consistent with the differences in OV infection, PD-L1 deletion reduced virus-induced cell death (Figure 3.2C), as measured by staining infected cells with Coomassie dye.

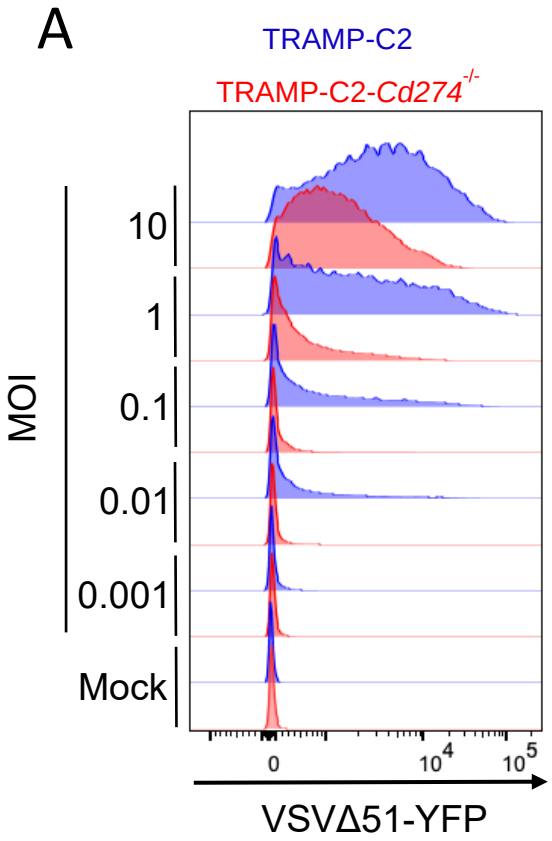
A
TRAMP-C2
TRAMP-C2-Cd274-/-
MOI
10
1
0.1
0.01
0.001
Mock
0
10^4
10^5
VSVΔ51-YFP

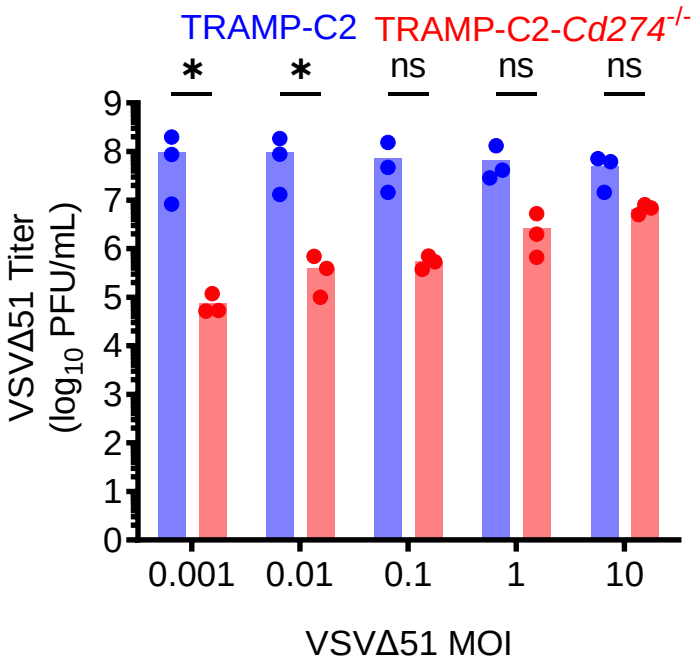
B
TRAMP-C2
TRAMP-C2-Cd274-/-
*
*
ns
ns
ns
VSVΔ51 Titer (log10 PFU/mL)
0
1
2
3
4
5
6
7
8
9
0.001
0.01
0.1
1
10
VSVΔ51 MOI

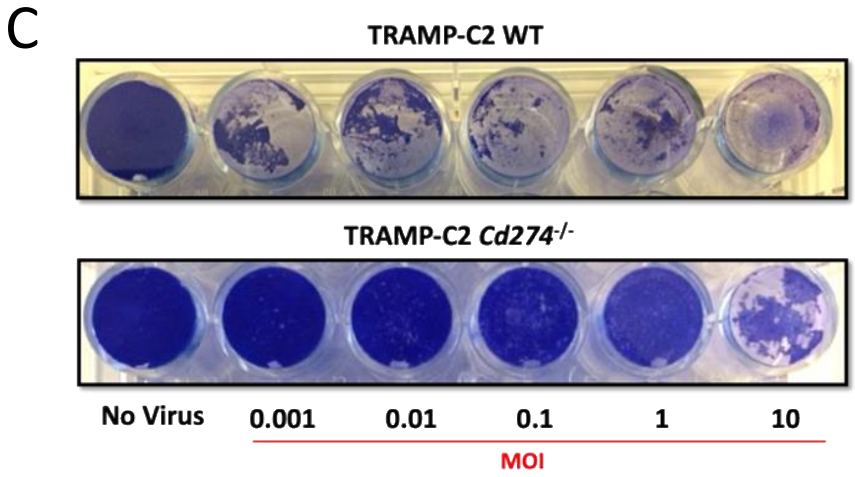
C
TRAMP-C2 WT
TRAMP-C2 Cd274-/-
No Virus
0.001
0.01
0.1
1
10
MOI

Figure 3.2. PD-L1 promotes VSVΔ51 infection and virus-induced cell death. TRAMP-C2 and TRAMP-C2 *Cd274*$^{-/-}$ cells were infected with VSVΔ51-YFP at indicated MOIs and subjected to flow cytometry to quantify the viral YFP reporter 24 hours post-infection (**A**), plaque assay to quantify viral titers 24 hours post-infection (**B**), or Coomassie staining to visualize cell death 48 hours post-infection (**C**). The data depicted are representative of 4 biological replicates performed with similar results, and N=3 biological replicates for the viral titer data. Statistical analysis by two-way ANOVA with Šídák's correction for multiple comparisons.

One potential mechanism by which PD-L1 could increase VSVΔ51 infection is by promoting entry of VSVΔ51 into cells. The viral N transcript was measured by qPCR to track viral replication in the cells during the first few hours of infection. This analysis revealed that there was no difference in viral transcript levels between parental and *Cd274*$^{-/-}$ TRAMP-C2 cells at 1 and 3 hours post-infection (Figure 3.3A), suggesting that VSVΔ51 can readily enter these cells regardless of PD-L1 expression. Furthermore, parental and *Cd274*$^{-/-}$ TRAMP-C2 cells express equal amounts of the VSV entry receptor LDL-R (Figure 3.3B), indicating that differences in viral receptor expression are not driving the differences in infection. At 8 hours post-infection and onwards, there was significantly less viral replication in TRAMP-C2 *Cd274*$^{-/-}$ cells compared to parental TRAMP-C2 (Figure 3.3A), consistent with the infection data in Figure 3.2.

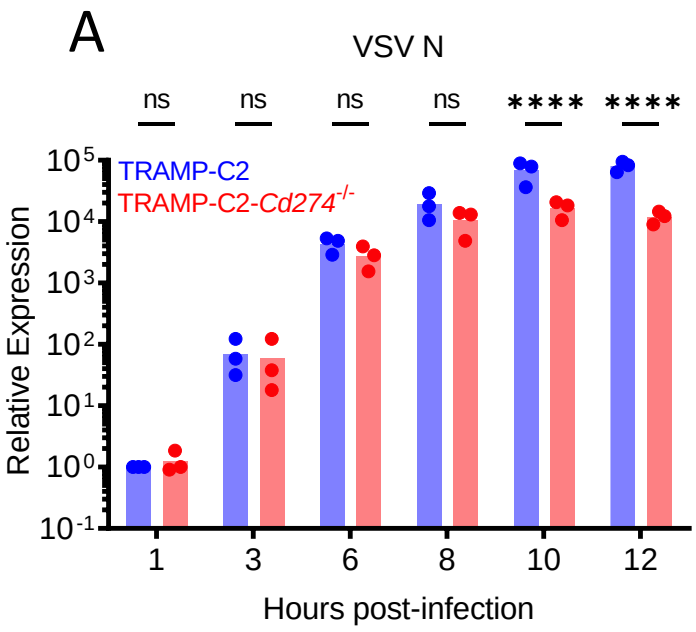
A
VSV N
ns
ns
ns
ns
****
****
TRAMP-C2
TRAMP-C2-Cd274-/-
Relative Expression
Hours post-infection
1
3
6
8
10
12

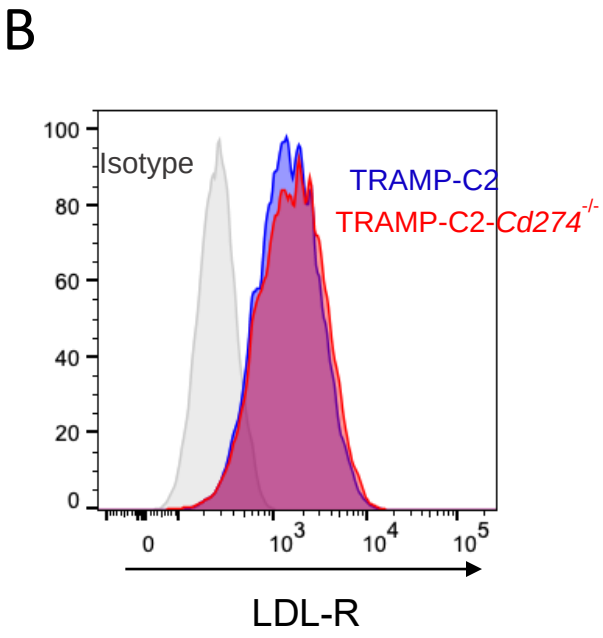
B
Isotype
TRAMP-C2
TRAMP-C2-Cd274-/-
LDL-R

Figure 3.3. PD-L1 does not regulate VSVΔ51 entry into TRAMP-C2 cells. (**A**) TRAMP-C2 and TRAMP-C2-*Cd274*$^{-/-}$ were infected with VSVΔ51-YFP at MOI 0.1, and RNA collected at indicated times post-infection for qPCR analysis of the viral nucleoprotein (N) transcript. N=3 biological replicates plotted. Statistical analysis by two-way ANOVA with Šídák's correction for multiple comparisons. (**B**) Expression of the VSV entry receptor LDL-R in TRAMP-C2 (blue) or TRAMP-C2-*Cd274*$^{-/-}$ (red) cells. Representative flow cytometry histograms are shown.

To confirm that PD-L1 deletion, and not an experimental artifact, resulted in differences in OV infection, PD-L1 expression (or an empty vector as a control) was restored in TRAMP-C2 *Cd274*$^{-/-}$ cells using retroviral methods (Figure 3.4A). Re-expression of PD-L1 in TRAMP-C2 *Cd274*$^{-/-}$ cells dramatically enhanced VSVΔ51 infection compared to the empty vector control (Figure 3.4B-C), confirming that PD-L1 is the cause of the observed viral phenotype, and not any off-target effects induced by the CRISPR-Cas9-mediated deletion.

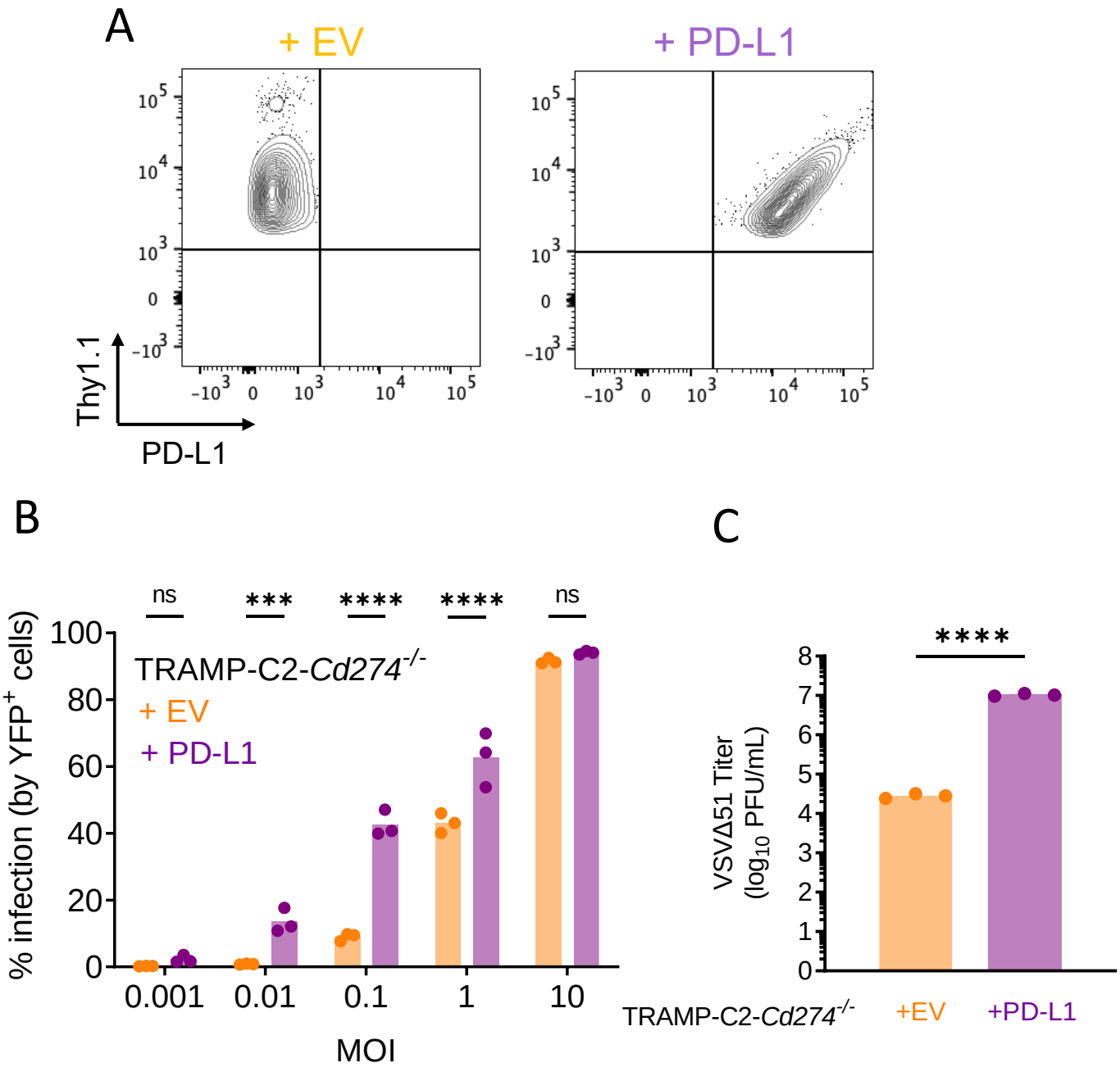
A
+ EV
+ PD-L1
Thy1.1
PD-L1
B
ns
***
****
****
ns
TRAMP-C2-Cd274-/-
+ EV
+ PD-L1
% infection (by YFP+ cells)
MOI
0.001
0.01
0.1
1
10
C
****
VSVΔ51 Titer
(log10 PFU/mL)
TRAMP-C2-Cd274-/-
+EV
+PD-L1

Figure 3.4. Restoration of PD-L1 expression in TRAMP-C2-*Cd274*$^{-/-}$ cells rescues phenotype. (A) Representative flow cytometry staining for PD-L1 and Thy1.1 following transduction of TRAMP-C2-*Cd274*$^{-/-}$ cells with empty vector (EV) or PD-L1-encoding vector. (**B-C**) TRAMP-C2-*Cd274*$^{-/-}$ transduced with PD-L1 or empty vector were infected with VSVΔ51-YFP at indicated MOIs for 24 hours and analyzed by flow cytometry (**B**), or by plaque assay (**C**). The data depicted are representative of 3 biological replicates performed with similar results. Statistical analysis by two-way ANOVA with Šídák's correction for multiple comparisons in B and two-tailed unpaired Student's t test in C.

There are multiple OV platforms today, many with distinct life cycles and host-virus interactions compared with VSVΔ51. To investigate if PD-L1 can promote infection of OVs besides VSVΔ51, we infected TRAMP-C2 cells with vaccinia virus, a more complex oncolytic DNA virus currently in clinical testing (*251*), TRAMP-C2 cells were better infected with vaccinia virus compared to TRAMP-C2 *Cd274*$^{-/-}$ (Figure 3.5), suggesting that the ability of PD-L1 to enhance OV infection is generalizable to other viral platforms.

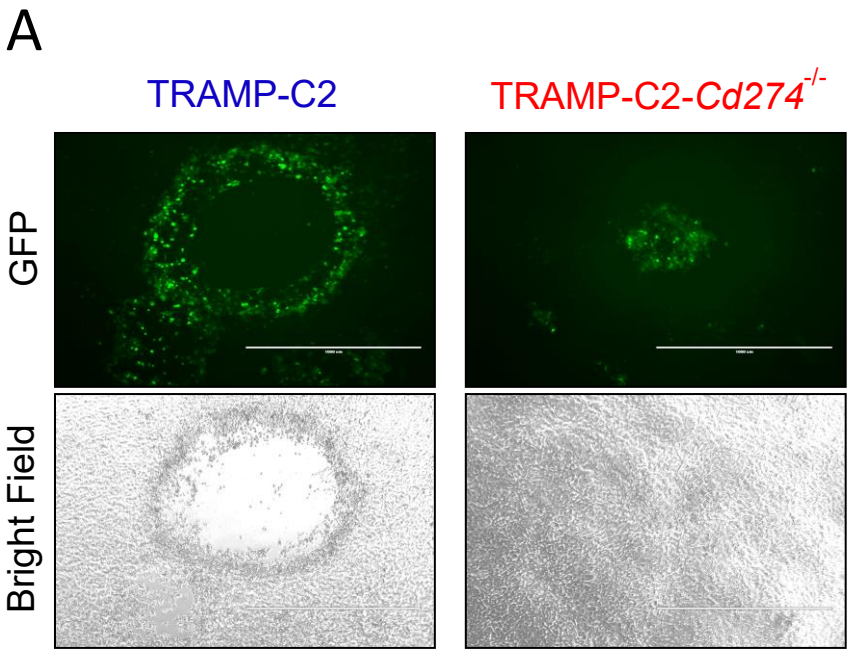
A
TRAMP-C2
TRAMP-C2-Cd274-/-
GFP
Bright Field

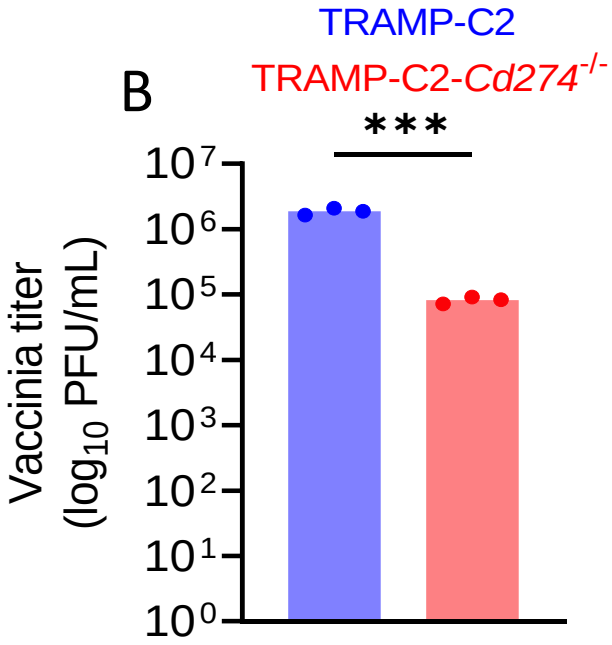
TRAMP-C2
TRAMP-C2-Cd274-/-
B
***
Vaccinia titer
(log10 PFU/mL)
10^7
10^6
10^5
10^4
10^3
10^2
10^1
10^0

Figure 3.5. PD-L1 promotes vaccinia virus infection. (**A**) TRAMP-C2 cells were infected with GFP-expressing vaccinia virus (Copenhagen strain) at MOI 0.1 for 48 hours, prior to fluorescence imaging. Representative of 2 experiments performed with similar results. (**B**) TRAMP-C2 cells were infected with GFP-expressing vaccinia virus (Copenhagen strain) at MOI 0.1 for 48 hours. Viral titer was assessed by plaque assay. The data depicted are representative of 3 biological replicates performed with similar results. Statistical analysis by two-tailed unpaired Student's t-test.

3.3 PD-L1 inhibits the type I interferon response

Given the link between PD-L1 and modulation of the type I interferon responses, and the importance of type I interferons for cellular anti-viral immunity and OV infection, we hypothesized that the PD-L1-mediated differences in OV infection stemmed from regulation of type I interferon responses by PD-L1.

To test this hypothesis, the production of type I interferon cytokines after OV infection was assessed. TRAMP-C2 *Cd274*$^{-/-}$ cells had 2-fold greater production of IFN-β compared to parental TRAMP-C2 cells (Figure 3.6A), suggesting that PD-L1 inhibits the production of type I interferon cytokines. Further, the difference in IFN-β production was closely mirrored at the transcriptional level (Figure 3.6B), suggesting that PD-L1 regulates type I interferon production at the transcriptional level. As expected, restoration of PD-L1 expression in TRAMP-C2 *Cd274*$^{-/-}$ cells dramatically inhibited IFN-β transcript levels compared to the empty vector control (Figure 3.6C). Importantly, these experiments were conducted at time points post-infection when there are approximately equal amounts of virus replication between the cells with and without PD-L1 (Figures 3.3A and 3.6D), to ensure that there is equal stimulus of the type I interferon pathway.

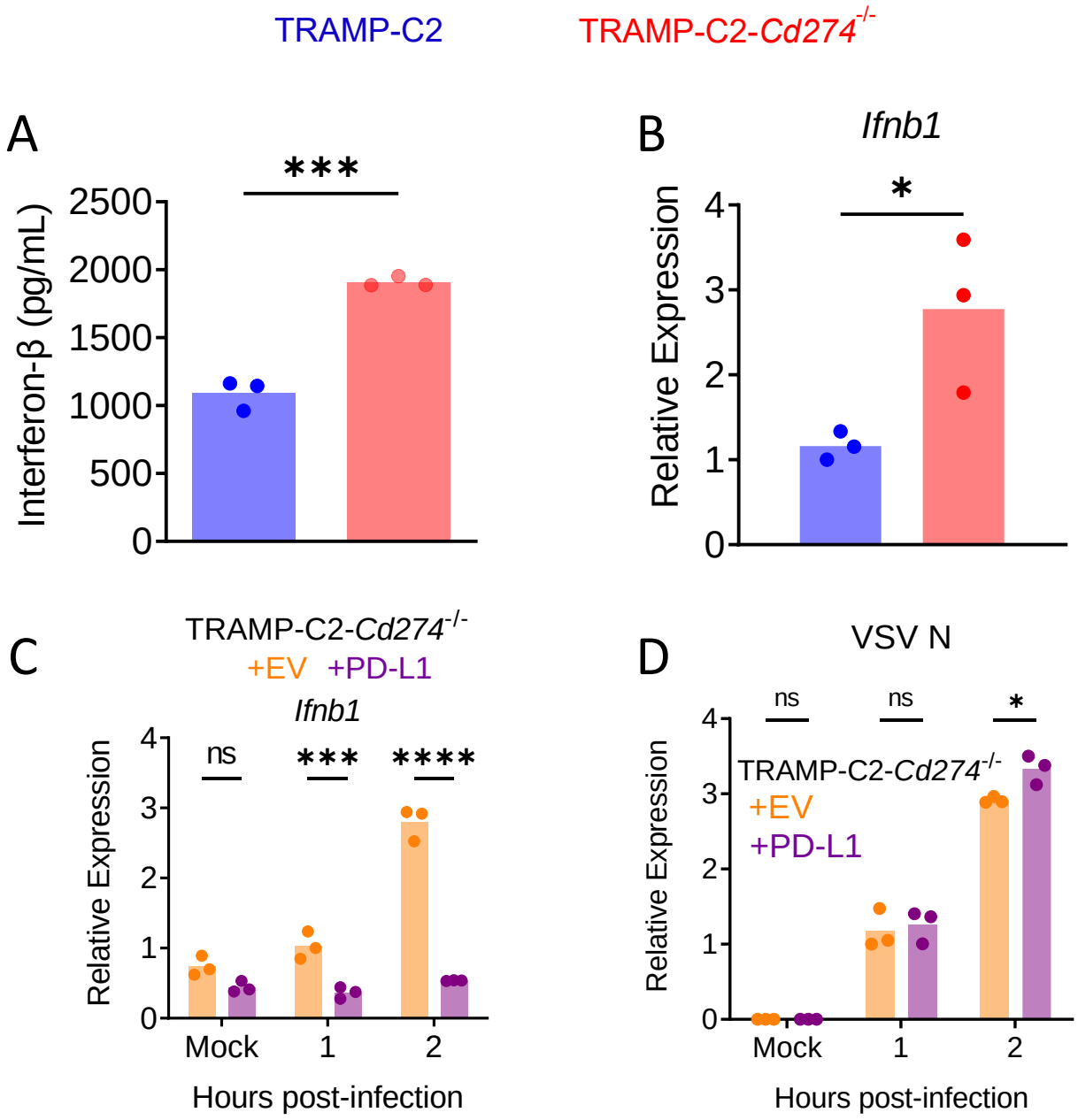
TRAMP-C2
TRAMP-C2-Cd274-/-
A
***
Interferon-β (pg/mL)
2500
2000
1500
1000
500
0
B
Ifnb1
*
Relative Expression
4
3
2
1
0
C
TRAMP-C2-Cd274-/-
+EV +PD-L1
Ifnb1
ns
***
****
Relative Expression
Mock
1
2
Hours post-infection
D
VSV N
ns
ns
*
TRAMP-C2-Cd274-/-
+EV
+PD-L1
Relative Expression
Mock
1
2
Hours post-infection

Figure 3.6. PD-L1 inhibits virus-induced production of type I interferon. (**A-B**) IFN-β protein in culture supernatant (by ELISA, **A**) or transcript levels (by qPCR, **B**) were quantified following infection with VSVΔ51-YFP for 8 hours. The data depicted are representative of 3 biological replicates performed with similar results. Statistical analysis with two-tailed unpaired Student's t-test. (**C-D**) TRAMP-C2 *Cd274*$^{-/-}$ transduced with PD-L1 or empty vector (EV) were infected with VSVΔ51-YFP at MOI 0.1 and analyzed by qPCR at indicated times post-infection to quantify *Ifnb1* (**C**) and VSV N (**D**) transcripts. The data depicted are representative of 3 biological replicates performed with similar results. Statistical analysis by two-way ANOVA with Šídák's correction for multiple comparisons.

Type I interferons execute anti-viral responses via expression of hundreds of interferon-stimulated genes (ISGs), which act by diverse mechanisms to restrict viral infection. Consistent with the difference in type I interferons, TRAMP-C2 *Cd274*$^{-/-}$ cells had greater expression of ISGs post-infection compared to parental TRAMP-C2 cells (Figure 3.7A). We next asked if the effects of PD-L1 on the type I interferon pathway are limited to VSVΔ51 as the trigger for activation of the anti-viral response, or if it can act on the type I interferon pathway downstream of different stimuli. Parental TRAMP-C2 and TRAMP-C2 *Cd274*$^{-/-}$ cells were transfected with the double-stranded RNA molecule poly(I:C), which is widely used as a viral mimic and is an agonist of the PRR RIG-I. In line with the virus data, TRAMP-C2 *Cd274*$^{-/-}$ cells had greater expression of IFN-β and ISGs compared to parental TRAMP-C2 after poly(I:C) transfection (Figure 3.7B-C).

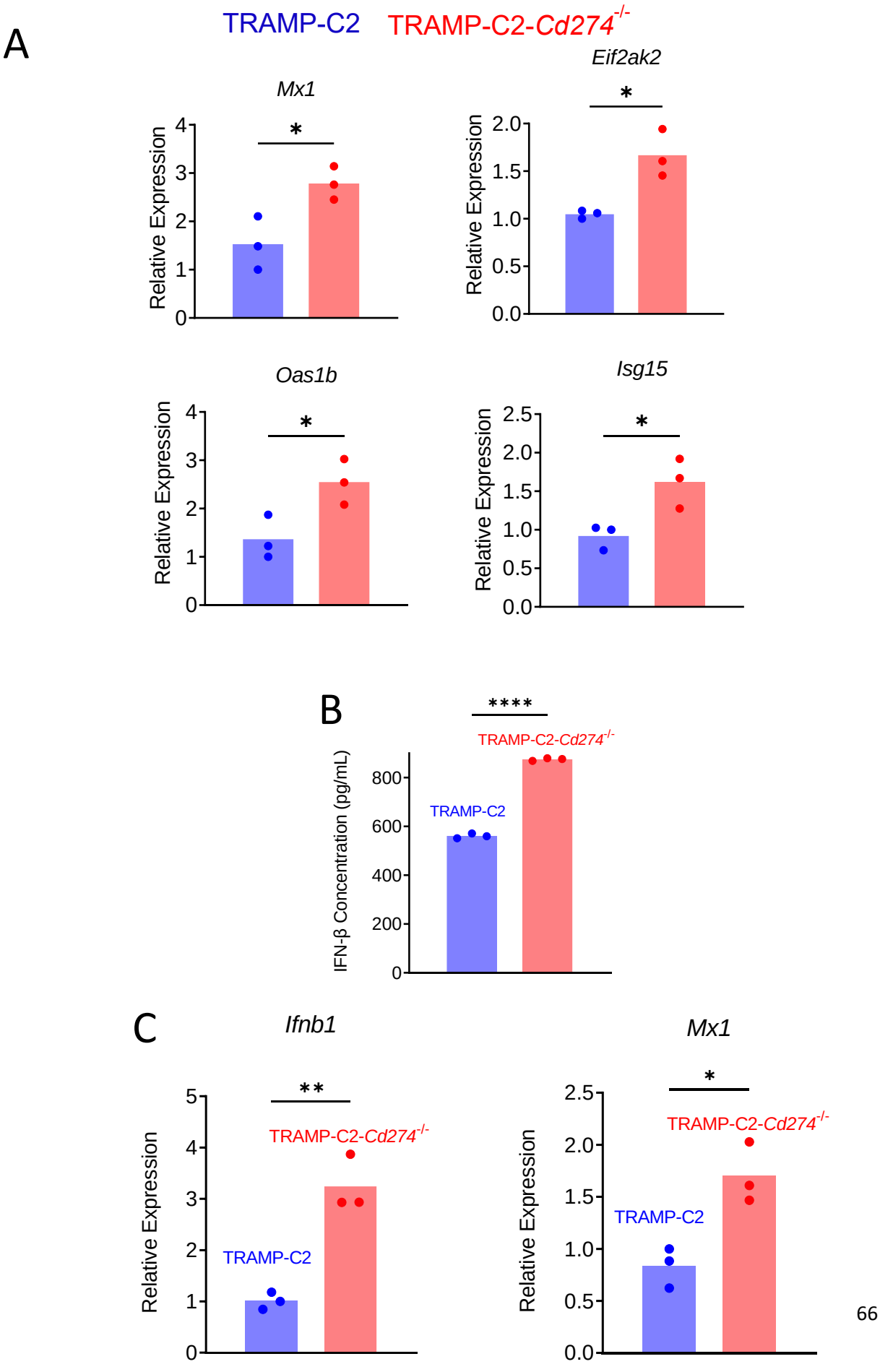
A
TRAMP-C2
TRAMP-C2-Cd274-/-
Mx1
Eif2ak2
Oas1b
Isg15
Relative Expression
B
IFN-β Concentration (pg/mL)
TRAMP-C2
TRAMP-C2-Cd274-/-
C
Ifnb1
Mx1

Figure 3.7. PD-L1 inhibits the type I interferon response induced by VSVΔ51 and poly(I:C). (**A**) Expression of ISGs was quantified following infection with VSVΔ51-YFP for 8 hours. Statistical analysis with two-tailed unpaired Student's t-test. (**B and C**) Cells were transfected with 1 μg of poly(I:C) for 8 hours prior to quantification of IFN-β (by ELISA, **B**) and IFN-β and MX1 transcripts (by qPCR, **C**). The experiments depicted are representative of 3 biological replicates performed with similar results. Statistical analysis by two-tailed unpaired Student's t-test.

Lastly, we asked if PD-L1 modulates signaling downstream of the type I interferon receptor, in addition to its ability to alter type I interferon cytokine production. To test this, TRAMP-C2 and TRAMP-C2 *Cd274*$^{-/-}$ cells were acutely treated with recombinant IFN-β and the phosphorylation and expression of key molecules involved in type I interferon signaling was analyzed. Interestingly, PD-L1 decreases the overall levels of the transcription factor STAT1, which is a key molecule (and ISG) involved in the transcriptional response induced by type I interferons (Figure 3.8A); additionally, PD-L1 promoted the phosphorylation of the transcription factor STAT3 at Tyr705 (Figure 3.8A). When PD-L1 was re-expressed in TRAMP-C2 *Cd274*$^{-/-}$ cells, PD-L1 similarly decreased STAT1 levels and promoted STAT3 phosphorylation at Tyr705, along with a dramatic decrease in TBK1 and IRF-3 phosphorylation at residues associated with their activation (Figure 3.8B). In all, this suggests that PD-L1 inhibits the type I interferon pathway in a two-pronged fashion: first, by inhibiting transcription and production of type I interferon cytokines, and secondly by modulating signaling downstream of the type I interferon receptor.

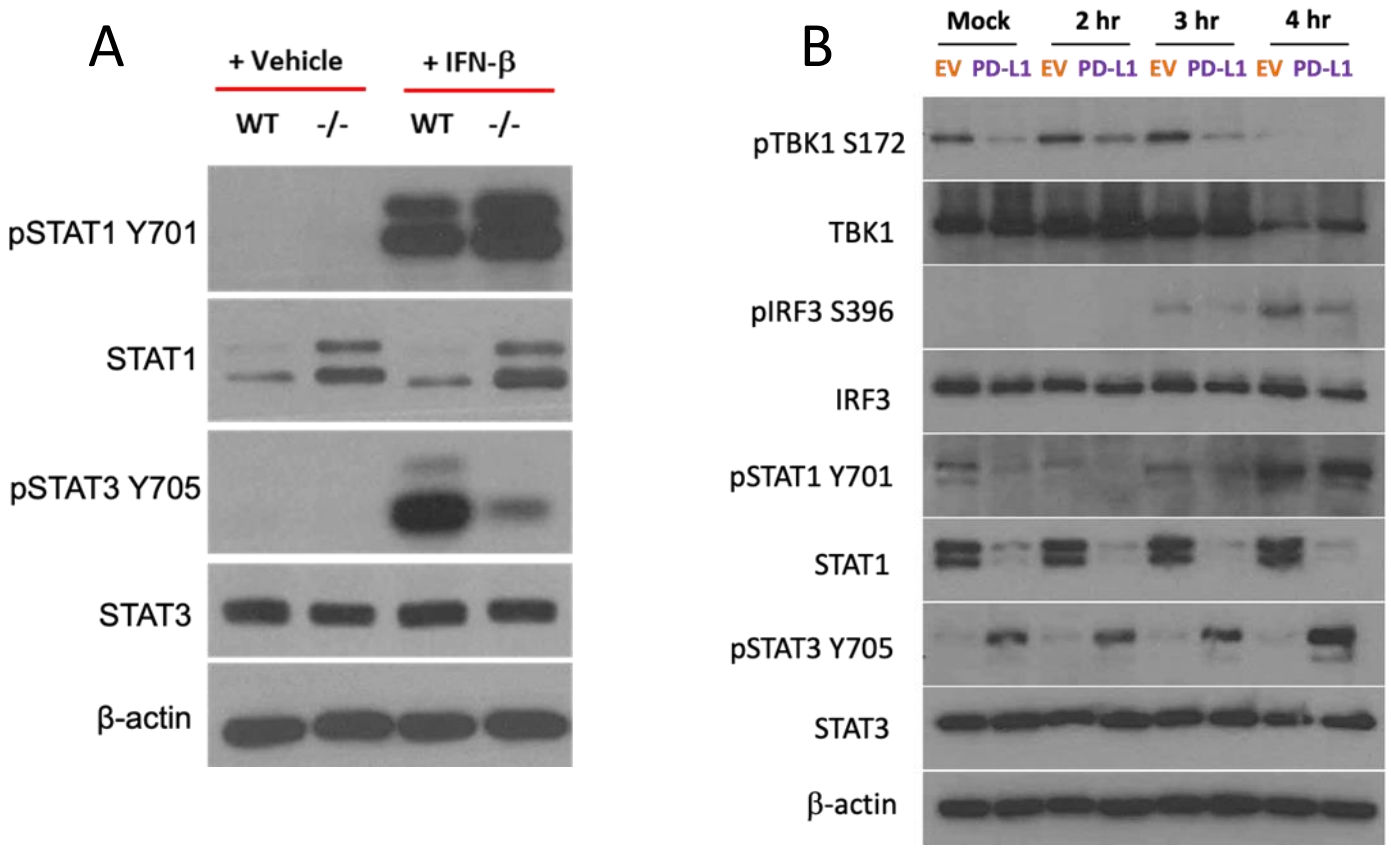
A
+ Vehicle
+ IFN-β
WT
-/-
WT
-/-
pSTAT1 Y701
STAT1
pSTAT3 Y705
STAT3
β-actin
B
Mock
2 hr
3 hr
4 hr
EV PD-L1 EV PD-L1 EV PD-L1 EV PD-L1
pTBK1 S172
TBK1
pIRF3 S396
IRF3
pSTAT1 Y701
STAT1
pSTAT3 Y705
STAT3
β-actin

Figure 3.8. PD-L1 inhibits type I interferon signaling. (**A**) TRAMP-C2 and TRAMP-C2 *Cd274*$^{-/-}$ cells were cultured in non-supplemented DMEM for 24 hours and treated with 200 units of recombinant murine IFN-β for 10 minutes prior to analysis by western blotting. The images depicted are representative of 3 performed with similar results. (**B)** TRAMP-C2 *Cd274*$^{-/-}$ cells transduced with PD-L1 or empty vector were infected with VSVΔ51-YFP at MOI 0.1 and analyzed by western blotting at indicated times post-infection. The experiments depicted are representative of 3 biological replicates performed with similar results.

To show that PD-L1 regulation of the type I interferon pathway results in its ability to promote viral infection, TRAMP-C2 and TRAMP-C2 *Cd274*$^{-/-}$ cells were pre-treated with a blocking antibody against a subunit of the type I interferon receptor (IFNAR1). Blockade of the type I interferon response with anti-IFNAR1 ablated all differences in VSVΔ51 infection between TRAMP-C2 and TRAMP-C2 *Cd274*$^{-/-}$ cells (Figure 3.9). Therefore, PD-L1 promotes viral infection by inhibiting the type I interferon response.

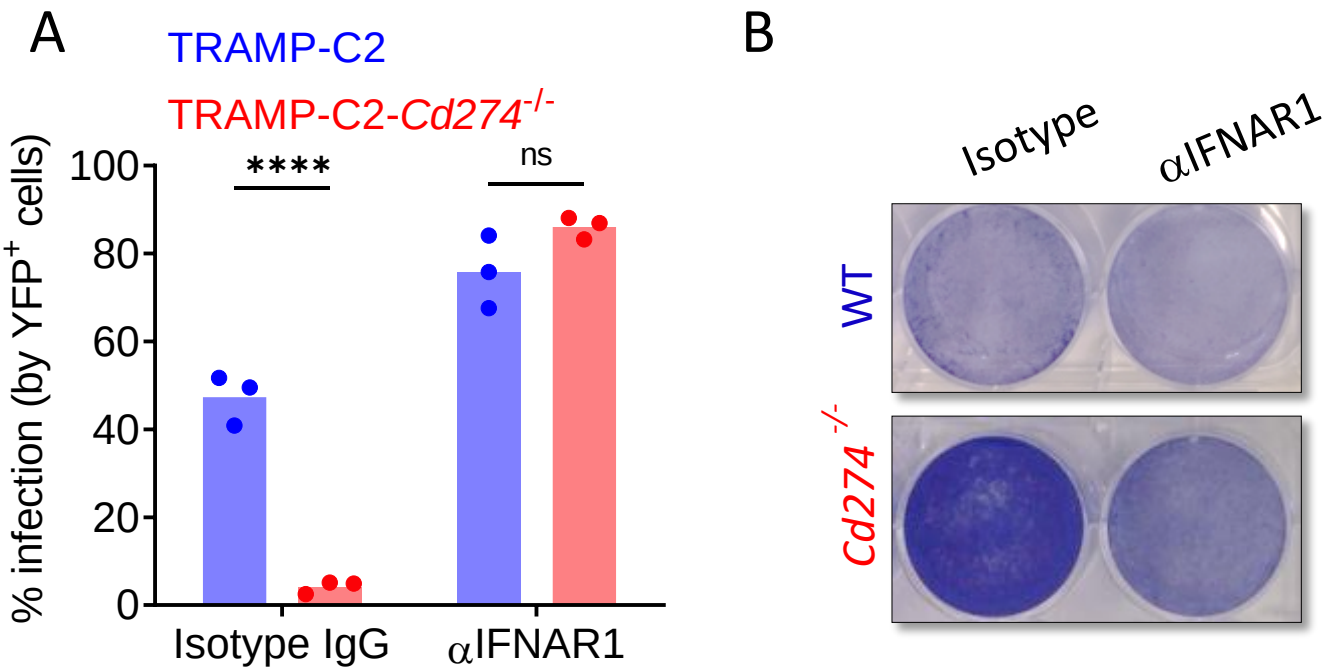
A
TRAMP-C2
TRAMP-C2-Cd274-/-
% infection (by YFP+ cells)
100
80
60
40
20
0
****
ns
Isotype IgG
αIFNAR1
B
Isotype
αIFNAR1
WT
Cd274-/-

Figure 3.9. PD-L1 promotes oncolytic virus infection via inhibition of the type I interferon pathway. (**A**) TRAMP-C2 and TRAMP-C2 *Cd274*$^{-/-}$ were pre-treated with 25 µg of anti-IFNAR1 for 24 hours, followed by infection with VSVΔ51-YFP at MOI 0.1 for 24 hours prior to analysis by flow cytometry (**A**) or Coomassie staining (**B**). The experiments depicted are representative of 3 biological replicates performed with similar results. Statistical analysis by two-way ANOVA with Šídák's correction for multiple comparisons.

3.4 PD-L1 inhibits the constitutive type I interferon response

Next, alternative methods were used to confirm the importance of the type I interferon response in the function of PD-L1. VSV WT has the intrinsic ability to block type I interferon production (in contrast with VSVΔ51, which no longer has this function due to its mutation). We hypothesized that PD-L1 should not enhance VSV WT infection due to the lack of type I interferons to act upon, in a similar fashion to the experiments blocking the type I interferon receptor in Figure 3.9. Surprisingly, PD-L1 still enhanced VSV WT infection in TRAMP-C2 cells (Figure 3.10A), contrary to our hypothesis. As expected, in VSV WT-infected TRAMP-C2 cells there was no production of type I interferon cytokine in the supernatant (Figure 3.10B).

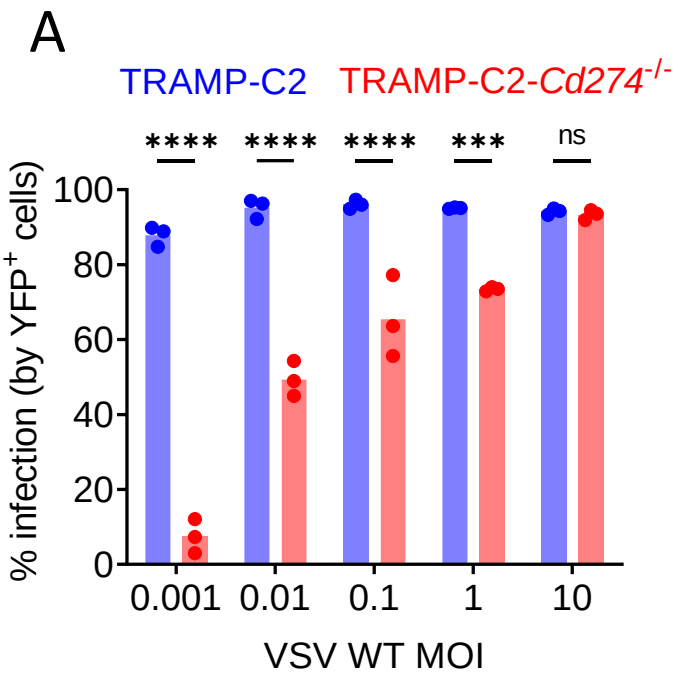
A
TRAMP-C2
TRAMP-C2-Cd274-/-
****
****
****
***
ns
% infection (by YFP+ cells)
100
80
60
40
20
0
0.001
0.01
0.1
1
10
VSV WT MOI

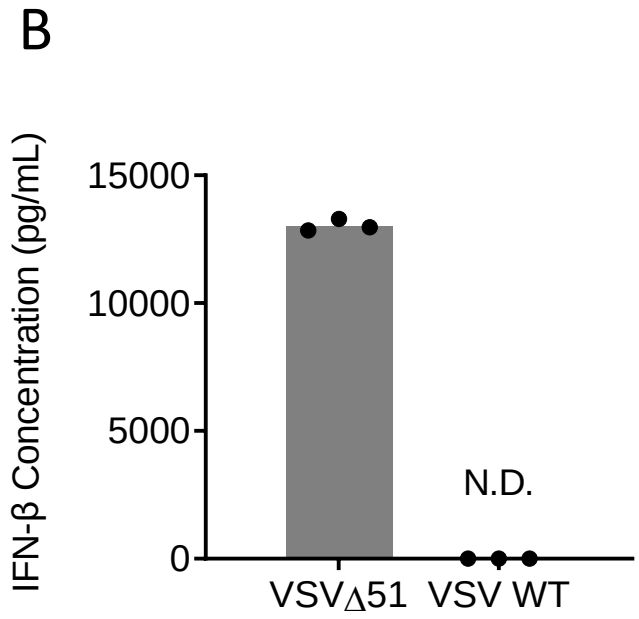
B
IFN-β Concentration (pg/mL)
15000
10000
5000
0
N.D.
VSVΔ51
VSV WT

Figure 3.10. PD-L1 promotes WT VSV infection. (**A**) TRAMP-C2 and TRAMP-C2 *Cd274*$^{-/-}$ cells were infected with VSV WT at indicated MOIs for 24 hours prior to analysis by plaque assay. The experiment depicted is representative of 3 performed with similar results. Statistical analysis by two-way ANOVA with Šídák's correction for multiple comparisons. (**B**). TRAMP-C2 cells were infected with VSVΔ51-YFP or VSV WT at MOI 0.1 for 12 hours prior to analysis by ELISA to quantify IFN-β in supernatant. The experiment depicted is representative of 2 biological replicates performed with similar results. N.D. = not detected.

To explain this puzzling result, we drew upon literature showing that cancer cells exhibit a constitutive/tonic type I interferon response (in the absence of any exogenous trigger), characterized by production of type I interferons and ISGs. Indeed, in the TRAMP-C2 cell line, there is expression of type I interferons and ISGs prior to infection (Figure 3.11). More importantly, PD-L1 inhibited constitutive type I interferon response, as we found lower expression (at the transcript level) in TRAMP-C2 versus TRAMP-C2 *Cd274*$^{-/-}$ cells (Figure 3.11). While IFN-β concentration was below the detection limit of ELISAs, biological activity of type I interferons was detected in uninfected TRAMP-C2 cells using a sensitive type I interferon luciferase reporter (Figure 3.12). Again, there was less biological activity of type I interferons in TRAMP-C2 versus TRAMP-C2 *Cd274*$^{-/-}$ cells (Figure 3.12), supporting the transcript analysis of type I interferons and ISGs. Therefore, during routine culture of TRAMP-C2 cells, there is an ongoing type I interferon response, which is inhibited by PD-L1.

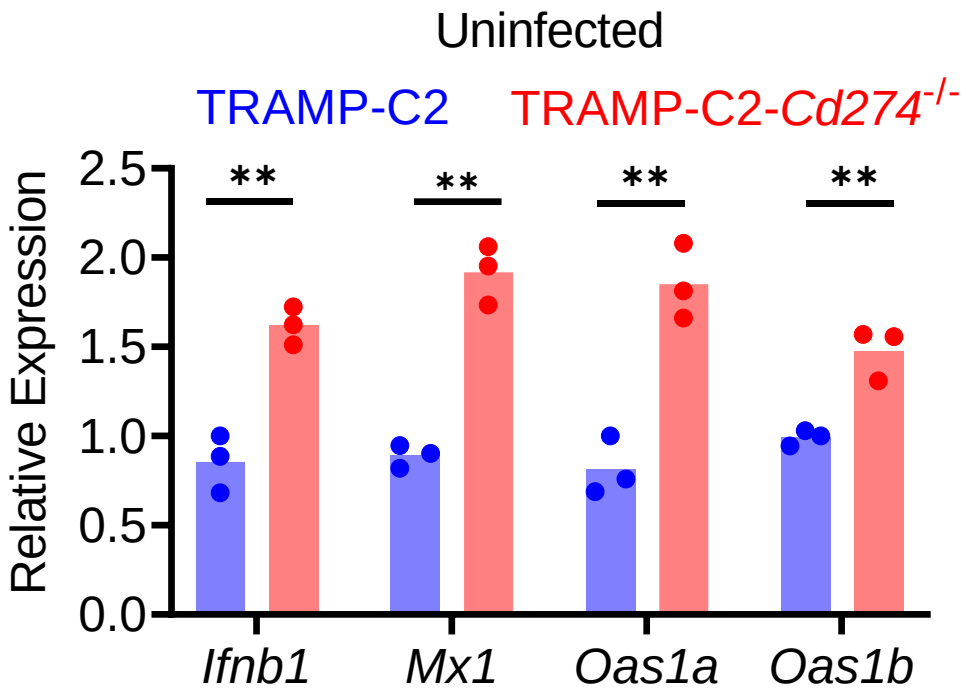
Uninfected
TRAMP-C2
TRAMP-C2-Cd274-/-
Relative Expression
2.5
2.0
1.5
1.0
0.5
0.0
**
**
**
**
Ifnb1
Mx1
Oas1a
Oas1b

Figure 3.11. TRAMP-C2 cells exhibit constitutive type I interferon response, which is inhibited by PD-L1. qPCR analysis of type I interferon and ISG transcripts expressed by TRAMP-C2 and TRAMP-C2 *Cd274*$^{-/-}$ cells prior to infection. N=3 biological replicates plotted. Statistical analysis by two-way ANOVA with Šídák's correction for multiple comparisons.

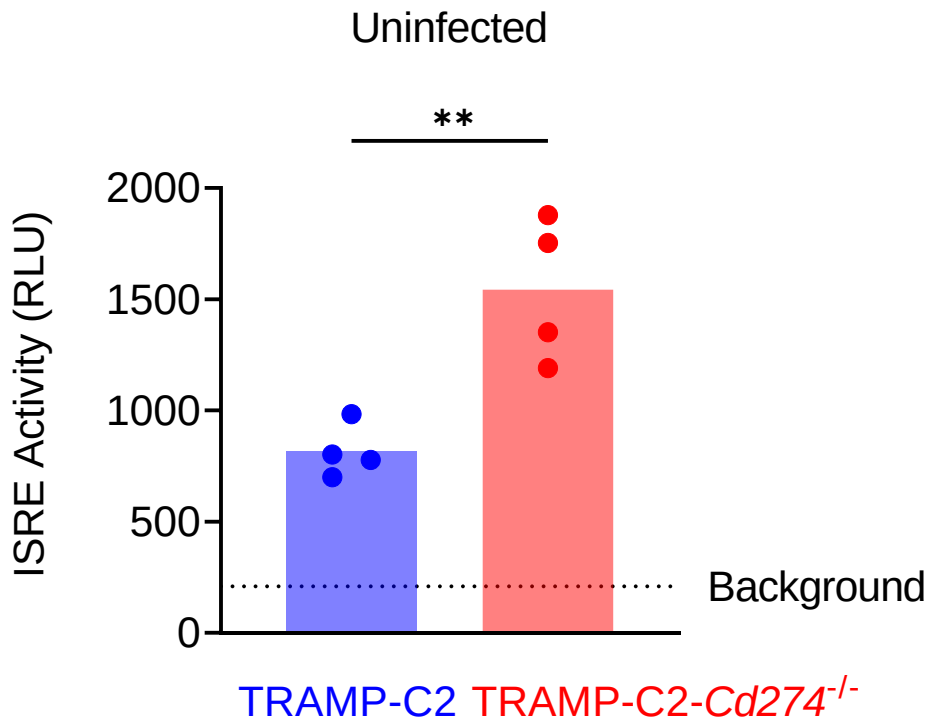
Uninfected
**
2000
1500
1000
500
0
ISRE Activity (RLU)
Background
TRAMP-C2
TRAMP-C2-Cd274-/-

Figure 3.12. TRAMP-C2 cells secrete type I interferon cytokine constitutively, which is inhibited by PD-L1. Measurement of type I IFN in uninfected TRAMP-C2 and TRAMP-C2 *Cd274*$^{-/-}$ supernatant using the L929-ISRE reporter line. The experiment depicted is representative of 3 biological replicates performed with similar results. Statistical analysis by two-tailed unpaired Student's t-test.

The constitutive type I interferon response (regulated by PD-L1) in TRAMP-C2 cells raised the possibility that the critical role of PD-L1 in promoting oncolytic viral infection comes prior to infection, rather than during infection. In other words, the ability of PD-L1 to inhibit the constitutive type I interferon response is more important to promote OV infection, rather than its ability to inhibit the virus-induced type I interferon response. This would explain why PD-L1-deficient TRAMP-C2 cells were still more resistant to VSV WT, as this virus would completely inhibit the virus-induced type I interferon response but have no impact on the constitutive type I interferon response that will confer an antiviral state to the tumour cells, which is inhibited by PD-L1.

To formally test this hypothesis, TRAMP-C2 and TRAMP-C2 *Cd274*$^{-/-}$ cells were treated with the transcription inhibitor actinomycin D at the time of infection with VSVΔ51, in order to block all cellular transcription, including virus-induced production of type I interferon. In this setting, the only source of type I interferons comes prior to infection, as part of the constitutive IFN response observed in cancer cells. Despite the absence of virus-induced interferon, there was still more VSV∆51 infection in TRAMP-C2 compared to TRAMP-C2-*Cd274*$^{-/-}$ cells (Figure 3.13), suggesting that the constitutive type I interferon response (regulated by PD-L1) drives the differences in OV infection. Further, it suggests that PD-L1 poises cancer cells to be more amenable to OV infection.

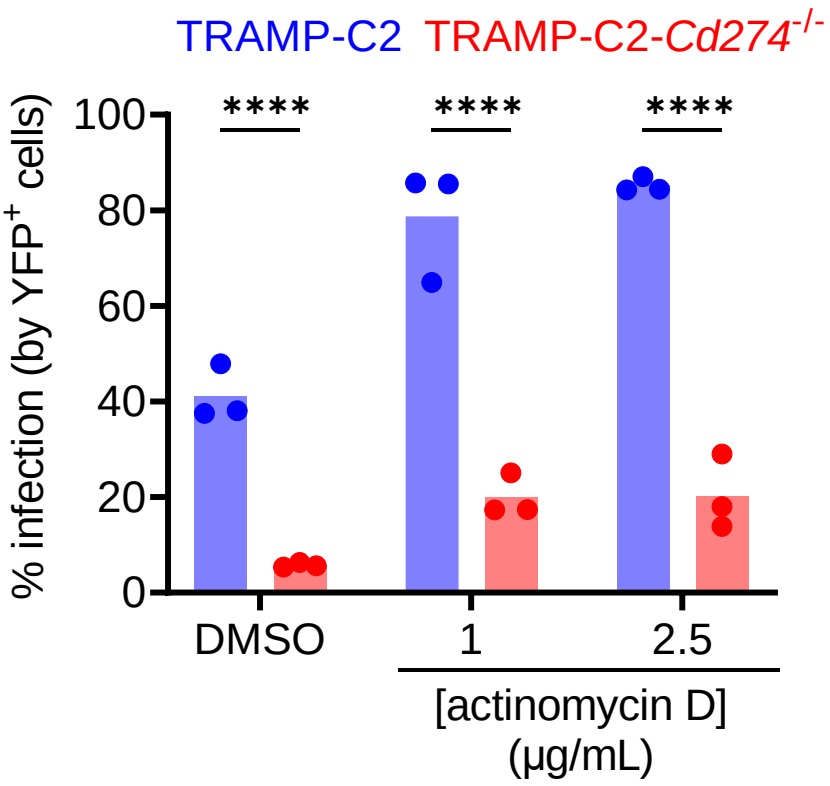
TRAMP-C2
TRAMP-C2-Cd274-/-
% infection (by YFP+ cells)
100
80
60
40
20
0
****
****
****
DMSO
1
2.5
[actinomycin D]
(µg/mL)

Figure 3.13. PD-L1 promotes oncolytic virus infection via inhibition of constitutive type I interferon response in TRAMP-C2 cells. TRAMP-C2 and TRAMP-C2 *Cd274*$^{-/-}$ cells were infected with VSVΔ51-YFP at MOI 0.1 and treated with indicated concentrations of actinomycin D (or DMSO as vehicle control) at the time of infection. 24 hours later, cells were analyzed by flow cytometry. The experiment depicted is representative of 3 biological replicates performed with similar results. Statistical analysis by two-way ANOVA with Šídák's correction for multiple comparisons.

3.5. PD-L1 requires engagement to inhibit type I interferons and promote OV infection

We next investigated whether PD-L1 required a binding partner to trigger its function, similar to many other cell-surface proteins. To date, there are two well-characterized binding partners of PD-L1: PD-1 and CD80.

First, the expression of PD-1 and CD80 in TRAMP-C2 cells was examined. PD-1 expression is generally limited to immune cells, and as expected TRAMP-C2 do not exhibit expression of PD-1 on the cell surface (Figure 3.14); however, TRAMP-C2 cells do express CD80 on the cell surface in approximately 40% of cells in culture (Figure 3.14).

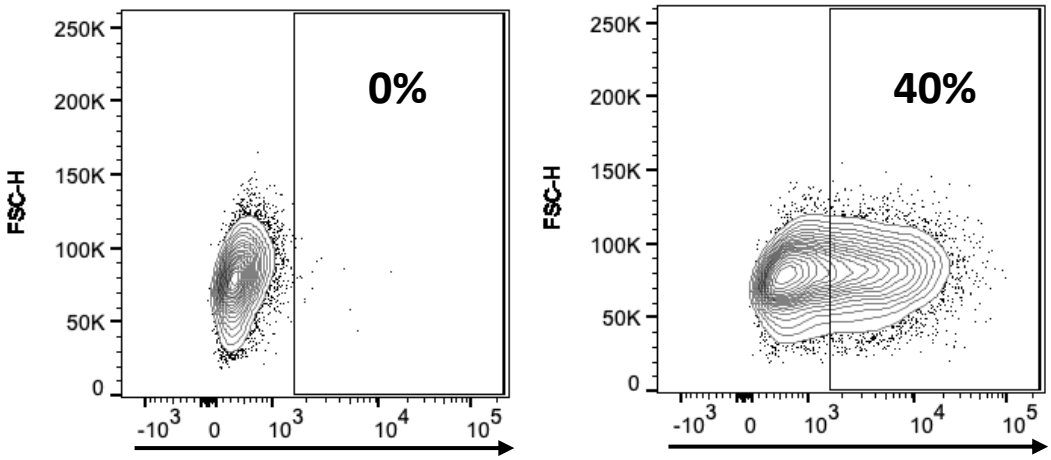
0%
40%
FSC-H
250K
200K
150K
100K
50K
0
-10^3
0
10^3
10^4
10^5
PD-1
CD80

Figure 3.14. TRAMP-C2 cells do not express PD-1 but do express CD80 on the cell surface. Expression of PD-1 and CD80 in TRAMP-C2 cells. Flow cytometry plots representative of 3 biological replicates are shown.

To determine if CD80 is required for PD-L1 function, the $CD80^+$ and $CD80^-$ cells from both parental TRAMP-C2 and TRAMP-C2 *Cd274*$^{-/-}$ cells were isolated, and all four of these cell populations were subjected to VSVΔ51 infection. If CD80 expression was required for PD-L1 function, we should only observe PD-L1 enhancement of OV infection in the $CD80^+$ TRAMP-C2 and *Cd274*$^{-/-}$ cells. In the cells expressing CD80, PD-L1 promoted OV infection (Figure 3.15A). In contrast, in $CD80^-$ cells, PD-L1 had no impact on OV infection (Figure 3.15A). Furthermore, CD80 expression is required for PD-L1 to inhibit the type I interferon pathway, since differences in type I interferon pathway activity are only observed in the $CD80^+$ TRAMP-C2 cells, and not the $CD80^-$ cells (Figure 3.15B). These data suggest that PD-L1 engagement is required to trigger its activity and promote permissiveness to OV infection.

A

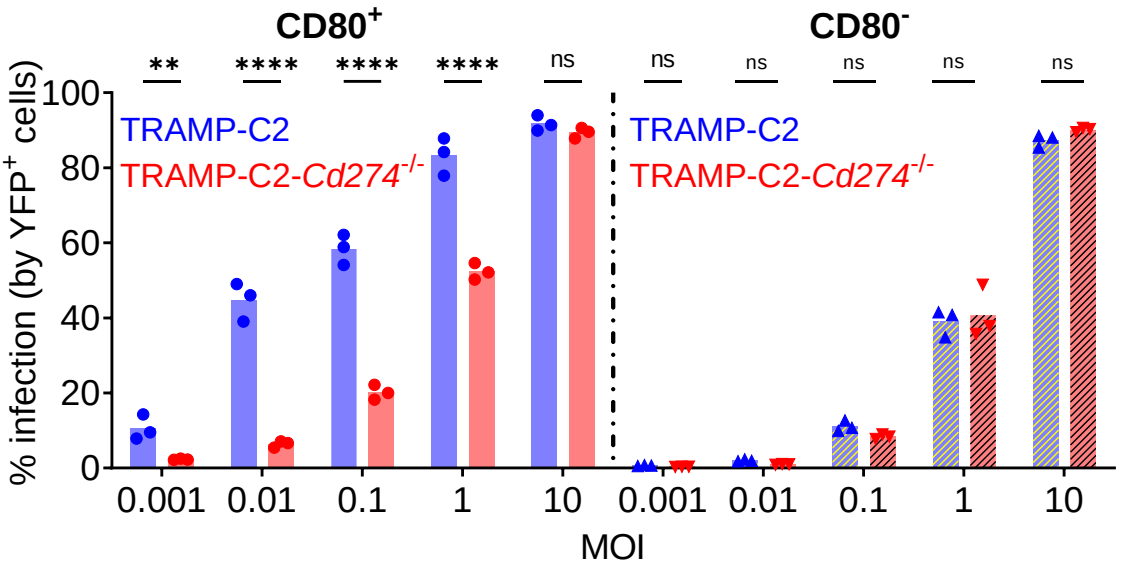
CD80+
CD80-
**
****
****
****
ns
ns
ns
ns
ns
ns
TRAMP-C2
TRAMP-C2-Cd274-/-
TRAMP-C2
TRAMP-C2-Cd274-/-
% infection (by YFP+ cells)
100
80
60
40
20
0
0.001
0.01
0.1
1
10
0.001
0.01
0.1
1
10
MOI

B

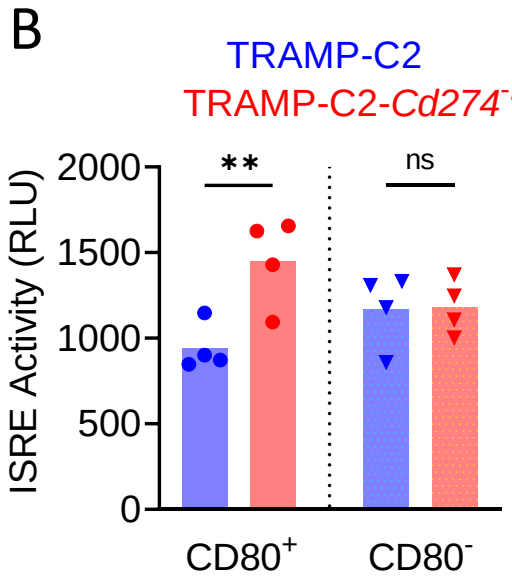
TRAMP-C2
TRAMP-C2-Cd274-/-
**
ns
ISRE Activity (RLU)
2000
1500
1000
500
0
CD80+
CD80-

Figure 3.15. CD80 is required for PD-L1 function in TRAMP-C2 cells. (A) $CD80^+$ and $CD80^-$ cells were isolated by FACS and subjected to VSVΔ51-YFP at indicated MOIs for 24 hours prior to flow cytometry to quantify viral YFP reporter. The experiment depicted is representative of 3 biological replicates performed with similar results. Statistical analysis by two-way ANOVA with Šídák's correction for multiple comparisons. (**B**) Type I interferon in culture supernatant was quantified using the L929-ISRE reporter cell line, in $CD80^+$ and $CD80^-$ cells isolated by FACS and infected with VSVΔ51-YFP for 8 hours. The experiment depicted is representative of 3 biological replicates performed with similar results. Statistical analysis by one-way ANOVA with Šídák's correction for multiple comparisons.

While PD-1 is not endogenously expressed by TRAMP-C2 cells, it could still serve to promote PD-L1 function (when present). To determine whether CD80 is uniquely required to engage PD-L1, or if PD-1 can also play this role, TRAMP-C2 cells were pre-treated with a recombinant PD-1-Fc chimera protein prior to VSVΔ51 infection. PD-1 treatment significantly enhanced VSVΔ51 infection in parental TRAMP-C2 cells compared to the isotype antibody treatment condition (Figure 3.16). PD-1 treatment had no impact on TRAMP-C2 *Cd274*$^{-/-}$ cells (Figure 3.16), which was expected given the lack of PD-L1 ligand expression.

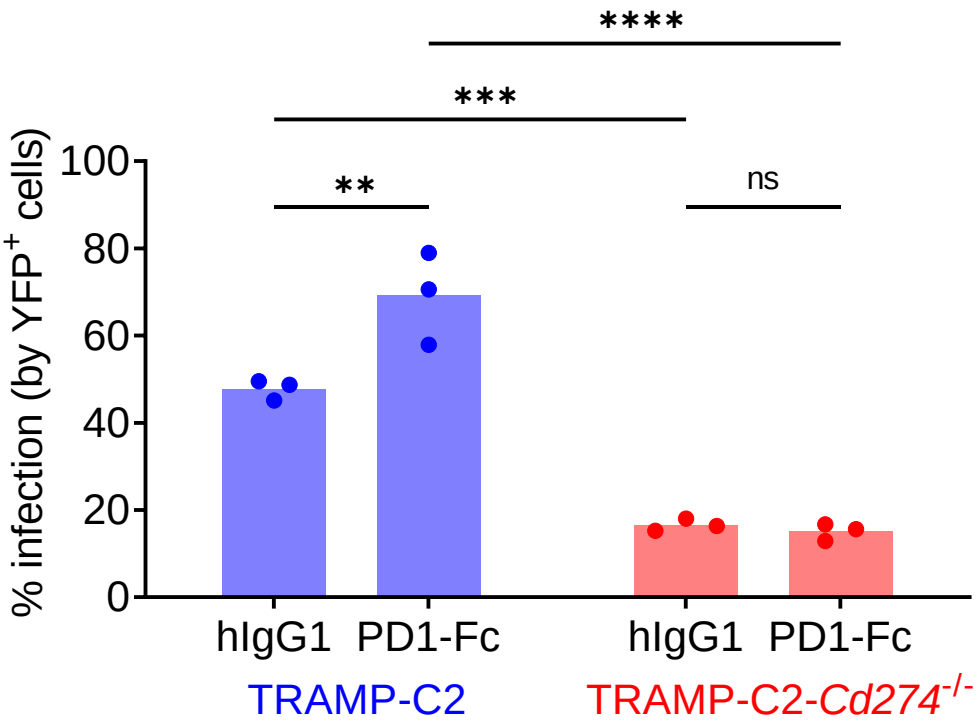
****
***
**
ns
% infection (by YFP+ cells)
100
80
60
40
20
0
hIgG1
PD1-Fc
hIgG1
PD1-Fc
TRAMP-C2
TRAMP-C2-Cd274-/-

Figure 3.16. Exogenous PD-1 can trigger PD-L1 function in TRAMP-C2 cells. TRAMP-C2 and TRAMP-C2 *Cd274*$^{-/-}$ were pre-treated for 24 hours with 500 ng of recombinant PD-1-Fc chimeric protein, and infected with VSVΔ51-YFP at MOI 0.1 for 24 hours prior to analysis by flow cytometry. The experiment depicted is representative of 3 biological replicates performed with similar results. Statistical analysis by two-way ANOVA with Šídák's correction for multiple comparisons.

Lastly, we explored if PD-L1 antibodies, typically used to block the interaction between PD-L1 and PD-1/CD80, could alter PD-L1 function. We used three PD-L1 blocking antibodies previously characterized to either block the PD-L1/PD-1 interaction (clone 27C11), the PD-L1/CD80 interaction (clone 17H9), or both (clone 6E11), prior to VSVΔ51 infection. Interestingly, pre-treatment with clones 27C11 and 6E11, but not 17H9, significantly enhanced VSVΔ51 infection in parental TRAMP-C2 cells compared to the isotype control condition (Figure 3.17A). Furthermore, treatment with these two antibody clones resulted in more significant inhibition of IFN-β and ISG expression in parental TRAMP-C2 cells compared to the isotype control condition (Figure 3.17B-C). None of the three PD-L1 antibodies had any significant impact on VSVΔ51 in TRAMP-C2 *Cd274*$^{-/-}$ cells (Figure 3.17), as expected given their lack of PD-L1 expression. Therefore, certain anti-PD-L1 clones have the ability to enhance/trigger PD-L1 function.

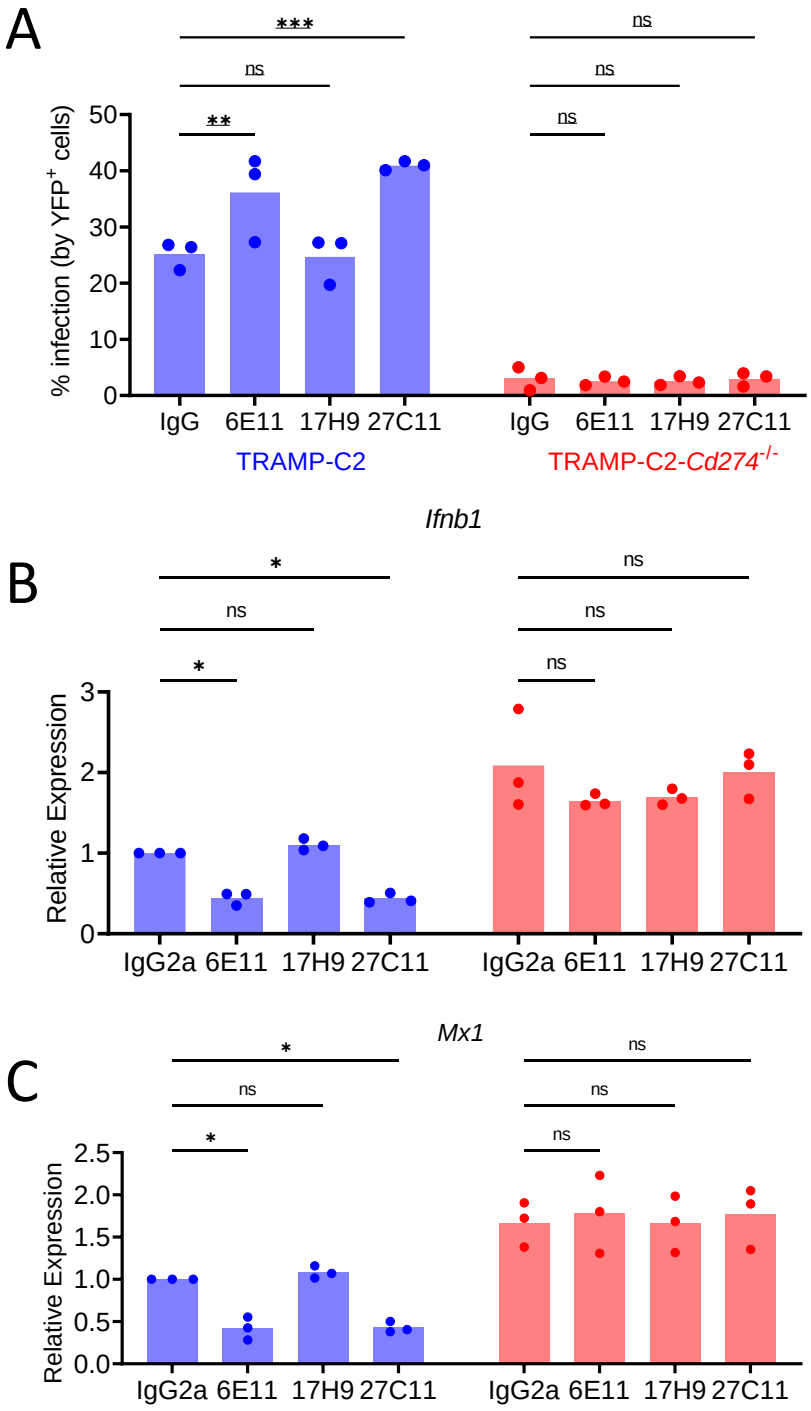
A
***
ns
**
ns
ns
ns
% infection (by YFP+ cells)
50
40
30
20
10
0
IgG 6E11 17H9 27C11
IgG 6E11 17H9 27C11
TRAMP-C2
TRAMP-C2-Cd274-/-
Ifnb1
B
*
ns
*
ns
ns
ns
Relative Expression
3
2
1
0
IgG2a 6E11 17H9 27C11
IgG2a 6E11 17H9 27C11
Mx1
C
*
ns
*
ns
ns
ns
Relative Expression
2.5
2.0
1.5
1.0
0.5
0.0
IgG2a 6E11 17H9 27C11
IgG2a 6E11 17H9 27C11

Figure 3.17. PD-L1 antibodies can trigger PD-L1 function. TRAMP-C2 and TRAMP-C2 *Cd274*$^{-/-}$ were pre-treated for 24 hours with 10 µg of PD-L1 antibodies (or isotype control), and infected with VSVΔ51-YFP at MOI 0.1 for (**A**) 24 hours prior to analysis by flow cytometry or (**B**) 8 hours prior to analysis by qPCR. The experiments depicted are representative of 3 biological replicates performed with similar results. Statistical analysis by two-way ANOVA with Šídák's correction for multiple comparisons.

3.6 PD-L1 promotes OV infection in vivo

To extend our findings beyond in vitro culture models, we tested if PD-L1 could enhance VSVΔ51 infection in the more complex in vivo tumour microenvironment. TRAMP-C2 and TRAMP-C2 *Cd274*$^{-/-}$ cells were implanted subcutaneously into immunodeficient NCG mice, and when tumours were established, they were injected intra-tumourally with VSVΔ51 expressing a luciferase reporter. In line with previous in vitro data, parental TRAMP-C2 tumours were better infected compared to TRAMP-C2 *Cd274*$^{-/-}$ tumours (Figure 3.18). Therefore, PD-L1 promotes OV infection in a physiologically relevant environment and is not limited to in vitro culture.

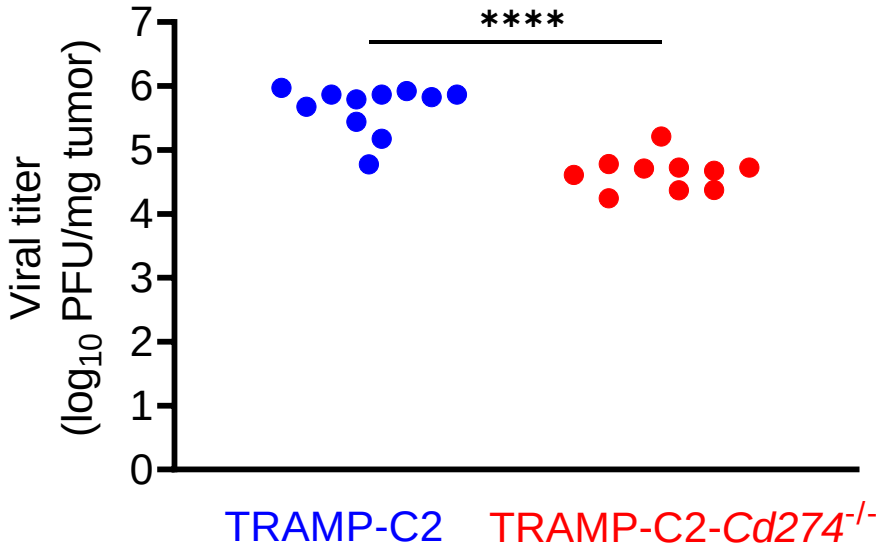

NCG - TRAMP-C2 tumours

NCG - TRAMP-C2-*Cd274*$^{-/-}$ tumours

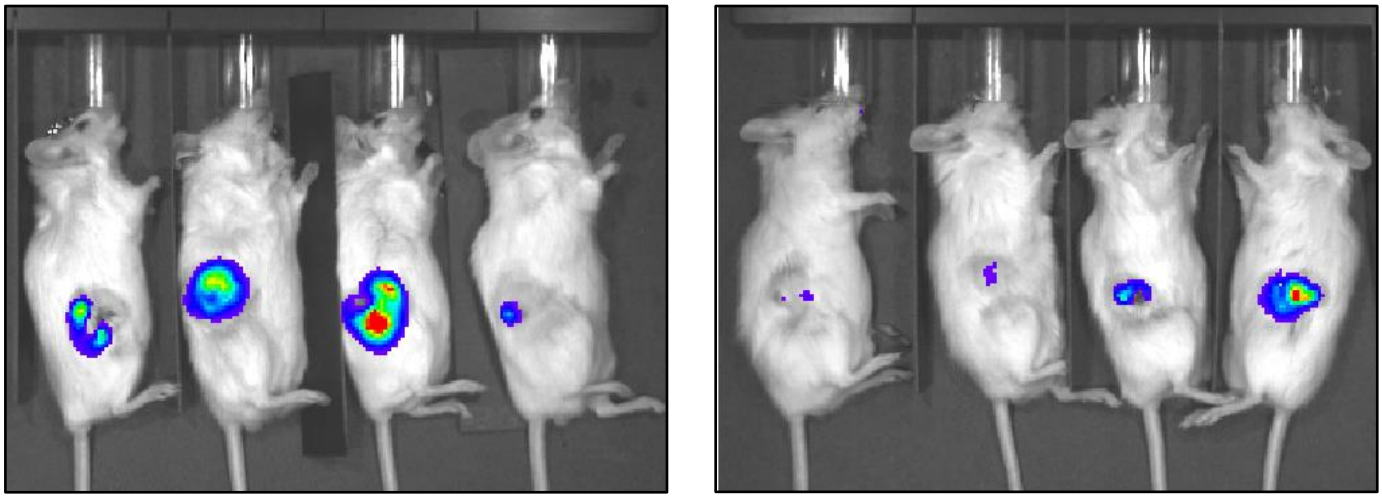

+ VSVΔ51-luciferase

Figure 3.18. PD-L1 promotes oncolytic virus infection in vivo. Male NCG mice were implanted with subcutaneous TRAMP-C2 or TRAMP-C2 *Cd274*$^{-/-}$ cells, and injected intra-tumourally with 10^8 PFU of VSVΔ51 expressing a luciferase reporter. 24 hours post-infection, mice were injected subjected to bioluminescence imaging (bottom), and tumours were homogenized to quantify viral titers by plaque assay (top). The bioluminescence images are representative of 2 experiments with similar results, and plaque assay data is a combination of N=2 biological replicates. Statistical analysis by unpaired two-tailed Student's t-test.

Chapter 4

PD-L1 inhibit the type I interferon pathway via a pro-glycolytic metabolic shift.

4.1 Introduction and Rationale

In the literature, PD-L1 expression is associated with alterations in the type I interferon pathway, but the mechanism by which PD-L1 regulates type I interferon signaling is unknown. Here, we describe how PD-L1 controls cellular metabolism resulting in inhibition of the type I interferon pathway, and identify glycolysis and lactate as a key pathway and metabolite involved in PD-L1 function.

Cellular and host metabolism are now well-appreciated to control inflammation and inflammatory pathways, including the type I interferon pathway. In particular, glycolysis and its associated metabolites have emerged as important regulators of interferon signaling and anti-viral defenses (*252–256*).

4.2. PD-L1 alters the cancer cell transcriptome

To begin understanding the mechanism by which PD-L1 inhibits the type I interferon pathway and promotes OV infection, a bulk RNA-seq experiment was conducted as an unbiased analysis of cellular status in the presence and absence of PD-L1. Four conditions were tested: TRAMP-C2 uninfected, TRAMP-C2 *Cd274*$^{-/-}$ uninfected, TRAMP-C2 VSVΔ51-infected, and TRAMP-C2 *Cd274*$^{-/-}$ VSVΔ51-infected. VSVΔ51-infected cells were collected after infection at MOI 0.1 for 8 hours, given that all previous experiments were conducted at MOI 0.1, and 8 hours post-infection is when differential regulation of the type I interferon pathway is observed post-infection. We also analyzed uninfected

cells, since our data shows that PD-L1 poises the cells to be more amenable to OV infection, prior to infection.

Comparing TRAMP-C2 and TRAMP-C2 *Cd274*$^{-/-}$ cells, we observed 2,690 and 5,486 differentially expressed genes in uninfected and infected samples respectively. This transcriptomic dataset was summarized using the Pathway RespOnsive GENes for activity inference (PROGENy) resource, which predicts pathways and transcription factors that might be dysregulated based on the differentially-expressed genes (Figure 4.1). Additionally, the transcriptomic dataset was analyzed using the DoRothEA resource, which predicts transcription factors that might be differentially active based on the gene expression patterns (Appendix I). Given our data showing the importance of the uninfected state for OV infection outcomes, we focused on the pathways dysregulated in the uninfected state and/or those previously described to regulate the type I interferon pathway. PROGENy analysis of the RNA-seq dataset predicted PD-L1-mediated regulation of several pathways and factors previously characterized to interact with and/or regulate the type I interferon pathway, including hypoxia, TGF-β signaling, hormone signaling, p53, and EGFR signaling.

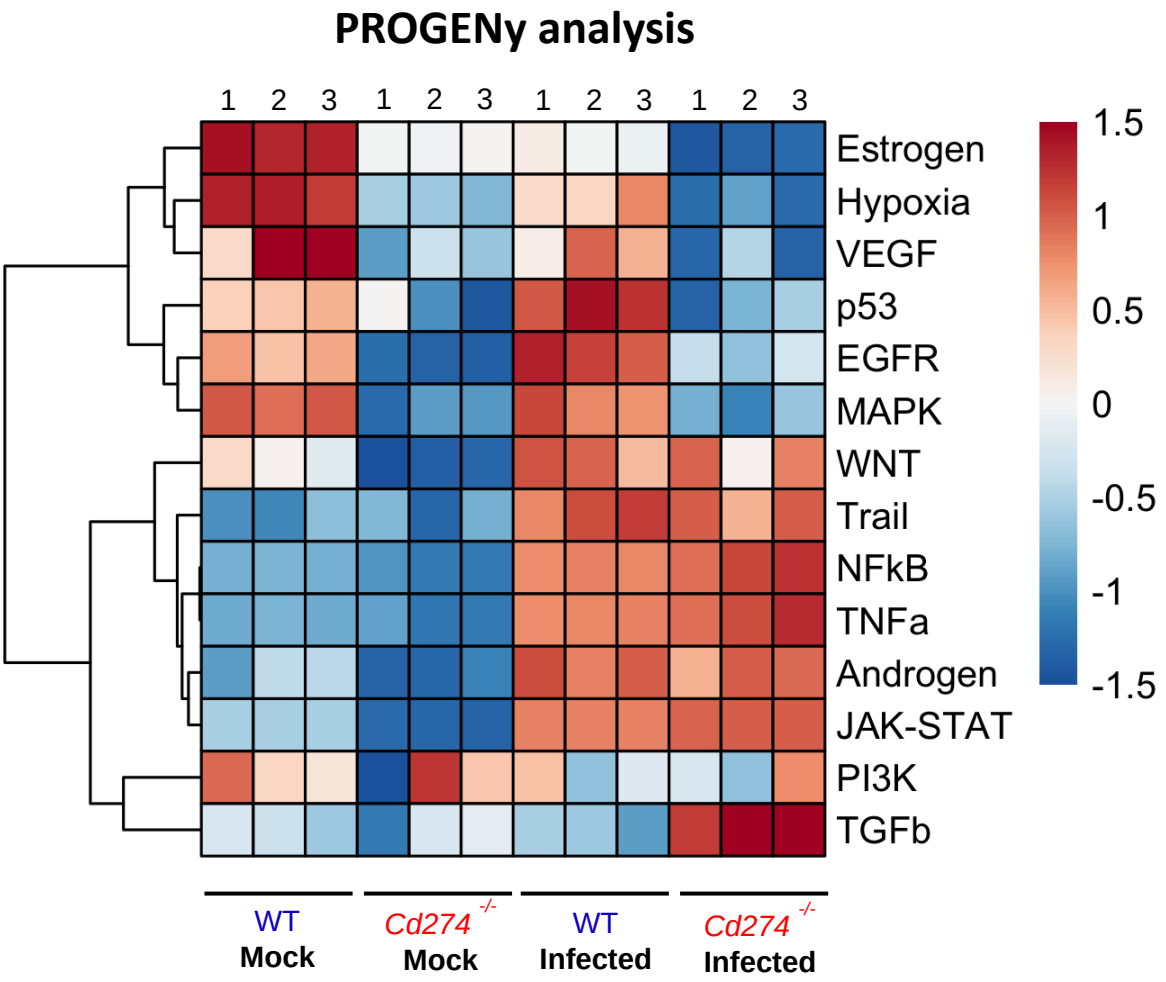
PROGENy analysis
1 2 3 1 2 3 1 2 3 1 2 3
Estrogen
Hypoxia
VEGF
p53
EGFR
MAPK
WNT
Trail
NFkB
TNFa
Androgen
JAK-STAT
PI3K
TGFb
1.5
1
0.5
0
-0.5
-1
-1.5
WT Mock
Cd274 -/- Mock
WT Infected
Cd274 -/- Infected

Figure 4.1. PD-L1 alters the cancer cell transcriptome. PROGENy pathway analysis of bulk RNA-seq performed on TRAMP-C2 and TRAMP-C2 *Cd274*$^{-/-}$ either mock-infected or infected with VSVΔ51-YFP at MOI 0.1 for 8 hours (3 biological replicates per condition).

To begin validating these transcriptomic signatures, a plate-based transcription factor activity assay was performed to test the DNA-binding activity of 48 transcription factors, including many identified from our RNA-seq dataset. TRAMP-C2 and TRAMP-C2 *Cd274*$^{-/-}$ cells were compared in the uninfected or infected (MOI 0.1, 12 hours post-infection) state. This study revealed a number of transcription factors with differential DNA-binding activity in the presence of PD-L1 (Figure 4.2), including Smad, c-Myc, and STAT3.

Based on the transcriptomic dataset and the transcription factor activity experiment, we began to pharmacologically perturb these proteins/pathways, and examine the impact of this perturbation on the ability of PD-L1 to promote OV infection.

A

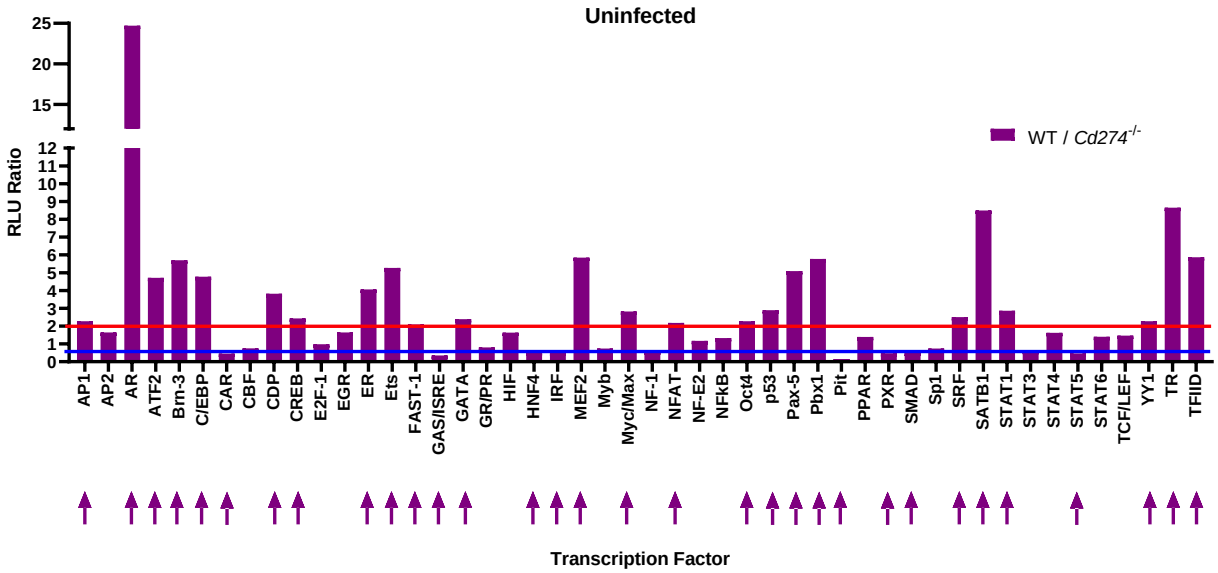
Uninfected
WT / Cd274-/-
RLU Ratio
AP1 AP2 AR ATF2 Brn-3 C/EBP CAR CBF CDP CREB E2F-1 EGR ER Ets FAST-1 GAS/ISRE GATA GR/PR HIF HNF4 IRF MEF2 Myb Myc/Max NF-1 NFAT NF-E2 NFkB Oct4 p53 Pax-5 Pbx1 Pit PPAR PXR SMAD Sp1 SRF SATB1 STAT1 STAT3 STAT4 STAT5 STAT6 TCF/LEF YY1 TR TFIID
Transcription Factor

B

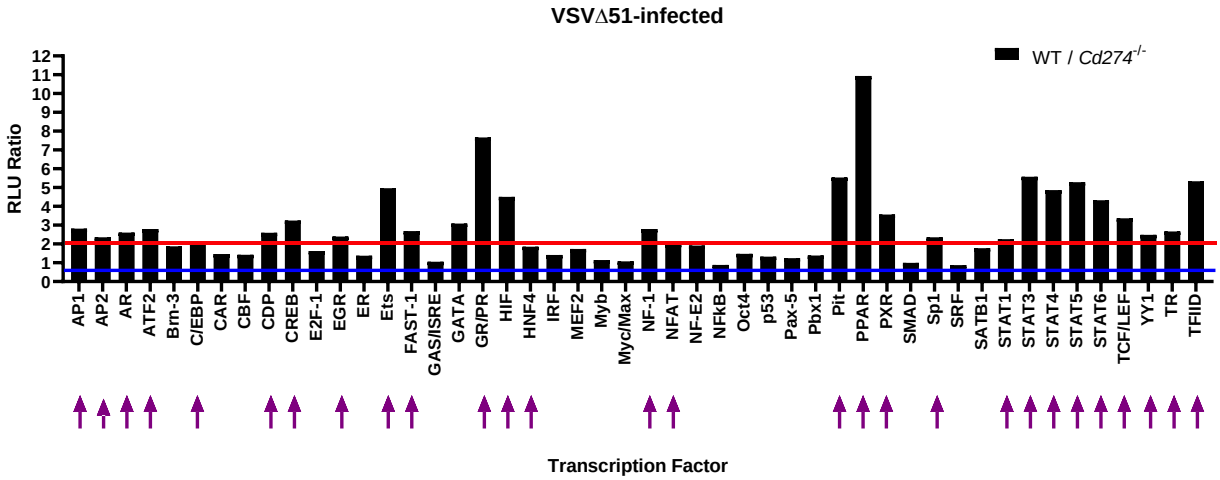
VSVΔ51-infected
WT / Cd274-/-
RLU Ratio
AP1 AP2 AR ATF2 Brn-3 C/EBP CAR CBF CDP CREB E2F-1 EGR ER Ets FAST-1 GAS/ISRE GATA GR/PR HIF HNF4 IRF MEF2 Myb Myc/Max NF-1 NFAT NF-E2 NFkB Oct4 p53 Pax-5 Pbx1 Pit PPAR PXR SMAD Sp1 SRF SATB1 STAT1 STAT3 STAT4 STAT5 STAT6 TCF/LEF YY1 TR TFIID
Transcription Factor

Figure 4.2. PD-L1 expression alters transcription factory activity. Summary of results from a luminescence-based plate array testing activity of 48 transcription factors. In (**A**), TRAMP-C2 cell were uninfected; in (**B**) TRAMP-C2 cells were infected with VSVΔ51 at MOI 0.1 for 12 hours. Raw luminescence units (RLU) of parental TRAMP-C2 were divided by RLU of TRAMP-C2 *Cd274*$^{-/-}$ for each transcription factor to assess relative activity. Red line and blue line indicate 2x and 0.5x difference, respectively. Purple arrows indicate those transcription factors with greater than 2-fold difference between TRAMP-C2 and TRAMP-C2 *Cd274*$^{-/-}$ cells. N=1 biological replicate.

We started with the TGF-β pathway, which has previously been described to alter type I interferon signaling and anti-viral responses, and was suggested to be regulated by PD-L1 in our transcriptomic dataset. The small-molecule inhibitor SB431542, which blocks the kinase activity of the TGFβ receptor (ALK5) (*257*), was used at relevant doses to inhibit the pathway. TRAMP-C2 and TRAMP-C2 *Cd274*$^{-/-}$ cells were pre-treated with the TGF-β inhibitor (or DMSO as vehicle control) for 24 hours prior to VSVΔ51 infection at MOI 0.1 for 24 hours. Treatment with SB431542 and inhibition of the TGF-β pathway resulted in no significant difference in infection in TRAMP-C2 and TRAMP-C2 *Cd274*$^{-/-}$ cells, and no change of the PD-L1-mediated enhancement of OV infection (Figure 4.3), suggesting this pathway is not involved in PD-L1 function.

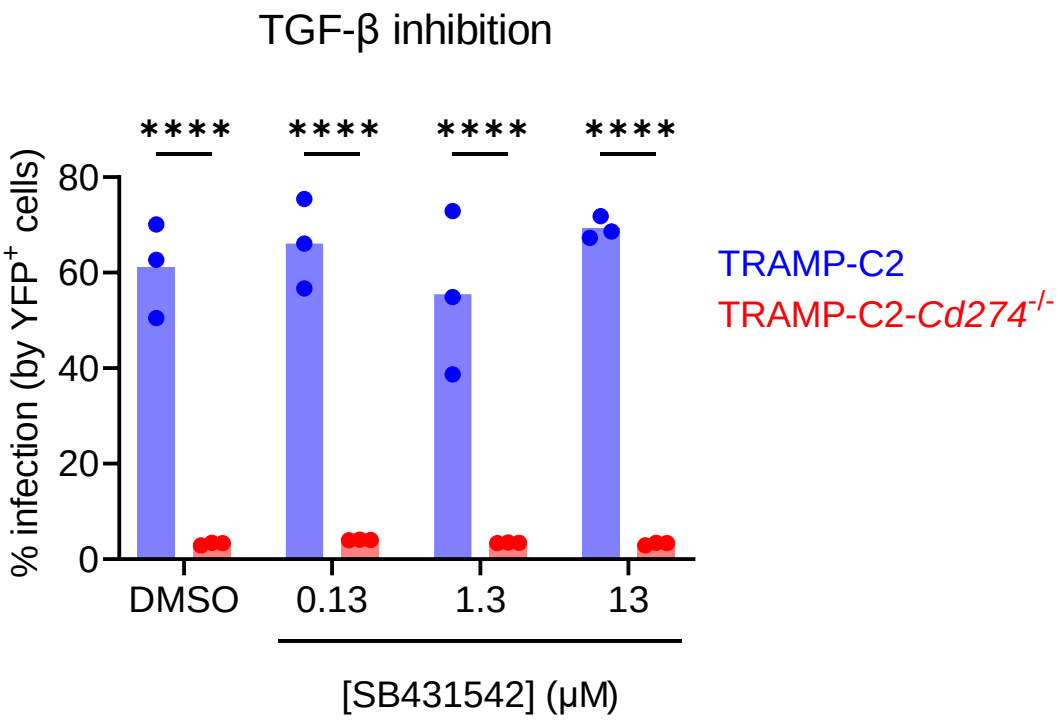
TGF-β inhibition
****
****
****
****
% infection (by YFP+ cells)
80
60
40
20
0
DMSO
0.13
1.3
13
[SB431542] (μM)
TRAMP-C2
TRAMP-C2-Cd274-/-

Figure 4.3. TGF-β signaling is not involved in PD-L1 function. TRAMP-C2 and TRAMP-C2 *Cd274*$^{-/-}$ cells were pre-treated with the TGF-βRI inhibitor SB431452 for 24 hours at indicated concentrations (or DMSO as vehicle control), followed by infection with VSVΔ51-YFP at MOI 0.1 for 24 hours. Infection was assessed by flow cytometry for viral YFP reporter expression. Experiment depicted is representative of 2 biological replicates with similar results. Statistical analysis by two-way ANOVA with Šídák's correction for multiple comparisons.

In a similar fashion, we inhibited the activity of EGFR using the irreversible inhibitor afatinib, which blocks the tyrosine kinase activity of the receptor and prevents downstream signaling (*258*). Parental TRAMP-C2 and TRAMP-C2 *Cd274*$^{-/-}$ cells were pre-treated with the EGFR inhibitor (or DMSO as vehicle control) for 6 hours prior to VSVΔ51 infection at MOI 0.1 for 24 hours. Treatment with afatinib and inhibition of EGFR signaling resulted in no significant difference in infection in TRAMP-C2 and TRAMP-C2 *Cd274*$^{-/-}$ cells, and no change of the PD-L1-mediated enhancement of OV infection (Figure 4.4), suggesting this pathway is not involved in PD-L1 function.

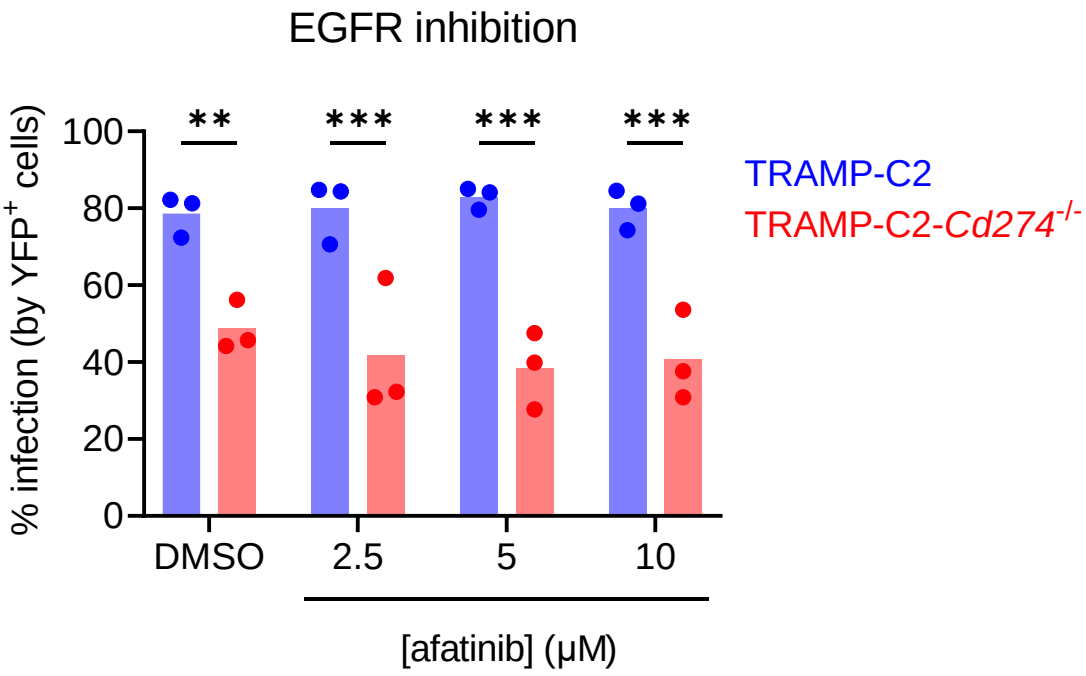
EGFR inhibition
% infection (by YFP+ cells)
100
80
60
40
20
0
**
***
***
***
DMSO
2.5
5
10
[afatinib] (μM)
TRAMP-C2
TRAMP-C2-Cd274-/-

Figure 4.4. EGFR signaling is not involved in PD-L1 function. TRAMP-C2 and TRAMP-C2 *Cd274*$^{-/-}$ cells were pre-treated with the irreversible EGFR inhibitor afatinib for 6 hours at indicated concentrations (or DMSO as vehicle control), followed by infection with VSVΔ51-YFP at MOI 0.1 for 24 hours. Infection was assessed by flow cytometry for viral YFP reporter expression. Experiment depicted is representative of 2 biological replicates with similar results. Statistical analysis by two-way ANOVA with Šídák's correction for multiple comparisons.

Next, we blocked the activity of the transcription factor c-Myc using the small-molecule inhibitor 10058-F4. This molecule blocks the dimerization between c-Myc and Max, which is required for transcriptional activity of c-Myc target genes (*259*). Parental TRAMP-C2 and TRAMP-C2 *Cd274*$^{-/-}$ cells were pre-treated with the c-Myc inhibitor (or DMSO as vehicle control) for 4 hours prior to VSVΔ51 infection at MOI 0.1 for 24 hours. Treatment with 10058-F4 and inhibition of c-Myc activity did not alter PD-L1-mediated enhancement of OV infection (Figure 4.5), suggesting this pathway is not involved in PD-L1 function.

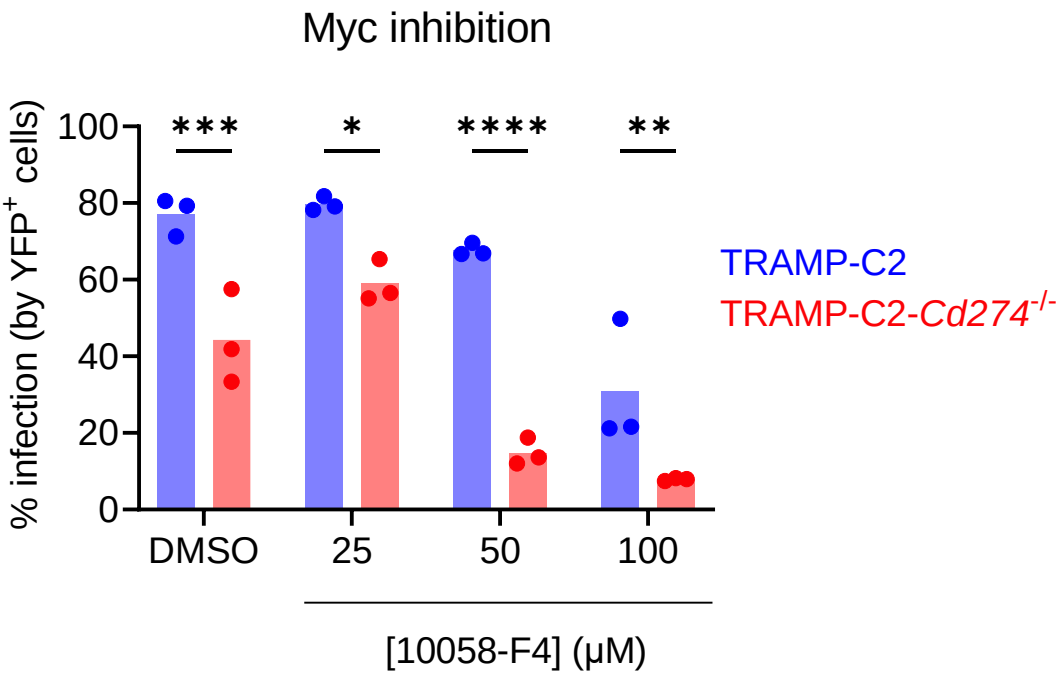
Myc inhibition
% infection (by YFP+ cells)
100
80
60
40
20
0
***
*
****
**
DMSO
25
50
100
[10058-F4] (μM)
TRAMP-C2
TRAMP-C2-Cd274-/-

Figure 4.5. Myc activity is not involved in PD-L1 function. TRAMP-C2 and TRAMP-C2 *Cd274*$^{-/-}$ cells were pre-treated with the c-Myc inhibitor 10058-F4 for 6 hours at indicated concentrations (or DMSO as vehicle control), followed by infection with VSVΔ51-YFP at MOI 0.1 for 24 hours. Infection was assessed by flow cytometry for viral YFP reporter expression. Experiment depicted is representative of 2 biological replicates with similar results. Statistical analysis by two-way ANOVA with Šídák's correction for multiple comparisons.

Next, we modulated androgen and estrogen signaling in TRAMP-C2 cells. Genes associated with estrogen activity were better expressed in TRAMP-C2 cells compared to TRAMP-C2 *Cd274*$^{-/-}$ cells in our RNA-seq dataset. Additionally, TRAMP-C2 cells are androgen-dependent prostate cancer cells that require a testosterone precursor (dehydroisoandrosterone) in the growth media for long-term culture, and androgen-associated genes were better expressed in parental TRAMP-C2 cells compared to TRAMP-C2 *Cd274*$^{-/-}$ cells in our RNA-seq dataset. Importantly, hormone signaling has been shown to modulate type I interferon responses and ISG expression (*260*, *261*). First, to eliminate androgen/estrogen signaling, TRAMP-C2 cells were cultured for 5 days in phenol red-free growth medium supplemented with charcoal-stripped FBS, without any testosterone precursor added, prior to VSVΔ51 infection. To stimulate hormone responses, estradiol and/or dihydrotestosterone were added to the cells for 48 hours prior to VSVΔ51 infection. While OV infection overall was reduced in cells cultured in phenol red-free media with charcoal-stripped serum, parental TRAMP-C2 cells still maintained higher OV infection compared to TRAMP-C2 *Cd274*$^{-/-}$ cells in all conditions (Figure 4.6), suggesting that androgen/estrogen responses do not play a role in PD-L1-mediated enhancement of OV infection.

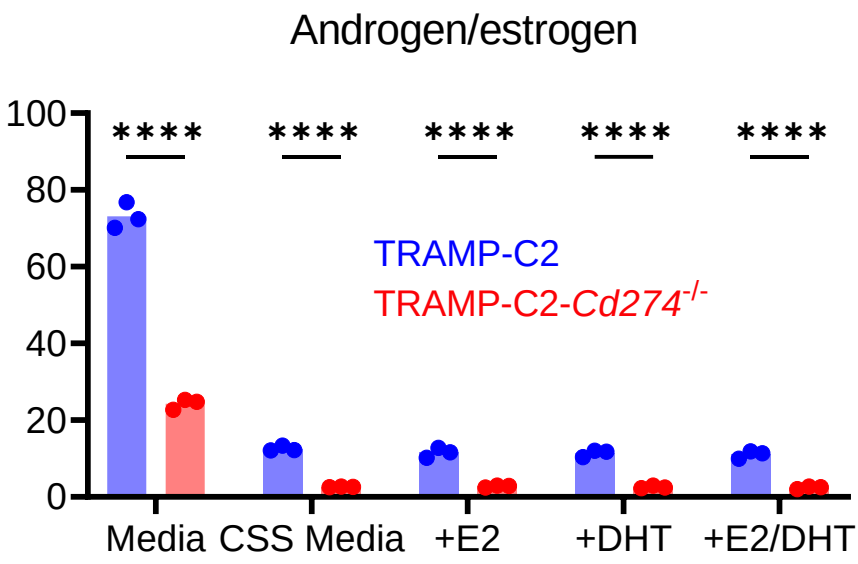
Androgen/estrogen
100
80
60
40
20
0
****
****
****
****
****
TRAMP-C2
TRAMP-C2-Cd274-/-
Media
CSS Media
+E2
+DHT
+E2/DHT

Figure 4.6. Hormone responses are not involved in PD-L1 function. TRAMP-C2 and TRAMP-C2 *Cd274*$^{-/-}$ cells were cultured in phenol red-free DMEM supplemented with 10% charcoal-stripped serum (CSS) for 48 hours prior to treatment with estradiol (E2, 100 nM) and/or dihydrotestosterone (DHT, 10 nM) for 24 hours. Following that, cells were infected with VSVΔ51-YFP at MOI 0.1 for 24 hours prior to analysis by flow cytometry for viral YFP reporter expression. Experiment depicted is representative of 2 biological replicates with similar results. Statistical analysis by two-way ANOVA with Šídák's correction for multiple comparisons.

Next, we blocked the activity of the transcription factor NRF2, which is a key regulator of cellular oxidants, with the small-molecule inhibitor ML385 (*262*). NRF2 has previously been implicated in regulation of the type I interferon response and OV infection (*263*, *264*). TRAMP-C2 and TRAMP-C2 *Cd274*$^{-/-}$ cells were pre-treated with the NRF2 (or DMSO as vehicle control) for 6 hours prior to VSVΔ51 infection at MOI 0.1 for 24 hours. Treatment with ML385 and inhibition of NRF2 activity resulted in no significant difference in infection in TRAMP-C2 and TRAMP-C2 *Cd274*$^{-/-}$ cells, and no change of the PD-L1-mediated enhancement of OV infection (Figure 4.7A). Additionally, pre-treatment of TRAMP-C2 and TRAMP-C2 *Cd274*$^{-/-}$ cells with the antioxidant N-acetylcysteine (NAC), which decreases reactive oxygen species concentration in cells (*265*), had no impact on PD-L1 function (Figure 4.7B). In all, this suggest that NRF2 and the cellular redox state is not involved in PD-L1 function.

A

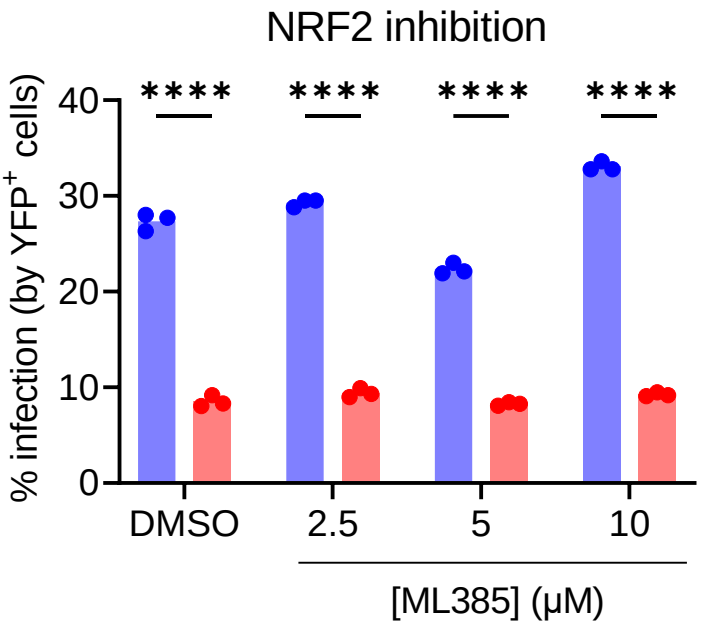

TRAMP-C2

TRAMP-C2-*Cd274*$^{-/-}$

B

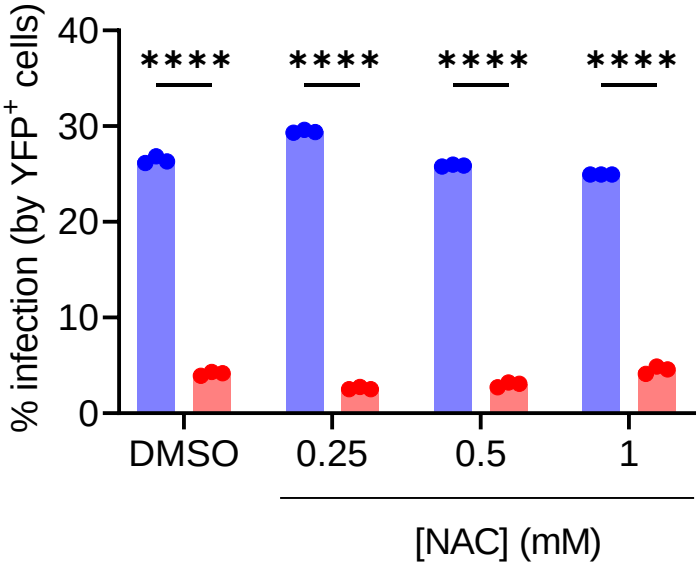

TRAMP-C2

TRAMP-C2-*Cd274*$^{-/-}$

Figure 4.7. Cellular ROS dynamics are not involved in PD-L1 function. TRAMP-C2 and TRAMP-C2 *Cd274*$^{-/-}$ cells were pre-treated with the NRF2 inhibitor ML385 (**A**) for 6 hours or N-acetylcysteine (NAC, **B**), or DMSO as control, for 24 hours prior to infection with VSVΔ51-YFP at MOI 0.1 for 24 hours. Infection was assessed by flow cytometry for viral YFP reporter expression. Experiment depicted is representative of 2 biological replicates with similar results. Statistical analysis by two-way ANOVA with Šídák's correction for multiple comparisons.

4.3. Hypoxia mimics the impact of PD-L1 on OV infection

Lastly, we explored the role of the hypoxia response in PD-L1 function, as hypoxia-related genes were suggested to be enhanced by PD-L1 in our RNA-seq dataset. Furthermore, the cellular changes associated with hypoxia are known to regulate type I interferon signaling and viral infection (*174*). To examine the possible role of hypoxic responses, TRAMP-C2 and TRAMP-C2 *Cd274*$^{-/-}$ cells were placed in hypoxic conditions (1% O_2) for 48 hours prior to VSVΔ51 infection for 24 hours (maintained in 1% O_2). Interestingly, culture of TRAMP-C2 cells in hypoxic conditions ablated differences in OV infection between TRAMP-C2 and TRAMP-C2 *Cd274*$^{-/-}$ cells (Figure 4.8), suggesting some role of the hypoxic response in PD-L1 function. Further, given that all our experiments were conducted in normoxic conditions (atmospheric 21% O_2) so far, some aspects of the hypoxia response must be activated in normoxic TRAMP-C2 cells, and play a role in PD-L1-mediated enhancement of OV infection.

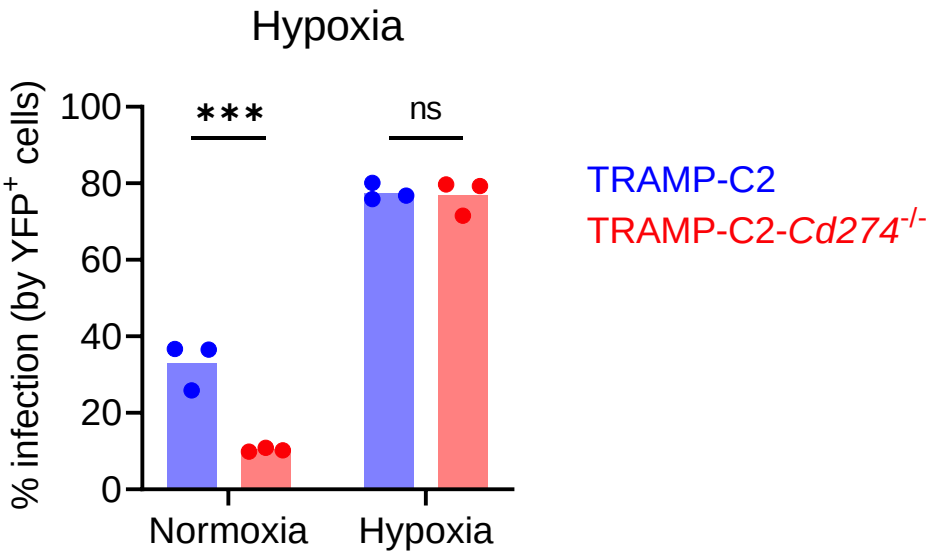
Hypoxia
% infection (by YFP+ cells)
100
80
60
40
20
0
***
ns
Normoxia
Hypoxia
TRAMP-C2
TRAMP-C2-Cd274-/-

Figure 4.8. Hypoxia mimics PD-L1 function. TRAMP-C2 and TRAMP-C2 *Cd274*$^{-/-}$ cells were cultured in normoxic or hypoxic (1% O_2) for 48 hours prior to infection with VSVΔ51-YFP at MOI 0.1 for 24 hours (in normoxic or hypoxic conditions). Infection was assessed by flow cytometry for viral YFP reporter expression. Experiment depicted is representative of 3 biological replicates performed with similar results. Statistical analysis by two-way ANOVA with Šídák's correction for multiple comparisons.

Given the essentiality of oxygen, mammalian cells respond dramatically to hypoxic conditions, including expression of hypoxia-inducible factors (*266*), changes in cellular ROS (*267*), and changes in cellular metabolism (*268*). Given that we already eliminated cellular ROS and redox state as a variable in PD-L1 function (Figure 4.7), we explored the role of hypoxia-inducible factors and cellular metabolism in PD-L1 function.

Hypoxia leads to the stabilization of hypoxia-inducible factors (HIFs) that act as transcription factors to alter gene expression patterns and adapt to the hypoxic conditions (*266*). The best-studied HIF is HIF-1, made up of the constitutively expressed and stable HIF-1β and the HIF-1α subunit that accumulates during hypoxia (but is otherwise degraded under normoxic conditions). We began investigating the potential regulation of HIF proteins by PD-L1 by analyzing expression of HIF-1α, HIF-1β, and the related hypoxia proteins PHD-2 and FIH. In particular, the expression of these proteins was examined in TRAMP-C2 cells infected with VSVΔ51, or treated with either of the two small-molecules known to stabilize HIF-1α, DMOG and DFX (*269*). In normoxic conditions, we did not observe any expression of HIF-1α in TRAMP-C2 cells infected with VSVΔ51 or untreated. While we did detect expression of HIF-1α in DFX-treated cells, surprisingly DMOG was unable to stabilize HIF-1α in TRAMP-C2 cells (Figure 4.9A). HIF-1β and FIH were equally expressed by TRAMP-C2 and TRAMP-C2 *Cd274*$^{-/-}$ cells, and only PHD-2 showed a reduction in expression in TRAMP-C2 *Cd274*$^{-/-}$ cells compared to parental TRAMP-C2 (Figure 4.9A). Therefore, under normoxic conditions, these cells

do not display robust stabilization of HIF-1α, despite the apparent pathway activity suggested in the RNA-seq analysis (Figure 4.1 and 4.2).

Consistent with this, pre-treatment of TRAMP-C2 cells with the HIF-1α-stabilizing agents DMOG and DFX did not alter PD-L1-mediated enhancement of OV infection, as parental TRAMP-C2 cells were still better infected compared to TRAMP-C2 *Cd274*$^{-/-}$ cells (Figure 4.9B).

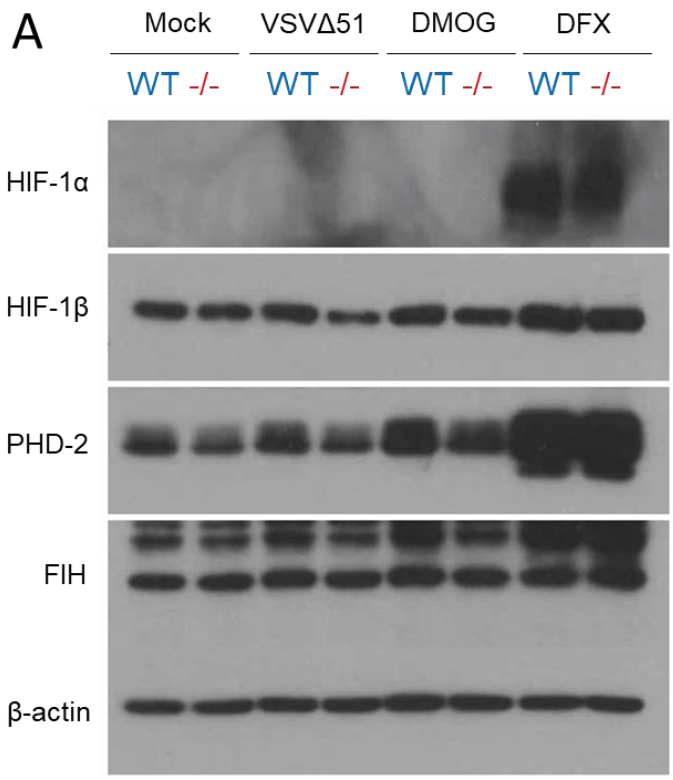
A
Mock
VSVΔ51
DMOG
DFX
WT -/-
WT -/-
WT -/-
WT -/-
HIF-1α
HIF-1β
PHD-2
FIH
β-actin

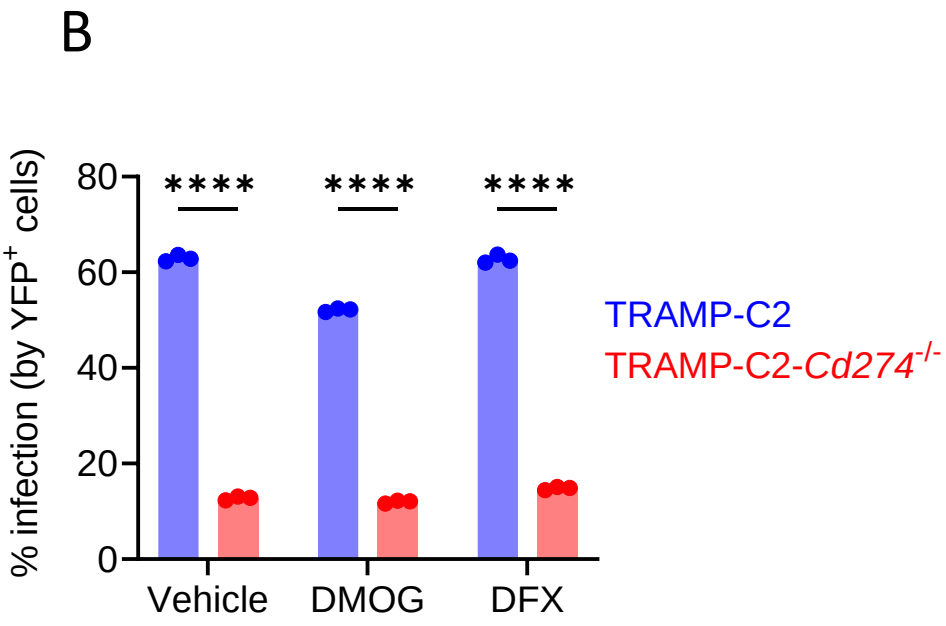
B
% infection (by YFP+ cells)
80
60
40
20
0
****
****
****
Vehicle
DMOG
DFX
TRAMP-C2
TRAMP-C2-Cd274-/-

Figure 4.9. TRAMP-C2 do not express HIF-1α under normoxic conditions, and HIF-1α-stabilizing agents do not phenocopy PD-L1 function. (**A**) TRAMP-C2 and TRAMP-C2 *Cd274*$^{-/-}$ cells were either infected with VSVΔ51-YFP at MOI 0.1 for 24 hours, treated with DMOG or DFX at 100 µM for 24 hours, or DMSO and mock-treated as control. Expression of hypoxia pathway proteins assessed by western blotting. Images depicted are representative of 2 biological replicates with similar results. (**B**) TRAMP-C2 and TRAMP-C2 *Cd274*$^{-/-}$ cells were pre-treated with DMOG or DFX at 100 µM for 24 hours (or DMSO as vehicle control) prior to infection with VSVΔ51-YFP at MOI 0.1 for 24 hours. Infection was assessed by flow cytometry for viral YFP reporter expression. Experiment depicted is representative of 2 biological replicates with similar results. Statistical analysis by two-way ANOVA with Šídák's correction for multiple comparisons.

To confirm the lack of HIF expression in normoxic TRAMP-C2 cells, the transcriptional activity of HIF proteins was assessed using a luciferase reporter plasmid expressing luciferase under the control of hypoxia response elements (HRE). TRAMP-C2 and TRAMP-C2 *Cd274*$^{-/-}$ cells were transfected with the HRE-luciferase plasmid (or empty vector) for 48 hours; for the last 24 hours, cells were cultured in either normoxic or hypoxic conditions. As expected, the luciferase reporter was expressed in cells under hypoxia at equal amounts in parental TRAMP-C2 and TRAMP-C2 *Cd274*$^{-/-}$ cells (Figure 4.10). Consistent with immunoblotting data, there was no luciferase reporter expression in normoxic TRAMP-C2 cells (compared to empty vector controls), suggesting that HIF proteins are not active in normoxic TRAMP-C2 cells, despite the apparent pathway activity at the transcriptional level (Figure 4.1).

In all, these data suggest that HIF proteins and the associated transcriptional response driven by HIF stabilization does not drive PD-L1 function in TRAMP-C2 cells. We subsequently turned our attention to the metabolic changes associated with the hypoxia response. It is well-known that hypoxia triggers a metabolic shift towards glycolysis to generate ATP and metabolites, with less reliance on oxidative phosphorylation (and the use of oxygen) for energy transduction and metabolism (*268*).

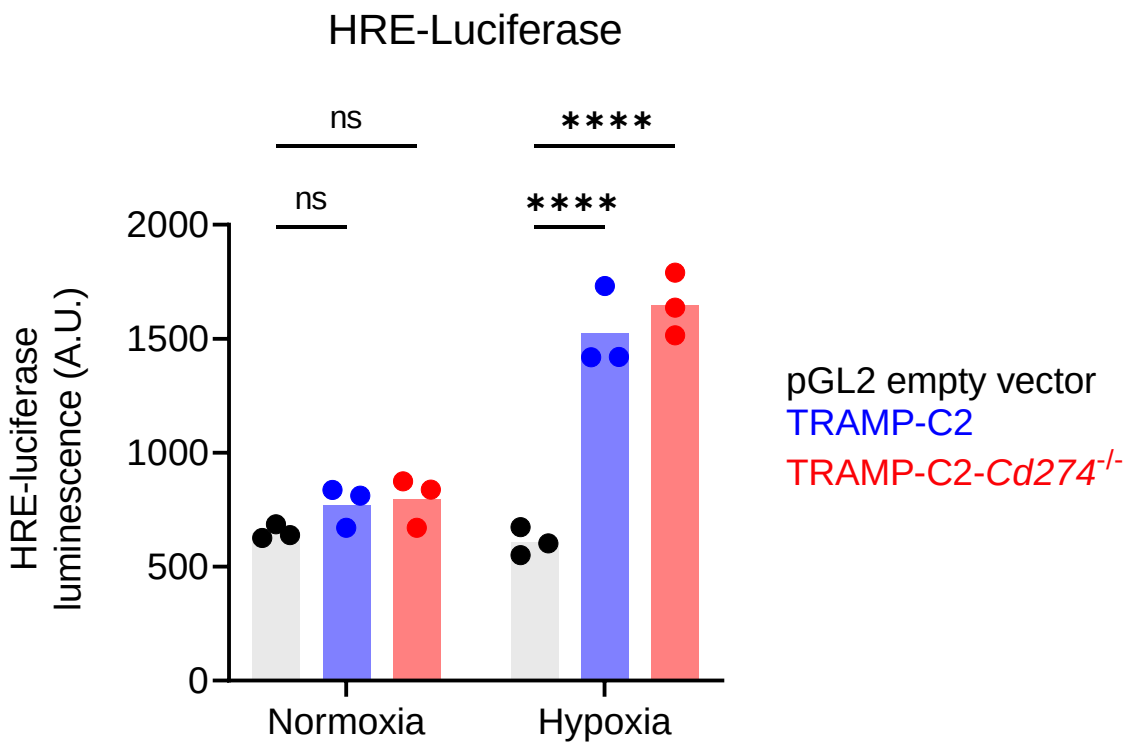
HRE-Luciferase
ns
****
ns
****
2000
1500
1000
500
0
HRE-luciferase luminescence (A.U.)
Normoxia
Hypoxia
pGL2 empty vector
TRAMP-C2
TRAMP-C2-Cd274-/-

Figure 4.10. TRAMP-C2 do not exhibit HIF-1α transcriptional activity in normoxic conditions. TRAMP-C2 and TRAMP-C2 *Cd274*$^{-/-}$ cells were transiently transfected with plasmid expressing HRE-luciferase reporter (or pGL2 empty vector as control) for 24 hours in normoxic conditions. Cells were either transferred to hypoxic conditions (1% O_2) or maintained in normoxic conditions (21% O_2) for another 24 hours prior to luciferase assay. Experiment depicted is representative of 2 biological replicates with similar results. Statistical analysis by two-way ANOVA with Šídák's correction for multiple comparisons.

4.4. PD-L1 promotes glycolytic metabolism

We began by re-examining the hypoxia gene signature detected by the PROGENy analysis in the bulk RNA-seq dataset (Figure 4.1). Interestingly, this gene signature in TRAMP-C2 cells was predominated by differentially-expressed metabolic enzymes (Figure 4.11A). Strikingly, almost every enzyme in the glycolysis pathway was down-regulated by deletion of PD-L1, giving rise to greater glycolysis gene set scores in TRAMP-C2 cells compared to TRAMP-C2 *Cd274*$^{-/-}$ cells (Figure 4.11B).

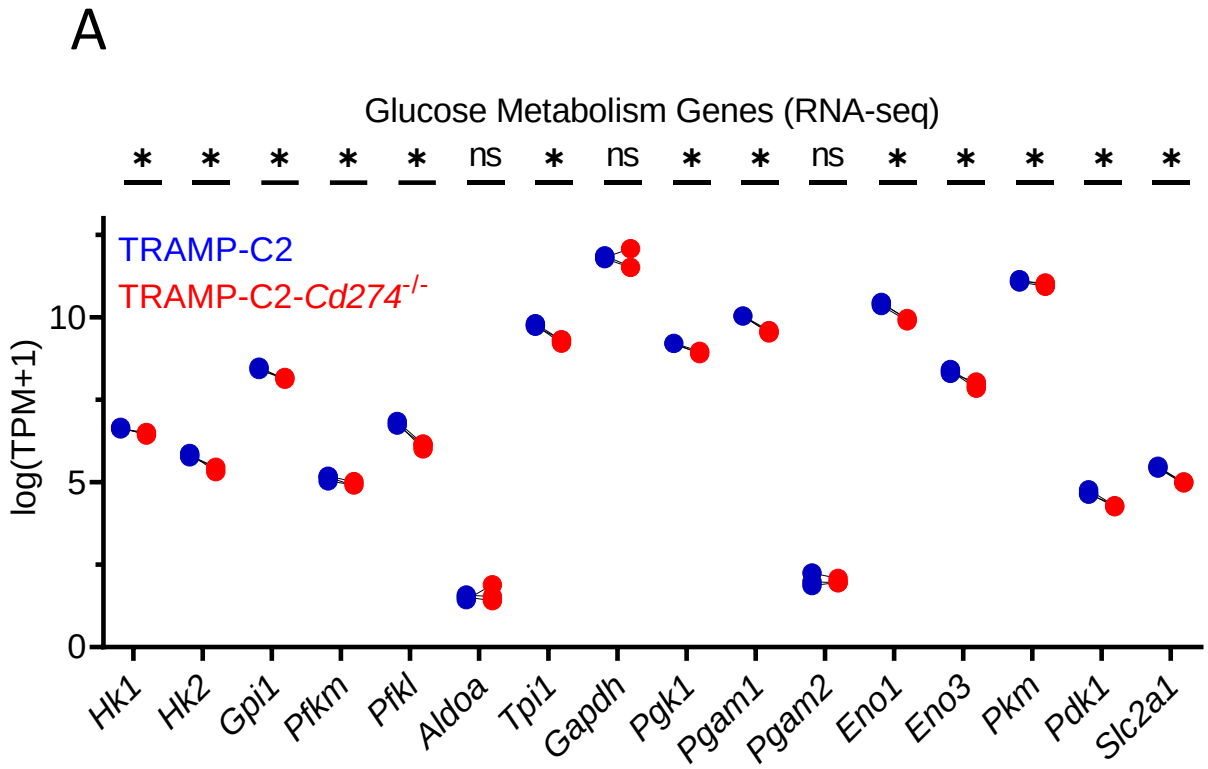
A
Glucose Metabolism Genes (RNA-seq)
* * * * * ns * ns * * ns * * * * *
TRAMP-C2
TRAMP-C2-Cd274-/-
log(TPM+1)
10
5
0
Hk1
Hk2
Gpi1
Pfkm
Pfkl
Aldoa
Tpi1
Gapdh
Pgk1
Pgam1
Pgam2
Eno1
Eno3
Pkm
Pdk1
Slc2a1

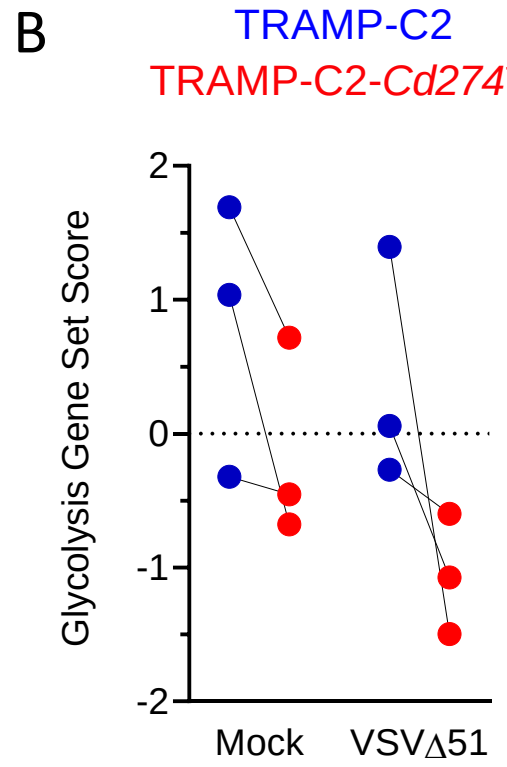
B
TRAMP-C2
TRAMP-C2-Cd274-/-
Glycolysis Gene Set Score
2
1
0
-1
-2
Mock
VSVΔ51

Figure 4.11. PD-L1 promotes expression of glycolysis-related genes. (**A**) Transcripts per million (TPM) for various glycolysis and glucose metabolism enzymes/transporters, from bulk RNA-seq experiment in uninfected TRAMP-C2 cells. 3 biological replicates per condition. Wald's test was used to test for differential expression between samples and the resultant *p*-values were adjusted to *q*-values using the Benjamini-Hochberg false discovery rate method. (**B**) Scoring for expression of genes included in the glycolysis gene set. RNA-seq dataset performed on TRAMP-C2 and TRAMP-C2 *Cd274*$^{-/-}$ either mock-infected or infected with VSVΔ51-YFP at MOI 0.1 for 8 hours (3 biological replicates per condition).

Furthermore, we observed a decrease in mitochondrial content in PD-L1-expressing TRAMP-C2 cells using MitoTracker dye and mtDNA quantification (Figure 4.12A-B). We investigated if PD-L1 impacted other aspects of mitochondrial biology, including the relative levels of mitochondrial ROS and alterations in mitochondrial dynamics. PD-L1 did not change mitochondrial ROS levels (Figure 4.12A), and had limited impact on mitochondrial morphology, as assessed by TOMM20 immunocytochemistry to label mitochondria (Figure 4.13). These data suggest that PD-L1 triggers a metabolic shift that promotes glycolysis-related gene expression while reducing mitochondrial mass.

A

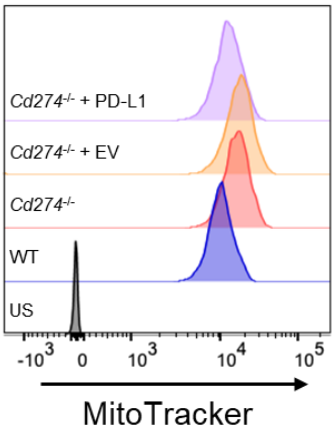
Cd274-/- + PD-L1
Cd274-/- + EV
Cd274-/-
WT
US
-10^3
0
10^3
10^4
10^5
MitoTracker

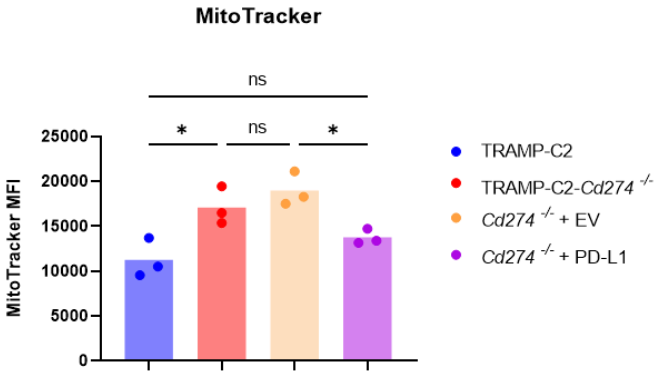
MitoTracker
ns
*
ns
*
MitoTracker MFI
25000
20000
15000
10000
5000
0
TRAMP-C2
TRAMP-C2-Cd274 -/-
Cd274 -/- + EV
Cd274 -/- + PD-L1

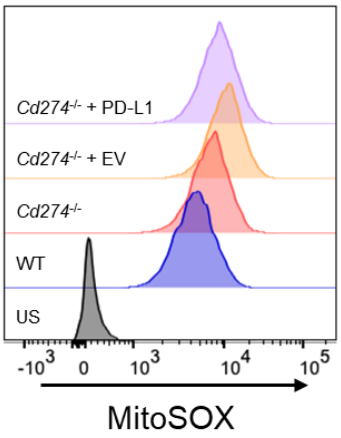
Cd274-/- + PD-L1
Cd274-/- + EV
Cd274-/-
WT
US
-10^3
0
10^3
10^4
10^5
MitoSOX

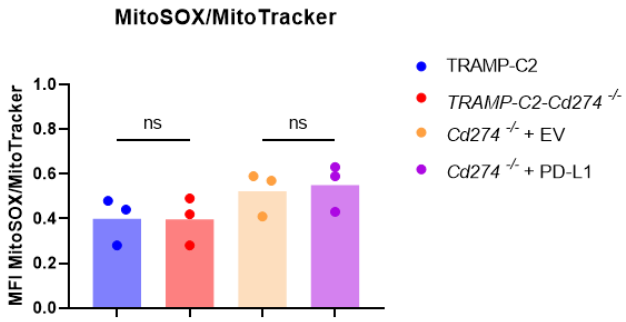
MitoSOX/MitoTracker
ns
ns
MFI MitoSOX/MitoTracker
1.0
0.8
0.6
0.4
0.2
0.0
TRAMP-C2
TRAMP-C2-Cd274 -/-
Cd274 -/- + EV
Cd274 -/- + PD-L1

B

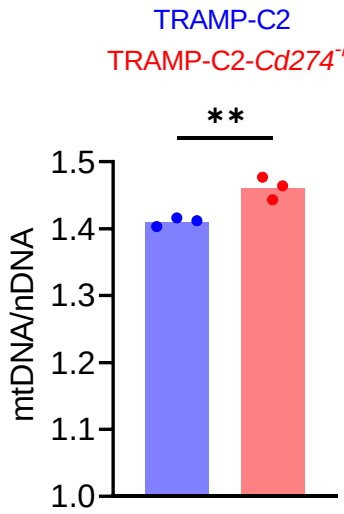
TRAMP-C2
TRAMP-C2-Cd274-/-
**
mtDNA/nDNA
1.5
1.4
1.3
1.2
1.1
1.0

Figure 4.12. PD-L1 reduces mitochondrial mass, without affecting mitochondrial ROS. (**A**) Mean fluorescence intensity (MFI) of MitoTracker and MitoSOX dyes by flow cytometry for uninfected TRAMP-C2, TRAMP-C2 *Cd274*$^{-/-}$, TRAMP-C2 *Cd274*$^{-/-}$ + EV, and TRAMP-C2 *Cd274*$^{-/-}$ + PD-L1 cells. MitoSOX MFI was corrected for total mitochondrial content by normalizing to MitoTracker MFI. Statistical analysis by one-way ANOVA with Šídák's correction for multiple comparisons. (**B**) Relative quantification of mitochondrial DNA/mtDNA by qPCR (normalized to nuclear DNA/nDNA in each sample), by qPCR analysis. N=3 biological replicates. Statistical analysis by two-tailed unpaired Student's t test.

Hoechst TOMM20

TRAMP-C2 WT

TRAMP-C2 *Cd274*$^{-/-}$

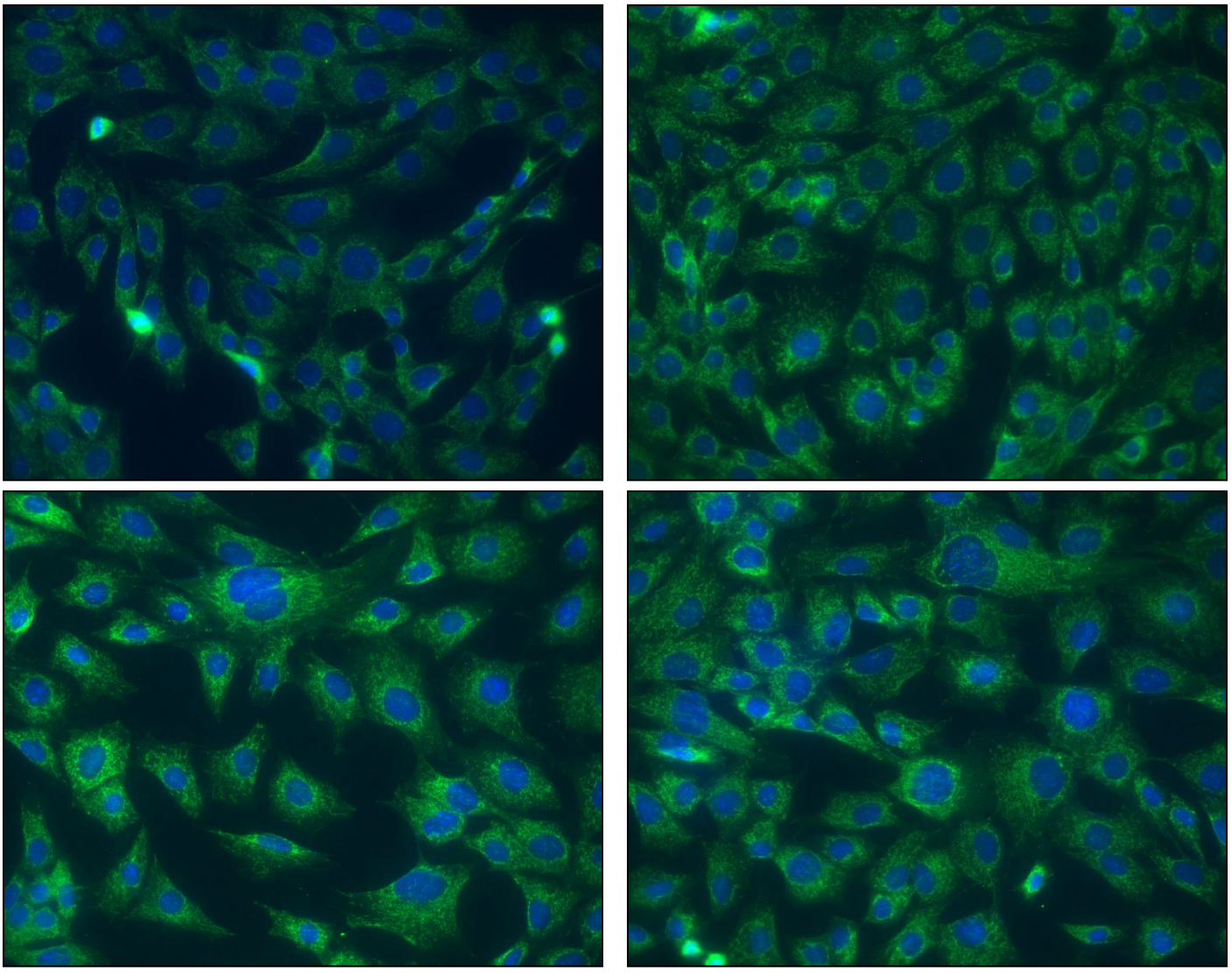

Figure 4.13. PD-L1 does not impact mitochondrial morphology. Mitochondria of cultured parental TRAMP-C2 and *Cd274*$^{-/-}$ cells were analyzed by immunofluorescent staining for TOMM20 and Hoechst dye. Representative images of N=2 biological replicates depicted.

Given the PD-L1-mediated differences in glycolysis enzyme expression and mitochondrial content, we tested for differences in glycolysis and mitochondrial metabolism using a mitochondrial stress test on the Seahorse metabolic flux platform. In agreement with our transcriptomic and mitochondrial quantification data, PD-L1 promoted the rate of glycolysis while inhibiting oxidative phosphorylation (Figure 4.14A-D). Additionally, bioenergetic calculations (*270*, *271*) suggest that in TRAMP-C2 cells, PD-L1 reduced ATP production from oxidative phosphorylation while increasing ATP production from glycolysis (Figure 4.14E-F).

Consistent with the increase in glycolysis rates, parental TRAMP-C2 had an enhanced rate of glucose uptake compared to TRAMP-C2 *Cd274*$^{-/-}$ cells (Figure 4.14G). This increase is restricted to the CD80^{+} cells, as CD80^{-} TRAMP-C2 and TRAMP-C2 *Cd274*$^{-/-}$ cells had similar glucose uptake rates (Figure 4.14H).

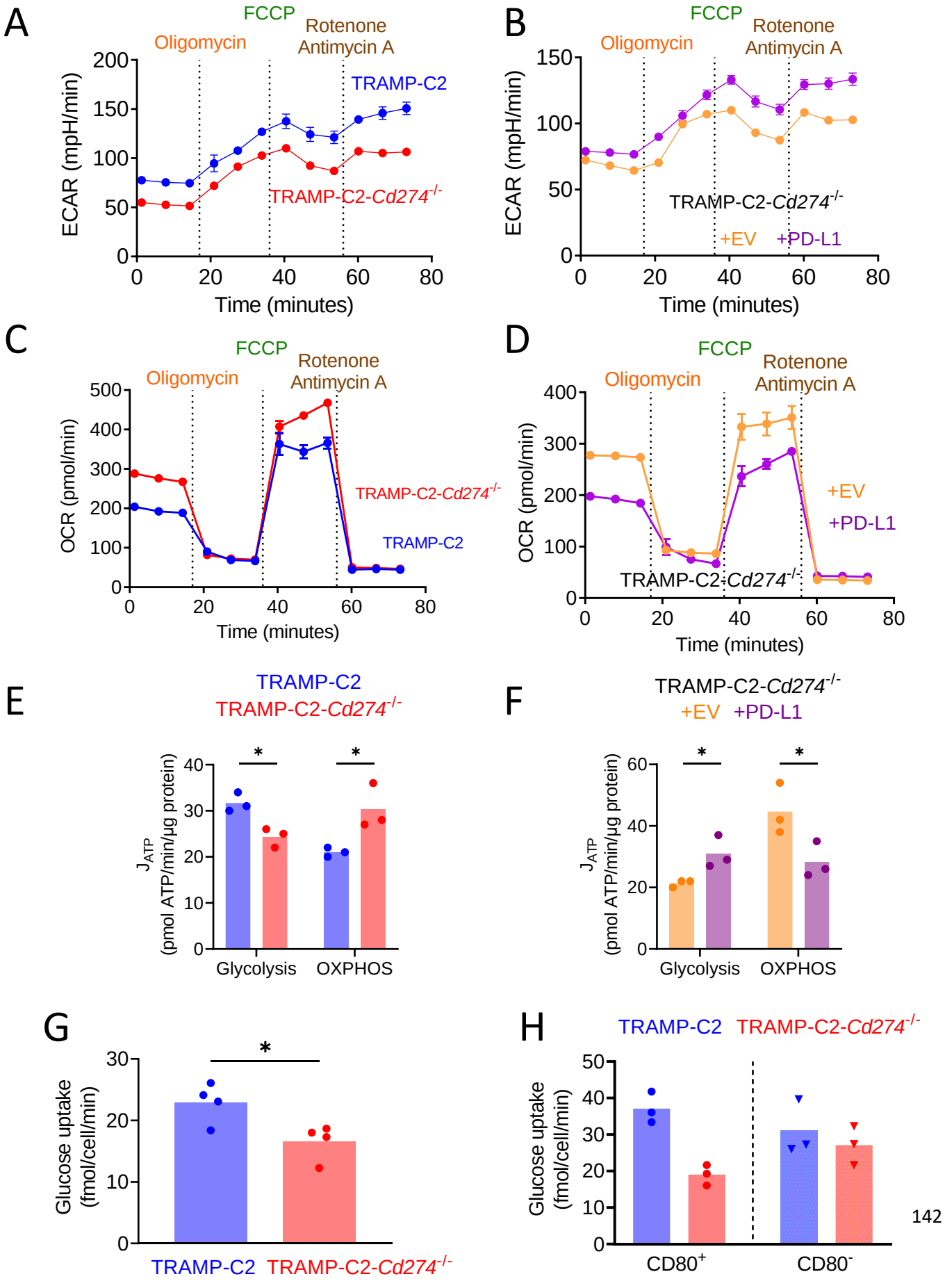
A
FCCP
Oligomycin
Rotenone
Antimycin A
TRAMP-C2
TRAMP-C2-Cd274-/-
ECAR (mpH/min)
Time (minutes)
B
FCCP
Oligomycin
Rotenone
Antimycin A
TRAMP-C2-Cd274-/-
+EV
+PD-L1
ECAR (mpH/min)
Time (minutes)
C
FCCP
Oligomycin
Rotenone
Antimycin A
TRAMP-C2-Cd274-/-
TRAMP-C2
OCR (pmol/min)
Time (minutes)
D
FCCP
Oligomycin
Rotenone
Antimycin A
+EV
+PD-L1
TRAMP-C2-Cd274-/-
OCR (pmol/min)
Time (minutes)
E
TRAMP-C2
TRAMP-C2-Cd274-/-
JATP (pmol ATP/min/µg protein)
Glycolysis
OXPHOS
F
TRAMP-C2-Cd274-/-
+EV
+PD-L1
JATP (pmol ATP/min/µg protein)
Glycolysis
OXPHOS
G
Glucose uptake (fmol/cell/min)
TRAMP-C2
TRAMP-C2-Cd274-/-
H
TRAMP-C2
TRAMP-C2-Cd274-/-
Glucose uptake (fmol/cell/min)
CD80+
CD80-

Figure 4.14. PD-L1 promotes glycolysis and glucose uptake, while inhibiting mitochondrial respiration. (**A-D**) Seahorse metabolic flux analysis on TRAMP-C2, TRAMP-C2 *Cd274*$^{-/-}$, TRAMP-C2 *Cd274*$^{-/-}$ + EV, and TRAMP-C2 *Cd274*$^{-/-}$ + PD-L1 (tested in n=6 technical replicates). Extracellular acidification rate (ECAR) and oxygen consumption rate (OCR) are measures of glycolysis and mitochondrial respiration, respectively. Images depicted are representative of 3 biological replicates with similar results. (**E-F**) Bioenergetic calculations based on Seahorse metabolic flux assay. N=3 biological replicates. (**G-H**) Glucose uptake was measured in TRAMP-C2 and TRAMP-C2 *Cd274*$^{-/-}$ cells (**G**), as well as CD80^{+} vs CD80^{-} cells FACS-isolated from TRAMP-C2 or TRAMP-C2 *Cd274*$^{-/-}$ cells (**H**). The experiments depicted are representative of 3 biological replicates performed with similar results. Statistical analysis by two-way ANOVA with Šídák's correction for multiple comparisons.

We confirmed the metabolic flux analysis with an unbiased metabolomics study, in order to assess the impact of PD-L1 on cell metabolism in a more comprehensive fashion. Approximately 100 water-soluble metabolites were quantified from both parental and PD-L1-deficient TRAMP-C2 cells. PD-L1 significantly altered the abundance of 52 of these metabolites (Figure 4.15A and Appendix II). As expected, several glycolysis metabolites had increased abundance in parental TRAMP-C2 compared to TRAMP-C2 *Cd274*$^{-/-}$ cells, including hexose sugars, fructose-1,6-bisphosphate, dihydroxyacetone phosphate, pyruvate, and lactate (Figure 4.15B). Interestingly, the concentrations of these same metabolites have previously been shown to be reliable indicators of glycolysis rates (*272*), in line with our previous data.

A

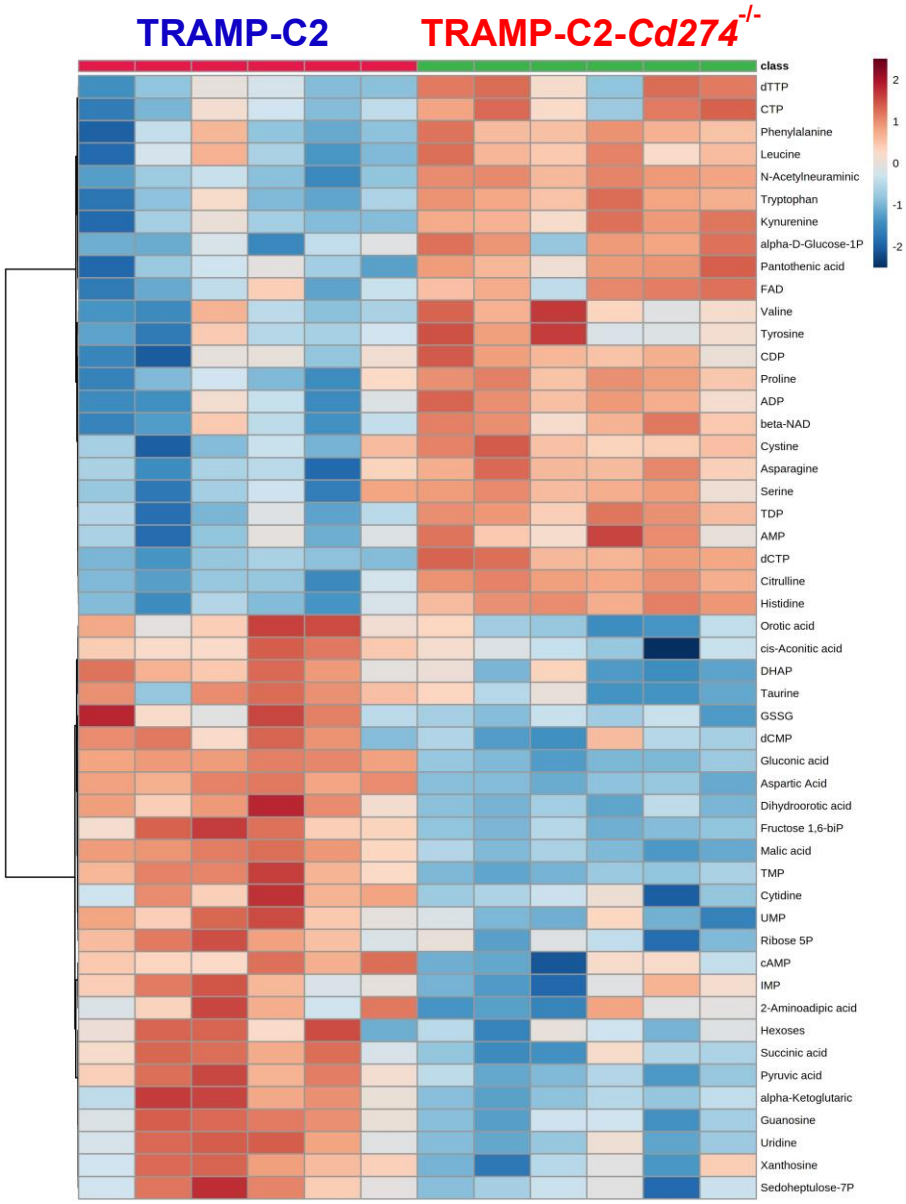
TRAMP-C2
TRAMP-C2-Cd274-/-
class
dTTP
CTP
Phenylalanine
Leucine
N-Acetylneuraminic
Tryptophan
Kynurenine
alpha-D-Glucose-1P
Pantothenic acid
FAD
Valine
Tyrosine
CDP
Proline
ADP
beta-NAD
Cystine
Asparagine
Serine
TDP
AMP
dCTP
Citrulline
Histidine
Orotic acid
cis-Aconitic acid
DHAP
Taurine
GSSG
dCMP
Gluconic acid
Aspartic Acid
Dihydroorotic acid
Fructose 1,6-biP
Malic acid
TMP
Cytidine
UMP
Ribose 5P
cAMP
IMP
2-Aminoadipic acid
Hexoses
Succinic acid
Pyruvic acid
alpha-Ketoglutaric
Guanosine
Uridine
Xanthosine
Sedoheptulose-7P
2
1
0
-1
-2

B

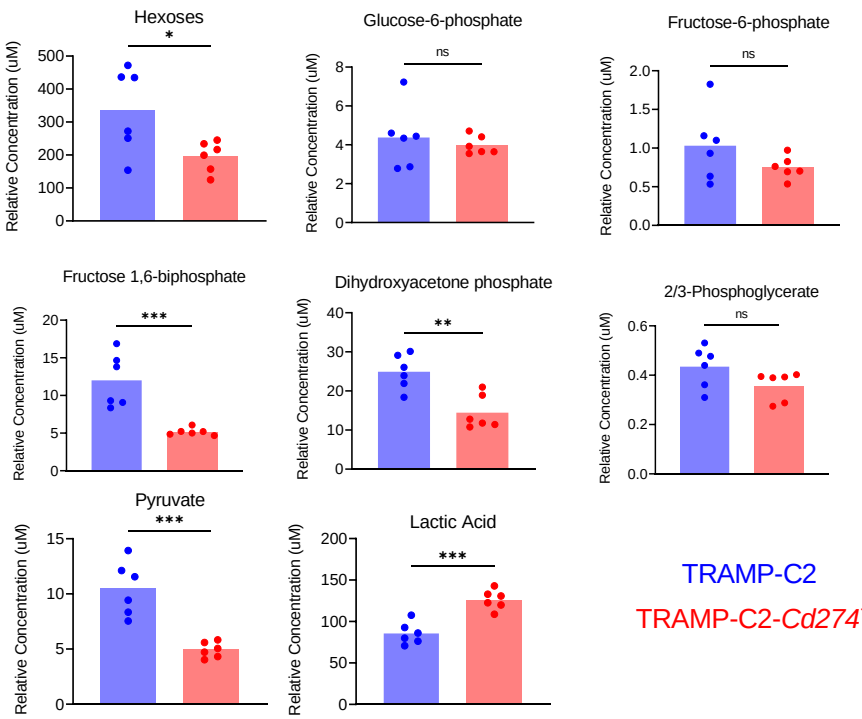
Hexoses
*
Glucose-6-phosphate
ns
Fructose-6-phosphate
ns
Fructose 1,6-biphosphate
***
Dihydroxyacetone phosphate
**
2/3-Phosphoglycerate
ns
Pyruvate
***
Lactic Acid
***
Relative Concentration (uM)
TRAMP-C2
TRAMP-C2-Cd274-/-

Figure 4.15. PD-L1 modulates the cancer cell metabolome. (**A**) Hierarchical clustered heat map depicting relative abundance of 50 metabolites quantified in untargeted metabolomics of TRAMP-C2 and TRAMP-C2 *Cd274*$^{-/-}$ cell lysates. 6 biological replicates per cell line are shown. (**B**) Relative abundance of glycolysis metabolites in TRAMP-C2 and TRAMP-C2 *Cd274*$^{-/-}$ cells, measured in the untargeted metabolomics study. 6 biological replicates per cell line. Statistical analysis by unpaired two-tailed Student's t-test.

Metabolic analysis of cells in culture is highly prone to artifacts due to the non-physiological conditions of typical in vitro culture, including (but not limited to) media composition and oxygen levels. Therefore, we verified that PD-L1 promotes glycolysis in vivo as well as in vitro, using [^{18}F]-fluorodeoxyglucose PET scanning, or [^{18}F]-FDG PET, on immunodeficient mice bearing TRAMP-C2 subcutaneous tumours. [^{18}F]-FDG PET is a clinical imaging method that employs a radiolabeled glucose analog that accumulates in highly glycolytic tissues, including tumours. When tumour-bearing mice were subjected to [^{18}F]-FDG PET, TRAMP-C2 tumours displayed significantly more [^{18}F]-FDG uptake compared to TRAMP-C2 *Cd274*$^{-/-}$ tumours (Figure 4.16A-B), consistent with our in vitro data. Tumour mass were equivalent between the two groups (Figure 4.16C).

Therefore, PD-L1 promotes glycolysis and glucose uptake and inhibits mitochondrial respiration. We next investigated if this PD-L1-driven metabolic shift plays a role in OV infection and inhibition of the type I interferon pathway.

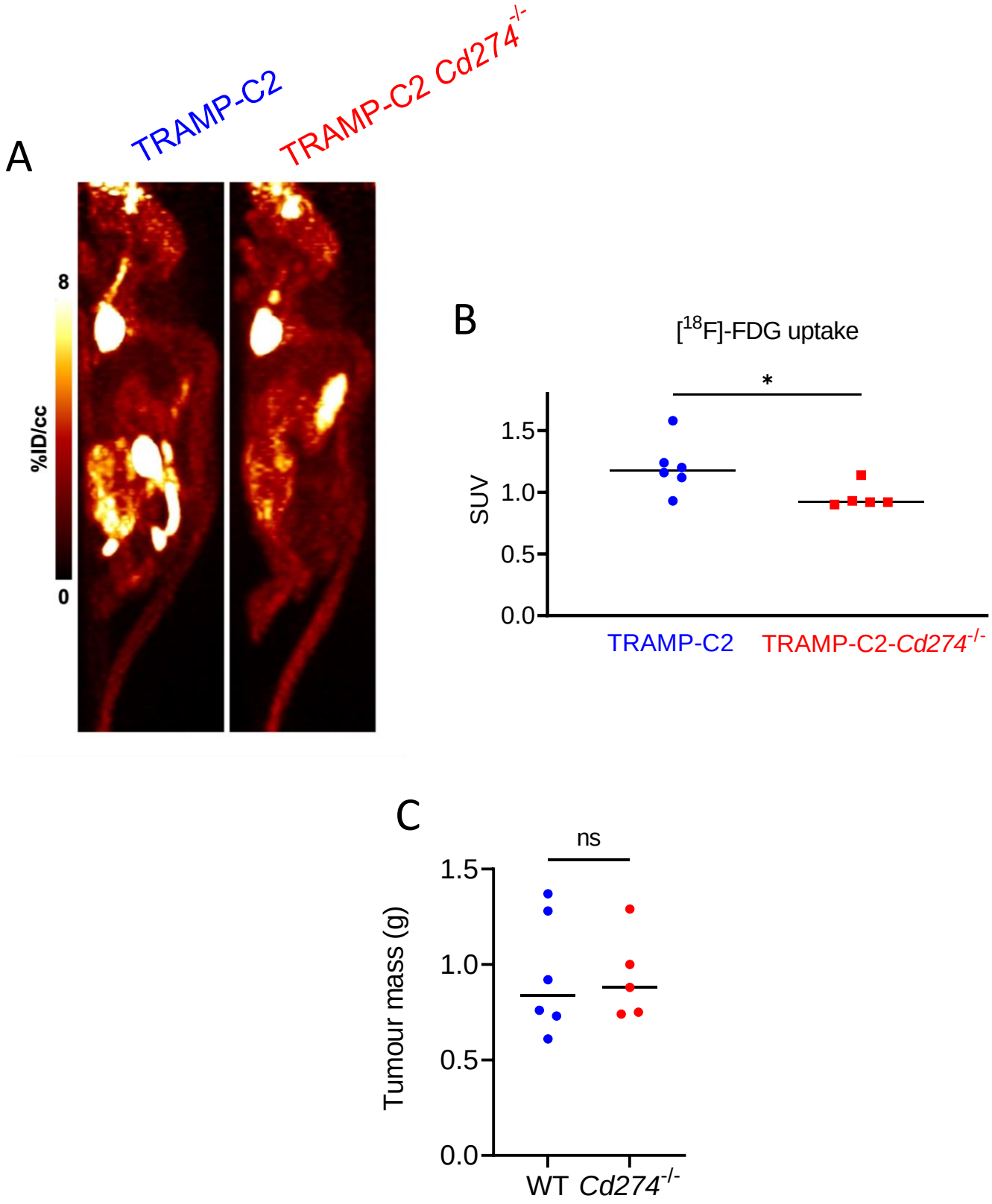
A
TRAMP-C2
TRAMP-C2 Cd274-/-
8
%ID/cc
0
B
[18F]-FDG uptake
*
SUV
1.5
1.0
0.5
0.0
TRAMP-C2
TRAMP-C2-Cd274-/-
C
ns
Tumour mass (g)
1.5
1.0
0.5
0.0
WT
Cd274-/-

Figure 4.16. PD-L1 promotes [^{18}F]-fluorodeoxyglucose uptake in vivo. Male NCG mice were implanted with subcutaneous TRAMP-C2 or TRAMP-C2-Cd274-/- tumours. Standardized uptake value (SUV) of [^{18}F]-fluorodeoxyglucose was assessed by PET imaging. Representative images displayed (**A**), with quantification of SUV in (**B**) and tumour masses in (**C**). Statistical analyses by two-tailed unpaired Student's t test.

4.5. PD-L1 relies on glycolytic metabolism to promote OV infection and inhibit type I interferons

It is well-recognized that metabolism is an important and potent regulator of inflammation and inflammatory pathways, and the type I interferon pathway is no exception. Glycolysis and particular metabolites generated by glycolysis reactions have been shown to modulate type I interferon signaling and cellular anti-viral responses. Therefore, we hypothesized that PD-L1 inhibits type I interferons and promotes OV infection via glycolysis.

To test our hypothesis that glycolysis is critical to PD-L1 function, we initially conducted studies using the glucose analog 2-deoxyglucose (2-DG) to inhibit glycolysis prior to VSVΔ51 infection (*273*). Treatment with 2-DG and inhibition of glycolysis ablated differences in viral infection between parental TRAMP-C2 and TRAMP-C2 *Cd274*$^{-/-}$ cells (Figure 4.17), suggesting that glycolysis is linked with PD-L1 function.

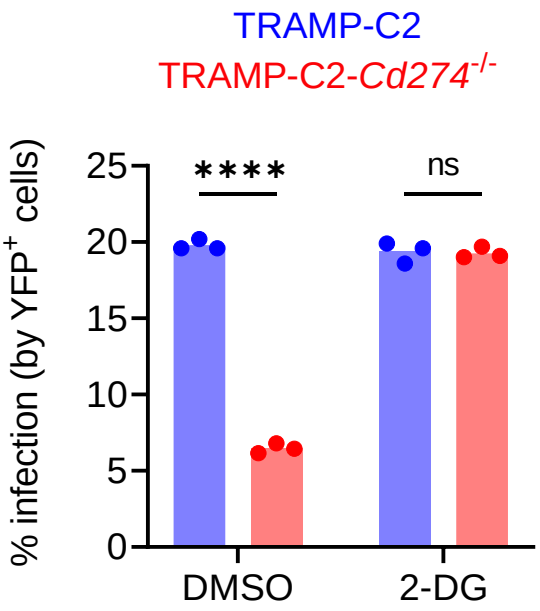
TRAMP-C2
TRAMP-C2-Cd274-/-
% infection (by YFP+ cells)
25
20
15
10
5
0
****
ns
DMSO
2-DG

Figure 4.17. Glycolysis is necessary for PD-L1 function. TRAMP-C2 and TRAMP-C2 *Cd274*$^{-/-}$ cells were pre-treated with 2-deoxy-D-glucose (2-DG) at 1.25 mM for 24 hours (or DMSO as vehicle control) prior to infection with VSVΔ51-YFP at MOI 0.1 for 24 hours. Infection was assessed by flow cytometry for viral YFP reporter expression. Experiment depicted is representative of 3 biological replicates with similar results. Statistical analysis by two-way ANOVA with Šídák's correction for multiple comparisons.

Previous studies have shown that PD-L1 regulates glycolysis via promotion of mTOR activity (*68*). We tested whether there is a role for mTOR in PD-L1 function (in this context) by inhibiting the function of mTORC1 and mTORC2 complexes with the inhibitor Torin1 (*274*). Pre-treatment with Torin1 followed by VSVΔ51 infection did not alter the ability of PD-L1 to promote OV infection (Figure 4.18A). Furthermore, there was no difference in the phosphorylation of S6K and 4E-BP1, two markers of mTORC1 function, nor phosphorylation of Akt, a marker of mTORC2 function, between parental TRAMP-C2 and TRAMP-C2 *Cd274*$^{-/-}$ cells (Figure 4.18B). These data suggest that PD-L1 does not influence mTOR activity in TRAMP-C2 cells, and that this metabolic sensor does not play a role in PD-L1 function in this particular context.

A

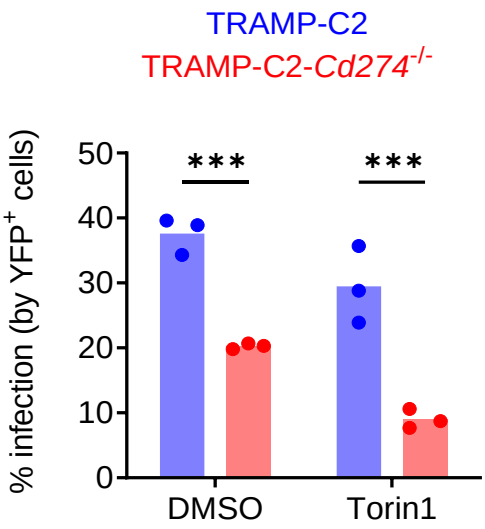
TRAMP-C2
TRAMP-C2-Cd274-/-
% infection (by YFP+ cells)
50
40
30
20
10
0
***
***
DMSO
Torin1

B

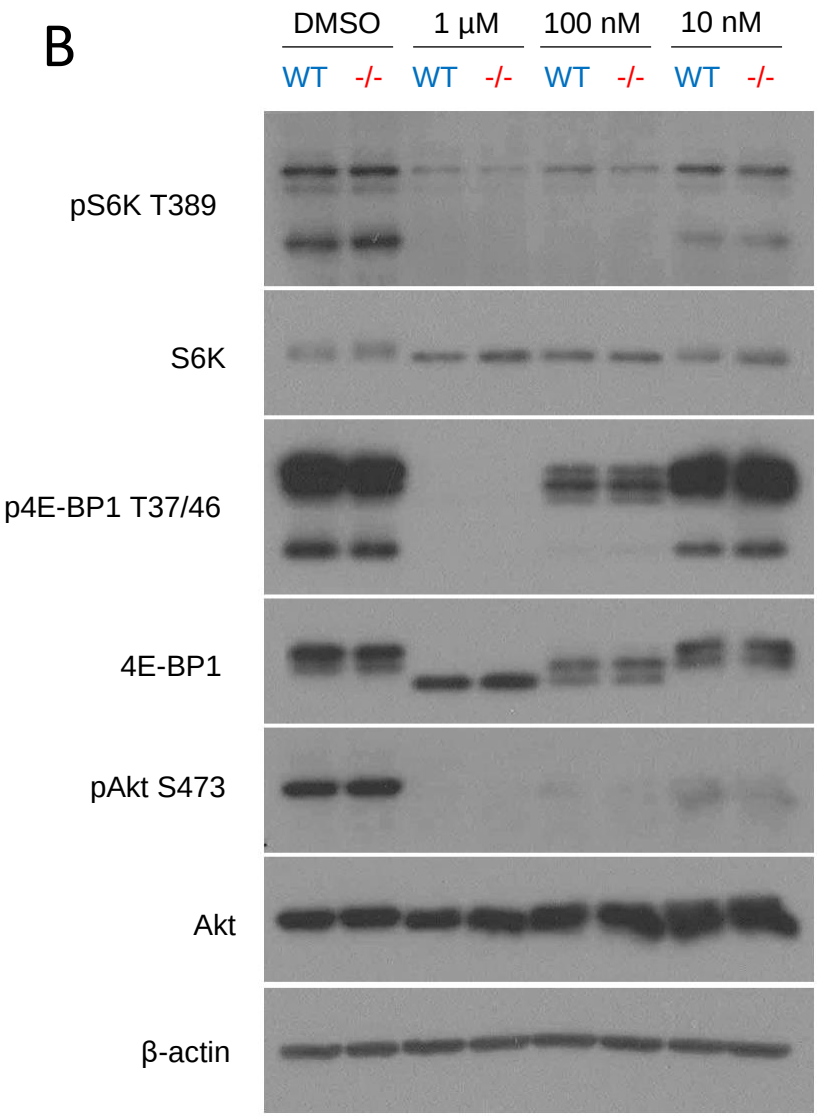
DMSO
1 µM
100 nM
10 nM
WT -/- WT -/- WT -/- WT -/-
pS6K T389
S6K
p4E-BP1 T37/46
4E-BP1
pAkt S473
Akt
β-actin

Figure 4.18. mTOR is not involved in PD-L1-mediated promotion of OV infection. (**A**) TRAMP-C2 and TRAMP-C2 *Cd274*$^{-/-}$ cells were pre-treated with Torin1 at 100 nM for 24 hours (or DMSO as vehicle control) prior to infection with VSVΔ51-YFP at MOI 0.1 for 24 hours. Infection was assessed by flow cytometry for viral YFP reporter expression. Experiment depicted is representative of 2 biological replicates with similar results. Statistical analysis by two-way ANOVA with Šídák's correction for multiple comparisons. (**B**) TRAMP-C2 and TRAMP-C2 *Cd274*$^{-/-}$ cells were pre-treated with Torin1 at indicated concentrations for 24 hours (or DMSO as vehicle control) prior to analysis by western blotting. Images presented are representative of 2 biological replicates.

Recent literature has suggested that lactate produced from glycolysis blocks activation of the type I interferon in response to RNA virus infection, including VSV (*275*). Therefore, we hypothesized that lactate from glycolysis is a key molecule used by PD-L1 to inhibit the type I interferon pathway and promote OV infection. First, we confirmed that TRAMP-C2 cells generated more lactate in the culture media in comparison to TRAMP-C2 *Cd274*$^{-/-}$ cells (Figure 4.19A, Basal). To address the hypothesis that lactate was critical for PD-L1 function, TRAMP-C2 cells were treated with two structurally distinct inhibitors of lactate dehydrogenase (LDH), the enzyme that generates lactate. Treatment with either of these two inhibitors (sodium oxamate or GNE-140) decreased lactate concentrations to undetectable levels (Figure 4.19A). Consistent with our hypothesis, LDH inhibition and removal of lactate from the culture eliminated PD-L1 function, as there was no longer any difference in VSVΔ51 infection between TRAMP-C2 and TRAMP-C2 *Cd274*$^{-/-}$ cells and PD-L1 could no longer promote infection (Figure 4.19B-C). Conversely, treatment with lactate itself was able to mimic the effects of PD-L1 on OV infection (Figure 4.19D). Along a similar vein, treatment with the respiratory inhibitor oligomycin, which causes a compensatory increase in glycolysis and lactate production (Figure 4.19A), phenocopied PD-L1 function on OV infection (Figure 4.19E).

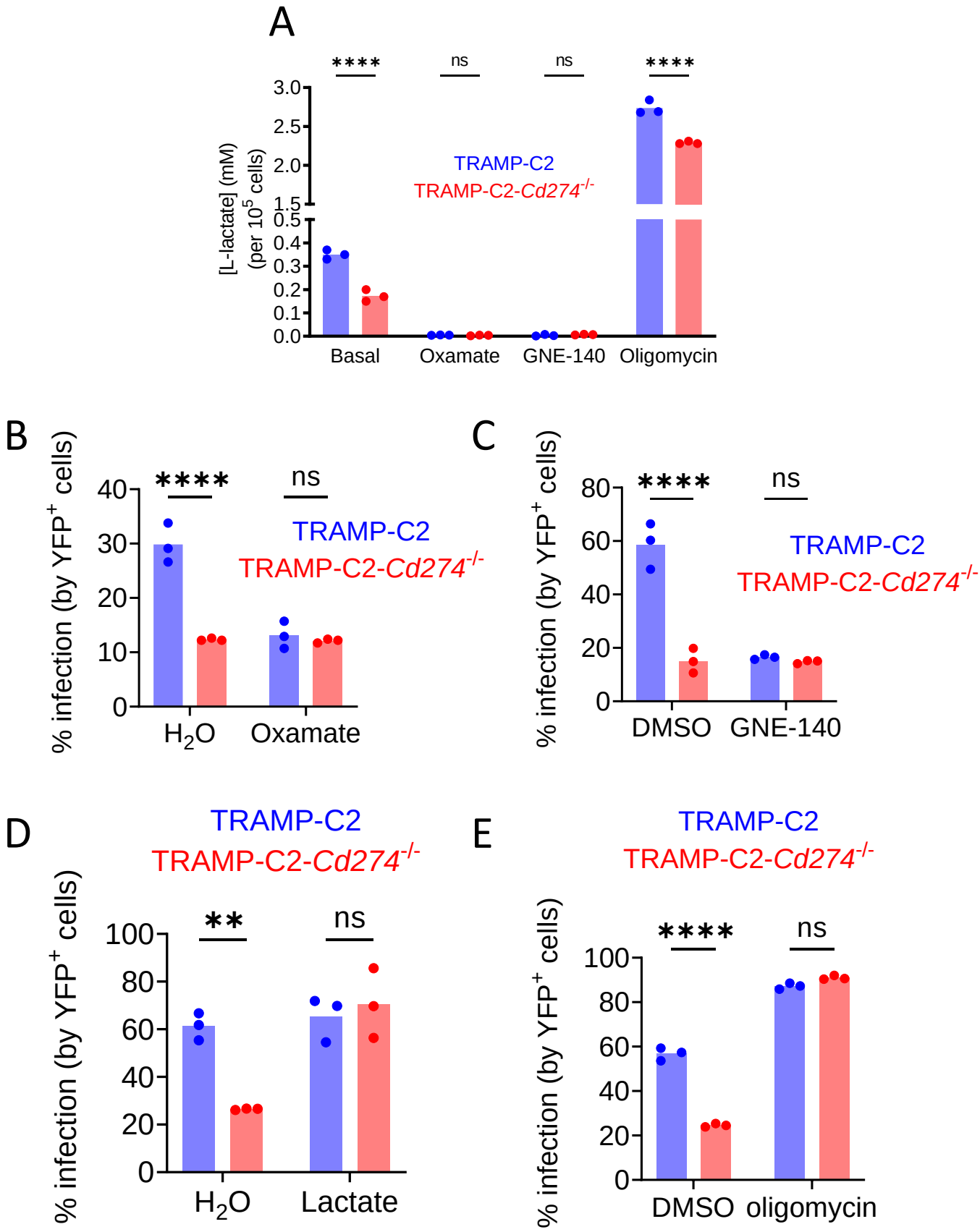
A
****
ns
ns
****
[L-lactate] (mM) (per 10^5 cells)
3.0
2.5
2.0
1.5
0.5
0.4
0.3
0.2
0.1
0.0
TRAMP-C2
TRAMP-C2-Cd274-/-
Basal
Oxamate
GNE-140
Oligomycin
B
% infection (by YFP+ cells)
****
ns
40
30
20
10
0
TRAMP-C2
TRAMP-C2-Cd274-/-
H2O
Oxamate
C
% infection (by YFP+ cells)
****
ns
80
60
40
20
0
TRAMP-C2
TRAMP-C2-Cd274-/-
DMSO
GNE-140
D
TRAMP-C2
TRAMP-C2-Cd274-/-
% infection (by YFP+ cells)
**
ns
100
80
60
40
20
0
H2O
Lactate
E
TRAMP-C2
TRAMP-C2-Cd274-/-
% infection (by YFP+ cells)
****
ns
100
80
60
40
20
0
DMSO
oligomycin

Figure 4.19. PD-L1 requires lactate to promote OV infection. (**A**) Lactate quantification in TRAMP-C2 culture supernatant in basal/untreated state, or after 24 hours of sodium oxamate (10 mM), GNE-140 (10 μM), or oligomycin (0.2 μM) treatment. N=3 biological replicates. Statistical analysis by two-way ANOVA with Šídák's correction for multiple comparisons. (**B-E**) TRAMP-C2 and TRAMP-C2 *Cd274*$^{-/-}$ cells were pre-treated with sodium oxamate at 10 mM (**B**); GNE-140 at 10 μM (**C**); lactate at 5 mM (**D**); oligomycin at 0.2 μM (**E**) for 24 hours, followed by infection with VSVΔ51-YFP at MOI 0.1 for 24 hours prior to analysis by flow cytometry. Experiments depicted are representative of 3 biological replicates performed with similar results. Statistical analysis by two-way ANOVA with Šídák's correction for multiple comparisons.

Importantly, treatment with these molecules (2-DG, lactate, oligomycin, GNE-140) did not lead to loss of PD-L1 expression (Figure 4.20), indicating that their effect on OV infection was not caused by down-regulation of PD-L1.

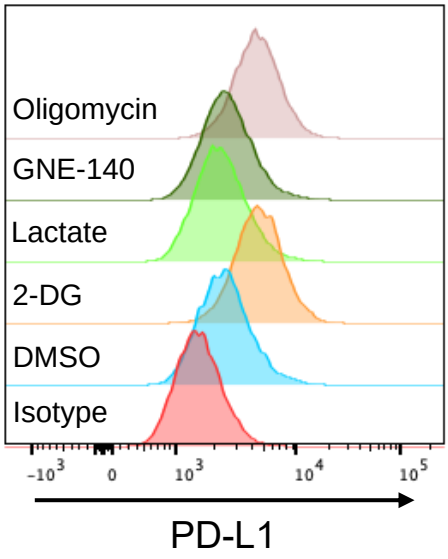
Oligomycin
GNE-140
Lactate
2-DG
DMSO
Isotype
-10^3
0
10^3
10^4
10^5
PD-L1

Figure 4.20. Metabolic inhibitors do not reduce PD-L1 expression in TRAMP-C2 cells. TRAMP-C2 cells were treated 2-DG (1.25 mM), sodium lactate (5 mM), GNE-140 (10 μM), oligomycin (0.2 μM), or DMSO for 24 hours prior to flow cytometry assessment of surface PD-L1 expression. Representative flow plots of N=2 biological replicates.

Lastly, we tested if lactate is responsible for the inhibition of type I interferon responses by PD-L1. TRAMP-C2 cells were pre-treated with equivalent concentrations of lactate, which resulted in a normalization of the type I interferon response (at the transcript level) between TRAMP-C2 and TRAMP-C2 *Cd274*$^{-/-}$ cells after VSVΔ51 infection (Figure 4.21A). Additionally, lactate normalized levels of STAT1 between TRAMP-C2 and TRAMP-C2 *Cd274*$^{-/-}$ cells, which is otherwise regulated by PD-L1 in these cells (Figure 4.21B).

Therefore, PD-L1 inhibits type I interferons and promotes OV infection via a metabolic shift that involves promotion of glycolysis and lactate production.

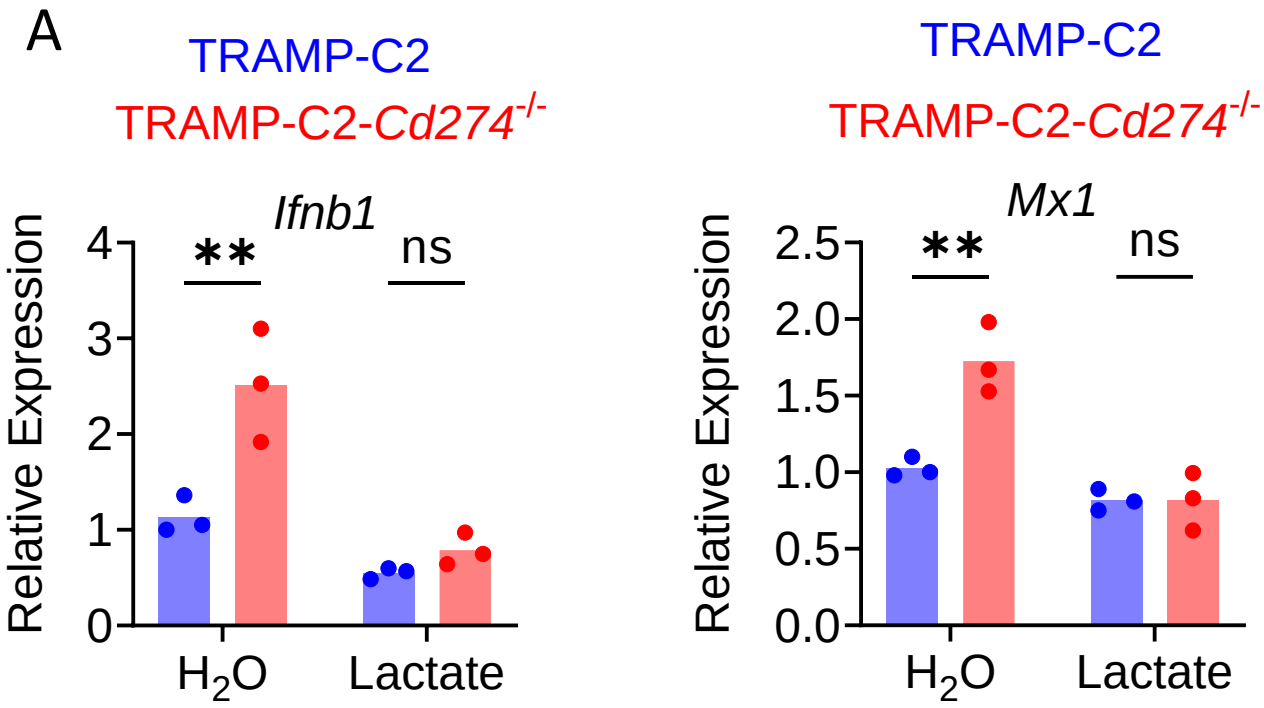
A
TRAMP-C2
TRAMP-C2-Cd274-/-
Ifnb1
Relative Expression
**
ns
H2O
Lactate
TRAMP-C2
TRAMP-C2-Cd274-/-
Mx1
Relative Expression
**
ns
H2O
Lactate

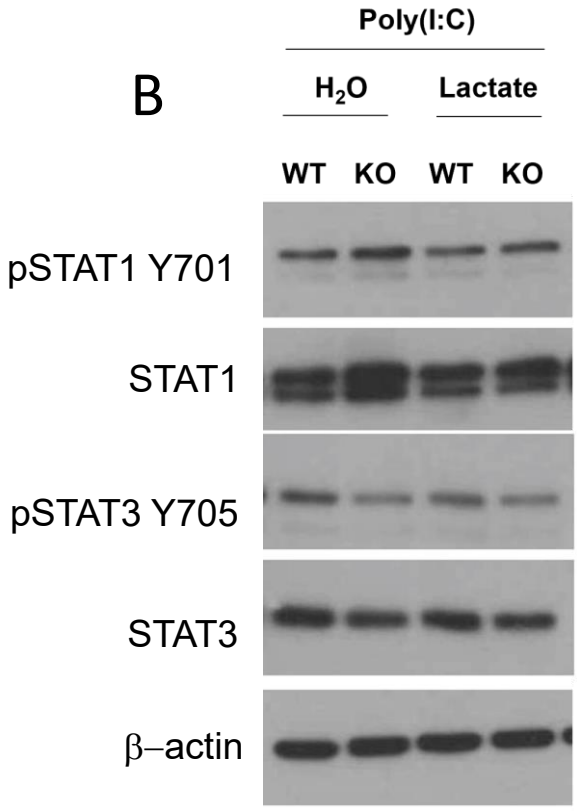
B
Poly(I:C)
H2O
Lactate
WT
KO
WT
KO
pSTAT1 Y701
STAT1
pSTAT3 Y705
STAT3
β–actin

Figure 4.21. PD-L1 inhibits the type I interferon pathway via lactate dynamics. (**A**) TRAMP-C2 and TRAMP-C2 *Cd274*$^{-/-}$ cells were pre-treated with lactate at 5 mM for 24 hours, followed by infection with VSVΔ51-YFP at MOI 0.1 for 8 hours prior to qPCR analysis for *Ifnb1* and *Mx1*. N=3 biological replicates. Statistical analysis by two-way ANOVA with Šídák's correction for multiple comparisons. (**B**) TRAMP-C2 and TRAMP C2-*Cd274*$^{-/-}$ cells were pre-treated with lactate at 5 mM for 24 hours, followed by transfection with poly(I:C) for 6 hours prior to western blotting analysis. Images depicted are representative of 3 biological replicates with similar results.

Chapter 5

PD-L1 has context-specific function.

5.1 Introduction and Rationale

So far, we have examined PD-L1 function in one murine prostate cancer cell line (TRAMP-C2). We next asked if PD-L1 function is specific to this cell line, or if PD-L1 enhancing OV infection is broadly applicable to other cell types. To answer this question, we sought to extend our investigation into other cancer cell types and expand into human cells, including primary patient samples.

Certainly, in the literature, it has been shown that PD-L1 impacts cell biology in diverse cancer cell types, as well as different immune cells. However, the proposed roles of PD-L1 in these different contexts rarely overlaps with other cell types, suggesting that PD-L1 biology has a degree of specificity, with as-of-yet undetermined mechanism(s). The specificity of PD-L1 function could be driven by differences in cellular context (such as cellular metabolism and/or mutational status) or tissue context.

5.2. PD-L1 does not impact OV infection in several murine cancer cell lines

We began by testing a panel of murine cancer cell lines (B16-BL6, MB49, YUMM1.1, C1498, MC38) commonly used in OV and immunotherapy research, all of which are known to express PD-L1. For all these lines, PD-L1 was deleted using CRISPR/Cas9. Parental and *Cd274*$^{-/-}$ cells for each of these cell lines were subsequently infected with VSVΔ51 at a range of MOIs. Surprisingly, deletion of PD-L1 had no impact on VSVΔ51 infection in these cell lines (Figure 5.1).

Parental *Cd274*$^{-/-}$

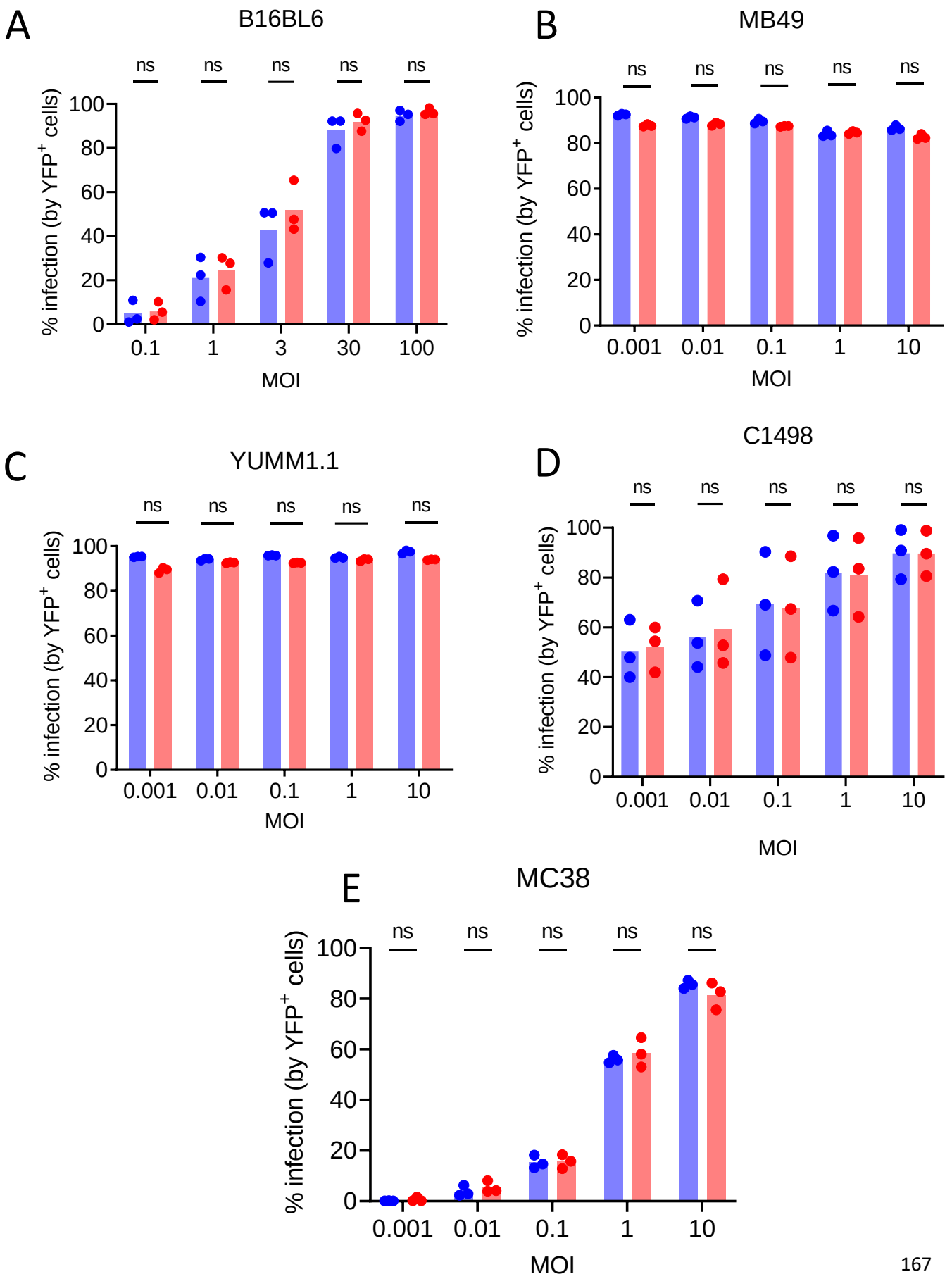

Figure 5.1. PD-L1 does not impact OV infection in a panel of murine cancer cell lines. (**A-E**) B16BL6 (**A**), MB49 (**B**), YUMM1.1 (**C**), C1498 (**D**), and MC38 (**E**) parental and *Cd274*$^{-/-}$ cells were infected with VSVΔ51-YFP at indicated MOIs for 24 hours prior to analysis by flow cytometry. N=3 biological replicates depicted. Statistical analysis by two-way ANOVA with Šídák's correction for multiple comparisons.

The expression of CD80 was examined in these cell lines since we previously showed in TRAMP-C2 cells that CD80 acts as an endogenous trigger for PD-L1 to enhance OV infection and induce metabolic changes. Both YUMM1.1 and MB49 cell lines express CD80 in a sub-clonal fashion (similar to TRAMP-C2), while B16BL6, C1498, and MC38 do not express surface CD80 (Figure 5.2). Therefore, in two of the five cell lines tested, PD-L1 does express the necessary binding partner (CD80), but in these cells PD-L1 does not modulate OV infection.

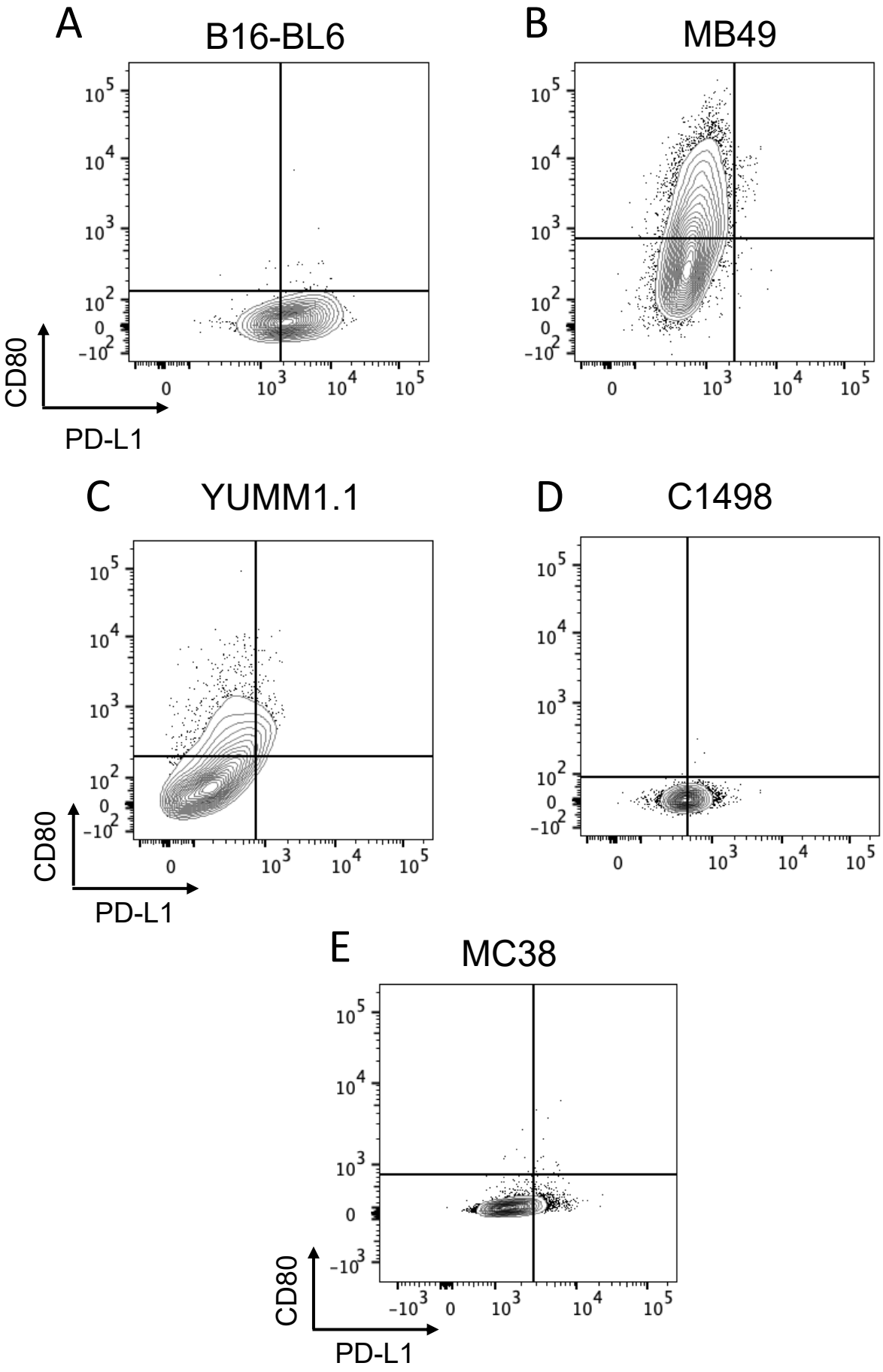
A
B16-BL6
B
MB49
C
YUMM1.1
D
C1498
E
MC38
CD80
PD-L1

Figure 5.2. CD80 and PD-L1 expression in panel of murine cancer cell lines. (**A-E**) B16BL6 (**A**), MB49 (**B**), YUMM1.1 (**C**), C1498 (**D**), and MC38 (**E**) cells were stained for surface CD80 and PD-L1. Representative flow plots of N=2 biological replicates.

5.3. PD-L1 expression correlates with glycolysis gene set scores

Since B16BL6, YUMM1.1, MB49, MC38, and C1498 were chosen based on their prevalence in the cancer immunology literature rather than any underlying biological reasoning, we developed a strategy to more rationally select cell types to assess PD-L1 function. Given that we have shown PD-L1 inhibits the type I interferon pathway and promotes OV infection via glycolysis, we attempted to choose cell lines based on their metabolic properties.

We made use of a publicly available dataset consisting of bulk RNA-seq of 675 human cell lines. In these cell lines, we scored PD-L1 (*CD274*) expression and expression of genes included in the Glycolysis Gene Set, which includes glycolysis and other metabolic enzymes (Figure 5.3). Interestingly, this analysis shows that cells with higher scoring for the Glycolysis Gene Set tend to have higher expression of PD-L1 (Figure 5.3), although it was not possible to determine cause and effect from such a dataset.

We chose two cell lines that score highly for the Glycolysis Gene Set, but with differing expression of PD-L1 – the gastric carcinoma line Hs746 and the renal cell carcinoma line 786-0. We anticipated that in these cells, PD-L1 may promote glycolysis, and therefore might also inhibit type I interferons and promote OV infection.

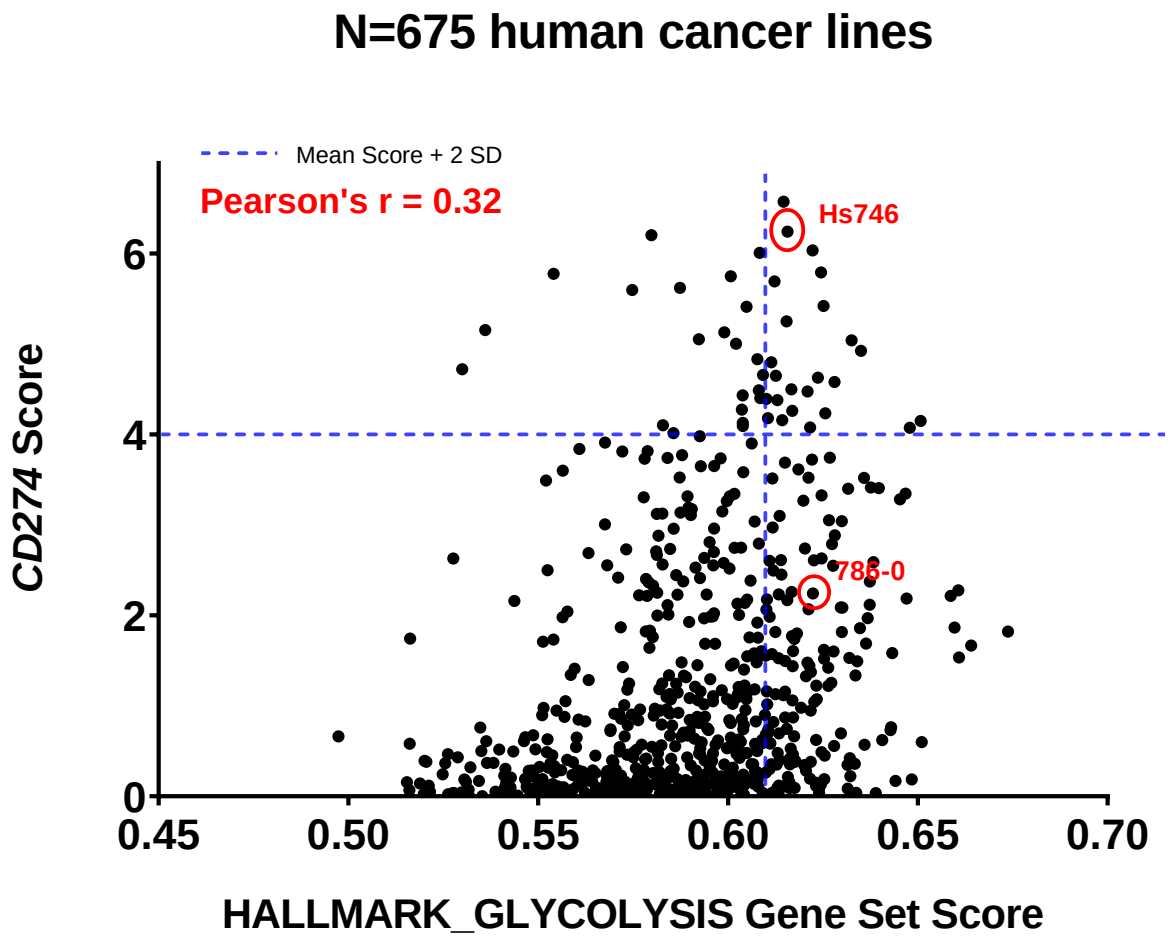
N=675 human cancer lines
Mean Score + 2 SD
Pearson's r = 0.32
Hs746
786-0
CD274 Score
0
2
4
6
0.45
0.50
0.55
0.60
0.65
0.70
HALLMARK_GLYCOLYSIS Gene Set Score

Figure 5.3. PD-L1 expression and glycolysis gene set scoring of human cell lines. Bioinformatic analysis of publicly available RNA-seq from 675 human cancer cell lines, scored for their expression of PD-L1 (*CD274*) and glycolysis gene signatures. Blue lines on plot indicate mean + 2 SD; Pearson correlation coefficient is indicated.

PD-L1 expression was deleted in both cell lines using CRISPR/Cas9 (Figure 5.4A-B), and both parental and *CD274*$^{-/-}$ cells were subjected to VSVΔ51 at a range of MOIs. Similar to TRAMP-C2, PD-L1 deletion reduced OV infection (Figure 5.4C-D), suggesting that PD-L1 does promote OV infection in these two human cancer cell lines.

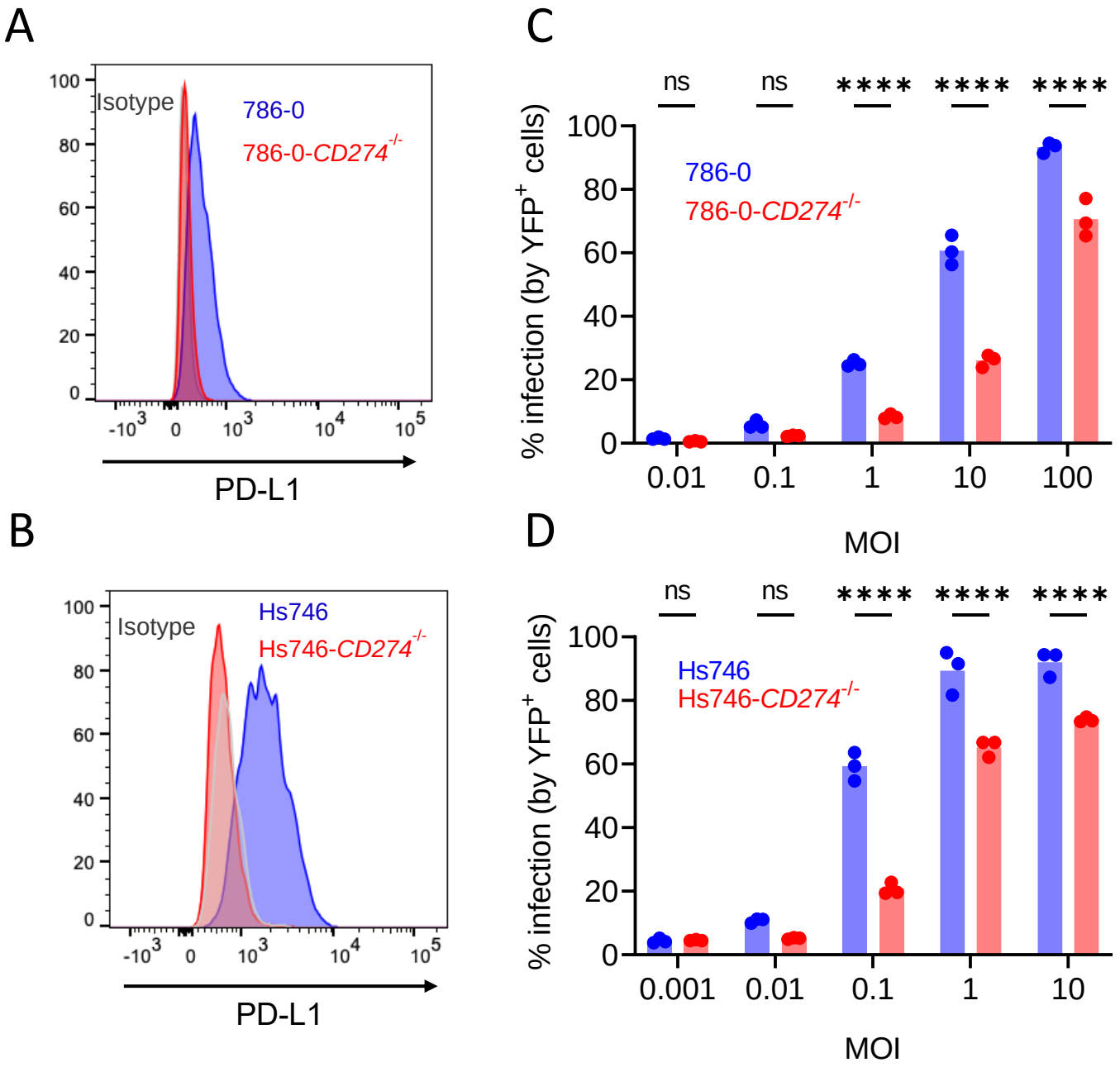
A
Isotype
786-0
786-0-CD274-/-
PD-L1
B
Isotype
Hs746
Hs746-CD274-/-
PD-L1
C
ns
ns
****
****
****
786-0
786-0-CD274-/-
% infection (by YFP+ cells)
MOI
D
ns
ns
****
****
****
Hs746
Hs746-CD274-/-
% infection (by YFP+ cells)
MOI

Figure 5.4. PD-L1 promotes OV infection in 786-0 and Hs746 cell lines. (**A-B**) 786-0 (**A**) and Hs746 (**B**) cells were electroporated with Cas9 and gRNA targeting PD-L1 to generate *CD274*$^{-/-}$ cells. Representative plots depicting PD-L1 expression are shown. (**C-D**) 786-0 (**C**) and Hs746 (**D**) parental and *CD274*$^{-/-}$ cells were infected with VSVΔ51-YFP at indicated MOIs for 24 hours prior to analysis by flow cytometry. Experiments depicted are representative of 3 biological replicates performed with similar results. Statistical analysis by two-way ANOVA with Šídák's correction for multiple comparisons.

5.4. PD-L1 inhibits the type I interferon pathway and promotes OV infection via lactate in Hs746 and 786-0

We next investigated if the mechanism of PD-L1-mediated OV enhancement was similar between TRAMP-C2 and Hs746 and 786-0. We examined the type I interferon pathway in Hs746 and Hs746 *CD274*$^{-/-}$ cells and 786-0 and 786-0 *CD274*$^{-/-}$ cells, in both mock-infected and VSVΔ51-infected conditions. Consistent with our previous findings, PD-L1 inhibited production of IFN-β and downstream ISGs (Figure 5.5A, C) in both the mock-infected and VSVΔ51-infected state. Additionally, PD-L1 modulated signaling downstream of the type I interferon receptor in both cell lines, to varying extents (Figure 5.5). In Hs746, PD-L1 inhibited phosphorylation of IRF-3, decreased levels of STAT1, and inhibited STAT3 phosphorylation at Tyr705 (Figure 5.5B). In 786-0 the impact of PD-L1 on signaling was far more modest, with PD-L1 inhibiting STAT1 phosphorylation at Tyr701 (Figure 5.5D).

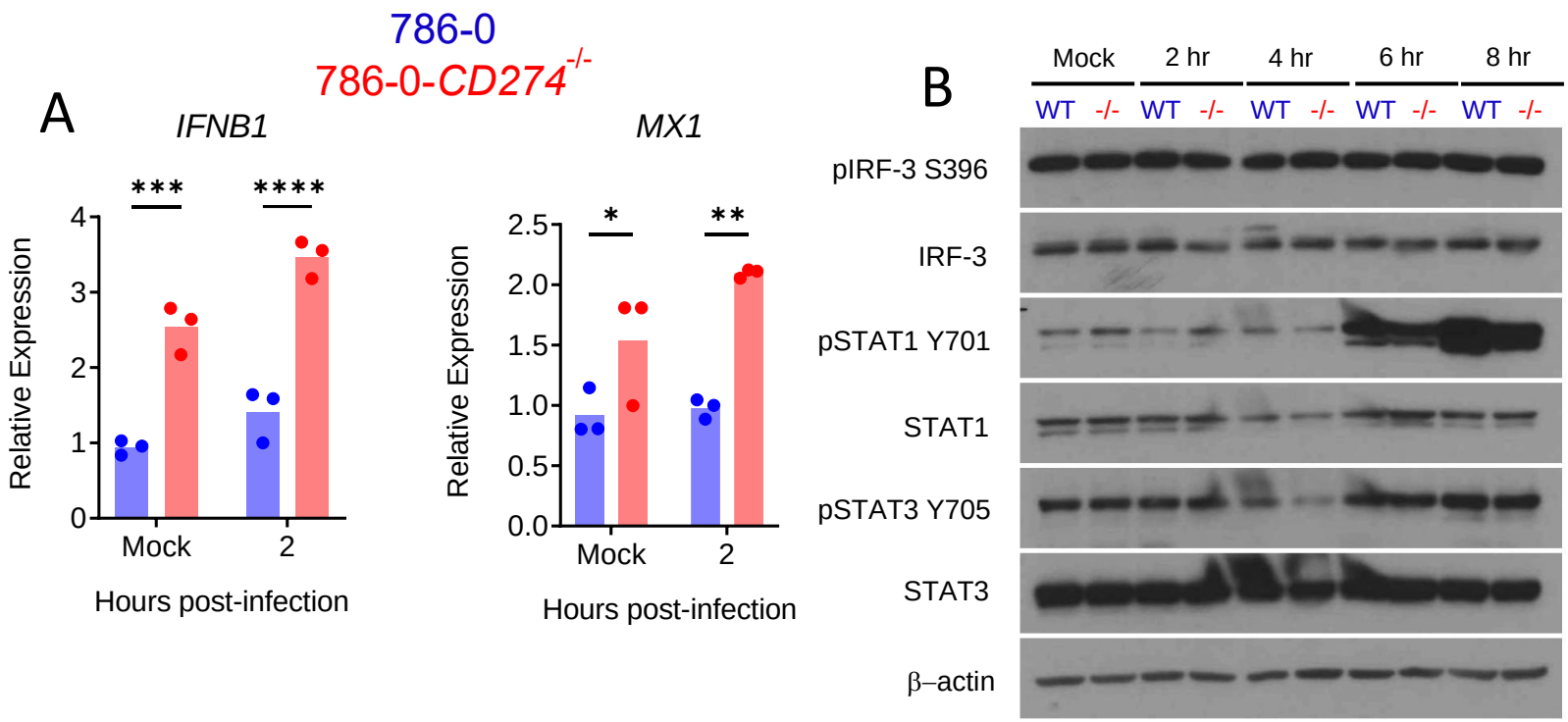
786-0
786-0-CD274-/-
A
IFNB1
MX1
***
****
*
**
Relative Expression
Mock
2
Hours post-infection
B
Mock
2 hr
4 hr
6 hr
8 hr
WT
-/-
pIRF-3 S396
IRF-3
pSTAT1 Y701
STAT1
pSTAT3 Y705
STAT3
β–actin

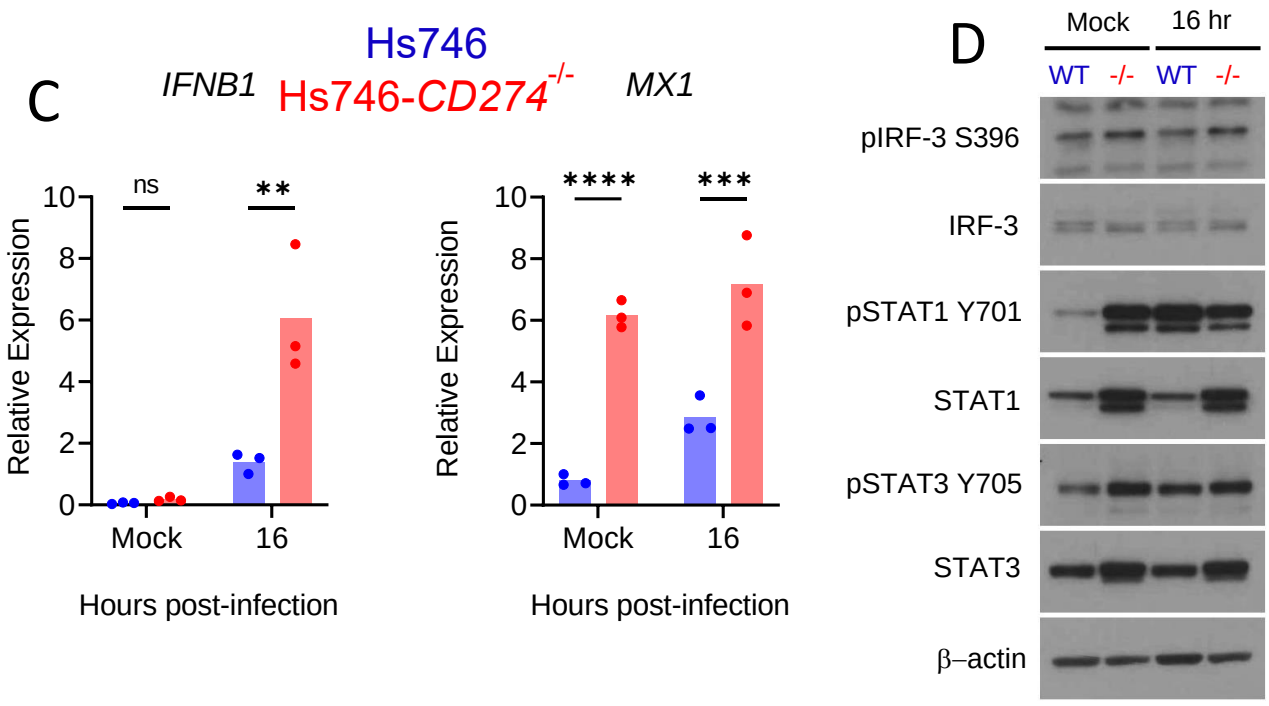
Hs746
Hs746-CD274-/-
C
IFNB1
MX1
ns
**
****
***
Relative Expression
Mock
16
Hours post-infection
D
Mock
16 hr
WT
-/-
pIRF-3 S396
IRF-3
pSTAT1 Y701
STAT1
pSTAT3 Y705
STAT3
β–actin

Figure 5.5. PD-L1 inhibits the type I interferon response in 786-0 and Hs746 cell lines. (**A**) 786-0 and 786-0 *CD274*$^{-/-}$ cells were infected with VSVΔ51-YFP at MOI 1 (or mock-infected) prior to qPCR analysis for *IFNB1* and *MX1* transcripts. N=3 biological replicates. Statistical analysis by two-way ANOVA with Šídák's correction for multiple comparisons. (**B**) 786-0 and 786-0 *CD274*$^{-/-}$ cells infected with VSVΔ51-YFP at MOI 1 (or mock-infected) and analyzed by western blotting at indicated times post-infection. Images depicted are representative of 3 with similar results. (**C**) Hs746 and Hs746 *CD274*$^{-/-}$ cells were infected with VSVΔ51-YFP at MOI 0.1 (or mock-infected) prior to qPCR analysis for *IFNB1* and *MX1* transcripts. N=3 biological replicates. Statistical analysis by two-way ANOVA with Šídák's correction for multiple comparisons. (**D**) Hs746 and Hs746 *CD274*$^{-/-}$ cells infected with VSVΔ51-YFP at MOI 0.1 (or mock-infected) and analyzed by western blotting at indicated times post-infection. Images depicted are representative of 3 biological replicates with similar results.

We also investigated if there are PD-L1-driven differences in lactate dynamics in Hs746 and 786-0 cells. In line with TRAMP-C2 cells, PD-L1 increased lactate production in both Hs746 and 786-0 (Figure 5.6A), suggesting an increased rate of glycolysis in parental Hs746 and 786-0 compared to their PD-L1-deficient counterparts. To link this difference in glycolysis and lactate to regulation of the type I interferon pathway, we blocked lactate production with the LDH inhibitor GNE-140 or spiked lactate into the media prior to VSVΔ51 infection. In both Hs746 and 786-0, reduction of lactate with the LDH inhibitor GNE-140 eliminated the ability of PD-L1 to promote OV infection with minimal impact on the *CD274*$^{-/-}$ cells (Figure 5.6B, D). Conversely, treatment with lactate mimicked the effect of PD-L1 on OV infection in both cell lines (Figure 5.6C, E). Therefore, PD-L1-driven differences in lactate levels is responsible for promoting OV infection in the Hs746 and 786-0 cell lines.

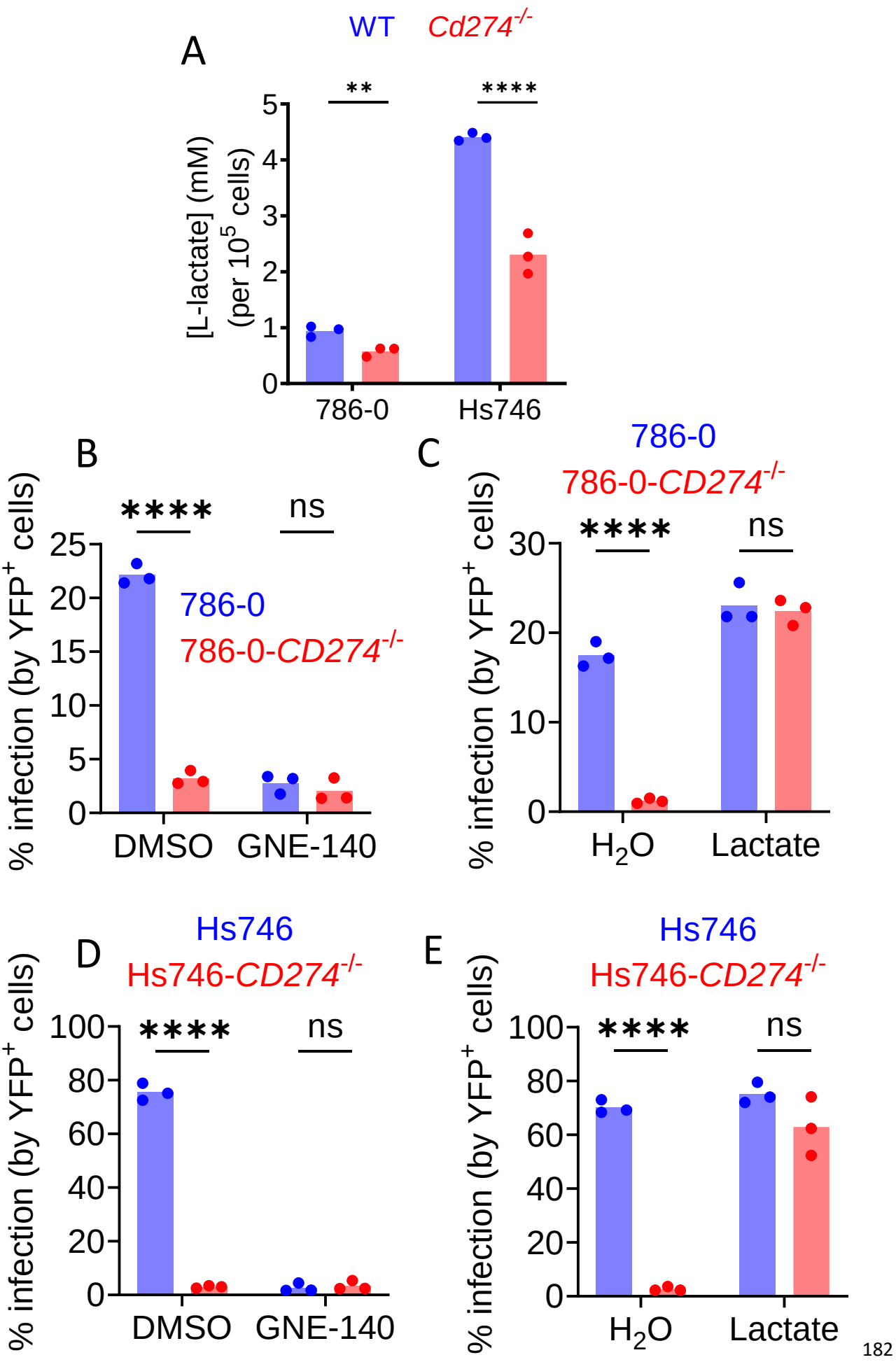
WT
Cd274-/-
A
**
****
[L-lactate] (mM) (per 10^5 cells)
786-0
Hs746
B
****
ns
786-0
786-0-CD274-/-
% infection (by YFP+ cells)
DMSO
GNE-140
C
786-0
786-0-CD274-/-
****
ns
% infection (by YFP+ cells)
H2O
Lactate
D
Hs746
Hs746-CD274-/-
****
ns
% infection (by YFP+ cells)
DMSO
GNE-140
E
Hs746
Hs746-CD274-/-
****
ns
% infection (by YFP+ cells)
H2O
Lactate

Figure 5.6. PD-L1 promotes OV infection via lactate in 786-0 and Hs746 cell lines. (**A**) Lactate quantification in 786-0 and Hs746 culture supernatant. N=3 biological replicates. Statistical analysis by two-tailed unpaired Student's t-test. (**B-C**) 786-0 and 786-0 *CD274*$^{-/-}$ cells were pre-treated with GNE-140 at 10 μM (**B**) or lactate at 5 mM (**C**) for 24 hours, followed by infection with VSVΔ51-YFP at MOI 1 for 24 hours prior to analysis by flow cytometry. Experiments depicted are representative of 3 biological replicates performed with similar results. Statistical analysis by two-way ANOVA with Šídák's correction for multiple comparisons. (**D-E**) Hs746 and Hs746 *CD274*$^{-/-}$ cells were pre-treated with GNE-140 at 10 μM (**D**) or lactate at 5 mM (**E**) for 24 hours, followed by infection with VSVΔ51-YFP at MOI 0.1 for 24 hours prior to analysis by flow cytometry. Experiments depicted are representative of 3 biological replicates performed with similar results. Statistical analysis by two-way ANOVA with Šídák's correction for multiple comparisons.

5.5. Atezolizumab promotes PD-L1 function in Hs746 and 786-0 cells

Lastly, we examined the expression of PD-1 and CD80 in Hs746 and 786-0 cells, given that we have previously shown the necessity of a binding partner for PD-L1 in the TRAMP-C2 model. Surprisingly, Hs746 and 786-0 do not express surface PD-1 or CD80 (Figure 5.7).

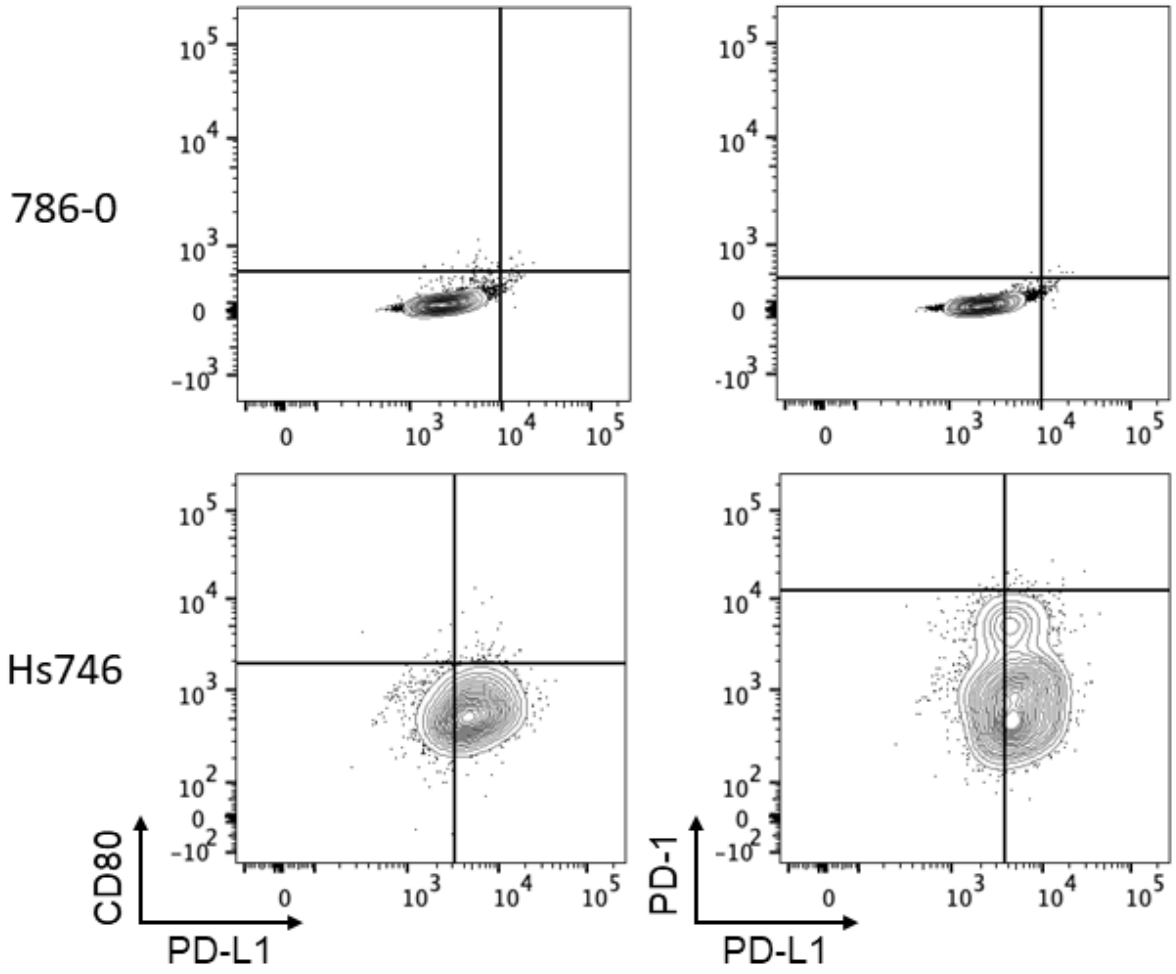
786-0
Hs746
CD80
PD-L1
PD-1
PD-L1

Figure 5.7. 786-0 and Hs746 cells do not express CD80 or PD-1. 786-0 and Hs746 cells were stained for surface CD80 and PD-1. Representative flow plots of N=2 biological replicates.

Despite the lack of PD-1/CD80 expression, in these cells PD-L1 may still be amenable to engagement by antibodies to enhance its functionality. To this end, we tested the ability of antibodies against human PD-L1 to trigger PD-L1 function and further promote OV infection, similar to our observations in the TRAMP-C2 model. We pre-treated Hs746 and 786-0 cells with atezolizumab, the clinically approved PD-L1 blockade antibody widely used in cancer therapy. Pre-treatment with atezolizumab significantly enhanced VSVΔ51 infection in parental Hs746 and 786-0 cells compared to the isotype control condition (Figure 5.8). Atezolizumab had no impact on *CD274*$^{-/-}$ cells (Figure 5.8), as expected based on their lack of PD-L1 expression. Therefore, the clinical PD-L1 antibody atezolizumab has the ability to enhance/trigger PD-L1 function, in addition to blocking the PD-L1:PD-1 interaction.

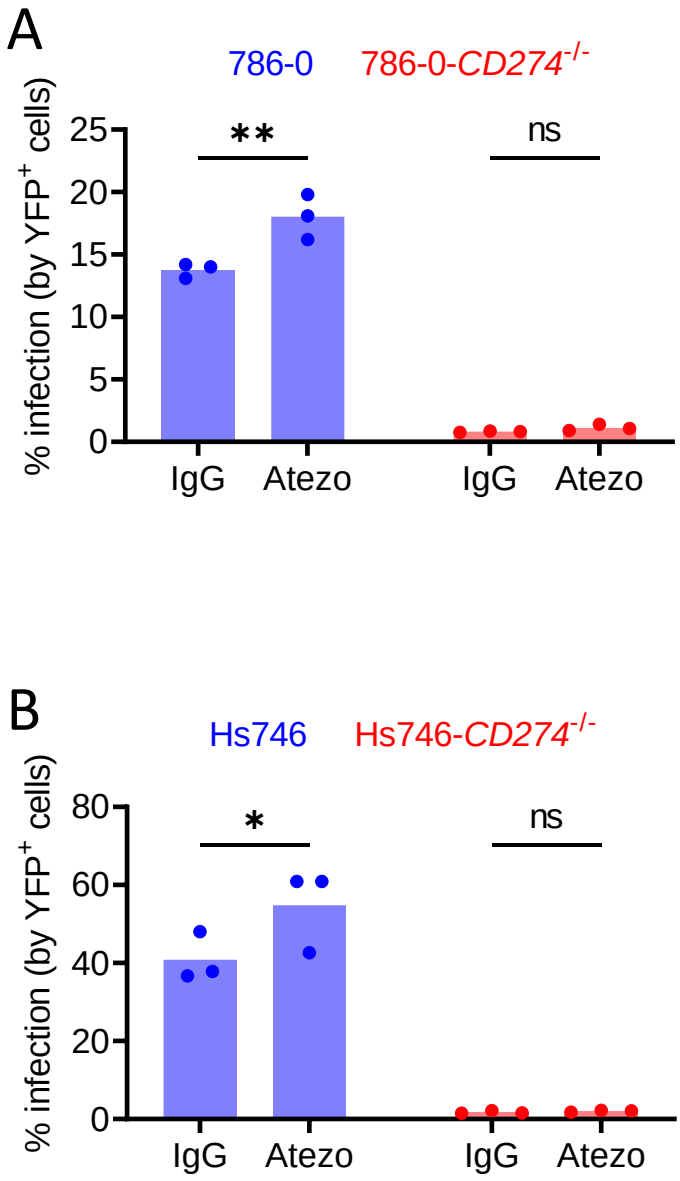
A
786-0
786-0-CD274-/-
% infection (by YFP+ cells)
25
20
15
10
5
0
**
ns
IgG
Atezo
IgG
Atezo
B
Hs746
Hs746-CD274-/-
% infection (by YFP+ cells)
80
60
40
20
0
*
ns
IgG
Atezo
IgG
Atezo

Figure 5.8. Atezolizumab promotes PD-L1 function in 786-0 and Hs746 cell lines. (**A-B**) 786-0 (**A**) and Hs746 (**B**) cells were treated with 5 μg of atezolizumab (Atezo) for 24 hours prior to VSVΔ51-YFP infection at MOI 1 or 0.1, respectively. 24 hours post-infection, cells were analyzed by flow cytometry to quantify the viral YFP reporter. Experiments depicted are representative of 3 biological replicates performed with similar results. Statistical analysis by two-way ANOVA with Šídák's correction for multiple comparisons.

5.6. PD-L1 promotes OV infection in primary human samples

To extend our findings beyond mice and cell lines, we tested if PD-L1 could enhance OV infection in primary human tumour samples. We obtained 21 tumour biopsies of diverse tissue origins (Appendix III) and assessed them for PD-L1 expression and infectability by VSVΔ51. To do so, we subjected the biopsy samples to PD-L1 IHC, Alamar Blue assay to assess biopsy viability, and ex vivo VSVΔ51 infection. We hypothesized that PD-L1^{+} tumours, defined in the clinical setting as tumours with ≥1% of tumour or immune cells expressing PD-L1 by IHC, would have greater VSVΔ51 infection compared to PD-L1^{-} tumours. In line with our hypothesis, we observed significantly more infection in PD-L1^{+} tumours compared to PD-L1^{-} tumours, although PD-L1 expression was not a perfect discriminator between well-infected tumour biopsies and poorly infected biopsies (Figure 5.9). We checked for potential confounding variables, including tumour biopsy viability, biopsy donor sex, and tissue origin of the tumour biopsy. There was no correlation between tumour viability (measured by Alamar Blue) or biopsy necrosis (measured by histology) and VSVΔ51 infection (Figure 5.10A-B), ruling out biopsy viability as a factor that might influence the results. Additionally, there was no difference in PD-L1 status or VSVΔ51 infection between male and female donors (Figure 5.10C-D), suggesting that sex does not play a role in the observed results. Lastly, PD-L1^{+} and PD-L1^{-} tumours were distributed across the 10 tumour types collected in this experiment, and no one tumour type was consistently better infected compared to others (Figure 5.10E). Therefore, PD-L1 marks patient tumour explants that are more likely to be infected with VSVΔ51.

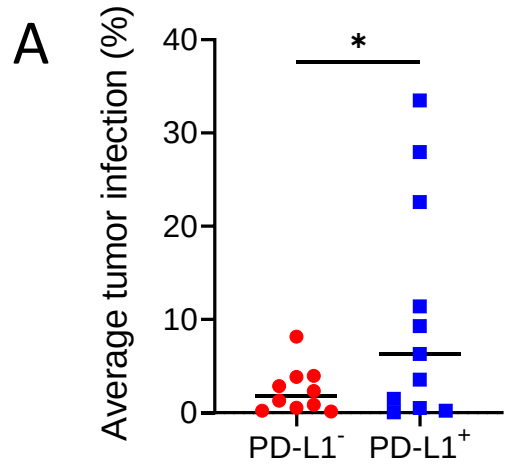
A
Average tumor infection (%)
40
30
20
10
0
*
PD-L1-
PD-L1+

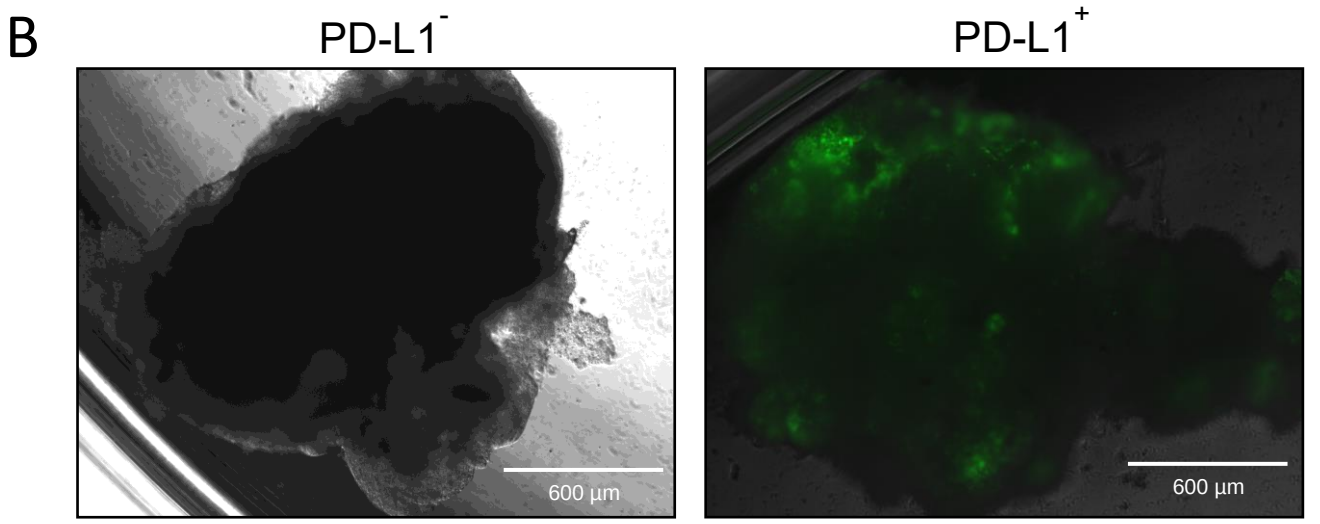
B
PD-L1-
PD-L1+
600 µm
600 µm

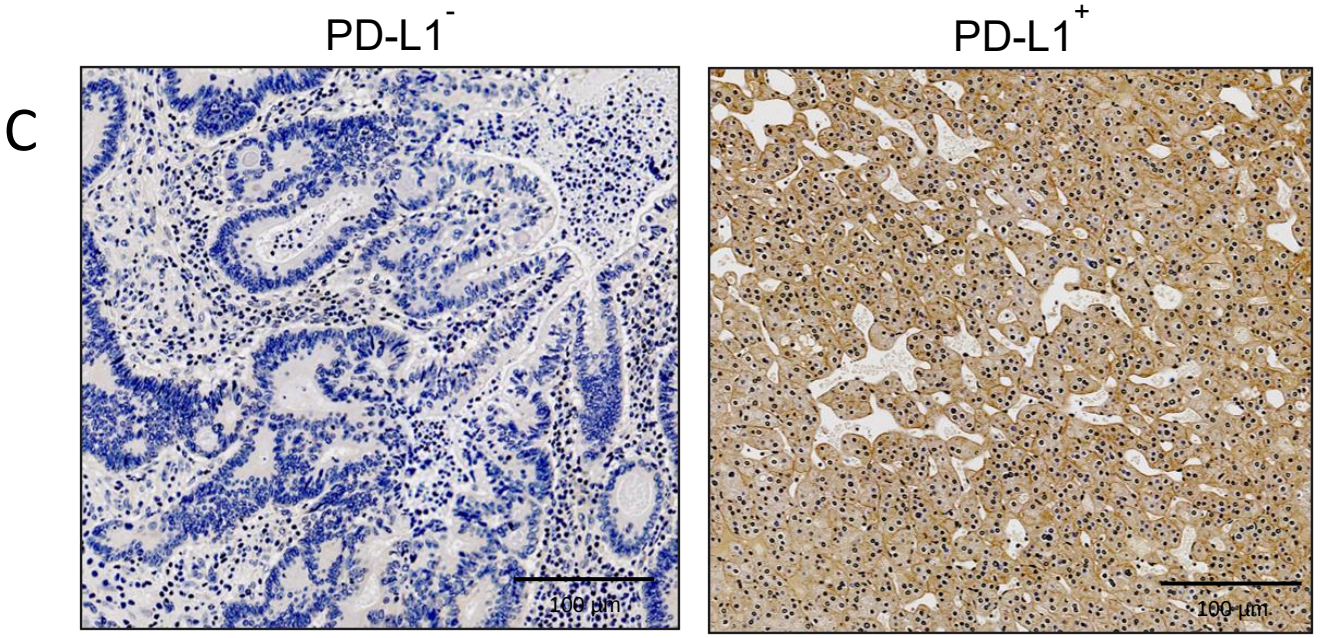
C
PD-L1-
PD-L1+
100 µm
100 µm

Figure 5.9. PD-L1 marks patient tumours best infected by VSVΔ51. (**A**) PD-L1 tumour status (where PD-L1$^+$ tumours are defined as ≥1% PD-L1$^+$ tumour/immune cells) plotted against average tumour infection (percentage of tumour explant area that is YFP$^+$). Statistical analysis by two-tailed unpaired Student's t-test. (**B**) Fluorescent imaging of tumour explant cores from patient biopsies infected with VSVΔ51-YFP for 48 hours prior to imaging for viral YFP reporter. Images of poorly infected (left) and well infected (right) tumours are depicted. (**C**) Patient tumour biopsies subjected to PD-L1 IHC to determine PD-L1 status of tumours. Images of PD-L1$^-$ (left) and PD-L1$^+$ (right) tumours are depicted.

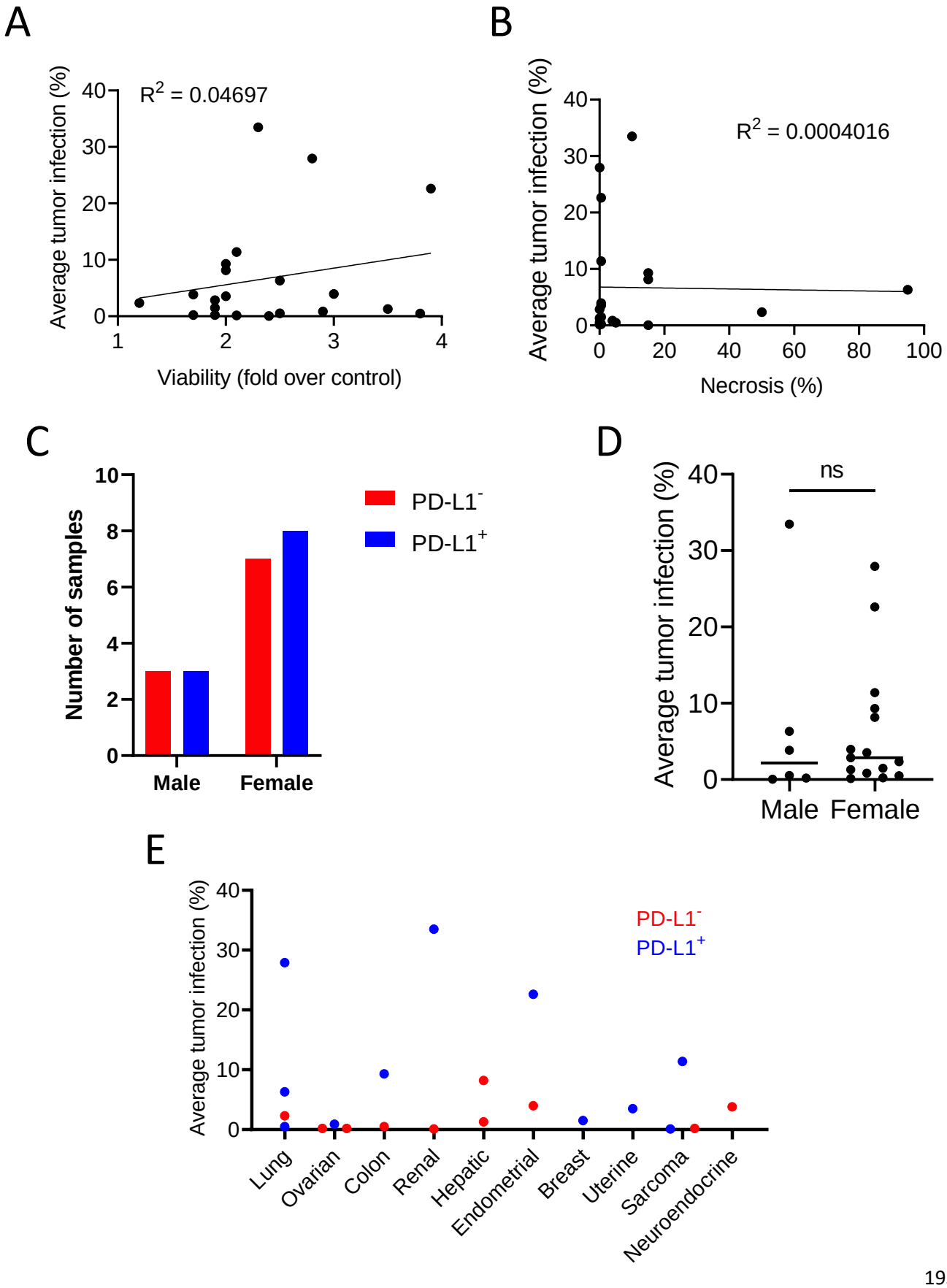
A
Average tumor infection (%)
R2 = 0.04697
Viability (fold over control)
B
Average tumor infection (%)
R2 = 0.0004016
Necrosis (%)
C
Number of samples
PD-L1-
PD-L1+
Male
Female
D
Average tumor infection (%)
ns
Male
Female
E
Average tumor infection (%)
PD-L1-
PD-L1+
Lung
Ovarian
Colon
Renal
Hepatic
Endometrial
Breast
Uterine
Sarcoma
Neuroendocrine

Figure 5.10. PD-L1 biomarker status is independent of tumour biopsy viability, donor sex, or tumour type. (A-B) Average tumour infection plotted against viability (assessed by Alamar Blue) and necrosis (% of tumour section necrotic, assessed by histology). (**C-D**) Distribution of PD-L1^{+} and PD-L1^{-} tumours, and average tumour infection, between male and female donors. Statistical analysis by two-tailed unpaired Student's t-test. (**E**) Distribution of PD-L1^{+} and PD-L1^{-} tumours, and their average infection level, across the 10 different tumour types collected.

Lastly, we investigated if PD-L1 can promote glycolysis in primary patient tumours. To do so, we assessed PD-L1 expression and Glycolysis Gene Set scores in a scRNA-seq dataset of 266 primary human tumours, spanning 8 types of cancer. The malignant cells in each tumour were scored for expression of PD-L1 transcripts and expression of genes included in the Glycolysis gene set. When we correlated the glycolysis score to PD-L1 expression in these cancers, we observed that tumours with high expression of PD-L1 had significantly higher glycolysis gene scores, in line with our hypothesis that PD-L1 drives glycolytic metabolism in cancer cells (Figure 5.11). Therefore, the effect of PD-L1 on OV infection, type I interferon responses, and cellular metabolism is not unique to the TRAMP-C2 model and is conserved in other contexts.

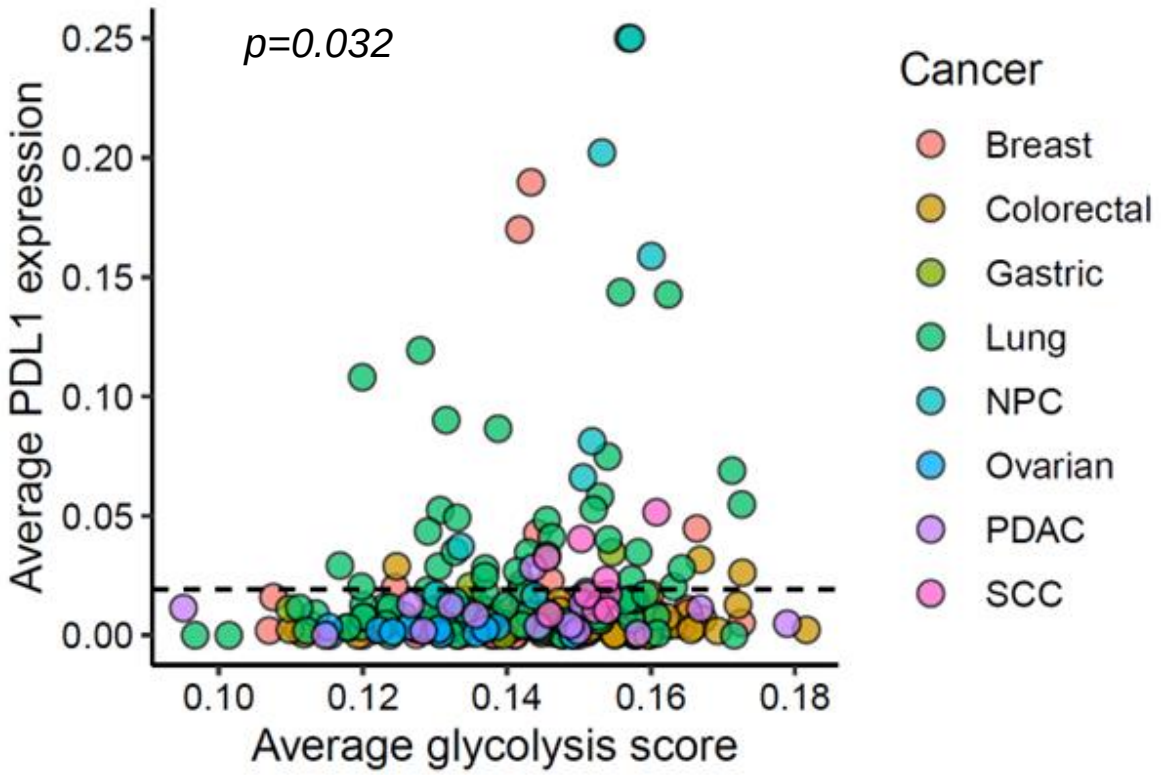
p=0.032
Average PDL1 expression
0.25
0.20
0.15
0.10
0.05
0.00
0.10
0.12
0.14
0.16
0.18
Average glycolysis score
Cancer
Breast
Colorectal
Gastric
Lung
NPC
Ovarian
PDAC
SCC

Figure 5.11. PD-L1 expression is associated with glycolysis gene scores in primary patient tumours. Association between the expression of PD-L1 and glycolysis-associated genes in the malignant cells of 266 tumours. Each point represents the average profile of malignant cells from scRNA-seq data sets, and dotted line represents mean PD-L1 expression of samples. Expression values reflect log-transformed gene counts per 10k transcripts and glycolysis activity represents gene set scores from the associated MSigDB Hallmark gene set. Statistical significance assessed by Wilcoxon rank-sum test to compare glycolysis scores of tumours expressing PD-L1 above or below mean expression. NPC: nasopharyngeal cancer, PDAC: pancreatic ductal adenocarcinoma, SCC: squamous cell carcinoma.

Chapter 6

Discussion

6.1. Summary

PD-L1 is quickly emerging as a regulator of many key pathways in cancer and immunity, and the idea that these functions are mediated by a poorly characterized, PD-1-independent signaling pathway is gaining more traction. Building on this PD-L1 “reverse signaling” literature, we have shown that PD-L1 inhibits the type I interferon response and enhances viral infection. Mechanistically, PD-L1 inhibits the type I interferon pathway via a pro-glycolytic metabolic shift in cancer cells. This function of PD-L1 requires engagement by an extracellular binding partner, which strongly suggests that this function is mediated by some signaling capacity of PD-L1. In the TRAMP-C2 model, engagement of PD-L1 is provided by CD80 expression, but treatment with recombinant PD-1 and even PD-L1 antibodies are able to engage and trigger PD-L1 activity in the TRAMP-C2 model and other cancer cell lines. Finally, we observed this phenotype in different in vitro and in vivo cellular contexts, suggesting our data is broadly relevant to cancer, rather than one particular cell line/type.

6.2. The elusive nature of PD-L1 signaling

PD-L1 has previously been demonstrated to modulate type I interferons, which was first characterized biochemically, and further observed using transcriptomic and bioinformatic approaches. In contrast with our findings, the earliest report from Gato-Cañas and colleagues did not observe PD-L1-mediated regulation of STAT1 dynamics, and conversely found that PD-L1 inhibited STAT3 phosphorylation and activation (*232*). In a similar vein, other groups have variously observed PD-L1 promoting or inhibiting type I

interferon responses in different cell types (*33*, *233*, *234*). Consistent with this idea, we have observed cell line-specific function of PD-L1 in the context of OV infection, where in some cell lines (TRAMP-C2, 786-0, Hs746) PD-L1 enhances OV infection, but in other cancer models like B16BL6 and MC38 (among others) PD-L1 has no impact on OV infection. The mechanism(s) underlying this context-specificity of PD-L1 function are unknown. It is possible that PD-L1 signals differently depending on the cell type, giving rise to different functionality. From a viral perspective it is possible that in some cellular contexts, type I interferon is not the major driver of OV infection. Indeed, other proteins/pathways, including Ras (*276*, *277*), have been implicated as driving OV infection in cancer cells and the cancer tropism of OVs. Different cell lines may have different activities of these OV regulators, potentially confounding our experiments.

On the other hand, what may be responsible for these signaling differences is the extensive glycosylation of PD-L1, which is responsible for approximately 50% of its observed molecular weight; importantly, different cell types/lines express different PD-L1 glycoforms (*278*, *279*). Differential glycosylation of PD-L1 influences its protein-protein interactions, which has thus far been exclusively studied in the context of PD-L1 ubiquitination by E3 ligases and subsequent proteasomal degradation (*278*). However, given the newfound realization that PD-L1 likely binds to intracellular signaling proteins to mediate its intrinsic effects, differential glycosylation of PD-L1 from one cell type to another could potentially alter its downstream signaling. Another contributor to the context-specific function of PD-L1 may be differential expression of those proteins involved in PD-L1 reverse signaling among different cancer cell types. Further

investigation into PD-L1 structure, and how that relates to its protein interactome and signaling, are required.

In terms of the biochemical underpinnings of PD-L1 signaling, there is a lack of data towards understanding if PD-L1 function requires cross-linking or conformational changes triggered by other proteins. Presumably, this engagement is provided by other cell surface receptors, provided in the TRAMP-C2 cells by CD80, but can be further triggered by addition of PD-1 or PD-L1 antibodies. In these experiments, only PD-L1 antibodies would be able to induce PD-L1 cross-linking, whereas CD80 and PD-1 likely do not (unless membrane CD80 and soluble PD-1 can oligomerize prior to/after engaging PD-L1).

In the data presented in Chapter 5, the human cell lines Hs746 and 786-0, where PD-L1 does promote glycolysis, inhibit the type I interferon pathway, and promote OV infection, there is no expression of CD80 or PD-1 to engage PD-L1. It is possible there are other, unidentified molecules in these cell lines triggering PD-L1 activity. However, it is also possible that PD-L1 does not always require an extracellular binding partner for its activity. Physiologically, there is a severe mismatch in the expression patterns of PD-L1 and CD80/PD-1, where PD-L1 is broadly expressed, while PD-1 and CD80 expression is generally limited to the immune system. This prompts one to question how PD-L1 is engaged in the diverse cellular contexts where it has been studied so far, and whether PD-L1 engagement is a strict requirement for its different biological functions. It should be noted that another surface protein, ephrin A3, has recently been described to bind to

PD-L1 (*280*), and there are likely other surface proteins (whose expression is not limited to immune cells) with PD-L1 binding activity. Additionally, in murine cancer cell lines where CD80 is expressed (for example, YUMM1.1 and MB49), PD-L1 does not promote OV infection, indicating that the presence of PD-L1 extracellular binding partners is not sufficient for functionality in this context.

6.3. PD-L1 as a novel metabolic regulator and its implications

Mechanistically, we found that PD-L1 regulates type I interferons by promoting increased rates of glucose uptake and glycolysis, with decreased reliance on respiration and mitochondria for energy and metabolites. To our knowledge, this is the first report showing that PD-L1 modulates type I interferons by altering cancer metabolism. However, previous work has suggested a link between PD-L1 expression and metabolism. Several studies in different cancer types and patient populations have shown a reproducible correlation between tumour PD-L1 expression and the radiolabeled glucose analog [^{18}F]-FDG PET avidity (*70*), similar to our in vivo data in the TRAMP-C2 model. Additionally, previous work has shown that PD-L1 may influence aerobic glycolysis in cancer cells, in addition to other metabolic pathways (*68*, *69*, *72*). Nevertheless, the biological consequences of PD-L1-mediated metabolic shifts are understudied, particularly given the fact that PD-L1 is expressed not only on cancer cells, but also on cells with metabolic function such as pancreatic islet cells (*19*). Future work investigating the impact of metabolic regulation by PD-L1 on processes including tumourigenesis, metastasis, and general host metabolism are warranted.

Interestingly, the effect of PD-L1 on cancer metabolism is reminiscent of the Warburg effect, wherein cells under aerobic conditions rely more on glycolysis than OXPHOS to meet energetic demands (*281*). The Warburg effect is frequently observed in cancer (*282*), and is thought to be an important driver of cancer cell proliferation and tumour biomass (*283*, *284*). This adds yet another important cancer process/pathway regulated by PD-L1, and further pinpoints PD-L1 as a key molecule in tumourigenesis.

One of the more interesting implications of PD-L1 as a metabolic regulator is in the field of immunometabolism. PD-L1 is expressed by almost every immune cell, and it is now well-appreciated that immune cell activity and fate is regulated by its metabolic properties (*285*). This raises the possibility that PD-L1 could be an important regulator of immune cell activity. Certainly, treatment with anti-PD-L1 is well-known to alter immune cells (*286*), but this is attributed to relief of PD-1-driven immunosuppression of T cells (and downstream consequences of that on other aspects of the immune response). As discussed below, one could now reasonably hypothesize that some of these changes are caused by direct changes in PD-L1 signaling in immune cells, rather than acting through the PD-1 receptor.

We have linked PD-L1 regulation of type I interferons to lactate, a metabolite highly associated with aerobic glycolysis and the Warburg effect. Beyond that, lactate is the subject of recent literature suggesting that it is not simply a waste product of aerobic

glycolysis. Reports have described active metabolism of lactate in healthy and cancer cells (*287*, *288*), the regulation of key oncogenes and tumour suppressor genes by lactate in cancer cells (*289*), regulation of inflammation (*290*) and other immune gene expression (*291*), and lactylation, a novel protein post-translational modification involving addition of lactate to various residues (*292*, *293*).

Additionally, lactate acts as a ligand for two GPCRs, GPR81 and GPR132, the latter of which is not well studied. GPR81 is known to be expressed on cancer cells (*294*), and interestingly the cellular roles of GPR81 overlap with known cell-intrinsic functions of PD-L1. For example, GPR81 has been described to induce resistance to chemotherapy by promoting expression of DNA repair proteins, including those involved in homologous recombination (*295*), which has been described for PD-L1 as well. Additionally, GPR81 and lactate can reduce type I interferon production by plasmacytoid DCs, albeit via a mechanism involving calcium signaling (*296*).

6.4. PD-L1 as a contributor to, and biomarker for, OV efficacy

We have shown that PD-L1 antibodies can trigger PD-L1 activity in vitro, leading to enhanced OV infection in PD-L1-expressing cells. This finding may shed new light on previous papers showing additive/synergistic effects on anti-tumour responses when OV therapy is combined with PD-L1 blockade in murine tumour models. Certainly, blocking the binding of PD-L1 to the inhibitory checkpoint receptor PD-1 is contributing to the boosted anti-tumour response in these models. However, it is now reasonable to

hypothesize that treatment with anti-PD-L1 is also triggering the OV-promoting properties of PD-L1 in these murine tumours, allowing for better OV infection (and the subsequent downstream effects such as tumour debulking and anti-tumour immunity). This hypothesis could be tested by analyzing OV infection in the tumour microenvironment in the presence and absence of anti-PD-L1; if a boost in OV infection is observed with anti-PD-L1 treatment, this could be a contributor to the therapeutic response.

Consistent with our in vitro and murine model data, PD-L1 marked patient tumour biopsies that were best infected with VSVΔ51 ex vivo. Therefore, PD-L1 may be a useful pre-treatment biomarker for those tumours that will best respond to OV therapy. Many ongoing OV clinical trials involve combination therapy with anti-PD-1 or anti-PD-L1, and therefore may collect data on tumour PD-L1 status, allowing for stratification of tumours into PD-L1^{+} and PD-L1^{-}. Based on our data, albeit limited, one would expect PD-L1^{-} tumours to not respond well to OV therapy, whereas PD-L1^{+} tumours would exhibit a variety of responses, ranging from poorly responsive to highly responsive.

6.5. Is it time to re-think PD-L1 blockade?

Lastly, from a clinical perspective, the fact that PD-L1 antibodies can trigger PD-L1 activity is highly relevant. It is tempting to speculate that these novel, cell-intrinsic functions of PD-L1 are modulated in tumours of patients undergoing anti-PD-L1 therapy, and this may contribute to anti-tumour efficacy (or lack thereof) of these therapeutic agents in different types of cancer. Investigation in appropriate murine models of cancer is needed to

elucidate the role of cell-intrinsic PD-L1 function on checkpoint blockade efficacy. To rigorously test the contribution of PD-L1 signaling to anti-PD-L1 treatment, PD-1-deficient murine models should be used to eliminate PD-1 as a potential variable in any observations. From there, the murine models could either be PD-L1-sufficient or PD-L1-deficient, along with PD-L1-sufficient/deficient tumour cells, to tease apart the relative contributions of host PD-L1 and tumour PD-L1.

If there is a role for PD-L1 intrinsic function in anti-PD-L1 therapy, it could shed much-needed insight into efforts to predict tumours that may respond best to this therapeutic agent. Currently, selecting patients with tumours that express PD-L1 and have high tumour mutational burden (TMB) enriches for those that will best respond to anti-PD-L1 checkpoint blockade therapy (*297*, *298*). Based on the known mechanism of action of anti-PD-L1, which is largely focused on preventing PD-1-driven T cell dysfunction, these biomarkers are biologically sound. However, despite the solid rationale behind these biomarkers, most patients with PD-L1^{+} and/or TMB^{high} tumours do not respond to anti-PD-L1 therapy, while responders can harbor PD-L1^{-} and TMB^{low} tumours (*299*). In the last few years, efforts to move beyond these 2 biomarkers and use tumour transcriptomic signatures have also not been greatly successful (*299*). Certainly, some of the difficulty may lie in the large degree of heterogeneity between tumour indications and between individual tumours. On the other hand, if one considers the possibility that PD-L1 checkpoint blockade succeeds in part by altering cancer cells via PD-L1 cell-intrinsic effects, this may prompt investigators to test for biomarkers (for example, certain metabolites or metabolic profiles) appropriate to this novel mechanism of action.

References

1. L. P. Andrews, H. Yano, D. A. A Vignali, Inhibitory receptors and ligands beyond PD-1, PD-L1 and CTLA-4: breakthroughs or backups. *Nat. Immunol.* **20**, 1425–1434 (2019).

2. J. L. Riley, PD-1 signaling in primary T cells. *Immunol. Rev.* **70**, 646–656 (2009).

3. A. O. Kamphorst, A. Wieland, T. Nasti, S. Yang, R. Zhang, D. L. Barber, B. T. Konieczny, C. Z. Daugherty, L. Koenig, K. Yu, G. L. Sica, A. H. Sharpe, G. J. Freeman, B. R. Blazar, L. A. Turka, T. K. Owonikoko, R. N. Pillai, S. S. Ramalingam, K. Araki, R. Ahmed, Rescue of exhausted CD8 T cells by PD-1-targeted therapies is CD28-dependent. *Science*. **355**, 1423–1427 (2017).

4. E. Hui, J. Cheung, J. Zhu, X. Su, M. J. Taylor, H. A. Wallweber, D. K. Sasmal, J. Huang, J. M. Kim, I. Mellman, R. D. Vale, T cell costimulatory receptor CD28 is a primary target for PD-1-mediated inhibition. *Science*. **355**, 1428–1433 (2017).

5. V. A. Boussiotis, Molecular and Biochemical Aspects of the PD-1 Checkpoint Pathway. *N. Engl. J. Med.* **375**, 1767–1778 (2016).

6. N. Patsoukis, Q. Wang, L. Strauss, V. A. Boussiotis, Revisiting the PD-1 pathway. *Sci. Adv.* **6**, 1–13 (2020).

7. X. Xiao, X. M. Lao, M. M. Chen, R. X. Liu, Y. Wei, F. Z. Ouyang, D. P. Chen, X. Y. Zhao, Q. Zhao, X. F. Li, C. L. Liu, L. Zheng, D. M. Kuang, PD-1hi identifies a novel regulatory b-cell population in human hepatoma that promotes disease progression. *Cancer Discov.* **6**, 546–559 (2016).

8. X. Wang, G. Wang, Z. Wang, B. Liu, N. Han, J. Li, C. Lu, X. Liu, Q. Zhang, Q. Yang, G. Wang, PD-1-expressing B cells suppress CD4+ and CD8+ T cells via PD-1/PD-L1-dependent pathway. *Mol. Immunol.* **109**, 20–26 (2019).

9. G. Oldenhove, E. Boucquey, A. Taquin, V. Acolty, L. Bonetti, B. Ryffel, M. Le Bert, K. Englebert, L. Boon, M. Moser, PD-1 Is Involved in the Dysregulation of Type 2 Innate Lymphoid Cells in a Murine Model of Obesity. *Cell Rep.* **25**, 2053-2060.e4 (2018).

10. J. A. Moral, J. Leung, L. A. Rojas, J. Ruan, J. Zhao, Z. Sethna, A. Ramnarain, B. Gasmi, M. Gururajan, D. Redmond, G. Askan, U. Bhanot, E. Elyada, Y. Park, D. A. Tuveson, M. Gönen, S. D. Leach, J. D. Wolchok, R. P. DeMatteo, T. Merghoub, V. P. Balachandran, ILC2s amplify PD-1 blockade by activating tissue-specific cancer immunity. *Nature*. **579**, 130–135 (2020).

11. Z. Davis, M. Felices, T. Lenvik, S. Badal, J. T. Walker, P. Hinderlie, J. L. Riley, D. A. Vallera, B. R. Blazar, J. S. Miller, Low-density PD-1 expression on resting human natural killer cells is functional and upregulated after transplantation. *Blood Adv.* **5**, 1069 (2021).

12. W. Chen, J. Wang, L. Jia, J. Liu, Y. Tian, Attenuation of the programmed cell death-1 pathway increases the M1 polarization of macrophages induced by

zymosan. *Cell Death Dis.* **7**, e2115–e2115 (2016).

13. S. R. Gordon, R. L. Maute, B. W. Dulken, G. Hutter, B. M. George, M. N. McCracken, R. Gupta, J. M. Tsai, R. Sinha, D. Corey, A. M. Ring, A. J. Connolly, I. L. Weissman, PD-1 expression by tumour-associated macrophages inhibits phagocytosis and tumour immunity. *Nature*. **545**, 495–499 (2017).

14. L. Strauss, M. A. A. Mahmoud, J. D. Weaver, N. M. Tijaro-Ovalle, A. Christofides, Q. Wang, R. Pal, M. Yuan, J. Asara, N. Patsoukis, V. A. Boussiotis, Targeted deletion of PD-1 in myeloid cells induces antitumor immunity. *Sci. Immunol.* **5** (2020), doi:10.1126/SCIIMMUNOL.AAY1863/SUPPL_FILE/AAY1863_TABLE_S5.XLSX.

15. T. Okazaki, T. Honjo, PD-1 and PD-1 ligands: from discovery to clinical application. *Int. Immunol.* **19**, 813–824 (2007).

16. A. H. Sharpe, K. E. Pauken, The diverse functions of the PD1 inhibitory pathway. *Nat. Rev. Immunol.* (2017), doi:10.1038/nri.2017.108.

17. H. Nishimura, M. Nose, H. Hiai, N. Minato, T. Honjo, Development of Lupus-like Autoimmune Diseases by Disruption of the PD-1 Gene Encoding an ITIM Motif-Carrying Immunoreceptor. *Immunity*. **11**, 141–151 (1999).

18. H. Nishimura, T. Okazaki, Y. Tanaka, K. Nakatani, M. Hara, A. Matsumori, S. Sasayama, A. Mizoguchi, H. Hiai, N. Minato, T. Honjo, Autoimmune Dilated Cardiomyopathy in PD-1 Receptor-Deficient Mice. *Science (80-.).* **291**, 319–322 (2001).

19. M. E. Keir, S. C. Liang, I. Guleria, Y. E. Latchman, A. Qipo, L. A. Albacker, M. Koulmanda, G. J. Freeman, M. H. Sayegh, A. H. Sharpe, Tissue expression of PD-L1 mediates peripheral T cell tolerance. *J. Exp. Med.* **203**, 883–895 (2006).

20. T. Yoshida, F. Jiang, T. Honjo, T. Okazaki, PD-1 deficiency reveals various tissue-specific autoimmunity by H-2b and dose-dependent requirement of H-2g7 for diabetes in NOD mice. *Proc. Natl. Acad. Sci. U. S. A.* **105**, 3533–3538 (2008).

21. A. J. Korman, S. C. Garrett-Thomson, N. Lonberg, The foundations of immune checkpoint blockade and the ipilimumab approval decennial. *Nat. Rev. Drug Discov.*, 1–20 (2021).

22. M. Ogishi, R. Yang, C. Aytekin, D. Langlais, M. Bourgey, T. Khan, F. Al Ali, M. Rahman, O. M. Delmonte, M. Chrabieh, P. Zhang, C. Gruber, S. J. Pelham, A. N. Spaan, J. Rosain, W.-T. Lei, S. Drutman, M. D. Hellmann, M. K. Callahan, M. Adamow, P. Wong, J. D. Wolchok, G. Rao, C. S. Ma, Y. Nakajima, T. Yaguchi, K. Chamoto, S. C. Williams, J.-F. Emile, F. Rozenberg, M. S. Glickman, F. Rapaport, G. Kerner, G. Allington, I. Tezcan, D. Cagdas, F. O. Hosnut, F. Dogu, A. Ikinciogullari, V. K. Rao, L. Kainulainen, V. Béziat, J. Bustamante, S. Vilarinho, R. P. Lifton, B. Boisson, L. Abel, D. Bogunovic, N. Marr, L. D. Notarangelo, S. G. Tangye, T. Honjo, P. Gros, S. Boisson-Dupuis, J.-L. Casanova, Inherited PD-1 deficiency underlies tuberculosis and autoimmunity in a child. *Nat. Med.* **15**, 41 (2021).

23. H. Dong, G. Zhu, K. Tamada, L. Chen, B7-H1, a third member of the B7 family, co-stimulates T-cell proliferation and interleukin-10 secretion. *Nat. Med.* **5**, 1365–1369 (1999).

24. G. J. Freeman, A. J. Long, Y. Iwai, K. Bourque, T. Chernova, H. Nishimura, L. J. Fitz, N. Malenkovich, T. Okazaki, M. C. Byrne, H. F. Horton, L. Fouser, L. Carter, V. Ling, M. R. Bowman, B. M. Carreno, M. Collins, C. R. Wood, T. Honjo, Engagement of the PD-1 Immunoinhibitory Receptor by a Novel B7 Family Member Leads to Negative Regulation of Lymphocyte Activation. *J. Exp. Med.* **192**, 1027–1034 (2000).

25. M. J. Butte, M. E. Keir, T. B. Phamduy, A. H. Sharpe, G. J. Freeman, Programmed Death-1 Ligand 1 Interacts Specifically with the B7-1 Costimulatory Molecule to Inhibit T Cell Responses. *Immunity*. **27**, 111–122 (2007).

26. D. Sugiura, T. Maruhashi, I.-M. Okazaki, K. Shimizu, T. K. Maeda, T. Takemoto, T. Okazaki, Restriction of PD-1 function by cis-PD-L1/CD80 interactions is required for optimal T cell responses. *Science*, eaav7062 (2019).

27. M. J. Butte, V. Peña-Cruz, M.-J. Kim, G. J. Freeman, A. H. Sharpe, Interaction of human PD-L1 and B7-1. *Mol. Immunol.* **45**, 3567–3572 (2008).

28. A. Chaudhri, Y. Xiao, A. N. Klee, X. Wang, B. Zhu, G. J. Freeman, PD-L1 Binds to B7-1 only in cis on the same cell surface. *Cancer Immunol. Res.* **6**, 921–929 (2018).

29. Y. Zhao, C. K. Lee, C. H. Lin, R. B. Gassen, X. Xu, Z. Huang, C. Xiao, C. Bonorino, L. F. Lu, J. D. Bui, E. Hui, PD-L1:CD80 Cis-Heterodimer Triggers the Co-stimulatory Receptor CD28 While Repressing the Inhibitory PD-1 and CTLA-4 Pathways. *Immunity*. **51**, 1059-1073.e9 (2019).

30. Y. Zhao, D. L. Harrison, Y. Song, J. Ji, J. Huang, E. Hui, Antigen-Presenting Cell-Intrinsic PD-1 Neutralizes PD-L1 in cis to Attenuate PD-1 Signaling in T Cells. *Cell Rep.* **24**, 379-390.e6 (2018).

31. J. Hou, R. Zhao, W. Xia, C.-W. Chang, Y. You, J.-M. Hsu, L. Nie, Y. Chen, Y.-C. Wang, C. Liu, W.-J. Wang, Y. Wu, B. Ke, J. L. Hsu, K. Huang, Z. Ye, Y. Yang, X. Xia, Y. Li, C.-W. Li, B. Shao, J. A. Tainer, M.-C. Hung, PD-L1-mediated gasdermin C expression switches apoptosis to pyroptosis in cancer cells and facilitates tumour necrosis. *Nat. Cell Biol.*, 1–12 (2020).

32. J. B. Schafer, E. D. Lucas, M. Dzieciettkowska, T. Forward, B. A. J. Tamburini, Programmed death ligand 1 intracellular interactions with STAT3 and focal adhesion protein Paxillin facilitate lymphatic endothelial cell remodeling. *J. Biol. Chem.* **0**, 102694 (2022).

33. Y. Gao, N. T. Nihira, X. Bu, C. Chu, J. Zhang, A. Kolodziejczyk, Y. Fan, N. T. Chan, L. Ma, J. Liu, D. Wang, X. Dai, H. Liu, M. Ono, A. Nakanishi, H. Inuzuka, B. J. North, Y. H. Huang, S. Sharma, Y. Geng, W. Xu, X. S. Liu, L. Li, Y. Miki, P. Sicinski, G. J. Freeman, W. Wei, Acetylation-dependent regulation of PD-L1 nuclear translocation dictates the efficacy of anti-PD-1 immunotherapy. *Nat. Cell*

Biol., 1–12 (2020).

34. X. Tu, B. Qin, Y. Zhang, C. Zhang, M. Kahila, S. Nowsheen, P. Yin, J. Yuan, H. Pei, H. Li, J. Yu, Z. Song, Q. Zhou, F. Zhao, J. Liu, C. Zhang, H. Dong, R. W. Mutter, Z. Lou, PD-L1 (B7-H1) Competes with the RNA Exosome to Regulate the DNA Damage Response and Can Be Targeted to Sensitize to Radiation or Chemotherapy. *Mol. Cell*. **74**, 1215-1226.e4 (2019).

35. H. Yao, J. Lan, C. Li, H. Shi, J. P. Brosseau, H. Wang, H. Lu, C. Fang, Y. Zhang, L. Liang, X. Zhou, C. Wang, Y. Xue, Y. Cui, J. Xu, Inhibiting PD-L1 palmitoylation enhances T-cell immune responses against tumours. *Nat. Biomed. Eng.* **3**, 306–317 (2019).

36. J. H. Cha, W. H. Yang, W. Xia, Y. Wei, L. C. Chan, S. O. Lim, C. W. Li, T. Kim, S. S. Chang, H. H. Lee, J. L. Hsu, H. L. Wang, C. W. Kuo, W. C. Chang, S. Hadad, C. A. Purdie, A. M. McCoy, S. Cai, Y. Tu, J. K. Litton, E. A. Mittendorf, S. L. Moulder, W. F. Symmans, A. M. Thompson, H. Piwnica-Worms, C. H. Chen, K. H. Khoo, M. C. Hung, Metformin Promotes Antitumor Immunity via Endoplasmic-Reticulum-Associated Degradation of PD-L1. *Mol. Cell*. **71**, 606-620.e7 (2018).

37. L.-C. Chan, C.-W. Li, W. Xia, J.-M. Hsu, H.-H. Lee, J.-H. Cha, H.-L. Wang, W.-H. Yang, E.-Y. Yen, W.-C. Chang, Z. Zha, S.-O. Lim, Y.-J. Lai, C. Liu, J. Liu, Q. Dong, Y. Yang, L. Sun, Y. Wei, L. Nie, J. L. Hsu, H. Li, Q. Ye, M. M. Hassan, H. M. Amin, A. O. Kaseb, X. Lin, S.-C. Wang, M.-C. Hung, IL-6/JAK1 pathway drives PD-L1 Y112 phosphorylation to promote cancer immune evasion. *J. Clin. Invest.* **129**, 3324–3338 (2019).

38. X. Zhao, Y. Wei, Y. Y. Chu, Y. Li, J. M. Hsu, Z. Jiang, C. Liu, J. L. Hsu, W. C. Chang, R. Yang, L. C. Chan, J. Qu, S. Zhang, H. Ying, D. Yu, M. C. Hung, Phosphorylation and Stabilization of PD-L1 by CK2 Suppresses Dendritic Cell Function. *Cancer Res.* **82**, 2185–2195 (2022).

39. H. Ghebeh, C. Lehe, E. Barhoush, K. Al-Romaih, A. Tulbah, M. Al-Alwan, S.-F. Hendrayani, P. Manogaran, A. Alaiya, T. Al-Tweigeri, A. Aboussekhra, S. Dermime, Doxorubicin downregulates cell surface B7-H1 expression and upregulates its nuclear expression in breast cancer cells: role of B7-H1 as an anti-apoptotic molecule. *Breast Cancer Res.* **12**, R48 (2010).

40. A. Satelli, I. S. Batth, Z. Brownlee, C. Rojas, Q. H. Meng, S. Kopetz, S. Li, Potential role of nuclear PD-L1 expression in cell-surface vimentin positive circulating tumor cells as a prognostic marker in cancer patients. *Sci. Rep.* **6**, 1–7 (2016).

41. K. Hee Shim, J. Eun Kwon, S. Gon Park, S. Ho Choo, S. Joong Kim, S. Il Kim, Prostate cancer Cell membrane and nuclear expression of programmed death ligand-1 in prostate needle biopsy tissue in prostate cancer patients undergoing primary radiation therapy. *Urol. Oncol.*, 1–8 (2021).

42. W. Du, J. Zhu, Y. Zeng, T. Liu, Y. Zhang, T. Cai, Y. Fu, W. Zhang, R. Zhang, Z. Liu, J. an Huang, KPNB1-mediated nuclear translocation of PD-L1 promotes non-

small cell lung cancer cell proliferation via the Gas6/MerTK signaling pathway. *Cell Death Differ.* (2020), doi:10.1038/s41418-020-00651-5.

43. W. Zhang, J. Jin, Y. Wang, L. Fang, L. Min, X. Wang, L. Ding, L. Weng, T. Xiao, T. Zhou, P. Wang, PD-L1 regulates genomic stability via interaction with cohesin-SA1 in the nucleus. *Signal Transduct. Target. Ther.* **6**, 1–3 (2021).

44. J. Yu, B. Qin, A. M. Moyer, S. Nowsheen, X. Tu, H. Dong, J. C. Boughey, M. P. Goetz, R. Weinshilboum, Z. Lou, L. Wang, Regulation of sister chromatid cohesion by nuclear PD-L1. *Cell Res.* **30**, 590–601 (2020).

45. X. Wu, Y. Li, X. Liu, C. Chen, S. M. Harrington, S. Cao, T. Xie, A. Orzechowski, T. Pham, A. S. Mansfield, Y. Yan, E. D. Kwon, L. Wang, K. Ling, H. Dong, Targeting B7-H1 (PD-L1) sensitizes cancer cells to chemotherapy. *Heliyon*. **4**, e01039 (2018).

46. C.-W. Li, S.-O. Lim, W. Xia, H.-H. Lee, L.-C. Chan, C.-W. Kuo, K.-H. Khoo, S.-S. Chang, J.-H. Cha, T. Kim, J. L. Hsu, Y. Wu, J.-M. Hsu, H. Yamaguchi, Q. Ding, Y. Wang, J. Yao, C.-C. Lee, H.-J. Wu, A. A. Sahin, J. P. Allison, D. Yu, G. N. Hortobagyi, M.-C. Hung, Glycosylation and stabilization of programmed death ligand-1 suppresses T-cell activity. *Nat. Commun.* (2016).

47. Y. Wang, Q. Sun, N. Mu, X. Sun, Y. Wang, S. Fan, L. Su, X. Liu, The deubiquitinase USP22 regulates PD-L1 degradation in human cancer cells. *Cell Commun. Signal.* **18**, 112 (2020).

48. C. Chen, S. Li, J. Xue, M. Qi, X. Liu, Y. Huang, J. Hu, H. Dong, K. Ling, PD-L1 tumor-intrinsic signaling and its therapeutic implication in triple-negative breast cancer. *JCI Insight*. **6**, 1–20 (2021).

49. R. Mezzadra, C. Sun, L. T. Jae, R. Gomez-Eerland, E. De Vries, W. Wu, M. E. W. Logtenberg, M. Slagter, E. A. Rozeman, I. Hofland, A. Broeks, H. M. Horlings, L. F. A. Wessels, C. U. Blank, Y. Xiao, A. J. R. Heck, J. Borst, T. R. Brummelkamp, T. N. M. Schumacher, Identification of CMTM6 and CMTM4 as PD-L1 protein regulators. *Nature*. **549**, 106–110 (2017).

50. M. L. Burr, C. E. Sparbier, Y.-C. Chan, J. C. Williamson, K. Woods, P. A. Beavis, E. Y. N. Lam, M. A. Henderson, C. C. Bell, S. Stolzenburg, O. Gilan, S. Bloor, T. Noori, D. W. Morgens, M. C. Bassik, P. J. Neeson, A. Behren, P. K. Darcy, S.-J. Dawson, I. Voskoboinik, J. A. Trapani, J. Cebon, P. J. Lehner, M. A. Dawson, CMTM6 maintains the expression of PD-L1 and regulates anti-tumour immunity. *Nature*. **549**, 101–105 (2017).

51. R. Q. Chen, X. H. Xu, F. Liu, C. Y. Li, Y. J. Li, X. R. Li, G. Y. Jiang, F. Hu, D. Liu, F. Pan, X. Y. Qiu, X. Q. Chen, The Binding of PD-L1 and Akt Facilitates Glioma Cell Invasion Upon Starvation via Akt/Autophagy/F-Actin Signaling. *Front. Oncol.* **9**, 1347 (2019).

52. C. A. Clark, H. B. Gupta, G. Sareddy, S. Pandeswara, S. Lao, B. Yuan, J. M. Drerup, A. Padron, J. Conejo-Garcia, K. Murthy, Y. Liu, M. J. Turk, K. Thedieck, V. Hurez, R. Li, R. Vadlamudi, T. J. Curiel, Tumor-intrinsic PD-L1 signals regulate

cell growth, pathogenesis, and autophagy in ovarian cancer and melanoma. *Cancer Res.* **76**, 6964–6974 (2016).

53. D. Zhang, R. M. Reyes, E. Osta, S. Kari, H. B. Gupta, A. S. Padron, A. V. R. Kornepati, A. Kancharla, X. Sun, Y. Deng, B. Wu, R. Vadlamudi, R. Li, R. S. Svatek, T. J. Curiel, Bladder cancer cell-intrinsic PD-L1 signals promote mTOR and autophagy activation that can be inhibited to improve cytotoxic chemotherapy. *Cancer Med.* **10**, 2137–2152 (2021).

54. F. Wang, L. Yang, M. Xiao, Z. Zhang, J. Shen, S. Anuchapreeda, S. Tima, S. Chiampanichayakul, Z. Xiao, PD-L1 regulates cell proliferation and apoptosis in acute myeloid leukemia by activating PI3K-AKT signaling pathway. *Sci. Rep.* **12**, 11444 (123AD).

55. S. Qu, Z. Jiao, G. Lu, B. Yao, T. Wang, W. Rong, J. Xu, T. Fan, X. Sun, R. Yang, J. Wang, Y. Yao, G. Xu, X. Yan, T. Wang, H. Liang, K. Zen, PD-L1 lncRNA splice isoform promotes lung adenocarcinoma progression via enhancing c-Myc activity. *Genome Biol.* **22**, 1–24 (2021).

56. S. Jalali, T. Price-Troska, C. Bothun, J. Villasboas, H.-J. Kim, Z.-Z. Yang, A. J. Novak, H. Dong, S. M. Ansell, Reverse signaling via PD-L1 supports malignant cell growth and survival in classical Hodgkin lymphoma. *Blood Cancer J.* **9**, 22 (2019).

57. M. Passariello, A. M. D'Alise, A. Esposito, C. Vetrei, G. Froechlich, E. Scarselli, A. Nicosia, C. De Lorenzo, Novel Human Anti-PD-L1 mAbs Inhibit Immune-Independent Tumor Cell Growth and PD-L1 Associated Intracellular Signalling. *Sci. Rep.* **9**, 1–13 (2019).

58. R. Saleh, R. Z. Taha, V. S. Nair, N. M. Alajez, E. Elkord, PD-L1 Blockade by Atezolizumab Downregulates Signaling Pathways Associated with Tumor Growth, Metastasis, and Hypoxia in Human Triple Negative Breast Cancer. *Cancers (Basel).* **11**, 1050 (2019).

59. T. Kong, R. Ahn, K. Yang, X. Zhu, Z. Fu, G. Morin, R. Bramley, N. C. Cliffe, Y. Xue, H. Kuasne, Q. Li, S. Jung, A. V. Gonzalez, S. Camilleri-Broet, M. C. Guiot, M. Park, J. Ursini-Siegel, S. Huang, CD44 promotes PD-L1 expression and its tumor-intrinsic function in breast and lung cancers. *Cancer Res.* **80**, 444–457 (2020).

60. H. B. Gupta, C. A. Clark, B. Yuan, G. Sareddy, S. Pandeswara, A. S. Padron, V. Hurez, J. Conejo-Garcia, R. Vadlamudi, R. Li, T. J. Curiel, Tumor cell-intrinsic PD-L1 promotes tumor-initiating cell generation and functions in melanoma and ovarian cancer. *Signal Transduct. Target. Ther.* **1**, 16030 (2016).

61. Y. Geng, X. Liu, J. Liang, D. M. Habiel, V. Kulur, A. L. Coelho, N. Deng, T. Xie, Y. Wang, N. Liu, G. Huang, A. Kurkciyan, Z. Liu, J. Tang, C. M. Hogaboam, D. Jiang, P. W. Noble, PD-L1 on invasive fibroblasts drives fibrosis in a humanized model of idiopathic pulmonary fibrosis. *JCI Insight*. **4** (2019), doi:10.1172/JCI.INSIGHT.125326.

62. S. Wang, J. Li, J. Xie, F. Liu, Y. Duan, Y. Wu, S. Huang, X. He, Z. Wang, X. Wu, Programmed death ligand 1 promotes lymph node metastasis and glucose metabolism in cervical cancer by activating integrin β4/SNAI1/SIRT3 signaling pathway. *Oncogene*. **37**, 4164–4180 (2018).

63. S. Ghosh, N. B. Nataraj, A. Noronha, S. Patkar, A. Sekar, S. Mukherjee, S. Winograd-Katz, L. Kramarski, A. Verma, M. Lindzen, D. D. Garcia, J. Green, G. Eisenberg, H. Gil-Henn, A. Basu, Y. Lender, S. Weiss, M. Oren, M. Lotem, B. Geiger, E. Ruppin, Y. Yarden, PD-L1 recruits phospholipase C and enhances tumorigenicity of lung tumors harboring mutant forms of EGFR. *Cell Rep.* **35** (2021), doi:10.1016/J.CELREP.2021.109181.

64. T. Li, F. Zhang, P. Qin, Y. Wang, A. Wang, L. Zhao, B. Xu, Q. Gao, Exploring a Tumor-Intrinsic PD-L1 Signal with Proximity-Dependent Biotin Identification in Lung Cancer Cells. *Biochemistry*. **58**, 2293–2296 (2019).

65. A. V. R. Kornepati, J. T. Boyd, C. E. Murray, J. Saifetiarova, B. de la Peña Avalos, C. M. Rogers, H. Bai, A. S. Padron, Y. Liao, C. Ontiveros, R. S. Svatek, R. Hromas, R. Li, Y. Hu, J. R. Conejo-Garcia, R. K. Vadlamudi, W. Zhao, E. Dray, P. Sung, T. J. Curiel, Tumor Intrinsic PD-L1 Promotes DNA Repair in Distinct Cancers and Suppresses PARP Inhibitor-Induced Synthetic Lethality. *Cancer Res.* **82**, 2156–2170 (2022).

66. Z. Xue, S. Zheng, D. Linghu, B. Liu, Y. Yang, M.-K. Chen, H. Huang, J. Song, H. Li, J. Wang, M.-C. Hung, D. Zhong, L. Sun, PD-L1 deficiency sensitizes tumor cells to DNA-PK inhibition and enhances cGAS-STING activation. *Am. J. Cancer Res.* **12**, 2363 (2022).

67. S. De, E. G. Holvey-Bates, K. Mahen, B. Willard, G. R. Stark, The ubiquitin E3 ligase FBXO22 degrades PD-L1 and sensitizes cancer cells to DNA damage. *Proc. Natl. Acad. Sci.* **118**, e2112674118 (2021).

68. C. H. Chang, J. Qiu, D. O'Sullivan, M. D. Buck, T. Noguchi, J. D. Curtis, Q. Chen, M. Gindin, M. M. Gubin, G. J. W. Van Der Windt, E. Tonc, R. D. Schreiber, E. J. Pearce, E. L. Pearce, Metabolic Competition in the Tumor Microenvironment Is a Driver of Cancer Progression. *Cell*. **162**, 1229–1241 (2015).

69. M. Garige, S. Ghosh, A. Norris, G. Li, S. Poncet, C.-K. Chou, W. W. Wu, R.-F. Shen, C. Sourbier, PD-L1 Mediates IFNγ-Regulation of Glucose but Not of Tryptophan Metabolism in Clear Cell Renal Cell Carcinoma. *Front. Oncol.* **12**, 1–13 (2022).

70. K. Kaira, I. Kuji, H. Kagamu, Value of 18F-FDG-PET to predict PD-L1 expression and outcomes of PD-1 inhibition therapy in human cancers. *Cancer Imaging*. **21**, 1–9 (2021).

71. S. Muralidharan, M. Sehgal, R. Soundharya, S. Mandal, S. S. Majumdar, M. Yeshwanth, A. Saha, M. K. Jolly, PD-L1 Activity Is Associated with Partial EMT and Metabolic Reprogramming in Carcinomas. *Curr. Oncol.* **29**, 8285–8301 (2022).

72. J. Pacheco-Torres, M.-F. Penet, Y. Mironchik, B. Krishnamachary, Z. M. Bhujwalla, The PD-L1 metabolic interactome intersects with choline metabolism and inflammation. *Cancer Metab.* **9**, 1–16 (2021).

73. G. Dock, THE INFLUENCE OF COMPLICATING DISEASES UPON LEUKAEMIA. *Am. J. Med. Sci.* **127**, 563 (1904).

74. L. Pelner, G. A. Fowler, H. C. Nauts, EFFECT OF CONCURRENT INFECTIONS AND THEIR TOXINS ON THE COURSE OF LEUKEMIA. *Acta Med. Scand.* **162**, 5–24 (1958).

75. G. Pasquinucci, POSSIBLE EFFECT OF MEASLES ON LEUKÆMIA. *Lancet*. **297**, 136 (1971).

76. S. Gross, MEASLES AND LEUKÆMIA. *Lancet*. **297**, 397–398 (1971).

77. C. Levaditi, S. Nicolau, Affinite du virus herpetique pour les neoplasmes epitheliaux. *Comptes Rendus Soc. Biol.* **87**, 498–500 (1922).

78. C. Dalba, D. Klatzmann, C. Logg, N. Kasahara, Beyond Oncolytic Virotherapy: Replication-Competent Retrovirus Vectors for Selective and Stable Transduction of Tumors. *Curr. Gene Ther.* **5**, 655–667 (2005).

79. C. M. Southam, A. E. Moore, CLINICAL STUDIES OF VIRUSES AS ANTINEOPLASTIC AGENTS, WITH PARTICULAR REFERENCE TO EGYPT 101 VIRUS. *Cancer*. **5**, 1025–1034 (1952).

80. S. K. Carter, IMMUNOTHERAPY OF CANCER IN MAN: CURRENT STATUS AND PROSPECTUS. *Ann. N. Y. Acad. Sci.* **277**, 722–740 (1976).

81. K. Garber, China Approves World's First Oncolytic Virus Therapy For Cancer Treatment. *JNCI J. Natl. Cancer Inst.* **98**, 298–300 (2006).

82. F. J. Kohlhapp, H. L. Kaufman, Molecular pathways: Mechanism of action for talimogene laherparepvec, a new oncolytic virus immunotherapy. *Clin. Cancer Res.* **22**, 1048–1054 (2016).

83. L. A. Pikor, J. C. Bell, J. S. Diallo, Oncolytic Viruses: Exploiting Cancer's Deal with the Devil. *Trends in Cancer*. **1**, 266–277 (2015).

84. R. M. L. Buller, G. L. Smith, K. Cremer, A. L. Notkins, B. Moss, Decreased virulence of recombinant vaccinia virus expression vectors is associated with a thymidine kinase-negative phenotype. *Nature*. **317**, 813–815 (1985).

85. R. L. Martuza, A. Malick, J. M. Markert, K. L. Ruffner, D. M. Coen, Experimental Therapy of Human Glioma by Means of a Genetically Engineered Virus Mutant. *Science (80-.).* **252**, 854–856 (1991).

86. M. Hengstschläger, M. Knöfler, E. W. Müllner, E. Ogris, E. Wintersberger, E. Wawra, Different regulation of thymidine kinase during the cell cycle of normal versus DNA tumor virus-transformed cells. *J. Biol. Chem.* **269**, 13836–13842 (1994).

87. J. A. Mccart, J. M. Ward, J. Lee, Y. Hu, H. R. Alexander, S. K. Libutti, B. Moss, D. L. Bartlett, Systemic Cancer Therapy with a Tumor-selective Vaccinia Virus Mutant Lacking Thymidine Kinase and Vaccinia Growth Factor Genes. *Cancer Res.* **61**, 8751–8757 (2001).

88. M. Puhlmann, M. Gnant, C. K. Brown, H. R. Alexander, D. L. Bartlett, Thymidine Kinase-Deleted Vaccinia Virus Expressing Purine Nucleoside Phosphorylase as a Vector for Tumor-Directed Gene Therapy. *Hum. Gene Ther.* **10**, 649–657 (2004).

89. S. H. Thorne, T. H. H. Hwang, W. E. O'Gorman, D. L. Bartlett, S. Sei, F. Kanji, C. Brown, J. Werier, J. H. Cho, D. E. Lee, Y. Wang, J. Bell, D. H. Kirn, Rational strain selection and engineering creates a broad-spectrum, systemically effective oncolytic poxvirus, JX-963. *J. Clin. Invest.* **117**, 3350–3358 (2007).

90. J. Hughes, P. Wang, G. Alusi, H. Shi, Y. Chu, J. Wang, V. Bhakta, I. McNeish, A. McCart, N. R. Lemoine, Y. Wang, Lister strain vaccinia virus with thymidine kinase gene deletion is a tractable platform for development of a new generation of oncolytic virus. *Gene Ther.* **22**, 476–484 (2015).

91. K. F. Hsu, C. L. Wu, S. C. Huang, J. L. Hsieh, Y. S. Huang, Y. F. Chen, M. R. Shen, W. J. Chung, C. Y. Chou, A. L. Shiau, Conditionally replicating E1B-deleted adenovirus driven by the squamous cell carcinoma antigen 2 promoter for uterine cervical cancer therapy. *Cancer Gene Ther.* **15**, 526–534 (2008).

92. J. C. Doloff, D. J. Waxman, Y. Jounaidi, Human Telomerase Reverse Transcriptase Promoter-Driven Oncolytic Adenovirus with E1B-19 kDa and E1B-55 kDa Gene Deletions. *Hum. Gene Ther.* **19**, 1383–1399 (2008).

93. O. Nakajima, A. Matsunaga, D. Ichimaru, Y. Urata, T. Fujiwara, K. Kawakami, Telomerase-specific virotherapy in an animal model of human head and neck cancer. *Mol. Cancer Ther.* **8**, 171–177 (2009).

94. J. L. Hsieh, C. H. Lee, M. L. Teo, Y. J. Lin, Y. S. Huang, C. L. Wu, A. L. Shiau, Transthyretin-driven oncolytic adenovirus suppresses tumor growth in orthotopic and ascites models of hepatocellular carcinoma. *Cancer Sci.* **100**, 537–545 (2009).

95. E. G. Cafferata, D. R. Macció, M. V. Lopez, D. L. Viale, C. Carbone, G. Mazzolini, O. L. Podhajcer, A novel A33 promoter-based conditionally replicative adenovirus suppresses tumor growth and eradicates hepatic metastases in human colon cancer models. *Clin. Cancer Res.* **15**, 3037–3049 (2009).

96. W. Pan, V. Bodempudi, T. Esfandyari, F. Farassati, Utilizing Ras Signaling Pathway to Direct Selective Replication of Herpes Simplex Virus-1. *PLoS One*. **4**, e6514 (2009).

97. M. Huch, A. Gros, A. José, J. R. González, R. Alemany, C. Fillat, Urokinase-Type Plasminogen Activator Receptor Transcriptionally Controlled Adenoviruses Eradicate Pancreatic Tumors and Liver Metastasis in Mouse Models. *Neoplasia*. **11**, 518–528 (2009).

98. B. D. Anderson, T. Nakamura, S. J. Russell, K.-W. Peng, High CD46 Receptor Density Determines Preferential Killing of Tumor Cells by Oncolytic Measles Virus. *Cancer Res.* **64**, 4919–4926 (2004).

99. J. Conner, L. Braidwood, S. M. Brown, A strategy for systemic delivery of the oncolytic herpes virus HSV1716: redirected tropism by antibody-binding sites incorporated on the virion surface as a glycoprotein D fusion protein. *Gene Ther.* **15**, 1579–1592 (2008).

100. C. Allen, G. Paraskevakou, I. Iankov, C. Giannini, M. Schroeder, J. Sarkaria, M. Schroeder, R. K. Puri, S. J. Russell, E. Galanis, Interleukin-13 Displaying Retargeted Oncolytic Measles Virus Strains Have Significant Activity Against Gliomas With Improved Specificity. *Mol. Ther.* **16**, 1556–1564 (2008).

101. J. Morrison, S. S. Briggs, N. Green, K. Fisher, V. Subr, K. Ulbrich, S. Kehoe, L. W. Seymour, Virotherapy of Ovarian Cancer With Polymer-cloaked Adenovirus Retargeted to the Epidermal Growth Factor Receptor. *Mol. Ther.* **16**, 244–251 (2008).

102. Y. Piao, H. Jiang, R. Alemany, V. Krasnykh, F. C. Marini, J. Xu, M. M. Alonso, C. A. Conrad, K. D. Aldape, C. Gomez-Manzano, J. Fueyo, Oncolytic adenovirus retargeted to Delta-EGFR induces selective antiglioma activity. *Cancer Gene Ther.* **16**, 256–265 (2008).

103. E. M. Gomes, M. S. Rodrigues, A. P. Phadke, L. D. Butcher, C. Starling, S. Chen, D. Chang, R. Hernandez-Alcoceba, J. T. Newman, M. J. Stone, A. W. Tong, Antitumor Activity of an Oncolytic Adenoviral-CD40 Ligand (CD154) Transgene Construct in Human Breast Cancer Cells. *Clin. Cancer Res.* **15**, 1317–1325 (2009).

104. L. Coughlan, S. Vallath, A. Saha, M. Flak, I. A. McNeish, G. Vassaux, J. F. Marshall, I. R. Hart, G. J. Thomas, In Vivo Retargeting of Adenovirus Type 5 to αvβ6 Integrin Results in Reduced Hepatotoxicity and Improved Tumor Uptake following Systemic Delivery. *J. Virol.* **83**, 6416–6428 (2009).

105. C. J. Breitbach, N. S. De Silva, T. J. Falls, U. Aladl, L. Evgin, J. Paterson, Y. Y. Sun, D. G. Roy, J. L. Rintoul, M. Daneshmand, K. Parato, M. M. Stanford, B. D. Lichty, A. Fenster, D. Kirn, H. Atkins, J. C. Bell, Targeting tumor vasculature with an oncolytic virus. *Mol. Ther.* **19**, 886–94 (2011).

106. R. Arulanandam, C. Batenchuk, F. A. Angarita, C. L. Addison, J. A. Mccart, J. C. B. Correspondence, VEGF-Mediated Induction of PRD1-BF1/Blimp1 Expression Sensitizes Tumor Vasculature to Oncolytic Virus Infection. *Cancer Cell*. **28**, 210–224 (2015).

107. C. S. Ilkow, M. Marguerie, C. Batenchuk, J. Mayer, D. Ben Neriah, S. Cousineau, T. Falls, V. A. Jennings, M. Boileau, D. Bellamy, D. Bastin, C. T. De Souza, A. Alkayyal, J. Zhang, F. Le Boeuf, R. Arulanandam, L. Stubbert, P. Sampath, S. H. Thorne, P. Paramanthan, A. Chatterjee, R. M. Strieter, M. Burdick, C. L. Addison, D. F. Stojdl, H. L. Atkins, R. C. Auer, J. S. Diallo, B. D. Lichty, J. C. Bell,

Reciprocal cellular cross-talk within the tumor microenvironment promotes oncolytic virus activity. *Nat. Med.* **21**, 530–536 (2015).

108. E. Ramelyte, A. Tastanova, M. Krauthammer, M. P. Levesque, R. Dummer, Z. Balá, D. Ignatova, P. Turko, U. Menzel, E. Guenova, C. Beisel, Oncolytic virotherapy-mediated anti-tumor response: a single-cell perspective. *Cancer Cell*. **39** (2021), doi:10.1016/j.ccell.2020.12.022.

109. S. Burke, A. Shergold, M. J. Elder, J. Whitworth, X. Cheng, H. Jin, R. W. Wilkinson, J. Harper, D. K. Carroll, Oncolytic Newcastle disease virus activation of the innate immune response and priming of antitumor adaptive responses in vitro. *Cancer Immunol. Immunother.*, 1–13 (2020).

110. T. F. Gajewski, H. Schreiber, Y. X. Fu, Innate and adaptive immune cells in the tumor microenvironment. *Nat. Immunol.* **14**, 1014–1022 (2013).

111. D. S. Chen, I. Mellman, Oncology meets immunology: The cancer-immunity cycle. *Immunity*. **39**, 1–10 (2013).

112. D. S. Chen, I. Mellman, Elements of cancer immunity and the cancer–immune set point. *Nature*. **541**, 321–330 (2017).

113. F. Errington, L. Steele, R. Prestwich, K. J. Harrington, H. S. Pandha, L. Vidal, J. de Bono, P. Selby, M. Coffey, R. Vile, A. Melcher, Reovirus activates human dendritic cells to promote innate antitumor immunity. *J. Immunol.* **180**, 6018–26 (2008).

114. A. Gauvrit, S. Brandler, C. Sapede-Peroz, N. Boisgerault, F. Tangy, M. Gregoire, Measles Virus Induces Oncolysis of Mesothelioma Cells and Allows Dendritic Cells to Cross-Prime Tumor-Specific CD8 Response. *Cancer Res.* **68**, 4882–4892 (2008).

115. C. Achard, J. B. Guillerme, D. Bruni, N. Boisgerault, C. Combredet, F. Tangy, N. Jouvenet, M. Grégoire, J. F. Fonteneaua, Oncolytic measles virus induces tumor necrosis factor-related apoptosis-inducing ligand (TRAIL)-mediated cytotoxicity by human myeloid and plasmacytoid dendritic cells. *Oncoimmunology*. **6** (2017), doi:10.1080/2162402X.2016.1261240/SUPPL_FILE/KONI_A_1261240_SM6457.PDF.

116. O. G. Donnelly, F. Errington-Mais, L. Steele, E. Hadac, V. Jennings, K. Scott, H. Peach, R. M. Phillips, J. Bond, H. Pandha, K. Harrington, R. Vile, S. Russell, P. Selby, A. A. Melcher, Measles virus causes immunogenic cell death in human melanoma. *Gene Ther.* **20**, 7–15 (2013).

117. M. H. Moehler, M. Zeidler, V. Wilsberg, J. J. Cornelis, T. Woelfel, J. Rommelaere, P. R. Galle, M. Heike, Parvovirus H-1-Induced Tumor Cell Death Enhances Human Immune Response In Vitro via Increased Phagocytosis, Maturation, and Cross-Presentation by Dendritic Cells. *Hum. Gene Ther.* **16**, 996–1005 (2005).

118. R. J. Prestwich, F. Errington, E. J. Ilett, R. S. M. Morgan, K. J. Scott, T. Kottke, J. Thompson, E. E. Morrison, K. J. Harrington, H. S. Pandha, P. J. Selby, R. G. Vile,

A. A. Melcher, Tumor Infection by Oncolytic Reovirus Primes Adaptive Antitumor Immunity. *Clin. Cancer Res.* **14**, 7358–7366 (2008).

119. J. B. Guillerme, N. Boisgerault, D. Roulois, J. Ménager, C. Combredet, F. Tangy, J. F. Fonteneau, M. Gregoire, Measles virus vaccine-infected tumor cells induce tumor antigen cross-presentation by human plasmacytoid dendritic cells. *Clin. Cancer Res.* **19**, 1147–1158 (2013).

120. T. Delaunay, M. Violland, N. Boisgerault, S. Dutoit, V. Vignard, C. Münz, M. Gannage, B. Dréno, K. Vaivode, D. Pjanova, N. Labarrière, Y. Wang, E. A. Chiocca, F. Le Boeuf, J. C. Bell, P. Erbs, F. Tangy, M. Grégoire, J. F. Fonteneau, Oncolytic viruses sensitize human tumor cells for NY-ESO-1 tumor antigen recognition by CD4+ effector T cells. *Oncoimmunology*. **7** (2018), doi:10.1080/2162402X.2017.1407897/SUPPL_FILE/KONI_A_1407897_SM9802.ZIP.

121. M. J. Atherton, K. B. Stephenson, F. Tzelepis, D. Bakhshinyan, J. K. Nikota, H. H. Son, A. Jirovec, C. Lefebvre, A. Dvorkin-Gheva, A. A. Ashkar, Y. Wan, D. F. Stojdl, E. C. Belanger, R. H. Breau, J. C. Bell, F. Saad, S. K. Singh, J. S. Diallo, B. D. Lichty, Transforming the prostatic tumor microenvironment with oncolytic virotherapy. *Oncoimmunology*. **7** (2018).

122. R. M. Diaz, F. Galivo, T. Kottke, P. Wongthida, J. Qiao, J. Thompson, M. Valdes, G. Barber, R. G. Vile, Oncolytic Immunovirotherapy for Melanoma Using Vesicular Stomatitis Virus. *Cancer Res.* **67**, 2840–2848 (2007).

123. R. J. Prestwich, E. J. Ilett, F. Errington, R. M. Diaz, L. P. Steele, T. Kottke, J. Thompson, F. Galivo, K. J. Harrington, H. S. Pandha, P. J. Selby, R. G. Vile, A. A. Melcher, Immune-mediated antitumor activity of reovirus is required for therapy and is independent of direct viral oncolysis and replication. *Clin. Cancer Res.* **15**, 4374–4381 (2009).

124. F. McNab, K. Mayer-Barber, A. Sher, A. Wack, A. O'Garra, Type I interferons in infectious disease. *Nat. Rev. Immunol.* **15**, 87–103 (2015).

125. J. W. Schoggins, S. J. Wilson, M. Panis, M. Y. Murphy, C. T. Jones, P. Bieniasz, C. M. Rice, A diverse range of gene products are effectors of the type I interferon antiviral response. *Nature*. **472** (2011), doi:10.1038/nature09907.

126. J. D. MacMicking, Interferon-inducible effector mechanisms in cell-autonomous immunity. *Nat. Rev. Immunol.* **12**, 367–382 (2012).

127. H. Kristiansen, H. H. Gad, S. Eskildsen-Larsen, P. Despres, R. Hartmann, The Oligoadenylate Synthetase Family: An Ancient Protein Family with Multiple Antiviral Activities. *J. Interf. Cytokine Res.* **31**, 41–47 (2011).

128. S. Balachandran, P. C. Roberts, L. E. Brown, H. Truong, A. K. Pattnaik, D. R. Archer, G. N. Barber, Essential Role for the dsRNA-Dependent Protein Kinase PKR in Innate Immunity to Viral Infection. *Immunity*. **13**, 129–141 (2000).

129. J. Verhelst, P. Hulpiau, X. Saelens, Mx Proteins: Antiviral Gatekeepers That

Restrain the Uninvited. *Microbiol. Mol. Biol. Rev.* **77**, 551–566 (2013).

130. A. Forero, S. Ozarkar, H. Li, S. K. Anderson, M. Gale, R. S. Correspondence, C. H. Lee, E. A. Hemann, M. S. Nadjsombati, M. R. Hendricks, L. So, R. Green, C. N. Roy, S. N. Sarkar, J. Von Moltke, R. Savan, Differential Activation of the Transcription Factor IRF1 Underlies the Distinct Immune Responses Elicited by Type I and Type III Interferons. *Immunity*. **51**, 451–464 (2019).

131. O. Takeuchi, S. Akira, Pattern Recognition Receptors and Inflammation. *Cell*. **140**, 805–820 (2010).

132. K. Newton, V. M. Dixit, Signaling in innate immunity and inflammation. *Cold Spring Harb. Perspect. Biol.* **4**, a006049 (2012).

133. J. C. Kagan, Signaling organelles of the innate immune system. *Cell*. **151**, 1168–1178 (2012).

134. H. Kato, S. Sato, M. Yoneyama, M. Yamamoto, S. Uematsu, K. Matsui, T. Tsujimura, K. Takeda, T. Fujita, O. Takeuchi, S. Akira, Cell Type-Specific Involvement of RIG-I in Antiviral Response. *Immunity*. **23**, 19–28 (2005).

135. H. Kato, O. Takeuchi, S. Sato, M. Yoneyama, M. Yamamoto, K. Matsui, S. Uematsu, A. Jung, T. Kawai, K. J. Ishii, O. Yamaguchi, K. Otsu, T. Tsujimura, C. S. Koh, C. Reis E Sousa, Y. Matsuura, T. Fujita, S. Akira, Differential roles of MDA5 and RIG-I helicases in the recognition of RNA viruses. *Nature*. **441**, 101–105 (2006).

136. H. Kato, O. Takeuchi, E. Mikamo-Satoh, R. Hirai, T. Kawai, K. Matsushita, A. Hiiragi, T. S. Dermody, T. Fujita, S. Akira, Length-dependent recognition of double-stranded ribonucleic acids by retinoic acid–inducible gene-I and melanoma differentiation–associated gene 5. *J. Exp. Med.* **205**, 1601–1610 (2008).

137. E. K. Crill, S. R. Furr-Rogers, I. Marriott, RIG-I is required for VSV-induced cytokine production by murine glia and acts in combination with DAI to initiate responses to HSV-1. *Glia*. **63**, 2168 (2015).

138. L. B. Ivashkiv, L. T. Donlin, Regulation of type I interferon responses. *Nat. Rev. Immunol.* **14**, 36–49 (2014).

139. P. Georgel, Z. Jiang, S. Kunz, E. Janssen, J. Mols, K. Hoebe, S. Bahram, M. B. A. Oldstone, B. Beutler, Vesicular stomatitis virus glycoprotein G activates a specific antiviral Toll-like receptor 4-dependent pathway. *Virology*. **362**, 304–313 (2007).

140. Z. Shi, Z. Cai, A. Sanchez, T. Zhang, S. Wen, J. Wang, J. Yang, S. Fu, D. Zhang, A Novel Toll-like Receptor That Recognizes Vesicular Stomatitis Virus. *J. Biol. Chem.* **286**, 4517 (2011).

141. D. J. Gough, N. L. Messina, C. J. P. Clarke, R. W. Johnstone, D. E. Levy, Constitutive Type I Interferon Modulates Homeostatic Balance through Tonic Signaling. *Immunity*. **36**, 166–174 (2012).

142. D. J. Gough, N. L. Messina, L. Hii, J. A. Gould, K. Sabapathy, A. P. S. Robertson, J. A. Trapani, D. E. Levy, P. J. Hertzog, C. J. P. Clarke, R. W. Johnstone, Functional Crosstalk between Type I and II Interferon through the Regulated Expression of STAT1. *PLOS Biol.* **8**, e1000361 (2010).

143. H. Cheon, E. G. Holvey-Bates, J. W. Schoggins, S. Forster, P. Hertzog, N. Imanaka, C. M. Rice, M. W. Jackson, D. J. Junk, G. R. Stark, IFNβ-dependent increases in STAT1, STAT2, and IRF9 mediate resistance to viruses and DNA damage. *EMBO J.* **32**, 2751–2763 (2013).

144. S. Mostafavi, H. Yoshida, D. Moodley, H. Leboité, K. Rothamel, T. Raj, C. J. Ye, N. Chevrier, S. Y. Zhang, T. Feng, M. Lee, J. L. Casanova, J. D. Clark, M. Hegen, J. B. Telliez, N. Hacohen, P. L. De Jager, A. Regev, D. Mathis, C. Benoist, Parsing the Interferon Transcriptional Network and Its Disease Associations. *Cell*. **164**, 564–578 (2016).

145. E. Platanitis, D. Demiroz, A. Schneller, K. Fischer, C. Capelle, M. Hartl, T. Gossenreiter, M. Müller, M. Novatchkova, T. Decker, A molecular switch from STAT2-IRF9 to ISGF3 underlies interferon-induced gene transcription. *Nat. Commun.* **10**, 1–17 (2019).

146. M. C. Abt, L. C. Osborne, L. A. Monticelli, T. A. Doering, T. Alenghat, G. F. Sonnenberg, M. A. Paley, M. Antenus, K. L. Williams, J. Erikson, E. J. Wherry, D. Artis, Commensal Bacteria Calibrate the Activation Threshold of Innate Antiviral Immunity. *Immunity*. **37**, 158–170 (2012).

147. S. C. Ganal, S. L. Sanos, C. Kallfass, K. Oberle, C. Johner, C. Kirschning, S. Lienenklaus, S. Weiss, P. Staeheli, P. Aichele, A. Diefenbach, Priming of Natural Killer Cells by Nonmucosal Mononuclear Phagocytes Requires Instructive Signals from Commensal Microbiota. *Immunity*. **37**, 171–186 (2012).

148. T. Kawashima, A. Kosaka, H. Yan, Z. Guo, R. Uchiyama, R. Fukui, D. Kaneko, Y. Kumagai, D. J. You, J. Carreras, S. Uematsu, M. H. Jang, O. Takeuchi, T. Kaisho, S. Akira, K. Miyake, H. Tsutsui, T. Saito, I. Nishimura, N. M. Tsuji, Double-Stranded RNA of Intestinal Commensal but Not Pathogenic Bacteria Triggers Production of Protective Interferon-β. *Immunity*. **38**, 1187–1197 (2013).

149. L. Deng, H. Liang, M. Xu, X. Yang, B. Burnette, A. Arina, X. D. Li, H. Mauceri, M. Beckett, T. Darga, X. Huang, T. F. Gajewski, Z. J. Chen, Y. X. Fu, R. R. Weichselbaum, STING-dependent cytosolic DNA sensing promotes radiation-induced type I interferon-dependent antitumor immunity in immunogenic tumors. *Immunity*. **41**, 843–852 (2014).

150. K. B. Chiappinelli, P. L. Strissel, A. Desrichard, T. A. Chan, S. B. Baylin, R. Strick Correspondence, H. Li, C. Henke, B. Akman, A. Hein, N. S. Rote, L. M. Cope, A. Snyder, V. Makarov, S. Buhu, D. J. Slamon, J. D. Wolchok, D. M. Pardoll, M. W. Beckmann, C. A. Zahnow, T. Merghoub, R. Strick, Inhibiting DNA Methylation Causes an Interferon Response in Cancer via dsRNA Including Endogenous Retroviruses Article Inhibiting DNA Methylation Causes an Interferon Response in Cancer via dsRNA Including Endogenous Retroviruses. *Cell*. **162**, 974–986

(2015).

151. C. Lu, J. Guan, S. Lu, Q. Jin, B. Rousseau, T. Lu, D. Stephens, H. Zhang, J. Zhu, M. Yang, Z. Ren, Y. Liang, Z. Liu, C. Han, L. Liu, X. Cao, A. Zhang, J. Qiao, K. Batten, M. Chen, D. H. Castrillon, T. Wang, B. Li, L. A. Diaz, G. M. Li, Y. X. Fu, DNA Sensing in Mismatch Repair-Deficient Tumor Cells Is Essential for Anti-tumor Immunity. *Cancer Cell*. **39**, 96-108.e6 (2021).

152. M. Tigano, D. C. Vargas, S. Tremblay-Belzile, Y. Fu, A. Sfeir, Nuclear sensing of breaks in mitochondrial DNA enhances immune surveillance. *Nature*. **591**, 477–481 (2021).

153. J. Guan, C. Lu, Q. Jin, H. Lu, X. Chen, L. Tian, Y. Zhang, J. Ortega, J. Zhang, S. Siteni, M. Chen, L. Gu, J. W. Shay, A. J. Davis, Z. J. Chen, Y. X. Fu, G. M. Li, MLH1 Deficiency-Triggered DNA Hyperexcision by Exonuclease 1 Activates the cGAS-STING Pathway. *Cancer Cell*. **39**, 109-121.e5 (2021).

154. L. Wang, I. Tassiulas, K. H. Park-Min, A. C. Reid, H. Gil-Henn, J. Schlessinger, R. Baron, J. J. Zhang, L. B. Ivashkiv, “Tuning” of type I interferon–induced Jak-STAT1 signaling by calcium-dependent kinases in macrophages. *Nat. Immunol. 2007 92*. **9**, 186–193 (2007).

155. L. F. Lu, M. P. Boldin, A. Chaudhry, L. L. Lin, K. D. Taganov, T. Hanada, A. Yoshimura, D. Baltimore, A. Y. Rudensky, Function of miR-146a in Controlling Treg Cell-Mediated Regulation of Th1 Responses. *Cell*. **142**, 914–929 (2010).

156. A. S. Papadopoulou, J. Dooley, M. A. Linterman, W. Pierson, O. Ucar, B. Kyewski, S. Zuklys, G. A. Hollander, P. Matthys, D. H. D. Gray, B. De Strooper, A. Liston, The thymic epithelial microRNA network elevates the threshold for infection-associated thymic involution via miR-29a mediated suppression of the IFN-α receptor. *Nat. Immunol. 2011 132*. **13**, 181–187 (2011).

157. D. T. Gracias, E. Stelekati, J. L. Hope, A. C. Boesteanu, T. A. Doering, J. Norton, Y. M. Mueller, J. A. Fraietta, E. J. Wherry, M. Turner, P. D. Katsikis, The microRNA miR-155 controls CD8+ T cell responses by regulating interferon signaling. *Nat. Immunol. 2013 146*. **14**, 593–602 (2013).

158. J. Liu, L. P. Carvalho, S. Bhattacharya, C. J. Carbone, K. G. S. Kumar, N. A. Leu, P. M. Yau, R. G. K. Donald, M. J. Weiss, D. P. Baker, K. J. McLaughlin, P. Scott, S. Y. Fuchs, Mammalian Casein Kinase 1α and Its Leishmanial Ortholog Regulate Stability of IFNAR1 and Type I Interferon Signaling. *Mol. Cell. Biol.* **29**, 6401–6412 (2009).

159. S. Bhattacharya, W. C. HuangFu, J. Liu, S. Veeranki, D. P. Baker, C. Koumenis, J. A. Diehl, S. Y. Fuchs, Inducible Priming Phosphorylation Promotes Ligand-independent Degradation of the IFNAR1 Chain of Type I Interferon Receptor. *J. Biol. Chem.* **285**, 2318–2325 (2010).

160. S. Bhattacharya, J. Qian, C. Tzimas, D. P. Baker, C. Koumenis, J. A. Diehl, S. Y. Fuchs, Role of p38 Protein Kinase in the Ligand-independent Ubiquitination and Down-regulation of the IFNAR1 Chain of Type I Interferon Receptor. *J. Biol.*

Chem. **286**, 22069 (2011).

161. J. Liu, W. C. HuangFu, K. G. S. Kumar, J. Qian, J. P. Casey, R. B. Hamanaka, C. Grigoriadou, R. Aldabe, J. A. Diehl, S. Y. Fuchs, Virus-Induced Unfolded Protein Response Attenuates Antiviral Defenses via Phosphorylation-Dependent Degradation of the Type I Interferon Receptor. *Cell Host Microbe*. **5**, 72–83 (2009).

162. Z. Du, Y. Shen, W. Yang, I. Mecklenbrauker, B. G. Neel, L. B. Ivashkiv, Inhibition of IFN-α signaling by a PKC- and protein tyrosine phosphatase SHP-2-dependent pathway. *Proc. Natl. Acad. Sci. U. S. A.* **102**, 10267–10272 (2005).

163. L. Wang, R. A. Gordon, L. Huynh, X. Su, K. H. P. Min, J. Han, J. S. Arthur, G. D. Kalliolias, L. B. Ivashkiv, Indirect Inhibition of Toll-like Receptor and Type I Interferon Responses by ITAM-Coupled Receptors and Integrins. *Immunity*. **32**, 518–530 (2010).

164. L. Huynh, L. Wang, C. Shi, K.-H. Park-Min, L. B. Ivashkiv, ITAM-Coupled Receptors Inhibit IFNAR Signaling and Alter Macrophage Responses to TLR4 and Listeria monocytogenes. *J. Immunol.* **188**, 3447–3457 (2012).

165. A. Yoshimura, T. Naka, M. Kubo, SOCS proteins, cytokine signalling and immune regulation. *Nat. Rev. Immunol.* **7**, 454–465 (2007).

166. M. Sarasin-Filipowicz, X. Wang, M. Yan, F. H. T. Duong, V. Poli, D. J. Hilton, D.-E. Zhang, M. H. Heim, Alpha Interferon Induces Long-Lasting Refractoriness of JAK-STAT Signaling in the Mouse Liver through Induction of USP18/UBP43. *Mol. Cell. Biol.* **29**, 4841–4851 (2009).

167. K. I. Arimoto, S. Löchte, S. A. Stoner, C. Burkart, Y. Zhang, S. Miyauchi, S. Wilmes, J. B. Fan, J. J. Heinisch, Z. Li, M. Yan, S. Pellegrini, F. Colland, J. Piehler, D. E. Zhang, STAT2 is an essential adaptor in USP18-mediated suppression of type I interferon signaling. *Nat. Struct. Mol. Biol.* **24**, 279–289 (2017).

168. H. H. Ho, L. B. Ivashkiv, Role of STAT3 in Type I Interferon Responses. *J. Biol. Chem.* **281**, 14111–14118 (2006).

169. W.-B. Wang, D. E. Levy, C.-K. Lee, STAT3 negatively regulates type I IFN-mediated antiviral response. *J. Immunol.* **187**, 2578–85 (2011).

170. L. Icardi, R. Mori, V. Gesellchen, S. Eyckerman, L. De Cauwer, J. Verhelst, K. Vercauteren, X. Saelens, P. Meuleman, G. Leroux-Roels, K. De Bosscher, M. Boutros, J. Tavernier, The Sin3a repressor complex is a master regulator of STAT transcriptional activity. *Proc. Natl. Acad. Sci. U. S. A.* **109**, 12058–63 (2012).

171. K. Shuai, B. Liu, Regulation of gene-activation pathways by PIAS proteins in the immune system. *Nat. Rev. Immunol.* **5**, 593–605 (2005).

172. J. H. Connor, C. Naczki, C. Koumenis, D. S. Lyles, Replication and Cytopathic Effect of Oncolytic Vesicular Stomatitis Virus in Hypoxic Tumor Cells In Vitro and In Vivo. *J. Virol.* **78**, 8960–8970 (2004).

173. I. I. L. Hwang, I. R. Watson, S. D. Der, M. Ohh, Loss of VHL Confers Hypoxia-Inducible Factor (HIF)-Dependent Resistance to Vesicular Stomatitis Virus: Role of HIF in Antiviral Response. *J. Virol.* **80**, 10712–10723 (2006).

174. A. Miar, E. Arnaiz, E. Bridges, S. Beedie, A. P. Cribbs, J. Downes, R. A. Beagrie, J. Rehwinkel, A. L. Harris, Hypoxia induces transcriptional and translational downregulation of the type I interferon (IFN) pathway in multiple cancer cell types. *Cancer Res.* (2020), doi:10.1158/0008-5472.CAN-19-2306.

175. A. Naldini, F. Carraro, W. R. Fleischmann, V. Bocci, Hypoxia Enhances the Antiviral Activity of Interferons. *J. Interferon Res.* **13**, 127–132 (2009).

176. H. Zheng, J. Qian, C. J. Carbone, N. A. Leu, D. P. Baker, S. Y. Fuchs, Vascular endothelial growth factor–induced elimination of the type 1 interferon receptor is required for efficient angiogenesis. *Blood*. **118**, 4003–4006 (2011).

177. M. Ghosh, S. Saha, J. Bettke, Mutant p53 suppresses innate immune signaling to promote tumorigenesis. *Cancer Cell*. **39**, 1–15 (2021).

178. B. T. Hummer, X.-L. Li, B. A. Hassel, Role for p53 in Gene Induction by Double-Stranded RNA. *J. Virol.* **75**, 7774–7777 (2001).

179. A. Takaoka, S. Hayakawa, H. Yanai, D. Stoiber, H. Negishi, H. Kikuchi, S. Sasaki, K. Imai, T. Shibue, K. Honda, T. Taniguchi, Integration of interferon-α/β signalling to p53 responses in tumour suppression and antiviral defence. *Nature*. **424**, 516–523 (2003).

180. C. Muñoz-Fontela, S. Macip, L. Martínez-Sobrido, L. Brown, J. Ashour, A. García-Sastre, S. W. Lee, S. A. Aaronson, Transcriptional role of p53 in interferon-mediated antiviral immunity. *J. Exp. Med.* **205**, 1929–1938 (2008).

181. J. Qing, C. Liu, L. Choy, R.-Y. Wu, J. S. Pagano, R. Derynck, Transforming Growth Factor β/Smad3 Signaling Regulates IRF-7 Function and Transcriptional Activation of the Beta Interferon Promoter. *Mol. Cell. Biol.* **24**, 1411–1425 (2004).

182. Y. Naiki, T. Komatsu, N. Koide, J. Dagvadorj, T. Yoshida, M. Arditi, T. Yokochi, TGF-β1 inhibits the production of IFN in response to CpG DNA via ubiquitination of TNF receptor-associated factor (TRAF) 6. *Innate Immun.* **21**, 770–777 (2015).

183. S. M. Pokharel, N. K. Shil, S. Bose, Autophagy, TGF-β, and SMAD-2/3 signaling regulates interferon-β response in respiratory syncytial virus infected macrophages. *Front. Cell. Infect. Microbiol.* **6**, 174 (2016).

184. J. R. Grunwell, S. M. Yeligar, S. Stephenson, X. Du Ping, T. W. Gauthier, A. M. Fitzpatrick, L. A. S. Brown, TGF-β1 Suppresses the Type I IFN Response and Induces Mitochondrial Dysfunction in Alveolar Macrophages. *J. Immunol.* **200**, 2115–2128 (2018).

185. J. Lupberger, F. H. T. Duong, I. Fofana, L. Zona, F. Xiao, C. Thumann, S. C. Durand, P. Pessaux, M. B. Zeisel, M. H. Heim, T. F. Baumert, Epidermal growth factor receptor signaling impairs the antiviral activity of interferon-alpha. *Hepatology*. **58**, 1225–1235 (2013).

186. Z. Liu, C. Han, C. Dong, A. Shen, E. Hsu, Z. Ren, C. Lu, L. Liu, A. Zhang, C. Timmerman, Y. Pu, Y. Wang, M. Chen, J. Qiao, Y. X. Fu, Hypofractionated EGFR tyrosine kinase inhibitor limits tumor relapse through triggering innate and adaptive immunity. *Sci. Immunol.* **4** (2019), doi:10.1126/SCIIMMUNOL.AAV6473/SUPPL_FILE/AAV6473_TABLE_S2.XLSX.

187. K. Gong, G. Guo, N. Panchani, M. E. Bender, D. E. Gerber, J. D. Minna, F. Fattah, B. Gao, M. Peyton, K. Kernstine, B. Mukherjee, S. Burma, C. M. Chiang, S. Zhang, A. Amod Sathe, C. Xing, K. H. Dao, D. Zhao, E. A. Akbay, A. A. Habib, EGFR inhibition triggers an adaptive response by co-opting antiviral signaling pathways in lung cancer. *Nat. Cancer*. **1**, 394–409 (2020).

188. R. J. Robb, E. Kreijveld, R. D. Kuns, Y. A. Wilson, S. D. Olver, A. L. J. Don, N. C. Raffelt, N. A. De Weerd, K. E. Lineburg, A. Varelias, K. A. Markey, M. Koyama, A. D. Clouston, P. J. Hertzog, K. P. A. MacDonald, G. R. Hill, Type I-IFNs control GVHD and GVL responses after transplantation. *Blood*. **118**, 3399–3409 (2011).

189. B. Drobits, M. Holcmann, N. Amberg, M. Swiecki, R. Grundtner, M. Hammer, M. Colonna, M. Sibilia, Imiquimod clears tumors in mice independent of adaptive immunity by converting pDCs into tumor-killing effector cells. *J. Clin. Invest.* **122**, 575–585 (2012).

190. S. R. Woo, M. B. Fuertes, L. Corrales, S. Spranger, M. J. Furdyna, M. Y. K. Leung, R. Duggan, Y. Wang, G. N. Barber, K. A. Fitzgerald, M. L. Alegre, T. F. Gajewski, STING-Dependent Cytosolic DNA Sensing Mediates Innate Immune Recognition of Immunogenic Tumors. *Immunity*. **41**, 830–842 (2014).

191. D. Zamarin, R. B. Holmgaard, S. K. Subudhi, J. S. Park, M. Mansour, P. Palese, T. Merghoub, J. D. Wolchok, J. P. Allison, Localized oncolytic virotherapy overcomes systemic tumor resistance to immune checkpoint blockade immunotherapy. *Sci. Transl. Med.* **6** (2014), doi:10.1126/SCITRANSLMED.3008095/SUPPL_FILE/5-226RA32_TABLES_S1_TO_S9.ZIP.

192. I. Melero, J. I. Quetglas, M. Reboredo, J. Dubrot, J. R. Rodriguez-Madoz, U. Mancheño, E. Casales, J. I. Riezu-Boj, M. Ruiz-Guillen, M. C. Ochoa, M. F. Sanmamed, N. Thieblemont, C. Smerdou, S. Hervas-Stubbs, Strict requirement for vector-induced type I interferon in efficacious antitumor responses to virally encoded IL12. *Cancer Res.* **75**, 497–507 (2015).

193. B. N. Bidwell, C. Y. Slaney, N. P. Withana, S. Forster, Y. Cao, S. Loi, D. Andrews, T. Mikeska, N. E. Mangan, S. A. Samarajiwa, N. A. De Weerd, J. Gould, P. Argani, A. Müller, M. J. Smyth, R. L. Anderson, P. J. Hertzog, B. S. Parker, Silencing of Irf7 pathways in breast cancer cells promotes bone metastasis through immune escape. *Nat. Med.* **18**, 1224–1231 (2012).

194. G. P. Dunn, A. T. Bruce, K. C. F. Sheehan, V. Shankaran, R. Uppaluri, J. D. Bui, M. S. Diamond, C. M. Koebel, C. Arthur, J. M. White, R. D. Schreiber, A critical function for type I interferons in cancer immunoediting. *Nat. Immunol.* **6**, 722–729 (2005).

195. J. B. Swann, Y. Hayakawa, N. Zerafa, K. C. F. Sheehan, B. Scott, R. D. Schreiber, P. Hertzog, M. J. Smyth, Type I IFN Contributes to NK Cell Homeostasis, Activation, and Antitumor Function. *J. Immunol.* **178**, 7540–7549 (2007).

196. H. M. Chen, N. Tanaka, Y. Mitani, E. Oda, H. Nozawa, J. Z. Chen, H. Yanai, H. Negishi, M. K. Choi, T. Iwasaki, H. Yamamoto, T. Taniguchi, A. Takaoka, Critical role for constitutive type I interferon signaling in the prevention of cellular transformation. *Cancer Sci.* **100**, 449–456 (2009).

197. M. Tschurtschenthaler, J. Wang, C. Fricke, T. M. J. Fritz, L. Niederreiter, T. E. Adolph, E. Sarcevic, S. Künzel, F. A. Offner, U. Kalinke, J. F. Baines, H. Tilg, A. Kaser, Type I interferon signalling in the intestinal epithelium affects Paneth cells, microbial ecology and epithelial regeneration. *Gut*. **63**, 1921–1931 (2014).

198. K. V. Katlinski, J. Gui, Y. V. Katlinskaya, A. Ortiz, R. Chakraborty, S. Bhattacharya, C. J. Carbone, D. P. Beiting, M. A. Girondo, A. R. Peck, E. Puré, P. Chatterji, A. K. Rustgi, J. A. Diehl, C. Koumenis, H. Rui, S. Y. Fuchs, Inactivation of Interferon Receptor Promotes the Establishment of Immune Privileged Tumor Microenvironment. *Cancer Cell*. **31**, 194–207 (2017).

199. L. A. Albacker, J. Wu, P. Smith, M. Warmuth, P. J. Stephens, P. Zhu, L. Yu, J. Chmielecki, Loss of function JAK1 mutations occur at high frequency in cancers with microsatellite instability and are suggestive of immune evasion. *PLoS One*. **12** (2017), doi:10.1371/JOURNAL.PONE.0176181.

200. D. S. Shin, J. M. Zaretsky, H. Escuin-Ordinas, A. Garcia-Diaz, S. Hu-Lieskovan, A. Kalbasi, C. S. Grasso, W. Hugo, S. Sandoval, D. Y. Torrejon, N. Palaskas, G. Abril-Rodriguez, G. Parisi, A. Azhdam, B. Chmielowski, G. Cherry, E. Seja, B. Berent-Maoz, I. P. Shintaku, D. T. Le, D. M. Pardoll, L. A. Diaz, P. C. Tumeh, T. G. Graeber, R. S. Lo, B. Comin-Anduix, A. Ribas, Primary resistance to PD-1 blockade mediated by JAK1/2 mutations. *Cancer Discov.* **7**, 188–201 (2017).

201. B. L. Wehde, P. D. Rädler, H. Shrestha, S. J. Johnson, A. A. Triplett, K. U. Wagner, Janus Kinase 1 Plays a Critical Role in Mammary Cancer Progression. *Cell Rep.* **25**, 2192-2207.e5 (2018).

202. S. R. Chan, C. G. Rickert, W. Vermi, K. C. F. Sheehan, C. Arthur, J. A. Allen, J. M. White, J. Archambault, S. Lonardi, T. M. McDevitt, D. Bhattacharya, M. V. Lorenzi, D. C. Allred, R. D. Schreiber, Dysregulated STAT1-SOCS1 control of JAK2 promotes mammary luminal progenitor cell survival and drives ERα+ tumorigenesis. *Cell Death Differ. 2014 212*. **21**, 234–246 (2013).

203. J. C. Paglino, A. N. van den Pol, Vesicular Stomatitis Virus Has Extensive Oncolytic Activity against Human Sarcomas: Rare Resistance Is Overcome by Blocking Interferon Pathways. *J. Virol.* **85**, 9346–9358 (2011).

204. D. Escobar-Zarate, Y. P. Liu, L. Suksanpaisan, S. J. Russell, K. W. Peng, Overcoming cancer cell resistance to VSV oncolysis with JAK1/2 inhibitors. *Cancer Gene Ther.* **20**, 582–589 (2013).

205. M. Moerdyk-Schauwecker, N. R. Shah, A. M. Murphy, E. Hastie, P. Mukherjee, V. Z. Grdzelishvili, Resistance of pancreatic cancer cells to oncolytic vesicular stomatitis virus: Role of type I interferon signaling. *Virology*. **436**, 221–234 (2013).

206. D. M. Knipe, P. M. Howley, in *Fields Virology* (Lippincott Williams & Wilkins, Philidelphia, ed. 5th, 2007), pp. 1364–1408.

207. D. Finkelshtein, A. Werman, D. Novick, S. Barak, M. Rubinstein, LDL receptor and its family members serve as the cellular receptors for vesicular stomatitis virus. *Proc. Natl. Acad. Sci. U. S. A.* **110**, 7306–7311 (2013).

208. D. K. Cureton, R. H. Massol, S. Saffarian, T. L. Kirchhausen, S. P. J. Whelan, Vesicular Stomatitis Virus Enters Cells through Vesicles Incompletely Coated with Clathrin That Depend upon Actin for Internalization. *PLOS Pathog.* **5**, e1000394 (2009).

209. D. K. Cureton, R. H. Massol, S. P. J. Whelan, T. Kirchhausen, The Length of Vesicular Stomatitis Virus Particles Dictates a Need for Actin Assembly during Clathrin-Dependent Endocytosis. *PLOS Pathog.* **6**, e1001127 (2010).

210. Y. Ito, L. Montagnier, Heterogeneity of the sensitivity of vesicular stomatitis virus to interferons. *Infect. Immun.* **18**, 23 (1977).

211. U. Müller, U. Steinhoff, L. F. L. Reis, S. Hemmi, J. Pavlovic, R. M. Zinkernagel, M. Aguet, Functional Role of Type I and Type II Interferons in Antiviral Defense. *Science (80-.).* **264**, 1918–1921 (1994).

212. J. E. Durbin, R. Hackenmiller, M. C. Simon, D. E. Levy, Targeted disruption of the mouse Stat1 gene results in compromised innate immunity to viral disease. *Cell*. **84**, 443–450 (1996).

213. M. A. Meraz, J. M. White, K. C. F. Sheehan, E. A. Bach, S. J. Rodig, A. S. Dighe, D. H. Kaplan, J. K. Riley, A. C. Greenlund, D. Campbell, K. Carver-Moore, R. N. DuBois, R. Clark, M. Aguet, R. D. Schreiber, Targeted disruption of the Stat1 gene in mice reveals unexpected physiologic specificity in the JAK-STAT signaling pathway. *Cell*. **84**, 431–442 (1996).

214. P. I. Marcus, M. J. Sekellick, Interferon induction by viruses. XIII. Detection and assay of interferon induction-suppressing particles. *Virology*. **142**, 411–415 (1985).

215. B. L. Black, D. S. Lyles, Vesicular stomatitis virus matrix protein inhibits host cell-directed transcription of target genes in vivo. *J. Virol.* **66**, 4058–4064 (1992).

216. P. I. Marcus, M. J. Sekellick, C. F. Spiropoulou, S. T. Nichol, Interferon induction by viruses. XXII. Vesicular stomatitis virus-Indiana: M-protein and leader RNA do not regulate interferon induction in chicken embryo cells. *J. Interferon Res.* **13**, 413–418 (1993).

217. B. L. Black, R. B. Rhodes, M. McKenzie, D. S. Lyles, The role of vesicular stomatitis virus matrix protein in inhibition of host-directed gene expression is genetically separable from its function in virus assembly. *J. Virol.* **67**, 4814–4821

(1993).

218. M. C. Ferran, J. M. Lucas-Lenard, The vesicular stomatitis virus matrix protein inhibits transcription from the human beta interferon promoter. *J. Virol.* **71**, 371–377 (1997).

219. S. A. Richards, K. L. Carey, I. G. Macara, Requirement of guanosine triphosphate-bound ran for signal-mediated nuclear protein export. *Science (80-.).* **276**, 1842–1844 (1997).

220. M. Ahmed, D. S. Lyles, Effect of Vesicular Stomatitis Virus Matrix Protein on Transcription Directed by Host RNA Polymerases I, II, and III. *J. Virol.* **72**, 8413–8419 (1998).

221. J. M. Petersen, L.-S. Her, V. Varvel, E. Lund, J. E. Dahlberg, The Matrix Protein of Vesicular Stomatitis Virus Inhibits Nucleocytoplasmic Transport When It Is in the Nucleus and Associated with Nuclear Pore Complexes. *Mol. Cell. Biol.* **20**, 8590–8601 (2000).

222. C. Von Kobbe, J. M. A. Van Deursen, J. P. Rodrigues, D. Sitterlin, A. Bachi, X. Wu, M. Wilm, M. Carmo-Fonseca, E. Izaurralde, Vesicular stomatitis virus matrix protein inhibits host cell gene expression by targeting the nucleoporin Nup98. *Mol. Cell*. **6**, 1243–1252 (2000).

223. M. Ahmed, M. O. McKenzie, S. Puckett, M. Hojnacki, L. Poliquin, D. S. Lyles, Ability of the Matrix Protein of Vesicular Stomatitis Virus To Suppress Beta Interferon Gene Expression Is Genetically Correlated with the Inhibition of Host RNA and Protein Synthesis. *J. Virol.* **77**, 4646–4657 (2003).

224. J. C. Bell, D. F. Stojdl, B. Lichty, S. Knowles, R. Marius, H. Atkins, N. Sonenberg, Exploiting tumor-specific defects in the interferon pathway with a previously unknown oncolytic virus. *Nat. Med.* **6**, 821–825 (2000).

225. D. F. Stojdl, B. D. Lichty, B. R. tenOever, J. M. Paterson, A. T. Power, S. Knowles, R. Marius, J. Reynard, L. Poliquin, H. Atkins, E. G. Brown, R. K. Durbin, J. E. Durbin, J. Hiscott, J. C. Bell, VSV strains with defects in their ability to shutdown innate immunity are potent systemic anti-cancer agents. *Cancer Cell*. **4**, 263–75 (2003).

226. M. C. Bourgeois-Daigneault, D. G. Roy, A. S. Aitken, N. El Sayes, N. T. Martin, O. Varette, T. Falls, L. E. St-Germain, A. Pelin, B. D. Lichty, D. F. Stojdl, G. Ungerechts, J. S. Diallo, J. C. Bell, Neoadjuvant oncolytic virotherapy before surgery sensitizes triple-negative breast cancer to immune checkpoint therapy. *Sci. Transl. Med.* **10**, 1641 (2018).

227. Z. Liu, R. Ravindranathan, P. Kalinski, Z. S. Guo, D. L. Bartlett, Rational combination of oncolytic vaccinia virus and PD-L1 blockade works synergistically to enhance therapeutic efficacy. *Nat. Commun.* **8** (2017), doi:10.1038/ncomms14754.

228. D. Zamarin, J. M. Ricca, S. Sadekova, A. Oseledchyk, Y. Yu, W. M.

Blumenschein, J. Wong, M. Gigoux, T. Merghoub, J. D. Wolchok, PD-L1 in tumor microenvironment mediates resistance to oncolytic immunotherapy. *J. Clin. Invest.* **128** (2018).

229. N. El-Sayes, S. Walsh, A. Vito, A. Reihani, K. Ask, Y. Wan, K. Mossman, IFNAR blockade synergizes with oncolytic VSV to prevent virus-mediated PD-L1 expression and promote antitumor T cell activity. *Mol. Ther. - Oncolytics*. **25**, 16–30 (2022).

230. M. Y. Bartee, K. M. Dunlap, E. Bartee, Tumor-Localized Secretion of Soluble PD1 Enhances Oncolytic Virotherapy. *Cancer Res.* **77**, 2952–2963 (2017).

231. W. Shen, M. M. Patnaik, A. Ruiz, S. J. Russell, K. W. Peng, Immunovirotherapy with vesicular stomatitis virus and PD-L1 blockade enhances therapeutic outcome in murine acute myeloid leukemia. *Blood*. **127**, 1449–1458 (2016).

232. M. Gato-Cañas, M. Zuazo, H. Arasanz, M. Ibañez-Vea, L. Lorenzo, G. Fernandez-Hinojal, R. Vera, C. Smerdou, E. Martisova, I. Arozarena, C. Wellbrock, D. Llopiz, M. Ruiz, P. Sarobe, K. Breckpot, G. Kochan, D. Escors, PDL1 Signals through Conserved Sequence Motifs to Overcome Interferon-Mediated Cytotoxicity. *Cell Rep.* **20**, 1818–1829 (2017).

233. B. Diskin, S. Adam, M. F. Cassini, G. Sanchez, M. Liria, B. Aykut, C. Buttar, E. Li, B. Sundberg, R. D. Salas, R. Chen, J. Wang, M. Kim, M. Saad Farooq, S. Nguy, C. Fedele, K. Ho Tang, T. Chen, W. Wang, M. Hundeyin, J. A. Kochen Rossi, E. Kurz, M. Israr Ul Haq, J. Karlen, E. Kruger, Z. Sekendiz, D. Wu, S. A. A Shadaloey, G. Baptiste, G. Werba, S. Selvaraj, C. Loomis, K.-K. Wong, J. Leinwand, G. Miller, PD-L1 engagement on T cells promotes self-tolerance and suppression of neighboring macrophages and effector T cells in cancer. *Nat. Immunol.* **21**, 442–454 (2020).

234. H. Cheon, E. G. Holvey-Bates, D. J. Mcgrail, G. R. Stark, L. A. Diaz, P. J. Hertzog, PD-L1 sustains chronic, cancer cell-intrinsic responses to type I interferon, enhancing resistance to DNA damage. *Proc. Natl. Acad. Sci.* **118**, 1–10 (2021).

235. L. Young, J. Sung, J. R. Masters, Detection of Mycoplasma in cell cultures. *Nat. Protoc.* **5**, 929–934 (2010).

236. N. E. Sanjana, O. Shalem, F. Zhang, Improved vectors and genome-wide libraries for CRISPR screening. *Nat. Methods*. **11**, 783 (2014).

237. N. L. Bray, H. Pimentel, P. Melsted, L. Pachter, Near-optimal probabilistic RNA-seq quantification. *Nat. Biotechnol.* **34**, 525–527 (2016).

238. H. Pimentel, N. L. Bray, S. Puente, P. Melsted, L. Pachter, Differential analysis of RNA-seq incorporating quantification uncertainty. *Nat. Methods*. **14**, 687–690 (2017).

239. M. Schubert, B. Klinger, M. Klünemann, A. Sieber, F. Uhlitz, S. Sauer, M. J. Garnett, N. Blüthgen, J. Saez-Rodriguez, Perturbation-response genes reveal

signaling footprints in cancer gene expression. *Nat. Commun.* **9**, 1–11 (2018).

240. M. Foroutan, D. D. Bhuva, R. Lyu, K. Horan, J. Cursons, M. J. Davis, Single sample scoring of molecular phenotypes. *BMC Bioinformatics*. **19**, 1–10 (2018).

241. W. Guo, L. Jiang, S. Bhasin, S. M. Khan, R. H. Swerdlow, DNA Extraction Procedures Meaningfully Influence qPCR-Based mtDNA Copy Number Determination. *Mitochondrion*. **9**, 261 (2009).

242. A. Subramanian, P. Tamayo, V. K. Mootha, S. Mukherjee, B. L. Ebert, M. A. Gillette, A. Paulovich, S. L. Pomeroy, T. R. Golub, E. S. Lander, J. P. Mesirov, Gene set enrichment analysis: A knowledge-based approach for interpreting genome-wide expression profiles. *Proc. Natl. Acad. Sci. U. S. A.* **102**, 15545–15550 (2005).

243. A. Liberzon, C. Birger, H. Thorvaldsdóttir, M. Ghandi, J. P. Mesirov, P. Tamayo, The Molecular Signatures Database (MSigDB) hallmark gene set collection. *Cell Syst.* **1**, 417 (2015).

244. D. P. Cook, B. C. Vanderhyden, Transcriptional census of epithelial-mesenchymal plasticity in cancer. *Sci. Adv.* **8**, 7640 (2022).

245. M. A. Savaikar, T. Whitehead, S. Roy, L. Strong, N. Fettig, T. Prmeau, J. Luo, S. Li, R. L. Wahl, K. I. Shoghi, Preclinical PERCIST and 25% of SUVmax Threshold: Precision Imaging of Response to Therapy in Co-clinical 18F-FDG PET Imaging of Triple-Negative Breast Cancer Patient–Derived Tumor Xenografts. *J. Nucl. Med.* **61**, 842–849 (2020).

246. S. Dupuis, E. Jouanguy, S. Al-Hajjar, C. Fieschi, I. Zaid Al-Mohsen, S. Al-Jumaah, K. Yang, A. Chapgier, C. Eidenschenk, P. Eid, A. Al Ghonaium, H. Tufenkeji, H. Frayha, S. Al-Gazlan, H. Al-Rayes, R. D. Schreiber, I. Gresser, J. L. Casanova, Impaired response to interferon-α/β and lethal viral disease in human STAT1 deficiency. *Nat. Genet.* **33**, 388–391 (2003).

247. Y. Minegishi, M. Saito, T. Morio, K. Watanabe, K. Agematsu, S. Tsuchiya, H. Takada, T. Hara, N. Kawamura, T. Ariga, H. Kaneko, N. Kondo, I. Tsuge, A. Yachie, Y. Sakiyama, T. Iwata, F. Bessho, T. Ohishi, K. Joh, K. Imai, K. Kogawa, M. Shinohara, M. Fujieda, H. Wakiguchi, S. Pasic, M. Abinun, H. D. Ochs, E. D. Renner, A. Jansson, B. H. Belohradsky, A. Metin, N. Shimizu, S. Mizutani, T. Miyawaki, S. Nonoyama, H. Karasuyama, Human Tyrosine Kinase 2 Deficiency Reveals Its Requisite Roles in Multiple Cytokine Signals Involved in Innate and Acquired Immunity. *Immunity*. **25**, 745–755 (2006).

248. T. Le Voyer, S. Sakata, M. Tsumura, T. Khan, A. Esteve-Sole, B. K. Al-Saud, H. E. Gungor, P. Taur, V. Jeanne-Julien, M. Christiansen, L.-M. Köhler, G. E. ElGhazali, J. Rosain, S. Nishimura, F. Sakura, M. Bouaziz, C. Oleaga-Quintas, A. Nieto-Patlán, À. Deyà-Martinez, Y. Altuner Torun, A.-L. Neehus, M. Roynard, S. E. Bozdemir, N. Al Kaabi, M. Al Hassani, I. Mersiyanova, F. Rozenberg, C. Speckmann, I. Hainmann, F. Hauck, M. H. Alzahrani, S. H. Alhajjar, S. Al-Muhsen, T. Cole, R. Fuleihan, P. D. Arkwright, R. Badolato, L. Alsina, L. Abel, M.

Desai, H. Al-Mousa, A. Shcherbina, N. Marr, S. Boisson-Dupuis, J.-L. Casanova, S. Okada, J. Bustamante, Genetic, Immunological, and Clinical Features of 32 Patients with Autosomal Recessive STAT1 Deficiency. *J. Immunol.* **207**, 133–152 (2021).

249. S. Varghese, S. D. Rabkin, R. Liu, P. G. Nielsen, T. Ipe, R. L. Martuza, Enhanced therapeutic efficacy of IL-12, but not GM-CSF, expressing oncolytic herpes simplex virus for transgenic mouse derived prostate cancers. *Cancer Gene Ther.* **13**, 253–265 (2006).

250. N. E. Annels, G. R. Simpson, M. Denyer, M. Arif, M. Coffey, A. Melcher, K. Harrington, R. Vile, H. Pandha, Oncolytic reovirus-mediated recruitment of early innate immune responses reverses immunotherapy resistance in prostate tumors. *Mol. Ther. - Oncolytics*. **20**, 434–446 (2021).

251. C. Monge, C. Xie, G. Brar, E. Akoth, S. Webb, D. Mabry, B. Redd, E. Levy, B. Wood, T. Greten, A phase I/II study of JX-594 oncolytic virus in combination with immune checkpoint inhibition in refractory colorectal cancer. *Eur. J. Cancer*. **138**, S57–S58 (2020).

252. J. D. Burke, L. C. Platanias, E. N. Fish, Beta interferon regulation of glucose metabolism is PI3K/Akt dependent and important for antiviral activity against coxsackievirus B3. *J. Virol.* **88**, 3485–3495 (2014).

253. B. Wang, T. Y. Liu, C. H. Lai, Y. H. Rao, M. C. Choi, J. T. Chi, J. W. Dai, J. C. Rathmell, T. P. Yao, Glycolysis-dependent histone deacetylase 4 degradation regulates inflammatory cytokine production. *Mol. Biol. Cell*. **25**, 3300–3307 (2014).

254. H. Jiang, H. Shi, M. Sun, Y. Wang, Q. Meng, P. Guo, Y. Cao, J. Chen, X. Gao, E. Li, J. Liu, PFKFB3-Driven Macrophage Glycolytic Metabolism Is a Crucial Component of Innate Antiviral Defense. *J. Immunol.* **197**, 2880–2890 (2016).

255. T. Shirai, R. R. Nazarewicz, B. B. Wallis, R. E. Yanes, R. Watanabe, M. Hilhorst, L. Tian, D. G. Harrison, J. C. Giacomini, T. L. Assimes, J. J. Goronzy, C. M. Weyand, The glycolytic enzyme PKM2 bridges metabolic and inflammatory dysfunction in coronary artery disease. *J. Exp. Med.* **213**, 337–354 (2016).

256. D. Ahmed, E. Cassol, Role of cellular metabolism in regulating type I interferon responses: Implications for tumour immunology and treatment. *Cancer Lett.* **409**, 20–29 (2017).

257. G. J. Inman, F. J. Nicol´as, N. Nicol´as, J. F. Callahan, J. D. Harling, L. M. Gaster, A. D. Reith, N. J. Laping, C. S. Hill, SB-431542 Is a Potent and Specific Inhibitor of Transforming Growth Factor-Superfamily Type I Activin Receptor-Like Kinase (ALK) Receptors ALK4, ALK5, and ALK7. *Mol. Pharmacol.* **62**, 65–74 (2002).

258. D. Li, L. Ambrogio, T. Shimamura, S. Kubo, M. Takahashi, L. R. Chirieac, R. F. Padera, G. I. Shapiro, A. Baum, F. Himmelsbach, W. J. Rettig, M. Meyerson, F. Solca, H. Greulich, K. K. Wong, BIBW2992, an irreversible EGFR/HER2 inhibitor highly effective in preclinical lung cancer models. *Oncogene*. **27**, 4702–4711

(2008).

259. A. Castell, Q. Yan, K. Fawkner, P. Hydbring, F. Zhang, V. Verschut, M. Franco, S. M. Zakaria, W. Bazzar, J. Goodwin, G. Zinzalla, L. G. Larsson, A selective high affinity MYC-binding compound inhibits MYC:MAX interaction and MYC-dependent tumor cell proliferation. *Sci. Rep.* **8**, 10064 (2018).

260. A. J. Asirvatham, M. Schmidt, B. Gao, J. Chaudhary, Androgens Regulate the Immune/Inflammatory Response and Cell Survival Pathways in Rat Ventral Prostate Epithelial Cells. *Endocrinology*. **147**, 257–271 (2006).

261. S. Kovats, Estrogen receptors regulate innate immune cells and signaling pathways. *Cell. Immunol.* **294**, 63–69 (2015).

262. A. Singh, S. Venkannagari, K. H. Oh, Y. Q. Zhang, J. M. Rohde, L. Liu, S. Nimmagadda, K. Sudini, K. R. Brimacombe, S. Gajghate, J. Ma, A. Wang, X. Xu, S. A. Shahane, M. Xia, J. Woo, G. A. Mensah, Z. Wang, M. Ferrer, E. Gabrielson, Z. Li, F. Rastinejad, M. Shen, M. B. Boxer, S. Biswal, Small molecule inhibitor of NRF2 selectively intervenes therapeutic resistance in KEAP1-deficient NSCLC tumors. *ACS Chem. Biol.* **11**, 3214–3225 (2016).

263. D. Olagnier, E. Farahani, J. Thyrsted, J. Blay-Cadanet, A. Herengt, M. Idorn, A. Hait, B. Hernaez, A. Knudsen, M. B. Iversen, M. Schilling, S. E. Jørgensen, M. Thomsen, L. S. Reinert, M. Lappe, H.-D. Hoang, V. H. Gilchrist, A. L. Hansen, R. Ottosen, C. G. Nielsen, C. Møller, D. van der Horst, S. Peri, S. Balachandran, J. Huang, M. Jakobsen, E. B. Svenningsen, T. B. Poulsen, L. Bartsch, A. L. Thielke, Y. Luo, T. Alain, J. Rehwinkel, A. Alcamí, J. Hiscott, T. Mogensen, S. R. Paludan, C. K. Holm, SARS-CoV2-mediated suppression of NRF2-signaling reveals potent antiviral and anti-inflammatory activity of 4-octyl-itaconate and dimethyl fumarate. *Nat. Commun.* **11**, 4938 (2020).

264. D. G. Ryan, E. V. Knatko, A. M. Casey, J. L. Hukelmann, S. Dayalan Naidu, A. J. Brenes, T. Ekkunagul, C. Baker, M. Higgins, L. Tronci, E. Nikitopolou, T. Honda, R. C. Hartley, L. A. J. O'Neill, C. Frezza, A. I. Lamond, A. Y. Abramov, J. S. C. Arthur, D. A. Cantrell, M. P. Murphy, A. T. Dinkova-Kostova, Nrf2 activation reprograms macrophage intermediary metabolism and suppresses the type I interferon response. *iScience*. **25**, 103827 (2022).

265. D. Ezerina, Y. Takano, K. Hanaoka, Y. Urano, T. P. Dick, N-Acetyl Cysteine Functions as a Fast-Acting Antioxidant by Triggering Intracellular H 2 S and Sulfane Sulfur Production. *Cell Chem. Biol.* **25**, 447–459 (2018).

266. K. E. Lee, M. C. Simon, *Cell*, in press, doi:10.1016/j.cell.2015.11.011.

267. T. Miyata, S. Takizawa, C. Van Ypersele De Strihou, Hypoxia. 1. Intracellular sensors for oxygen and oxidative stress: Novel therapeutic targets. *Am. J. Physiol. - Cell Physiol.* **300**, 226–231 (2011).

268. W. W. Wheaton, N. S. Chandel, Hypoxia. 2. Hypoxia regulates cellular metabolism. *Am. J. Physiol. - Cell Physiol.* **300** (2011), doi:10.1152/ajpcell.00485.2010.

269. D. Duscher, M. Januszyk, Z. N. Maan, A. J. Whittam, M. S. Hu, G. G. Walmsley, Y. Dong, S. M. Khong, M. T. Longaker, G. C. Gurtner, J. Distinguished Professor, P. Reconstr Surg Author manuscript, Comparison of the Hydroxylase Inhibitor DMOG and the Iron Chelator Deferoxamine in Diabetic and Aged Wound Healing. *Plast Reconstr Surg*. **139**, 695–706 (2017).

270. S. A. Mookerjee, A. A. Gerencser, D. G. Nicholls, M. D. Brand, Quantifying intracellular rates of glycolytic and oxidative ATP production and consumption using extracellular flux measurements. *J. Biol. Chem.* **292**, 7189–7207 (2017).

271. S. A. Mookerjee, A. A. Gerencser, D. G. Nicholls, M. D. Brand, Quantifying intracellular rates of glycolytic and oxidative ATP production and consumption using extracellular flux measurements. *J. Biol. Chem.* **292**, 12649 (2018).

272. L. B. Tanner, A. G. Goglia, M. H. Wei, T. Sehgal, L. R. Parsons, J. O. Park, E. White, J. E. Toettcher, J. D. Rabinowitz, Four Key Steps Control Glycolytic Flux in Mammalian Cells. *Cell Syst.* **7**, 49-62.e8 (2018).

273. A. N. Wick, D. R. Drury, H. I. Nakada, J. B. Wolfe Withtee, A. Gbabowski, LOCALIZATION OF THE PRIMARY METABOLIC BLOCK PRODUCED BY 2-DEOXYGLUCOSE. *J. Biol. Chem.* **224**, 963–969 (1957).

274. Q. Liu, J. W. Chang, J. Wang, S. A. Kang, C. C. Thoreen, A. Markhard, W. Hur, J. Zhang, T. Sim, D. M. Sabatini, N. S. Gray, Discovery of 1-(4-(4-propionylpiperazin-1-yl)-3-(trifluoromethyl)phenyl)-9-(quinolin-3-yl)benzo[h] [1,6]naphthyridin-2(1H)-one as a highly potent, selective Mammalian Target of Rapamycin (mTOR) inhibitor for the treatment of cancer. *J. Med. Chem.* **53**, 7146–7155 (2010).

275. W. Zhang, G. Wang, Z. G. Xu, H. Tu, F. Hu, J. Dai, Y. Chang, Y. Chen, Y. Lu, H. Zeng, Z. Cai, F. Han, C. Xu, G. Jin, L. Sun, B. S. Pan, S. W. Lai, C. C. Hsu, J. Xu, Z. Z. Chen, H. Y. Li, P. Seth, J. Hu, X. Zhang, H. Li, H. K. Lin, Lactate Is a Natural Suppressor of RLR Signaling by Targeting MAVS. *Cell*. **178**, 176-189.e15 (2019).

276. J. E. Strong, M. C. Coffey, D. Tang, P. Sabinin, P. W. Lee, The molecular basis of viral oncolysis: usurpation of the Ras signaling pathway by reovirus. *EMBO J.* **17**, 3351–3362 (1998).

277. B. P. Cuddington, K. L. Mossman, Permissiveness of Human Cancer Cells to Oncolytic Bovine Herpesvirus 1 Is Mediated in Part by KRAS Activity. *J. Virol.* **88**, 6885–6895 (2014).

278. C. W. Li, S. O. Lim, W. Xia, H. H. Lee, L. C. Chan, C. W. Kuo, K. H. Khoo, S. S. Chang, J. H. Cha, T. Kim, J. L. Hsu, Y. Wu, J. M. Hsu, H. Yamaguchi, Q. Ding, Y. Wang, J. Yao, C. C. Lee, H. J. Wu, A. A. Sahin, J. P. Allison, D. Yu, G. N. Hortobagyi, M. C. Hung, Glycosylation and stabilization of programmed death ligand-1 suppresses T-cell activity. *Nat. Commun.* **7** (2016).

279. H. H. Lee, Y. N. Wang, W. Xia, C. H. Chen, K. M. Rau, L. Ye, Y. Wei, C. K. Chou, S. C. Wang, M. Yan, C. Y. Tu, T. C. Hsia, S. F. Chiang, K. S. C. Chao, I. I. Wistuba, J. L. Hsu, G. N. Hortobagyi, M. C. Hung, Removal of N-Linked

Glycosylation Enhances PD-L1 Detection and Predicts Anti-PD-1/PD-L1 Therapeutic Efficacy. *Cancer Cell*. **36**, 168-178.e4 (2019).

280. E. Verschueren, B. Husain, K. Yuen, Y. Sun, S. Paduchuri, Y. Senbabaoglu, I. Lehoux, T. A. Arena, B. Wilson, S. Lianoglou, C. Bakalarski, Y. Franke, P. Chan, A. W. Wong, L. C. Gonzalez, S. Mariathasan, S. J. Turley, J. R. Lill, N. Martinez-Martin, The Immunoglobulin Superfamily Receptome Defines Cancer-Relevant Networks Associated with Clinical Outcome. *Cell*. **182**, 1–16 (2020).

281. R. J. DeBerardinis, N. S. Chandel, We need to talk about the Warburg effect. *Nat. Metab.* **2**, 127–129 (2020).

282. W. H. Koppenol, P. L. Bounds, C. V. Dang, Otto Warburg's contributions to current concepts of cancer metabolism. *Nat. Rev. Cancer*. **11**, 325–337 (2011).

283. M. G. Vander Heiden, L. C. Cantley, C. B. Thompson, Understanding the Warburg Effect: The Metabolic Requirements of Cell Proliferation. *Science (80-.).* **324**, 1029–1033 (2009).

284. A. Luengo, Z. Li, D. Y. Gui, L. B. Sullivan, M. Zagorulya, B. T. Do, R. Ferreira, A. Naamati, A. Ali, C. A. Lewis, C. J. Thomas, S. Spranger, N. J. Matheson, M. G. Vander Heiden, Increased demand for NAD+ relative to ATP drives aerobic glycolysis. *Mol. Cell*. **81**, 691-707.e6 (2021).

285. R. M. Loftus, D. K. Finlay, Immunometabolism: Cellular metabolism turns immune regulator. *J. Biol. Chem.* **291**, 1–10 (2016).

286. S. L. Topalian, J. M. Taube, R. A. Anders, D. M. Pardoll, S. Kimmel, S. Kimmel, S. Kimmel, S. Kimmel, Mechanism-driven biomarkers to guide immune checkpoint blockade in cancer therapy. *Nat. Rev. Cancer*. **16**, 275–287 (2017).

287. B. Faubert, K. Y. Li, L. Cai, C. T. Hensley, J. Kim, L. G. Zacharias, C. Yang, Q. N. Do, S. Doucette, D. Burguete, H. Li, G. Huet, Q. Yuan, T. Wigal, Y. Butt, M. Ni, J. Torrealba, D. Oliver, R. E. Lenkinski, C. R. Malloy, J. W. Wachsmann, J. D. Young, K. Kernstine, R. J. DeBerardinis, Lactate Metabolism in Human Lung Tumors. *Cell*. **171**, 358-371.e9 (2017).

288. A. Karagiannis, T. Gallopin, A. Lacroix, F. Plaisier, J. Piquet, H. Geoffroy, R. Hepp, J. Naude, B. Le Gac, R. Egger, B. Lambolez, D. Li, J. Rossier, J. F. Staiger, H. Imamura, S. Seino, J. Roeper, B. Cauli, Lactate is an energy substrate for rodent cortical neurons and enhances their firing activity. *Elife*. **10**, 1–40 (2021).

289. I. San-Millán, C. G. Julian, C. Matarazzo, J. Martinez, G. A. Brooks, Is Lactate an Oncometabolite? Evidence Supporting a Role for Lactate in the Regulation of Transcriptional Activity of Cancer-Related Genes in MCF7 Breast Cancer Cells. *Front. Oncol.* **9**, 1536 (2020).

290. R. Haas, J. Smith, V. Rocher-Ros, S. Nadkarni, T. Montero-Melendez, F. D'Acquisto, E. J. Bland, M. Bombardieri, C. Pitzalis, M. Perretti, F. M. Marelli-Berg, C. Mauro, Lactate Regulates Metabolic and Pro-inflammatory Circuits in

Control of T Cell Migration and Effector Functions. *PLoS Biol.* **13** (2015).

291. Q. Feng, Z. Liu, X. Yu, T. Huang, J. Chen, J. Wang, J. Wilhelm, S. Li, J. Song, W. Li, Z. Sun, B. D. Sumer, B. Li, Y. X. Fu, J. Gao, Lactate increases stemness of CD8+ T cells to augment anti-tumor immunity. *Nat. Commun.* **13**, 1–13 (2022).

292. R. S. Jansen, R. Addie, R. Merkx, A. Fish, S. Mahakena, O. B. Bleijerveld, M. Altelaar, L. IJlst, R. J. Wanders, P. Borst, K. Van De Wetering, N-lactoyl-amino acids are ubiquitous metabolites that originate from CNDP2-mediated reverse proteolysis of lactate and amino acids. *Proc. Natl. Acad. Sci. U. S. A.* **112**, 6601–6606 (2015).

293. D. Zhang, Z. Tang, H. Huang, G. Zhou, C. Cui, Y. Weng, W. Liu, S. Kim, S. Lee, M. Perez-Neut, J. Ding, D. Czyz, R. Hu, Z. Ye, M. He, Y. G. Zheng, H. A. Shuman, L. Dai, B. Ren, R. G. Roeder, L. Becker, Y. Zhao, Metabolic regulation of gene expression by histone lactylation. *Nature*. **574**, 575–580 (2019).

294. C. L. Roland, T. Arumugam, D. Deng, S. H. Liu, B. Philip, S. Gomez, W. R. Burns, V. Ramachandran, H. Wang, Z. Cruz-Monserrate, C. D. Logsdon, Cell surface lactate receptor GPR81 is crucial for cancer cell survival. *Cancer Res.* **74**, 5301 (2014).

295. W. Wagner, K. D. Kania, W. M. Ciszewski, Stimulation of lactate receptor (HCAR1) affects cellular DNA repair capacity. *DNA Repair (Amst).* **52**, 49–58 (2017).

296. D. Raychaudhuri, R. Bhattacharya, B. P. Sinha, C. S. C. Liu, A. R. Ghosh, O. Rahaman, P. Bandopadhyay, J. Sarif, R. D'rozario, S. Paul, A. Das, D. K. Sarkar, S. Chattopadhyay, D. Ganguly, Lactate induces pro-tumor reprogramming in intratumoral plasmacytoid dendritic cells. *Front. Immunol.* **10**, 1878 (2019).

297. N. A. Rizvi, M. D. Hellmann, A. Snyder, P. Kvistborg, V. Makarov, J. J. Havel, W. Lee, J. Yuan, P. Wong, T. S. Ho, M. L. Miller, N. Rekhtman, A. L. Moreira, F. Ibrahim, C. Bruggeman, B. Gasmi, R. Zappasodi, Y. Maeda, C. Sander, E. B. Garon, T. Merghoub, J. D. Wolchok, T. N. Schumacher, T. A. Chan, Mutational landscape determines sensitivity to PD-1 blockade in non-small cell lung cancer. *Science*. **348**, 124–128 (2015).

298. J. J. Havel, D. Chowell, T. A. Chan, The evolving landscape of biomarkers for checkpoint inhibitor immunotherapy. *Nat. Rev. Cancer 2019 193*. **19**, 133–150 (2019).

299. R. Banchereau, N. Leng, O. Zill, E. Sokol, G. Liu, D. Pavlick, S. Maund, L.-F. Liu, E. Kadel, N. Baldwin, S. Jhunjhunwala, D. Nickles, Z. J. Assaf, D. Bower, N. Patil, M. McCleland, D. Shames, L. Molinero, M. Huseni, S. Sanjabi, C. Cummings, I. Mellman, S. Mariathasan, P. Hegde, T. Powles, Molecular determinants of response to PD-L1 blockade across tumor types. *Nat. Commun.* **12**, 1–11 (2021).

Appendix I: DoRothEA analysis of bulk RNA-seq dataset.

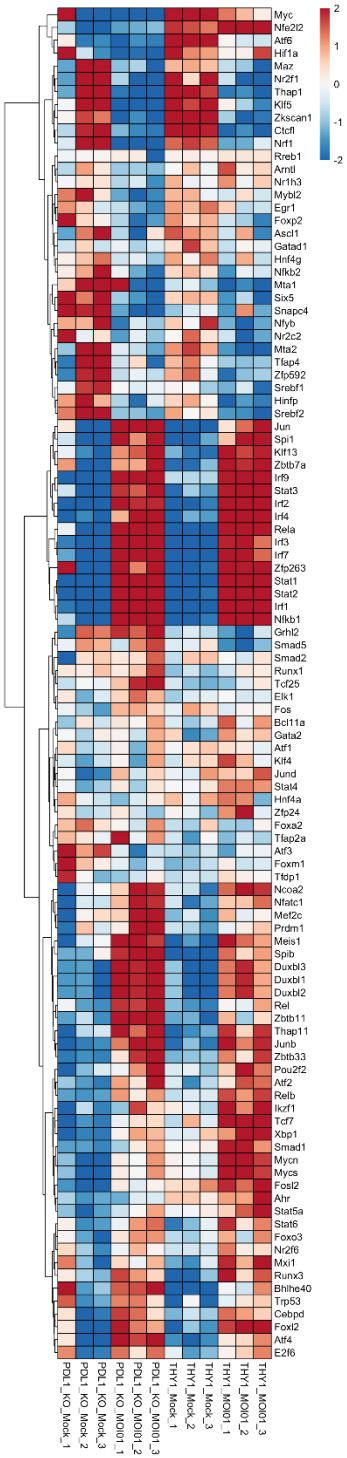

Appendix Figure 1: DoRothEA analysis of TRAMP-C2 bulk RNA-seq experiment. DoRothEA transcription factor analysis of bulk RNA-seq performed on TRAMP-C2 and TRAMP-C2 *Cd274*$^{-/-}$ either mock-infected or infected with VSVΔ51-YFP at MOI 0.1 for 8 hours (3 biological replicates per condition).

Appendix II: Summary of metabolomics results.

Appendix Table 1: metabolomics results of cell culture supernatant.

	Average		SD		WT vs KO	
Name	**WT**	**KO**	**WT**	**KO**	**p-value (t test)**	**Fold change, WT/KO**
2/3-Phosphoglyceric acid	12.29	24.26	2.58	5.52	0.0007155	-1.973
2-Aminoadipic acid	-8.55	-9.03	0.59	0.62	0.1995900	0.947
2-Deoxyuridine	-12.86	-6.85	0.50	0.66	0.0000000	-0.532
Alanine/Sarcosine	80.58	117.30	6.19	3.75	0.0000002	-1.456
alpha-Ketoglutaric acid	20.26	31.11	2.66	1.38	0.0000048	-1.536
Asparagine	22.40	56.63	4.08	9.06	0.0000073	-2.528
Aspartic Acid	38.09	75.56	6.14	3.76	0.0000002	-1.984
cis-Aconitic acid	13.90	19.99	3.08	2.29	0.0030363	-1.438
Citramalic acid	-5.72	-5.81	0.71	0.44	0.7986033	0.985
Citric acid / Isocitric acid	13.66	19.91	8.74	24.52	0.5693939	-1.457
Citrulline	1045.12	1971.99	219.00	115.06	0.0000035	-1.887
Cystine	-14.50	-17.62	1.29	0.68	0.0003806	0.823
Dihydroxyacetone phosphate	162.14	303.07	16.34	7.35	0.0000000	-1.869
Disaccharide	-2.26	-6.09	4.05	2.56	0.0790873	0.372
Gluconic acid	-4.64	-4.40	0.70	0.45	0.5009291	-0.949
Glutamic acid	16.88	33.56	2.83	1.61	0.0000002	-1.988
Glutamine	-10.98	-13.05	1.79	0.98	0.0328533	0.842
Glyceric acid	-2.11	-0.14	1.55	1.25	0.0364177	-0.066
Hexoses	-6.64	-8.21	1.99	1.00	0.1145680	0.808
Histidine	-3.17	-2.24	1.99	1.17	0.3452549	-0.705
Hydroxyglutaric acid	-3.34	-2.03	0.59	0.28	0.0006388	-0.608
Isoleucine	-7.85	-8.88	0.72	0.82	0.0447085	0.885
Kynurenine	-3.80	-3.68	0.82	0.50	0.7667542	-0.968
Lactic acid	85.56	126.32	13.22	11.84	0.0002193	-1.476
Leucine	-8.68	-9.77	0.55	0.48	0.0045699	0.889
Malic acid	11.28	30.25	2.79	1.18	0.0000000	-2.681
Methionine	-6.27	-6.50	0.81	0.62	0.5995274	0.965
N-Acetylaspartic acid	-6.87	-7.31	0.89	0.56	0.3323878	0.940
N-Acetylglutamic acid	5.56	9.27	1.80	4.00	0.0651678	-1.667
N-Acetylneuraminic acid	-4.18	-4.33	1.11	0.91	0.8011052	0.965
Orotic acid	27.04	39.52	2.78	4.66	0.0002182	-1.462
Pantothenic acid	-6.28	-7.12	0.44	0.34	0.0043207	0.882
Phenylalanine	-7.32	-8.51	0.72	0.44	0.0064752	0.861
Phenylpyruvic acid	116.60	243.72	41.77	4.56	0.0000229	-2.090

Phosphoenolpyruvic acid	-7.35	-3.75	2.31	3.03	0.0427803	-0.509
Pyridoxal	21.17	35.77	3.21	1.89	0.0000023	-1.689
Pyridoxine	-7.02	-8.27	0.79	0.63	0.0130610	0.849
Pyroglutamic acid	-5.41	-3.69	3.69	3.23	0.4094152	-0.681
Pyruvic acid	-12.99	-18.19	0.29	0.16	0.0000000	0.714
Riboflavin	-6.95	-7.63	0.90	0.58	0.1532879	0.911
Salicylic Acid	2.23	4.30	2.66	3.85	0.3051208	-1.925
Serine	-13.10	-14.06	1.06	0.84	0.1135042	0.932
Succinic acid	-4.89	-5.48	0.88	0.44	0.1761132	0.893
Taurine	-7.14	-1.42	2.77	5.42	0.0441185	-0.199
Thiamine	4.71	7.21	2.86	1.66	0.0930260	-1.533
Threonine	2.81	5.18	1.04	2.34	0.0473259	-1.843
Thymidine	-17.55	-12.71	0.54	0.64	0.0000001	-0.724
Thymine	24.55	50.34	6.47	7.52	0.0000817	-2.051
Tryptophan	-6.73	-7.55	0.45	0.59	0.0212810	0.891
Tyrosine	-6.53	-7.31	0.82	0.61	0.0898680	0.893
Uracil	2.23	8.74	4.07	3.34	0.0126879	-3.917
Uric acid	3.30	6.26	1.60	1.20	0.0045192	-1.900
Uridine	-9.87	-4.07	1.39	1.75	0.0000807	-0.412
Valine	-6.14	-7.28	0.55	0.60	0.0064479	0.843
Xanthine	-16.95	-21.31	0.44	0.09	0.0000000	0.795
Xanthosine	-1.79	-3.00	1.20	0.89	0.0752383	0.596

Appendix Table 2: metabolomics results of cell lysates.

	Average		**Standard Deviation**		**WT vs KO**	
Name	**WT**	**KO**	**WT**	**KO**	**p-value (t test)**	**Fold change, WT/KO**
2/3-Phosphoglyceric acid	0.4346	0.3569	0.0838	0.0591	0.0931850	1.218
2-Aminoadipic acid	0.3025	0.2632	0.0277	0.0312	0.0437940	1.149
2-Deoxycytidine 5-monophosphate	0.0161	0.0121	0.0027	0.0020	0.0160202	1.330
2-Deoxyribose 5-phosphate	0.0164	0.0147	0.0032	0.0011	0.2557608	1.113
Acetyl-CoA	0.1869	0.1681	0.0263	0.0231	0.2163911	1.112
Adenosine 3-5-cyclic monophosphate	0.0184	0.0122	0.0025	0.0032	0.0040407	1.503
Adenosine 5-diphosphate	30.3317	39.0144	3.7496	2.5526	0.0008561	-1.286
Adenosine 5-monophosphate	80.5812	106.3058	9.6735	12.1462	0.0022937	-1.319
Adenosine 5-triphosphate	38.5665	43.5172	5.1298	7.6610	0.2177761	-1.128
Alanine/Sarcosine	241.4903	281.3969	42.3592	46.6056	0.1516831	-1.165

alpha-D-Glucose-1-phosphate	0.0311	0.0972	0.0130	0.0373	0.0021705	-3.121
alpha-Ketoglutaric acid	0.7771	0.5253	0.1518	0.0378	0.0027569	1.479
Asparagine	0.0880	0.1575	0.0267	0.0217	0.0005812	-1.790
Aspartic Acid	11.4569	6.6351	0.6063	0.2671	0.0000000	1.727
beta-Nicotinamide adenine dinucleotide	7.2449	9.4539	1.0102	0.6518	0.0011419	-1.305
cis-Aconitic acid	0.1236	0.0948	0.0137	0.0168	0.0084481	1.304
Citramalic acid	0.1664	0.1632	0.0416	0.0338	0.8855367	1.020
Citric acid / Isocitric acid	10.6491	11.3728	1.8088	6.0594	0.7849350	-1.068
Citrulline	0.8303	1.7028	0.1461	0.0960	0.0000002	-2.051
Coenzyme A	0.2933	0.2997	0.0264	0.0197	0.6445873	-1.022
Creatine	356.0217	330.9007	67.2106	72.5008	0.5475937	1.076
Creatinine	0.2874	0.2531	0.0567	0.0406	0.2558087	1.136
Cystine	0.0034	0.0078	0.0019	0.0023	0.0048215	-2.288
Cytidine	0.1000	0.0743	0.0139	0.0102	0.0044384	1.345
Cytidine 5-diphosphate	8.9790	11.2808	1.3210	0.8569	0.0050052	-1.256
Cytidine 5-monophosphate	1.7751	1.8109	0.2221	0.2048	0.7776850	-1.020
Cytidine 5-triphosphate	5.6172	7.0726	0.5874	0.8963	0.0076602	-1.259
Deoxycytidine 5-triphosphate	0.0821	0.1355	0.0054	0.0115	0.0000012	-1.651
Deoxythymidine 5-triphosphate	0.4373	0.5820	0.0453	0.0902	0.0056119	-1.331
Dihydroorotic acid	0.1904	0.1075	0.0376	0.0096	0.0003846	1.772
Dihydroxyacetone phosphate	24.9115	14.4485	4.4456	4.3677	0.0021025	1.724
Flavin adenine dinucleotide	0.2109	0.2736	0.0289	0.0289	0.0037282	-1.297
Fructose 1,6-biphosphate	12.0123	5.1786	3.5542	0.4852	0.0008858	2.320
Fructose 6-phosphate	1.0313	0.7486	0.4618	0.1461	0.1833202	1.378
gamma-Glu-Cys	0.4150	0.4228	0.0372	0.0681	0.8106087	-1.019
Gluconic acid	0.3142	0.1477	0.0148	0.0112	0.0000000	2.127
Glucose 6-phosphate	4.3793	3.9803	1.6149	0.4757	0.5744478	1.100
Glutamic acid	103.5862	93.9370	14.7983	13.2852	0.2620961	1.103
Glutamine	320.4917	277.4456	55.4964	42.0322	0.1608271	1.155
Glutathione (oxidized)	0.9969	0.7316	0.1931	0.0547	0.0089148	1.363
Glutathione (reduced)	32.0422	32.3146	1.2314	1.1558	0.7009988	-1.009
Glyceric acid	0.2294	0.2017	0.0547	0.0558	0.4060357	1.137
Guanine	0.3827	0.3545	0.0544	0.0747	0.4713718	1.080
Guanosine	0.5496	0.2960	0.1295	0.0522	0.0012353	1.857

Guanosine 5-diphosphate	4.0029	5.7996	1.4089	0.8943	0.0248519	-1.449
Guanosine 5-triphosphate	15.2618	16.0167	1.9584	4.8704	0.7319403	-1.049
Hexoses	336.6635	196.1445	128.6744	46.6527	0.0306604	1.716
Histidine	5.8866	9.5934	0.7957	0.5076	0.0000023	-1.630
Hydroxyglutaric acid	0.2080	0.1991	0.0181	0.0120	0.3409206	1.044
Hypotaurine	0.4336	0.3669	0.0944	0.0838	0.2249736	1.182
Inosine	4.1588	4.3587	0.4840	0.5334	0.5121592	-1.048
Inosine 5-monophosphate	0.2345	0.1819	0.0348	0.0405	0.0367227	1.289
Isoleucine	53.0592	61.3778	7.5593	10.4812	0.1459222	-1.157
Kynurenine	0.2386	0.3548	0.0353	0.0320	0.0001371	-1.487
Lactic acid	334.6749	320.4600	89.5998	61.9012	0.7557546	1.044
Leucine	50.5030	63.9697	7.8798	4.2761	0.0042507	-1.267
Malic acid	5.7409	2.5814	0.7758	0.3307	0.0000035	2.224
Methionine	21.2308	23.1960	3.3881	1.3564	0.2165747	-1.093
N-Acetylaspartic acid	0.0075	0.0082	0.0009	0.0007	0.1524145	-1.095
N-Acetylglutamic acid	0.0273	0.0281	0.0025	0.0016	0.4992381	-1.031
N-Acetylneuraminic acid	3.4473	6.1589	0.4441	0.3428	0.0000003	-1.787
O-Phosphorylethanolamine	1.4355	1.2858	0.2420	0.1015	0.1925887	1.116
Orotic acid	0.1666	0.1188	0.0276	0.0182	0.0053489	1.402
Pantothenic acid	2.9505	3.7708	0.2959	0.2398	0.0003599	-1.278
Phenylalanine	29.1591	37.9478	4.6187	1.9273	0.0015576	-1.301
Phenylpyruvic acid	2.7581	2.8436	0.9232	0.4171	0.8403362	-1.031
Proline	23.2369	38.1857	5.3885	3.1144	0.0001545	-1.643
Pyridoxal	0.0222	0.0227	0.0064	0.0026	0.8655432	-1.022
Pyridoxine	0.4326	0.3846	0.1493	0.0576	0.4788275	1.125
Pyroglutamic acid	37.7283	29.9736	11.0528	4.5365	0.1429509	1.259
Pyruvic acid	10.4876	4.9266	2.4491	0.7074	0.0003267	2.129
Riboflavin	0.1569	0.1476	0.0387	0.0144	0.5933422	1.063
Ribose 5-phosphate	0.4471	0.2807	0.0805	0.0613	0.0024057	1.593
S-5-Adenosyl-L-homocysteine	0.8451	0.7042	0.1382	0.1484	0.1195058	1.200
Sedoheptulose-7-phosphate	0.1362	0.0768	0.0427	0.0175	0.0103672	1.772
Serine	14.7701	17.6787	1.8614	0.7565	0.0053049	-1.197
Succinic acid	1.8341	1.2016	0.3039	0.2107	0.0018608	1.526
Taurine	151.5445	116.3657	20.2695	17.0454	0.0086665	1.302
Thiamine	0.4164	0.3837	0.1002	0.0753	0.5382272	1.085

Threonine	187.8586	219.3041	31.9800	32.1650	0.1203193	-1.167
Thymidine 5-diphosphate	0.3825	0.5281	0.0436	0.0295	0.0000483	-1.381
Thymidine 5-monophosphate	0.0921	0.0551	0.0125	0.0032	0.0000375	1.670
Tryptophan	30.9187	45.2060	4.6518	2.6956	0.0000681	-1.462
Tyrosine	36.7731	49.0738	6.0291	9.0061	0.0194473	-1.335
UDP-Glucose / UDP-Galactose	13.8707	13.6677	2.4325	0.6979	0.8481077	1.015
UDP-Glucuronic Acid	3.9667	3.5598	0.3579	0.3131	0.0625030	1.114
Uracil	0.0385	0.0290	0.0107	0.0066	0.0922647	1.328
Uric acid	5.2643	4.5929	1.3516	0.4349	0.2736816	1.146
Uridine	0.8404	0.5953	0.1319	0.0649	0.0022033	1.412
Uridine 5-diphosphate	5.7722	6.8697	1.0295	0.5583	0.0445907	-1.190
Uridine 5-monophosphate	5.0701	4.0607	0.4481	0.4251	0.0025055	1.249
Uridine 5-triphosphate	45.5040	53.9743	6.4448	9.9933	0.1116110	-1.186
Valine	51.6877	71.1841	10.1750	11.8952	0.0122332	-1.377
Xanthine	1.0497	1.1771	0.3081	0.2512	0.4506658	-1.121
Xanthosine	0.0369	0.0237	0.0069	0.0062	0.0060500	1.558
Adenylate Energy Charge	0.35984	0.33399	0.03082	0.03455	0.2014357	1.07739
GSH/GSSG	33.11328	44.45266	6.18321	4.71946	0.0050888	-1.34244

Appendix III: Summary of patient tumour biopsy cohort.

Sample ID	Sex	Age	Diagnosis	PD-L1 status	Average % infection	Biopsy Viability (fold over control)	% Necrosis
203	62	Female	lung squamous cell carcinoma	+	0.5	3.8	5%
204	83	Female	endometrial cancer	-	4.0	3	<1%
205	63	Male	papillary renal cell carcinoma	+	33.5	2.3	10%
215	57	Female	ovarian cancer	-	0.9	2.9	4-5%
221	67	Female	endometrial cancer	+	22.6	3.9	<1%
223	68	Female	lung cancer	+	27.9	2.8	0%
224	70	Female	hepatocellular carcinoma	-	1.3	3.5	0%
225	73	Male	lung squamous cell carcinoma	+	6.3	2.5	95%
226	48	Male	colon adenocarcinoma	-	0.5	2.5	0%
227	74	Female	lung non-small cell carcinoma	-	2.3	1.2	50%
241	57	Female	ovarian cancer	+	0.2	1.7	<1%
242	73	Female	chromophobe renal cell carcinoma	-	0.1	2.1	0%
247	62	Female	colon adenocarcinoma	+	9.3	2	15%
248	63	Female	ovarian cancer	-	2.9	1.9	0%
249	56	Male	dermatofibrosarcoma protuberans	-	0.2	1.9	<1%
253	62	Male	neuroendocrine tumor	-	3.8	1.7	<1%
257	67	Female	uterine fibroid	+	3.5	2	<1%
260	61	Female	fibrous tumor of the abdomen	+	11.4	2.1	<1%
283	52	Female	breast carcinoma	+	1.5	1.9	1%
289	79	Female	hepatic adenocarcinoma	-	8.2	2	15%
291	59	Male	leiomyosarcoma	+	0.1	2.4	15%